REFERENCE ONLY

UNIVERSITY OF LONDON THESIS

Degree	Year	Name of Author
PhD	2006	BISHOP, L. J.

A Quantitative Study of Volcanic Processes on Mars Using Data from the Mars Global Surveyor Spacecraft

A thesis submitted to the University of London
for the degree of Doctor of Philosophy
by

Louise Jane Bishop

Department of Earth Sciences
University College London
Gower Street
London WC1E 6BT

Submitted December 2004

ProQuest LLC
789 East Eisenhower Parkway
P.O. Box 1346
Ann Arbor, MI 48106-1346

Abstract

Volcanic processes on Mars were investigated using topographic profiles derived with the help of IDL software from data collected by the Mars Orbiter Laser Altimeter (MOLA) on the Mars Global Surveyor Mission (MGS) in 1997-2001 and images obtained by the MGS Mars Orbiter Camera (MOC) and by the earlier Viking mission. Thickness and slope values for lava flows at both Elysium Mons and Alba Patera made it possible to compute flow emplacement times and effusion rates using the flow growth model proposed by C. R. J. Kilburn and R. M. C Lopes in 1990.

Geological mapping of the Elysium volcanic region showed that Elysium Mons was emplaced as a result of a single shift in vent position on top of an older volcanic edifice, here termed the Ancient Volcanic Edifice (AVE). This implies that there have been substantial variations in both position and time for the magma supply.

Calculations suggest that the flows at Alba Patera were emplaced more quickly than those at Elysium Mons, possibly owing to differences in fissure width and lava composition. There is evidence for both aa and pahoehoe on the summit areas of Elysium Mons and Alba Patera. The presence of aa is consistent with the view that long lava flows on Mars are emplaced quickly. Pahoehoe flows imply slow emplacement, and their inferred presence on Mars provides support for the theory that long terrestrial lavas are often emplaced as sheets of inflated pahoehoe.

MOC image analysis indicated that late-stage explosive activity has occurred at several Martian volcanoes where it was previously undetected, contrary to the prevalent view that Martian volcanism evolves from explosive to effusive activity. To resolve the many ambiguities inherent in morphological data and imagery the need remains for ground truthing by experienced observers and detailed geochemical analyses in situ or by means of a sample return mission

Acknowledgements

I would like to gratefully acknowledge and thank the following for their valuable input throughout the duration of this work:

- The Natural Environmental Research Council for the funding for the first three years of this project.
- I would like to thank my main supervisor Professor John Guest for all his help, ideas and constant interest in all things Martian.
- Thanks also go to my second supervisor Dr Christopher Kilburn for the use of his lava growth model and also for all his patient explanations of how to use it!
- I gratefully acknowledge the help of Professor Claudio Vita-Finzi, who genuinely had to plough through some of my work during the writing-up, and I want to thank him for helping to keep me motivated, and for all the discussions we had.
- I would also like to say thank you to all the other people who have provided me with useful and interesting discussions about my work, in particular Dr Gerald Roberts, Dr Francis Nimmo and Dr Charlie Bristow.
- I want to thank all the guys in the RPIF for making it a nice place to work, especially Dr Dominic Fortes and Dr Emma Bowden for being excellent gossip partners, Peter Grindrod for putting up with me both at college and at the Natural History Museum, and lastly, but not least, Joyce Vetterlein for being genuinely great, as well as being the only other person I know who doesn't tire of talking about Mars/MOLA etc.

On a personal note I want to thank my family for being so supportive, especially my parents John and Elaine Bishop, who have never doubted that I can achieve whatever I put my mind to.

My final and biggest thank you goes to my partner Christopher Martin. Chris has lived and breathed this work almost as much as me, and I can't begin to tell him how much his love, support and endless patience have helped me through this work. **Thank you.**

Contents

		Page
Title Page		1
Abstract		2
Acknowledgements		3
Contents		4
Lists of Tables		11
Lists of Figures		12
Chapter 1		20
1.1	**Spacecraft exploration of Mars**	21
1.11	Previous missions	21
1.12	Mars Global Surveyor	24
1.2	**Volcanic processes on Mars**	27
1.21	Comparative volcanology	27
1.22	General geology and types of volcanoes on Mars	28
(a)	Crustal Dichotomy and relative ages on Mars	28
(b)	The distribution of Martian volcanoes	32
(c)	Shields, domes and paterae	34
(d)	Alba Patera	36
(e)	Evolution and growth of Martian volcanoes	39
1.3	**Geology of Elysium**	41
1.31	Geological setting of the Elysium Montes	41
1.32	Geological history of Elysium	44
1.33	Characteristics of the volcanoes	45
1.34	The presence of volatiles in Elysium	46
1.4	**Lava flow studies**	47

1.41 Rheological behaviour of lava 48
1.42 Factors that affect flow dimensions 52
1.43 Factors affecting magma discharge rates 52
1.44 Factors affecting flow behaviour 53
1.45 Modelling lava flow growth 55
1.5 This study 56

Chapter 2 59

2.1 Sources of data 59
2.11 Viking images 59
(a) Data collection 60
(b) Availability for use 61
2.12 MGS MOC images 61
(a) Data collection 61
(b) Availability for use 62
2.13 MGS MOLA data 64
(a) Data collection 64
(i) Specifications of MOLA 64
(ii) How does MOLA work? 66
(iii) How does MOLA tell the difference between clouds and the ground? 72
(iv) Surface reflectivity and atmospheric opacity 73
(b) Availability for use 74
(c) Major corrections applied to MOLA data 76
(i) Orbit determination 76
(ii) Altimetric crossovers 77
(iii) Overall errors 77
2.2 Manipulation of data 78
2.21 Viking images 78
(a) Use of software 78
(b) Errors and difficulties 79
(i) Digital data 79

(ii) Printed material 80

2.22 MOC images 81

(a) Manipulation of images 81

(b) MOC footprints 81

(c) Errors and difficulties 82

2.23 MOLA data 83

(a) Co-ordinate systems 83

(b) Production of orbit profiles 86

(c) Determining the positions of MOLA ground-tracks 87

(i) Finding orbits in a specific area 87

(ii) Mapping of orbits 88

(iii) Matching profiles to photomosaics 88

(d) Gridded data 90

(e) Errors in results produced using MOLA data 90

Chapter 3 92

3.1 Introduction 92

3.2 Methods 92

3.3 Volcanic Features 93

3.31 Olympus Mons 95

3.32 Alba Patera 103

3.33 Elysium Mons 108

3.34 Hecates Tholus 115

3.35 Unit boundaries 119

3.4 Periglacial Features **123**

3.5 Fluvial Features and Elysium Fossae **129**

3.6 Aeolian Features **134**

3.61 Erosional processes 134

3.62 Small-scale processes 137

3.63 Dunes 140

3.7 Impact Cratering **143**

3.71 Impact cratering processes 144

3.72 Impact crater modification 146

3.8 Conclusions about the surface of Mars **150**

Chapter 4 **152**

4.1 Methods of geological mapping 152
4.11 Aims 152
4.12 Boundaries and choice of units 153
4.13 Ages of units 153
4.14 Photogeological analysis 155
4.15 Analysis of MOLA data 155
4.16 Errors and difficulties 156
4.2 Physiographic Setting of Mapping Area 157
4.3 Mapping units 160
4.31 Volcanics 162
4.32 Fossae Materials and Altered Plains 170
(a) Fossae Materials 171
(b) Fossae Plains (**Fap**) 173
(c) Altered plains materials 182
4.3 Plains Materials 187
(a) Highland Materials 188
(b) Hilly Plains Units 190
4.4 Features of interest 196
4.41 Elysium Fossae 196
4.42 Volcanic calderas 198
(a) Elysium Mons 199
(b) Albor Tholus 200
(c) Hecates Tholus 202
4.43 Slopes of the volcanoes 204
4.44 Hecates Tholus collapse feature 204
4.45 Volcanic ridge features 205
4.5 Stratigraphic observations 207
4.6 Models 209
4.7 Geologic summary 215

4.8 Additional data 219
4.81 TES data 219
4.82 Gravity data 220
4.83 Mars Odyssey 221
4.9 Conclusions 222

Chapter 5 223

5.1 Types of lava flows 225
5.2 Selection of lava flows for this study 231
5.21 Selection of lava flows 232
(a) Elysium Mons 232
(b) Alba Patera 234
5.22 Determination of type of flow 236
(a) Downstream resistance 236
(b) Fractal analysis 241
5.3 Modelling **246**
5.31 The flow growth model 246
5.32 Flow measurements 254
(a) Flow growth model measurements 254
(b) Maximum length 255
(c) Maximum width 256
(d) Thickness 256
(e) Slope 258
(f) Area and volume 259
(g) Other measurements 260

5.4 Conclusion **261**

Chapter 6 **263**

6.1 Results of aa flows 263
6.11 Elysium Mons aa flows 263

(a) Appearance 264
(b) Emplacement 267
6.12 Alba Patera aa flows 280
(a) Appearance 280
(b) Emplacement 284

6.2 Modelling 289
6.21 Elysium Mons 289
6.22 Alba Patera aa flows 292
6.23 Analysis 294

6.3 Results of pahoehoe flows 296
6.31 Elysium Mons pahoehoe flows 296
(a) Appearance 297
(b) Emplacement 304
6.32 Alba Patera pahoehoe flows 311
a) Appearance 312
(b) Emplacement 313
6.33 Analysis 319

6.4 Initial conclusions of lava flow study results 321

Chapter 7 **323**

7.1 The geology of the area surrounding the Elysium Montes 323
7.11 Evolution of volcanic centres 323
7.12 Explosive activity 327
7.13 Eruptions from the Fossae 328
7.14 Overall implications 330
7.2 **Lava flow studies** 331
7.21 Comparisons with results from similar studies 331
7.22 Comparisons with results for other lava flow studies on Mars 339
7.23 Comparisons to terrestrial flow values 343
7.24 Overall implications 345

a) Aa flow studies 345
b) Pahoehoe flow studies 346
7.3 Martian surface processes 348
7.4 **MOLA as a geological tool** 350
7.5 Conclusions 353
7.51 Summary of major conclusions 353
7.52 Further work 354
References **359**
Appendix **397**

Tables

Chapter 1: **Page**

Table: 1.1	Categorisation of Martian ages	31
1.2	Absolute ages of selected Martian geological features	31

Chapter 2:

Table: 2.1	Summary of MOC characteristics	62
2.2	Specifications for MOLA instrument	65
2.3	MOLA matched filter characteristics	72
2.4	Values for Martian reference spheroid	84

Chapter 5:

Table: 5.1	Results of fractal analysis highlighting aa and pahoehoe flows	244
5.2	Results of fractal analysis highlighting intermediate flows	245

Chapter 6:

Table

6.1	Measurements of Elysium Mons aa lava flows	290
6.2	Calculations for the Elysium lavas	290
6.3	Measurements of Alba Patera aa lava flows	292
6.4	Calculations for the Alba lavas	293
6.5	Measurements of Elysium Mons pahoehoe lava flows	298
6.6	Measurements of Alba Patera pahoehoe lava flows	313

Chapter 7:

Table: 7.1	Calculations of flow emplacement times for Martian volcanoes studied in previous work	340

Figures

Chapter 1:

Figure		Page
1.1	The planet Mars	20
1.2	Mariner 4 image of cratered terrain	22
1.3	Mariner 9 image of waning dust storm	23
1.4	Diagram of MGS spacecraft	24
1.5	MOLA topographic map of Mars with major surface features and mission landing sites labelled	26
1.6	Sketch map of major geological features on Mars	33
1.7	MOC image of cones in western Isidis Planitia	35
1.8	Viking Orbiter image of Tyrrhena Patera	36
1.9	Viking Orbiter image of Alba Patera	37
1.10	General geological map of Alba Patera	39
1.11	Viking image mosaic of the Elysium Montes region of Mars	41
1.12	General geological map of Elysium Montes	42
1.13	Plot of shear stress versus strain for Newtonian and Bingham liquids	49
1.14	Diagram to demonstrate lateral flow of fluids	50
1.15	Apollo photograph of lunar sinuous rilles	54

Chapter 2:

2.1	Illustration of a Gaussian trace	67
2.2	Diagram explaining the position of the Vernal Equinox	69
2.3	Illustration of the way MOLA makes measurements	70
2.4	Illustration of MOLA ground-track positioning	76
2.5	Diagrams to illustrate areocentric and areographic latitudes	84
2.6	Example of MOLA profiles constructed using IDL	87

Chapter 3:

3.1	Sketch map of Mars showing the positions of the major geological features	95
3.2	Sketch showing locations of MOC images on the flanks of Olympus Mons	96
3.3	MOC image of edge of Olympus Mons caldera and a sheet flow	97
3.4	MOC image of channel leading from a crater/depression on the flanks of Olympus Mons	98
3.5	Aerial photo of Bear Crater (Idaho, USA) and associated channel	98
3.6	MOC image of leveed flows on the flanks of Olympus Mons	99
3.7	'Dust' filled channels on the flanks of Olympus Mons	99
3.8	MOC image of leveed flows emplaced on ridges on Olympus Mons	100
3.9	MOC image of thick lava flows at the base of Olympus Mons	101
3.10	Aerial photograph of Big Glass Mountain, California, USA	101
3.11	Image of an area of basal scarp of Olympus Mons where layering is exposed	103
3.12	Sketch showing the locations of MOC images on the flanks of Alba Patera	104
3.13	MOC image of part of Alba Patera caldera complex	104
3.14	Image of hummocky material on the summit of Alba Patera	105
3.15	Aerial photograph of the Wapi flow field in Idaho, USA	106
3.16	Hummocky terrain and loose material in image of part of the upper flanks of Alba Patera	106
3.17	MOC image of outer summit area of Alba Patera	107
3.18	Image of possible yardangs at the summit of Alba Patera	107
3.19	Image of lava flow edges of boundaries at Alba Patera	108
3.20	Sketch of Elysium Mons showing the locations covered by several MOC images	109
3.21	MOC image of Elysium Mons caldera showing possible inflated flows	110
3.22	Aerial photograph of terrestrial inflated pahoehoe flows	110
3.23	MOC image of the flank of Elysium Mons which displays a surface texture like that found at the summit	111
3.24	MOC image of lava surfaces covered in fine-grained deposits	112

3.25	Aerial photograph of terrestrial inflated pahoehoe flows covered with aeolian materials	112
3.26	MOC image of the boundary of a lava flow on Elysium Mons	113
3.27	Aerial photograph of the boudary of a terrestrial aa flow	113
3.28	MOC image of boundaries of flows and partially buried flows on Elysium Mons	114
3.29	MOC image of lava flows on Elysium Mons that exhibit channels, yardangs and dunes	114
3.30	Sketch of Hecates Tholus showing the locations covered by several MOC images	115
3.31	MOC image of an area inside the caldera of Hecates Tholus	116
3.32	MOC image of linear features occurring on the flanks of Hecates Tholus	117
3.33	Images of terrestrial yardangs	118
3.34	MOC image of channels on the flanks of Hecates Tholus	119
3.35	MOC image showing boundary between Hecates Tholus and the surrounding plains	120
3.36	MOC image highlighting the boundary between Elysium lavas and plains underlain by ground-ice	120
3.37	Close-up images of plains in Figure 36	121
3.38	MOC images showing various examples of pitted and patterned terrain north of Elysium Mons	125
3.39	Photographs and a sketch of terrestrial pingoes and remnants of frost mounds	126
3.40	MOC images of the area around and in the Chaotic Terrain that suggest the presence of ground-ice	128
3.41	Various MOC images supporting the theory that water was erupted from the Elysium Fossae	132
3.42	MOC images of the northern Elysium plains showing erosional features within channels and the Fossae	133
3.43	MOC images demonstrating the erosional power of the wind on Mars	136
3.44	MOC images highlighting the way that winds are channelled by topography	139
3.45	MOC images of different dune types and dune fields observed in this Study	143

3.46 MOC images showing different aspects of Martian impact craters 146
3.47 MOC images that demonstrate some different ways in which Martian Impact craters can be modified 147/148
3.48 Photomosaic of part of Enceladus 149

Chapter 4:

4.1 Shaded MOLA topography map of entire mapping area 158
4.2 Sketch map of entire mapping area 159
4.3 Small reference map of mapping area 160
4.4 Detailed map of the northwestern part of mapping area 161
4.5 Small map of 'volcanic' geological units 162
4.6 Contour map of entire mapping area 163
4.7 Shaded DEM of the Elysium Montes 166
4.8 Image of Elysium Fossae embayed by lava flows 167
4.9 Shaded MOLA image of area immediately west of Elysium Mons 168
4.10 MOC image of the summit of Elysium Mons 169
4.11 Small map of 'altered plains' geological units 171
4.12 MOC image of impact craters penetrating Martian surface layers 172
4.13 Shaded DEM of layered deposits from the Elysium Fossae 173
4.14 Viking image of pitted flow material 174
4.15 Image of phreatic explosion craters in pumice flow deposits 175
4.16 Viking image of sources of flow material 176
4.17 MOLA profile across Fossae Materials with different units labelled 177
4.18 Viking image of material at the distal end of a set of Fossae 178
4.19 Viking image of an area of the Smoothed Flow unit (**Fsm**) 179
4.20 Viking image of part of the Ridged Fractured Material unit (**Rfr**) 180
4.21 Viking image showing part of the Disrupted Materials unit (**Dr**) 182
4.22 Viking image of one of the Volcanic Ridge features (**Vr**) and part of the Textured Plains unit (**Txp**) 184
4.23 Viking image of some of the Fossae and the surrounding Disrupted Flow (**Df**) unit 185
4.24 Viking image of the Vent flows (**Vf**) unit 186
4.25 Small map of the 'Plains Materials' geological units 188

4.26 Part of Viking photomosaic of quadrangle MC15 showing the appearance of the Ridged Plains (**rp**) 191
4.27 Shaded MOLA image of small, relatively young volcano 193
4.28 Viking image showing an example of the Chaotic Terrain (unit **Ct**) 194
4.29 Small sketch map of major geological features of interest in the Elysium mapping area 196
4.30 Viking image of one of the Elysium Fossae 197
4.31 MOC image of part of wall of the Elysium Mons caldera 199
4.32 MOC image traversing the Elysium Mons caldera, and a sketch map constructed from this image 201
4.33 MOC image showing part of the wall and floor of the Alba Patera Caldera 202
4.34 MOC image of the northern edge of the caldera of Hecates Tholus 203
4.35 DEM of the western flank of Hecates Tholus highlighting the shape of the 'collapse feature' 205
4.36 MOC image exhibiting the small-scale features occurring on one of the Volcanic Ridge features (**Vr**) 206
4.37 Correlation of mapping units 208
4.38 Map of arcuate graben surrounding Elysium Mons 211
4.39 Geological map of the Ardnamurchan volcanic complex 212
4.40(a) MOLA profile across Elysium Mons 212
(b) Shaded MOLA image indicating the position of the MOLA profile in Figure 40(a) 213
4.41 Contour map of the summit of Elysium Mons and the surrounding area 214

Chapter 5:

5.1 Photograph of the 1983 aa flow of Mount Etna, Sicily 227
5.2 Photograph of the 1651 lava flow of Mount Etna, Sicily 228
5.3 Photograph of a tumulus from the Balze Soprane pahoehoe flow of Mount Etna, Sicily 230
5.4 Map showing the positions of the Elysium Mons lava flows studied using the flow growth model 234
5.5 Map showing the positions of the Alba Patera lava flows studied using

	the flow growth model	235
5.6	Plot of thickness against slope for young lava flows on Mount Etna.	237
5.7	Plot of thickness against slope for all measured points along all of the Alba Patera lava flows	237
5.8	Plot of thickness against slope for all measured points along all of the Elysium Mons lava flows	238
5.9(a)	Plot showing h against sinα for all the Alba Patera lava flows	239
(b)	Plot showing h against sinα for (a) all the Elysium Mons lava flows	239
5.10	Plot of thickness against sine of the angle of slope for all thickness measurements made along flow 3 on Alba Patera	240
5.11	Diagram comparing the typical shapes of the boundaries of aa and pahoehoe flows	242
5.12	Plan views of S-type and M-type lava flows	248
5.13	Simplified diagram of a typical aa lava flow front	250
5.14	Diagram showing how flow length was measured	255
5.15	Diagram showing positions of MOLA ground tracks crossing flow 39	257
5.16	Graph of single MOLA ground track traversing a lava flow	258
5.17	Diagram to explain how slope was measured along each lava flow	259
5.18	Diagram to show how measurements were made on each flow	261

Chapter 6:

6.1	Sketch map showing position of Elysium Mons aa flows	264
6.2	Viking image of flow 39 showing surface features	265
6.3	Viking image showing depressions on surface of flow 44	265
6.4	Viking image of flow 17 highlighting central channel	266
6.5	Image, thickness and slope of flow 28	268
6.6(a)	Viking image of flows 35 and 36	270
(b)	Graph of thickness and slope for flow 35	270
6.7	Viking image of flow 24 showing diversion of flow	271
6.8(a)	Viking image of flows 45 and 46	272
(b)	Graph of thickness and slope for flow 46	272

6.9	Diagram showing different modes of lava flow advance	273
6.10	Aerial photograph of the Laki flow field, Iceland	274
6.11	Image, thickness and downstream resistance of flow 21	276
6.12	Diagram explaining lateral resistance of lava flows	277
6.13	Plot of thickness against width for flow 24	277
6.14	Plot of thickness/width against slope for flow 21	278
6.15	Sketch map showing position of Alba Patera aa flows	280
6.16	Viking image of part of the summit of Alba Patera, locating flow 8	282
6.17	Image of Alba Patera showing flow 7	282
6.18	Images of Alba flows that may have been emplaced via channels	283
6.19	Image plus thickness and slope profiles for flow 4	284
6.20	Image related to thickness and slope profiles for flow 1	285
6.21	Plot of flow velocity for flow 8	288
6.22	Sketch map showing the positions of the Elysium Mons pahoehoe flows	297
6.23	Viking image of flow 31, which exhibits surface ridges	299
6.24	Viking image of flow 23 highlighting surface ridges and depressions	299
6.25	Viking image showing pitted appearance of flow 32	300
6.26	Image and thickness profile of flow 26	301
6.27	Image of channel/lava tube at surface of flow 50	302
6.28	Image of proximal end of flow 30, showing potential vent	303
6.29	Viking image of flow 47 indicating possible breakouts	303
6.30	Image of central region of flow 30 where it has been diverted	304
6.31	Surface and underlying surface plot for flow 30	305
6.32	Surface and underlying surface plot for flow 32	306
6.33	Image and thickness and slope plots for flow 22	307
6.34	Image and thickness and slope plots for flow 45	308
6.35	Velocity plots for an aa and a pahoehoe flow on Elysium Mons	310
6.36	Sketch map showing the positions of the Alba Patera aa flows	311
6.37	Image of flows 2 and 3 separated by a topographic high	314
6.38	Thickness and slope profiles related to an image of flow 10	315
6.39(a)	Image and thickness and slope profiles for flow 2 indicating breakouts	316
(b)	Thickness and slope profiles for flow 9 compared to an image of the flow	316
6.40	Plot of velocity for Alba Patera pahoehoe flow 9	318

Chapter7:

7.1	Diagram to show a model for the evolution of Elysium Mons	326
7.2	Diagram to show a model for the eruptions from the Elysium Fossae	329
7.3	MOLA profile along a 'segmented' flow	334
7.4	Stylised sketch of lava flows showing different modes of advance	334

1.0 Introduction

Figure 1.1: This image of Mars was taken by the Wide Field Camera of the Hubble Space Telescope, when Mars was 87 million kilometres from Earth. This image is centred on the volcanic region of Elysium. The white patches are clouds in the Martian atmosphere. **Image Credit:** Steve Lee (University of Colorado), Jim Bell (Cornell University), Mike Wolff (Space Science Institute), and NASA

Mars has fascinated people ever since they began to observe the night sky. The pinkish-red colour of this planet (see Figure 1.1) has lead to it being a symbol of fire, war and malignancy in the mythologies of many civilisations, and the ancient Greeks named it Ares (Mars) after their God of War. Observations by telescope began in the early 17th century, and maps of the planet began to be drawn using telescope observations from the end of the 19th century until well into the 20th century. The 'discovery' by Schiaparelli in 1877 of linear features (which he called 'canali') on the surface of Mars, was built upon by Percival Lowell who began mapping Mars in 1894. Lowell sparked the interest of the general public by calling these features canals, and fuelled speculation that Mars was inhabited by an intelligent race of aliens living in a drought-stricken world.

Although belief in canals within the scientific community was not strong, it was not until the 1960's when images from spacecraft missions to Mars were returned, that the existence of canals on Mars was finally disproved. Images from later missions did, however, show that Mars has undergone extensive geological activity in the past, and also showed dendritic channels that pointed to a warmer, wetter, more Earth-like Mars at some time in the past. Since it is thought that where water was present there was the chance for life to evolve, the existence of these channels was an important discovery

and laid the foundations for further missions to Mars. The Viking mission to Mars in the 1970's was an attempt to search for evidence for life on Mars, but no unequivocal evidence was found. Recent information returned from the two Mars Exploration Rovers currently working on the surface of Mars has shown that in at least one place on the planet, Meridiani Planum (see Figure 1.5), there had probably been a standing body of water present for a substantial period of time in the past (Squyres et al., 2004a). At the other landing site in Gusev crater evidence for the involvement of water in the formation of mineral veins, filled vugs in the rocks, and mineral coatings on the surface of the rocks has also been found (Squyres et al., 2004b). Therefore, public and scientific interest in Mars still remains strong. Not only is there still the real possibility that life may once have flourished on the Red Planet, but Mars also presents an opportunity to explore a world other than the Earth, and compare its features and processes to those on our own planet.

1.1 Spacecraft exploration of Mars

Telescope observations of Mars could not provide a clear view of the surface, therefore all of our current knowledge of surface processes and features on Mars has come from the return of data from spacecraft missions. Some were flyby missions, while some involved spacecraft orbiting the planet and returning data for several years. Others have involved the combined use of orbiters and robotic landers, such as the most recent Mars mission that landed the two Mars Exploration Rovers, Spirit and Odyssey, at two different locations on the planet earlier this year (2004). The Mars Global Surveyor spacecraft collected the new data being used in this thesis, so details of this mission will be given in this section. Also, some data from previous missions will be used in this thesis and so these will be discussed briefly for background information.

1.11 Previous missions

In 1965 Mariner 4 took the first photographs of the Martian surface during a flyby of the planet. The spacecraft passed over the southern highland region of Mars and the 19 images taken revealed highly cratered terrain (Figure 1.2). It had been

expected from telescope observations that Mars would be Earth-like in appearance because polar ice caps, surface colour changes (thought to be vegetation) and clouds had all been seen. It was therefore a surprise to find that the surface of Mars was covered in craters, particularly in the numbers seen in these images and, for a while after the Mariner 4 mission, the surface of Mars was thought to be Moon-like in appearance. A radio-occultation experiment using the spacecraft also permitted measurements of the atmospheric surface pressure to be made. This proved that the atmosphere was much thinner than had been previously expected and early designs for Mars landing probes had to be rethought.

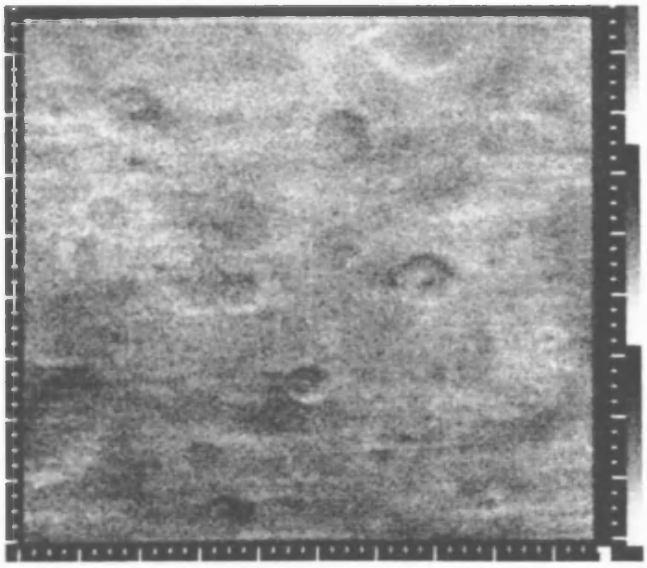

Figure 1.2: This image, taken by the Mariner 4 spacecraft, shows heavily cratered terrain in western Memnonia Fossae (centred at 24 S, 169 W) on Mars. It shows at least twenty craters of various sizes that make this surface resemble that of the Moon. The image was taken from 13,000 km and measures 253 by 225 km. A central peak in the crater right of the centre can be seen. North is towards the top left of the image. (Mariner 4, frame 09D)

Several further Mariner spacecraft were sent to Mars to obtain images of the surface but it was not until Mariner 9 reached the planet, that scientists began to realise that Mars was actually different from the Moon. Mariner 9 went into orbit around Mars in November 1971 but had to wait several weeks for a global dust storm that was shrouding the planet to begin to dissipate before it could begin to photograph the surface (Figure 1.3). The imagery obtained revolutionised our understanding of Mars, showing the great diversity of the surface geology. It was during this mission that all the major geological features were discovered, such as the giant volcano Olympus Mons, the huge 3000km long canyon of Valles Marineris, evidence for catastrophic floods and also dendritic drainage systems that suggested that Mars may have had a

different climate at some time in the past. Enough photographic coverage (over 7000 photographs) of the planet was obtained to produce maps of its entire surface, which was divided into 30 mapping quadrangles. It was also at this time that the relative ages of Martian units were studied using sizes, degradation states and numbers of superposed impact craters (Masursky et al., 1978; Wise, 1979; Moore, 1980). The first formal global geological map was produced by Scott and Carr (1978), in which the three time-stratigraphic units (see section 1.22) were first used, based on the work of Condit (1978). Apart from the imagery, the Mariner 9 mission also provided a wealth of information about the atmosphere and allowed some measurements of the gravity field and topography to be obtained.

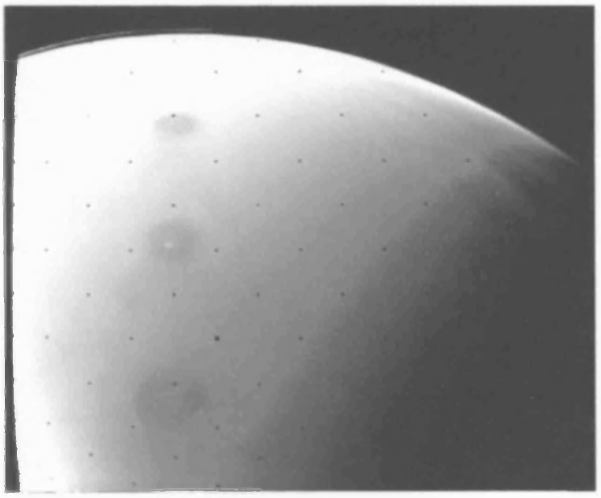

Figure 1.3: As the dust started to settle from the global dust storm encountered by Mariner 9, dark features started to show through the clouds, three of which are shown in this image. Further settling of dust showed these features to be the summits of the large volcanoes of the Tharsis region of Mars. (Mariner 9, image ID: 71-051A-04c)

The next mission of major importance in the study of Mars, was the US Viking mission. The mission built upon the previous data obtained not only by the US Mariner missions but also the Mars missions launched by the USSR, and provided a greater variety, quality and quantity of data. There were two identical Viking spacecraft, each consisting of an orbiter and a lander. The Viking 1 orbiter went into orbit around Mars on 19th June 1976, and deployed the lander on 20th July after a suitable landing site had been found using the orbiter camera. Viking 2 went into orbit on 7th August and its lander touched down on 3rd September. The cameras on the orbiters were of a similar design to those on the Mariner spacecraft but could take pictures at a higher resolution than in previous missions, with the highest resolution being 7.5 metres, although

resolution was usually at a scale of 10 to 100 m/pixel. Overall, the orbiters returned 52,603 images, which covered the entire planet and enabled more detailed mapping to be carried out (Scott et al., 1981a; Scott and Tanaka, 1986; Greeley and Guest, 1987; Tanaka and Scott, 1987). One of the main aims of the Viking mission was to search for evidence of life on Mars, and so included on the landers were 4 experiments, each designed to test for micro-organisms in the Martian soil. No definite evidence for life on Mars was found. Viking also provided a great deal of other data and a summary of the scientific results can be found in the paper by Snyder (1979). The images that were gathered by the Orbiters in this mission are used in the present study as a base upon which to use the new data from MGS.

1.12 Mars Global Surveyor

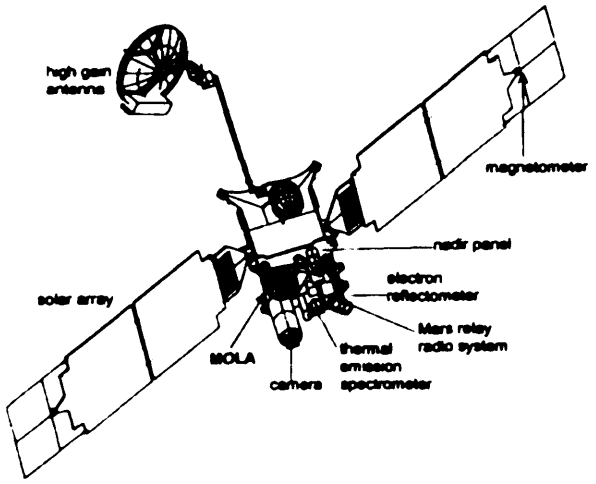

Figure 1.4: This is a diagram of the MGS spacecraft. All the instruments carried onboard MGS have been labelled. Image taken from the paper by Abshire et al. (2000).

The Mars Global Surveyor (MGS) spacecraft has been an important mission in terms of furthering current knowledge of Mars. It reached Mars on 11th September 1997 and after several phases of aerobraking (where the spacecraft is slowed by passing through the Martian atmosphere), a polar, circular orbit was achieved, with a height of ~400 kilometres above the Martian surface. At present (in 2004) it is still collecting data and transmitting it back to Earth. The spacecraft carries four on-board science instruments (see Figure 1.4), a camera, a spectrometer, a laser altimeter and a magnetometer. The Mars Orbiter Camera (MOC) has two modes, wide-angle for global coverage, and narrow-angle with a resolution of 1.4 metres/pixel for smaller areas of the

surface (Malin et al., 1992; 1998). The high-resolution mode is intended to be used to study small-scale surface features. The Mars Orbiter Laser Altimeter (MOLA) has now stopped working, but was used to gather elevation data of the surface and allow global mapping of the topography of the planet (see Figure 1.5) at a level suitable for addressing problems in geology and geophysics (Zuber et al., 1992; Smith et al., 1998). It also characterised the 1.064-micrometer wavelength surface reflectivity of Mars to contribute to analyses of global surface mineralogy and seasonal albedo changes. It is these two instruments that provided much of the new data used in this thesis and therefore the way the instruments collect the data and the types of data available during this study are discussed in Chapter 2. The Thermal Emission Spectrometer (TES) measures infrared radiation and is used to determine the general mineral composition of patches of ground 9 km^2 (Christensen et al., 1992; 1998). Although this information is useful for mapping, the data from this instrument were not used in the present study because the resolution is too coarse for detailed mapping. TES can also be used to scan the atmosphere to provide data that is used in the study of the Martian clouds and weather. The final instrument, the Magnetometer/Electron Reflectometer (MAG/ER) is designed to measure the global magnetic properties of Mars in order to provide an insight into the internal structure of the planet (Acua et al., 1992;1998).

Prior to MGS, the mean atmospheric pressure surface of 6.1 mbars had been used as a reference level for the topography on Mars. MOLA topography is based on a new mean radius of the planet and a new equipotential surface for the areoid (the areoid being a surface of constant gravity potential on Mars). The areoid of the zero level (the reference surface which can be thought of as being similar to sea-level on Earth) is defined to be the surface with the same gravitational potential as the mean equatorial radius (3396 kilometres). Initially the areoid was based on the Goddard Mars potential Model GMM-1 (Smith et al., 1993), which was derived solely from data returned from the Viking and Mariner 9 missions. However, as new data was returned from MGS, the gravity field of Mars could be continuously refined, and a new Martian gravity field solution GMM-2B is now being used as the reference surface from which MOLA elevations can be determined (Lemoine et al., 2001).

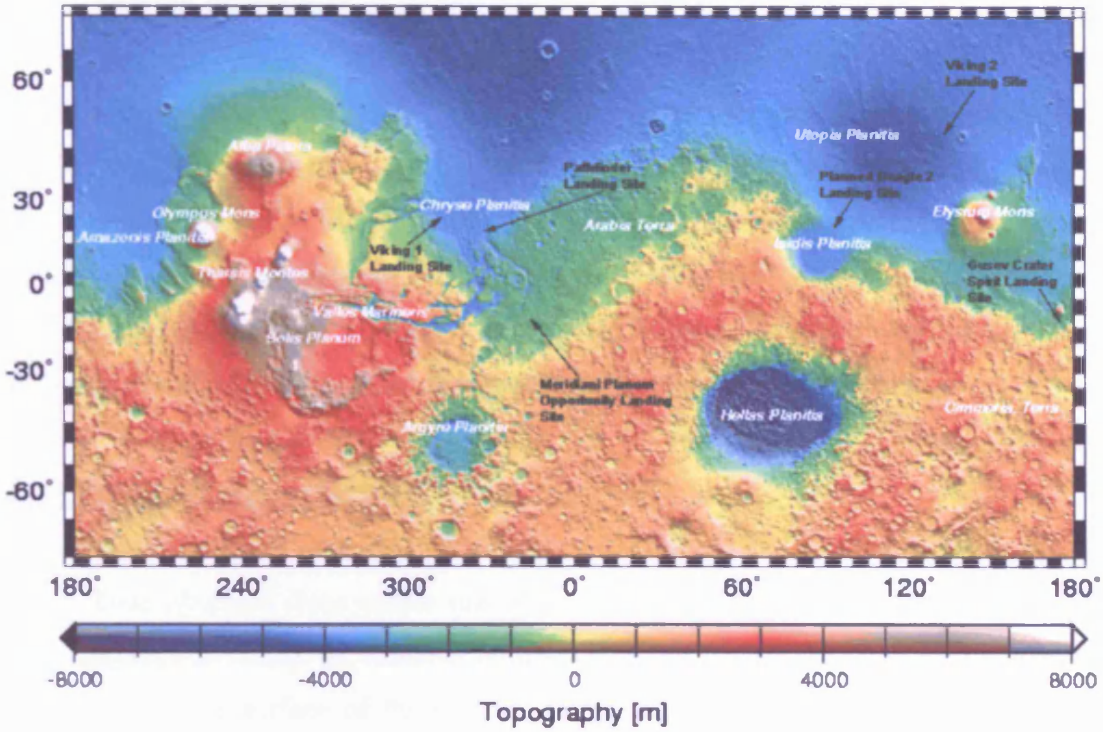

Figure 1.5: Global topographic map of Mars with major surface features labelled. The difference in elevation between the northern and southern hemispheres is clearly shown in this map. Labelled arrows show the positions of landing sites of various Mars missions, including the Mars Exploration Rovers (Spirit and Opportunity). Longitude is given in degrees East. This image has been adapted from one created by the MOLA Science Team.

The MGS mission was designed to be the first in a series of U.S space missions in which the aims are to: understand present and past climate conditions on Mars; to determine whether life, or at least pre-biotic compounds, did develop on Mars; and to identify the types and locations of resources that could utilised by humans in manned missions. MGS has provided data on a global scale regarding the characteristics and dynamics of the magnetosphere, atmosphere, surface and interior, and this information can now be used as a basis for future missions. There were several main aims of the MGS mission. Firstly it was to image the surface morphology of the planet at a scale small enough for individual landforms, features and geological processes to be studied. Secondly it was to determine the composition and map the distribution of surface minerals, and also to determine physical properties of the surface layer using data both from TES and from MOLA. The mission also aimed to map the global topography, and to determine the geodetic figure and the gravitational field. The MAG/ER instrument

was to provide information regarding the magnetic field of Mars and to globally map the magnetic properties of the surface layer. MGS was also intended to show that Mars is still a dynamic planet with ongoing environmental processes, and as such it was to provide information regarding the weather and structure of the atmosphere, as well as monitoring seasonal variations in surface features, the polar caps, dust levels and clouds. The scale of much of the data provided by MGS could be used to study the planet in detail in a way that was not possible beforehand. The aims of the present study for which these new data will be used are discussed in section 1.5.

1.2 Volcanic Processes on Mars

Data obtained from earlier missions, such as Mariner 9 and Viking showed that Mars displays a variety of volcanic features that attest to a long and varied history of volcanism on the surface of the planet. Large volcanic edifices, what appeared to be plains of flood lavas, and long lava flows could all be observed in images returned from these missions (Carr, 1973, 1981; Carr et al., 1977). Images from MGS MOC have indicated that volcanism may have occurred far more recently than previously thought, perhaps less than 10 million years ago (Hartmann and Berman, 2000). The data from MGS has also given rise to the idea that there are still potentially areas of ongoing geothermal activity (Burr et al., 2002). Thus Mars presents an ideal place to study extra-terrestrial volcanic processes.

1.21 Comparative Volcanology

The study of volcanology on Earth involves not only mapping the distribution and type of volcanoes and associated volcanic material world-wide, but also the study of the physical factors governing the type of activity and products found at each location. Another major goal of the study is to work out whether there are patterns to the type of activity and products observed, if these have changed over time, and why this should be. Data collected both in the field and from experiments are used to further understanding of the subject, and to produce theoretical models that can be used to predict the behaviour of volcanic processes. One of the major aims of modelling is to

try to predict how lava flows travel, since this is of high importance for the risk analysis of built-up areas near active volcanoes.

Until information about extra-terrestrial planets was returned from spacecraft missions, the Earth was the only case study available to volcanologists. However, once they were returned, the images of the surfaces of many planets (and moons) clearly showed that volcanism is one of the most important processes that shaped the surfaces of the rocky planets and moons in our solar system. All the planetary bodies are thought to have formed from the same solar nebula, but at varying distances from the Sun. Therefore each planetary body will have a different mass, volume, internal structure, surface temperature and different atmospheric properties, so it would be expected that each would have evolved in a different way. These different factors manifest themselves in the different geomorphologies observed on the surface of each planetary body, and also in the types of volcanic products found. In comparing volcanic features and products found on extra-terrestrial planets with those found on the Earth, our knowledge of the factors affecting volcanism can be tested as scientists try to explain the differences or similarities observed. Also, any new features or processes observed can lead geologists to have a more enlightened view of volcanism on Earth. Thus, it was one of the aims of this study to apply present geological knowledge to the new data returned from MGS, and not only discover new information about features and processes in the areas studied on Mars, but to note if they are different from terrestrial examples and try to explain why this should be.

1.22 General geology and types of volcanoes on Mars

1.22a Crustal Dichotomy and relative ages on Mars

Although the geological history is varied across the whole of Mars, the planet can generally be divided into two areas that are physiographically and geologically different. These areas are the northern lowlands and the southern highlands. The transition zone between the two areas is called the crustal dichotomy and is a large, irregular circle centred at latitude 50°N, longitude 190°W. Most of it is marked by an irregular scarp and clusters of low hills (several hundreds of metres high as measured by

MOLA). The difference in elevations between the northern lowlands and southern highlands can be as much as 4 kilometres (Frey et al., 1998). The origin of the dichotomy is unknown, although several ideas have been put forward, which include subcrustal erosion due to mantle convection (Wise et al., 1979a; McGill and Dimitriou, 1990), a large impact (Wilhelms and Squyres, 1984), and several impact events (Frey and Shultz, 1988). There has also been much debate over the idea that the northern lowlands may have been the site of a large, ancient ocean (Parker et al., 1989, 1993; Head et al, 1998, 1999a,b), and that the dichotomy boundary represents the coastline of this ocean. Whatever their origins, the two regions have distinct characteristics. Most of the highland terrain is ancient, rough, densely cratered rock, thought to have been formed early in the history of the planet when the rate of impacts was high. The northern lowlands are mostly covered with lava flows and younger sediments, and are therefore younger and generally smoother than the southern highlands.

Using stratigraphy it is often possible to determine the relative ages of Martian terrain units by examining the images to determine which rock units overlie others, and which units are modified by features that must have formed after the units were emplaced. Also, it is possible to use crater-counting techniques to establish a relative time scale of rock units and features, since, as a general rule, if impacting rates are constant then older surfaces will exhibit higher numbers of impact craters than younger ones. However, due to the fact that there are no returned rock samples from Mars, it is not possible to assign absolute ages to the rock units. Crater counting can be used to produce possible absolute ages but it is necessary to have a fixed age to base the record on, and also to know the cratering rate subsequent to this fixed point.

By plotting the size of impact craters against the frequency at which craters of each size occur, it is possible to produce a curve that provides information about the population of impacting objects responsible for the cratering record at a particular period of time. Using these crater statistical techniques together with stratigraphy, relative chronologies for Mars indicate that Martian terrain units formed during two major cratering periods: late heavy bombardment and post late heavy bombardment (Hartmann, 1973; Soderblom et al., 1974; Neukum and Wise, 1976; Hartmann, 1978; Scott and Carr, 1978; Neukum and Hiller, 1981; Barlow 1988). Several of these studies differ in both the data sets used and the crater diameters used but the curves produced for the period of late heavy bombardment on Mars are all similar to that for the same

period on the Moon. Therefore, if the period of late heavy bombardment ended at the same time as it did on the Moon (3.8 Gyr ago as found for the returned samples of lunar highland rocks), then surfaces showing the crater size/frequency curve of late heavy bombardment are older than 3.8 Gyr. This provides a basis for the possible absolute age record, since all units that do not show this signature must be younger than 3.8 Gyr. Absolute chronologies for terrain units were then obtained by extrapolation to the lunar cratering chronology, assuming that the impacting populations at the Moon and Mars were the same, and by using a model of the cratering rate through time. However, the chronologies produced by these studies vary widely, with the major differences between each being the estimates of impact cratering rates used. Using these various chronologies, Martian stratigraphic boundaries could then be produced according to the number of craters of a certain diameter that were found to cover an area of a specific size (Hartman, 1973; Soderblom et al., 1974; Mutch et al., 1976; Neukum and Wise, 1976; Condit, 1978; Carr, 1981; Neukum and Hiller, 1981).

Formal definition of the Martian time-stratigraphic units began with the 1:25M-scale geological map produced by Scott and Carr (1978), where Martian geological history was split into three periods; Noachian (the oldest), Hesperian and then Amazonian (the youngest). Mapping at the 1:15M-scale allowed more stratigraphic detail to be discerned and enabled Tanaka (1986) to subdivide the three periods into early, middle and late epochs, as shown in Table 1.1. The Noachian system comprises of the oldest discernible rocks on Mars (Scott and Carr, 1978). These are ancient crustal rocks formed during heavy to waning impact flux. In contrast to this, the impact crater flux declined during the Hesperian period. It records extensive ridged plains volcanism (Early Hesperian epoch), followed by more centralised volcanic activity and widespread resurfacing of the northern plains (Late Hesperian epoch). The youngest units on Mars are included in the Amazonian system, as defined by Scott and Carr (1978), and most of these occur in the northern lowlands.

	Crater diameter and density range			Absolute age range (Gyr)	
Epoch	**2km**	**5km**	**16km**	**HT**	**NW**
Late Amazonian	<40			0.25-0	0.70-0
Middle Amazonian	40-150	<25		0.70-0.25	2.50-0.70
Early Amazonian	150-400	25-67		1.80-0.70	3.55-2.50
Late Hesperian	400-750	67-125		3.10-1.80	3.70-3.55
Early Hesperian	750-1200	125-200	<25	3.50-3.10	3.80-3.70
Late Noachian		200-400	25-100	3.85-3.50	4.30-3.80
Middle Noachian		>400	100-200	3.92-3.85	4.50-4.30
Early Noachian			>200	4.60-3.92	4.60-4.50

Table 1.1 showing the way Martian geological history has been split by Tanaka (1986) into periods and epochs. The data has been taken from Tanaka (1986) and Tanaka et al. (1988), based on the Hartmann-Tanaka (HT) and Neukum-Wise (NW) ages.

Table 1.2 displays the results of some crater counting studies using different absolute age models. The large range of values for some of the features helps to highlight the errors inherent in not only the crater counting process, but also the differences between the different models. Plescia and Saunders (1979) used the chronologies of both Neukum and Wise (1976) and Soderblom (1977) to give absolute ages of some volcanic constructs as shown in Table 1.2, but favoured the values produced using the Soderblom time scale since these were more consistent with thermal models.

Feature	**Hartmann (1973)**	**Soderblom et al. (1974)**	**Neukum and Wise (1976)**	**Neukum and Hiller (I) (1981)**	**Neukum and Hiller (II) (1981)**	**Plescia and Saunders (1979)**
Highlands	3.0 – 4.0	≥ 3.2	4.4	3.8 – 4.2	4.0 – 4.2	-
Ridged Plains	-	2.1 – 1.8	3.9	3.9	2.7 – 4.0	-
Elysium Montes	-	1.5 – 0.8	3.7	3.2 – 3.9	1.7 – 4.0	1.4 – 2.2
Alba Patera	-	-	3.7	0.5 – 3.8	0.3 – 3.7	1.7
Olympus Mons	0.1	≤ 1.7	2.5	0.3 – 3.3	0.3 – 2.0	0.003

Table 1.2: Comparison of Absolute Ages (Gyr) for selected features, taken from Strom et al., 1992.

1.22b The distribution of Martian volcanoes

A map of the major Martian volcanoes and other geologic features is given in Figure 1.6. The largest volcanic province on Mars is called Tharsis, and all of the volcanoes in this area are situated on either the crest of, or on the northwestern side of, a large rise called the Tharsis Bulge. The Tharsis Bulge is a region of major doming and uplift, which extends 4000 kilometres from north to south, 3000 kilometres from east to west, and has a mean elevation of between 10 and 11 kilometres above Mars Mean Datum (as measured by MOLA). The tectonic stresses occurring during the growth of the Tharsis Bulge are likely to have been a key element in the formation of Valles Marineris (see Figure 1.6), which is a canyon system just south of the equator that extends for 4000 kilometres. Although termed 'bulge' the Tharsis region is actually more like a broad, gentle rise, with slopes of between 0.2 and 0.4 degrees on the northern side, and values of around half this on the southern side. The most prominent group of volcanoes in this region consists of Arsia, Pavonis and Ascraeus Mons, collectively known as the Tharsis Montes. They are aligned in a southwest-northeast direction along the crest of the Bulge, and probably formed along a major fracture zone, since major fractures continue the same trend even beyond the Tharsis volcanic province (Cattermole, 1996). Some smaller shields and also some tholi (volcanic domes) occur near these three major volcanoes (see Figure 1.6), some continuing along the same trend as the major Tharsis Montes. Olympus Mons, the highest and youngest of the major Martian volcanoes, occurs to the northwest of the Tharsis Montes. At the edge of the Tharsis Bulge, north of the Tharsis Montes, lies Alba Patera, which is a low relief shield that covers an extensive area, and is associated with a large, circumferential fracture system.

A second, yet smaller volcanic rise occurs in the Elysium region of Mars, where another complex of volcanoes occurs. These volcanoes are Hecates Tholus, Elysium Mons and Albor Tholus. Hecates and Albor Tholi, as the names suggest, are both dome-type volcanoes that appear to have been heavily buried and embayed by younger lavas, but Elysium Mons is a shield volcano. There is much evidence for volcano/volatile activity in this region, particularly at Hecates Tholus where a late-stage pyroclastic fall deposit has been identified (Mouginis-Mark et al., 1982), and to the north west of Elysium Mons where many, potentially fluvial, channels are observed (Baker, 1982; Mouginis-Mark et al., 1984; Mouginis-Mark, 1985; MacKinnon and

Tanaka, 1989). These volcanoes have been mapped as part of this study, so the work carried out in

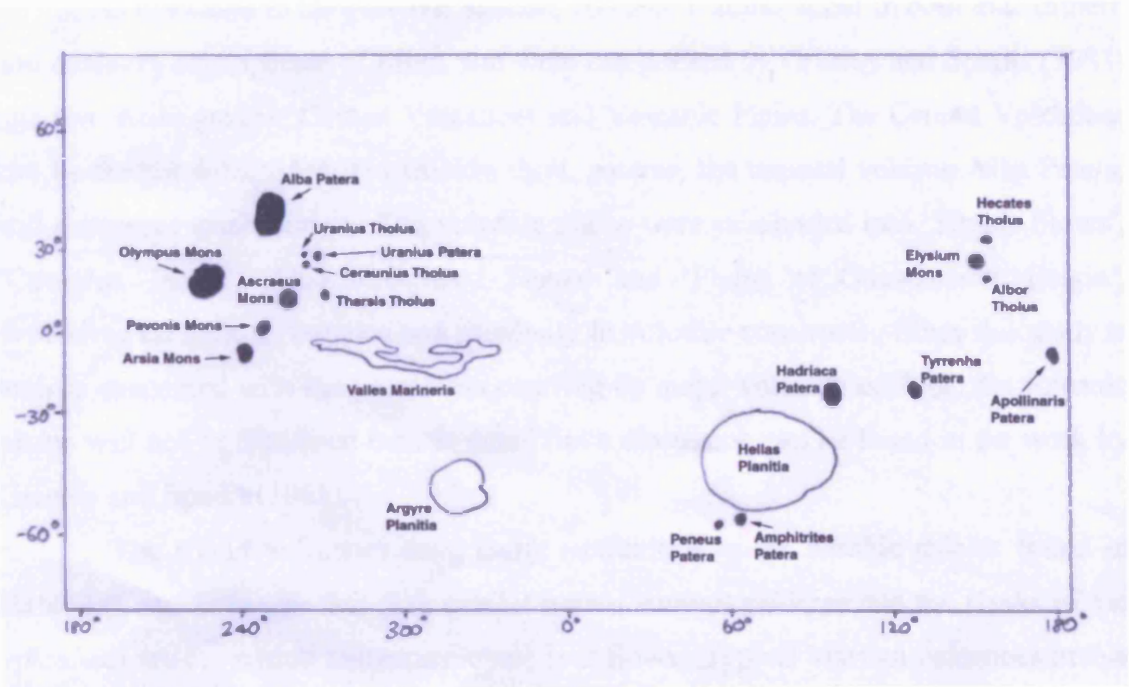

Figure 1.6: Sketch map of the major geological features on Mars. Dark areas are volcanic constructs, unfilled circular areas are impact basins, and the outline of the canyon system Valles Marineris is also shown.

previous studies of this area is discussed in section 1.3 to provide the reader with background information. To the south east of the Elysium Montes, is Apollinaris Patera, which occurs just to the north of the dichotomy boundary. This volcano is a broad shield that terminates in a scarp on all sides except the south. The southern flank of the volcano is covered with a fan of material that appears to have flowed from the edge of the caldera. The fan is cut by many channels but it is unclear whether the deposit is composed of lavas or pyroclastic materials (Thornhill et al., 1993).

In the southern hemisphere of Mars is the Hellas impact basin (see Figure 1.6), which is thought to have been formed from a giant meteorite impact, has a rim diameter of ~2300 kilometres, and is the dominant surface feature of the southern highlands. The major volcanic centres that occur in the southern highlands are situated around this basin. At least two of these volcanoes, Hadriaca and Tyrrhena Paterae, are thought to have formed from a mixture of lava and ash (Greeley and Spudis, 1981; Cattermole, 1996).

1.22c Shields, Domes and Paterae

As discussed in the previous section, volcanic features occur in both the northern and southern hemispheres of Mars, and were categorised by Greeley and Spudis (1981) into two main groups: Central Volcanoes and Volcanic Plains. The Central Volcanoes can be further subdivided into shields, tholi, paterae, the unusual volcano Alba Patera, and numerous small domes. The volcanic plains were subdivided into 'Simple Flows', 'Complex Flows', 'Undifferentiated Flows' and 'Plains of Questionable Origin', depending on their appearance and proximity to volcanic constructs. Since this study is mainly concerned with the processes occurring on major volcanic edifices, the volcanic plains will not be discussed here in detail but a discussion can be found in the work by Greeley and Spudis (1981).

The shield volcanoes have many similarities to the basaltic shields found in Hawaii (Carr, 1973), in that they exhibit nested summit calderae and the flanks of the volcanoes are covered in numerous lobate lava flows. Typical Martian volcanoes in this group are the Tharsis Montes (Arsia Mons, Ascraeus Mons and Pavonis Mons) and Olympus Mons (see Figure 1.6). One of the major differences between terrestrial shields and Martian ones is the fact that the Martian volcanoes are far larger in size than terrestrial ones. As an example, the summit of Olympus Mons reaches 23 kilometres above the surrounding plains (as measured with MOLA), and has a base which is in excess of 600 kilometres in diameter (Wu et al., 1984). This has been attributed mainly to the lack of plate tectonics on Mars, which allows a volcano to grow over the same hotspot for millions of years without being transported away on a moving plate as is thought to occur on Earth. It may also be partly due to the fact such large volcanoes would not be supported by the crust on Earth even if they had been able to form, thus implying that the Martian lithosphere must be thicker than on Earth (Soloman and Head, 1982).

The tholi volcanoes are smaller both in height and diameter than the shield volcanoes. They are dome shaped with steep lower flanks and shallower upper flanks and summit areas. Often the lower flanks of these volcanoes have been buried by lava flows of the surrounding plains or volcanoes (as in the case of Albor Tholus as discussed in Chapter 4 of this study), and some of the volcanoes in this group appear to have undergone explosive activity. One example of this is the volcano Hecates Tholus, which is discussed in section 1.3 and also in Chapter 4. Many small domes have also

been observed all over Mars. Studies carried out using the Viking images showed that there are thousands of sub-kilometre sized hills within the northern plains (Frey et al., 1979; Frey and Jarosewich, 1982), which may be volcanic in origin. Also, Plescia (1981) and Tanaka and Davis (1988) identified several breached cones in Tempe Terra and Syria Planum, which they found to be similar in appearance to terrestrial cinder cones formed by pyroclastic activity, and some additionally having produced lava flows. More recently MOC images of Isidis Planitia have shown small, sub-kilometre sized hills also thought to be cinder cones (Fagents et al., 2002; Greeley and Fagents, 2001) (see Figure 1.7).

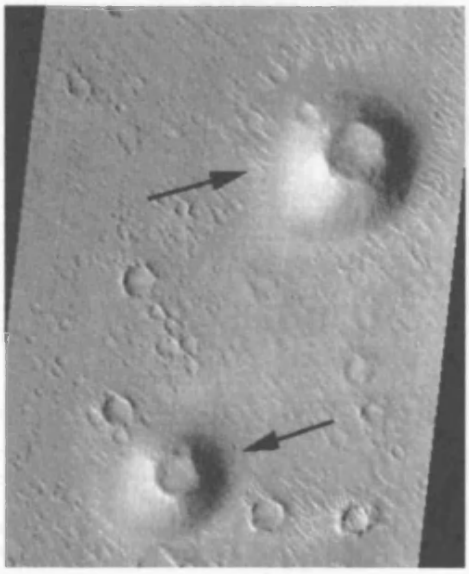

Figure 1.7: Part of MOC image AB1-03405 showing two cones (arrowed) in western Isidis Planitia. These may be features similar to terrestrial volcanic cinder cones and measurements have shown that the summits of these features reach several tens of metres above the surrounding surface (Greeley and Fagents, 2001). This area measures 2.6 kilometres across the middle of the image, north is towards the top and the sun direction is from the bottom left of the image.

The third group of volcanoes, the paterae, are shield-like in appearance but with low relief and have irregular summit craters. There are two sub-groups of paterae: highland and lowland. The lowland paterae are northern hemisphere lava shields. The highland paterae, found in the southern hemisphere, are also low-relief shields but the flanks are often covered in numerous radial channels (Plescia and Saunders, 1979). West (1974) suggested that these volcanoes were probably composed of ash flow deposits rather than lava flows due to the shape of their topographic profiles. This later prompted Greeley and Spudis (1981) and Greeley and Crown (1990) to carry out more detailed mapping of Tyrrhena Patera (a typical example of this type of volcano), (see Figure 1.8). Their conclusion agreed with that of West (1974) in that, with the exception of some lava flows near the summit, the flanks of this volcano are likely to be composed of unconsolidated materials that were probably ash deposits. The highland paterae are

therefore believed to be mixed lava and pyroclast edifices. Since these volcanoes are found in the oldest areas of Mars, it follows that they may represent early central volcanism and that as Mars evolved, volcanism became more effusive to produce the Hawaiian-style type of volcanoes observed in the northern lowlands (Francis and Wood, 1982; Cattermole, 1990).

Figure 1.8: Viking Orbiter image 87A14 showing the volcano Tyrrhena Patera. This volcano is probably composed of ash flow deposits (West, 1974), and the numerous channels on the flanks indicate the easily erodible nature of the flank materials. The image represents an area 200 kilometres across and the direction of the sunlight is from the left-hand side of the image.

1.22d Alba Patera

Alba Patera is a volcano that is located in the northern part of the Tharsis region of Mars (see Figure 1.6). It has been the focus of much study (see Carr et al., 1977; Scott et al., 1981a,b; Cattermole, 1987 & 1990; Mouginis-Mark et al., 1988; and Lopes and Kilburn, 1990) over the past several decades, because it appears to be a unique landform. It is because it is unique that Greeley and Spudis (1981) gave it a separate grouping during their categorisation of volcanic features on Mars. As several of the lava flows on the summit of this volcano are the focus of study in Chapters 5 and 6, the form and history of the volcano will be discussed in this section.

therefore believed to be mixed lava and pyroclast edifices. Since these volcanoes are found in the oldest areas of Mars, it follows that they may represent early central volcanism and that as Mars evolved, volcanism became more effusive to produce the Hawaiian-style type of volcanoes observed in the northern lowlands (Francis and Wood, 1982; Cattermole, 1990).

Figure 1.8: Viking Orbiter image 87A14 showing the volcano Tyrrhena Patera. This volcano is probably composed of ash flow deposits (West, 1974), and the numerous channels on the flanks indicate the easily erodible nature of the flank materials. The image represents an area 200 kilometres across and the direction of the sunlight is from the left-hand side of the image.

1.22d Alba Patera

Alba Patera is a volcano that is located in the northern part of the Tharsis region of Mars (see Figure 1.6). It has been the focus of much study (see Carr et al., 1977; Scott et al., 1981a,b; Cattermole, 1987 & 1990; Mouginis-Mark et al., 1988; and Lopes and Kilburn, 1990) over the past several decades, because it appears to be a unique landform. It is because it is unique that Greeley and Spudis (1981) gave it a separate grouping during their categorisation of volcanic features on Mars. As several of the lava flows on the summit of this volcano are the focus of study in Chapters 5 and 6, the form and history of the volcano will be discussed in this section.

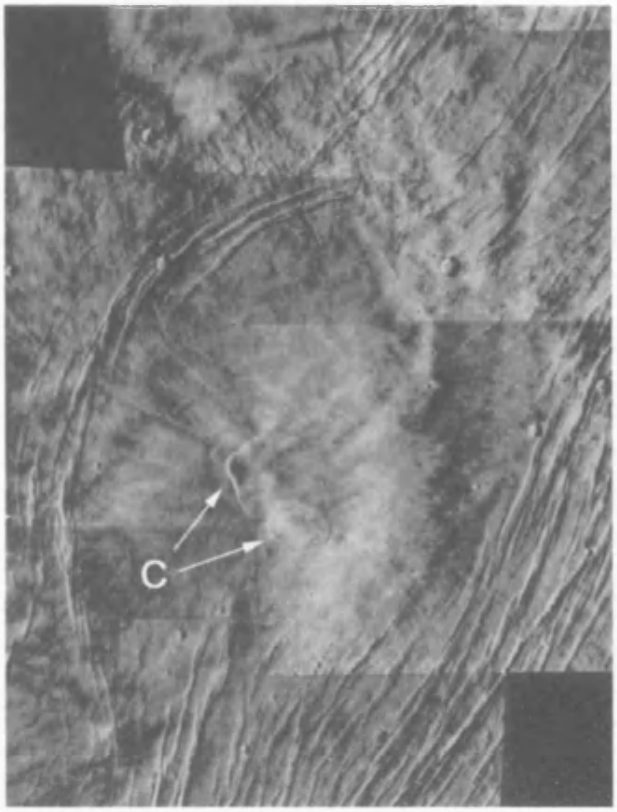

Figure 1.9: Viking photomosaic (frames 783A12 to 17) of the summit of Alba Patera showing the double caldera complex (C) and zone of ring fractures. The total image is ~550 kilometres across and is illuminated from the lower right.

Alba Patera is a broad, low relief structure, which has a diameter of 2700 kilometres, and has a topographic profile similar in shape to an upturned saucer. The summit rises to a maximum of 6500 metres above the Mars Mean Datum (as measured by MOLA), and lies at the centre of an oval ring-fracture zone. It is the site of a double caldera complex (see Figure 1.9) that is thought to have formed as a direct result of magma supply to the flanks of the volcano (Cattermole, 1990). Using MOLA it was determined that the summit of the volcano has low slope values of around 0.6°, and that this value remains the same for the southern and eastern outer flank areas. Flank slope values are found to increase to around 1.7° in some places on the outer northern and western flanks, outside of the main ring fracture zone. The flanks of the volcano are covered by many individual lava flows and lava flow complexes, many of which have flowed great distances (100's of kilometres) even over the shallower slopes, and this led Cattermole (1989) to infer low viscosity and high volume for the individual flows. The type and form of the lava flows on the volcano have been the subject of studies carried out by Carr et al., (1977), and also Cattermole (1989).

It is generally accepted that the growth of Alba Patera began during the early period of lava flooding, before the more localised central vent eruptions that formed the

Tharsis and Elysium Montes began (Plescia and Saunders, 1979; Scott and Tanaka, 1980, 1986; Cattermole, 1989). Timescales are subject to a great deal of uncertainty, since the works of Neukum and Wise (1976) and Neukum and Hiller (1981), do not agree with the timescale worked out by Soderblom (1977) as discussed in section 1.22a. However, they give a range for the peak of activity on Alba Patera to have occurred between 3600 +/- 40 million years and 1725 +/- 123 million years ago. Stratigraphic relations observed on the images show that the earliest recognisable Alba units predate those of the Tharsis Montes, while the youngest ones postdate some of the rocks on Arsia Mons (Scott and Tanaka, 1980). Therefore, the total eruptive life of Alba Patera must have been at least 1.5×10^9 years (Neukum and Wise, 1976), and possibly as much as 2.8×10^9 years (Hartmann, 1978).

The eruptive activity at Alba Patera has therefore been long and has varied over time. The area has been mapped by Scott and Tanaka (1980, 1986), who established that there were three main phases of patera growth, and also several large flow-fields that may have been related to major fractures on the flanks on the volcano. This was later confirmed in detailed mapping (see Figure 1.10) carried out by Cattermole (1987, 1990). The first phase in the development of the volcano involved the emplacement of fissure-fed flood lavas of Lower Hesperian age (Scott and Tanaka, 1986), which can now only be observed to occupy distal locations around the volcano. Also around this time, the extrusion of high-volume sheet and tube-fed lavas occurred mainly from fissures located at the edge of the rising dome of the volcano. After this, volcanism became more centralised, with sheet flows and tube-fed lavas being erupted at high effusion rates from linear vents on or near the edge of the present summit. These complex flow fields represent the majority of patera-building activity. Subsequent to this in the Amazonian era, volcanism became restricted to the extrusion of shorter, narrow flows from the two summit calderas. In the late stages of the eruptive history of the volcano, more viscous materials were erupted from NNE-SSW trending fissures, which formed en echelon spatter ridges on the flanks.

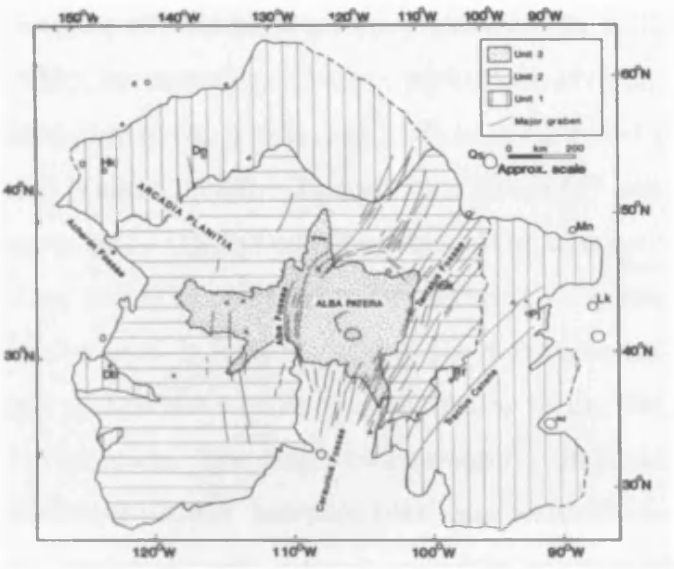

Figure 1.10: General geological map of Alba Patera showing the three major volcanic units (unit 3 being the youngest). The figure is taken from Cattermole (1990).

Interestingly, one of the characteristics of Alba Patera is the presence of dendritic channel networks that occur on the flanks of the volcano, mainly to the north of the summit. They have incised into relatively smooth-surfaced units which show a paucity of obvious flow lobes, and which appear to separate the two main stages of the growth of the volcano (Cattermole, 1996). An analysis of images and thermal inertia data for the volcano led Mouginis-Mark et al. (1988), to conclude that the channels were fluvial in origin. They also concluded that they had been formed by sapping caused by the release of non-juvenile water, the source of which was from within relatively unconsolidated deposits on the flanks of the volcano. They suggested that the unconsolidated materials were of pyroclastic origin, and were most likely to have been emplaced as long run-out pyroclastic flows. Mouginis-Mark et al. (1988) suggested that the pyroclastics were emplaced after the eruption of the sheet and tube-fed lavas on the lower flanks and that the ash deposit contained water-ice. The emplacement of the high-volume summit flows over the ash is suggested to have released melt water from the ice within the ash and carved the channels. They also suggested that the existence of pyroclastics within the lava pile may also explain the low relief of the volcano, and the form and distribution of the circumferential fractures.

1.22e Evolution and growth of Martian volcanoes.

It is difficult to determine the internal structure of the Martian volcanoes because of the lack of appropriate field data. Terrestrial studies to determine the internal

structure of volcanoes on Earth use analysis of field data such as seismic data (Ryan, 1988), the mapping of vent distributions (Porter, 1972; Nakamura, 1977; Munro and Mouginis-Mark, 1990), and analysis of exposed dyke swarms (Walker, 1987; Knight and Walker, 1988). This enables laboratory models of volcanic edifices (Fiske and Jackson, 1972), and numerical modelling of eruptive episodes (Wilson and Head, 1988; Head and Wilson, 1989) to be produced. The models produced using these techniques can be used to infer something about the internal workings of the Martian volcanoes, and comparisons between observations in the images, and field observations on Earth can be made. The major observation for the large Martian volcanoes is that they have relatively simple morphologies compared to terrestrial volcanoes. These simple morphologies seem to be controlled by deep-seated regional tectonic forces (Mouginis-Mark et al., 1992), and are rarely influenced by the tectonic forces imposed by other volcanic edifices, unlike volcanic centres on Earth (Fiske and Jackson, 1972). One area where Martian volcanoes do appear to influence the tectonic setting of others is in Tharsis where mapping of vent distribution has revealed incipient rift zones trending roughly perpendicular to the major NE-SW trend of the Tharsis ridge volcanoes (Carr et al., 1977; Crumpler and Aubele, 1978).

As mentioned earlier, many of the large shield volcanoes have nested summit calderas. This implies that the volcanoes have undergone multiple collapse events, inferred by Mouginis-Mark (1981) to have been the result of large-volume flank eruptions partially evacuating each magma chamber. Work by Mouginis-Mark and Mathews (1987) on the rim heights of the caldera of Olympus Mons showed that dike intrusions appeared to have played a major role in the growth of the volcano, in a similar way to some volcanoes on Earth (Walker, 1987, 1988). More recent work by Scott and Wilson (2000) showed that the nested caldera of Ascraeus Mons shows evidence for an alternating pattern of variations over time in both position and rate for the magma supply from the mantle, and also in the distribution of stresses within the volcanic edifice.

The large size of many of the lava flows associated with volcanic edifices (Carr, 1973; Carr et al., 1977; Cattermole, 1987), has led to the idea that the sizes of the Martian magma reservoirs could be much larger than terrestrial ones (Mouginis-Mark et al, 1992; Mouginis-Mark and Rowland, 2001). Also, the spacing of the volcanoes may be related to the size of the volcanoes as suggested by Whitford-Stark (1982) in a study of Tharsis. Whitford-Stark suggested that in the case of smaller groups of volcanoes,

they shared a magma source and thus the volcanoes could not reach such large scales. If the larger volcanoes do not share a magma source they must be spaced far enough apart to achieve this. These observations could have important implications in the mapping section of this thesis, given the new findings concerning the growth of Elysium Mons (see Chapter 4).

1.3 Geology of Elysium

The Elysium Montes represent the second largest volcanic province on Mars. Although the region is older than Tharsis, it still exhibits many well-preserved lava flows. It is because of this, and the fact that there is substantial evidence for volcano/volatile interactions here (see section 1.34), that the volcanoes in this region have been the subject of much study in the past. The Elysium Montes and surrounding region therefore present an interesting area to analyse with the data from MGS in the present study, both in terms of studying individual features such as lava flows, and also in the production of a geological map of the area.

1.31 Geological Setting of the Elysium Montes

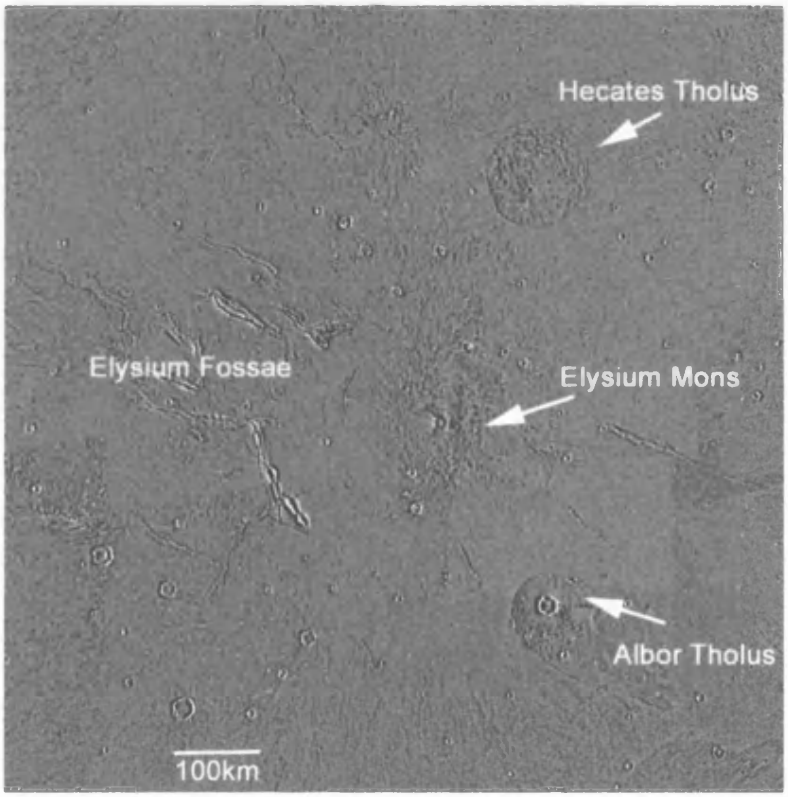

Figure 1.11: Composite of Viking images showing the Elysium Montes, the Elysium Fossae and the surrounding area.

The Elysium Montes and the area surrounding them are shown in Figure 1.11. It is centred at 25°N, 212°W (148°E), and consists of a broad dome topped by three volcanic constructs; Hecates Tholus, Elysium Mons and Albor Tholus. Early mapping of the area was carried out using Mariner 9 images (Scott and Allingham, 1976; Malin, 1977), and then later using images from the Viking mission (Greeley and Guest, 1987; Mouginis-Mark et al., 1984; Tanaka et al., 1992). A general morphologic map of surface units in the region is shown in Figure 1.12, in order to highlight the major features and surface morphologies in this area.

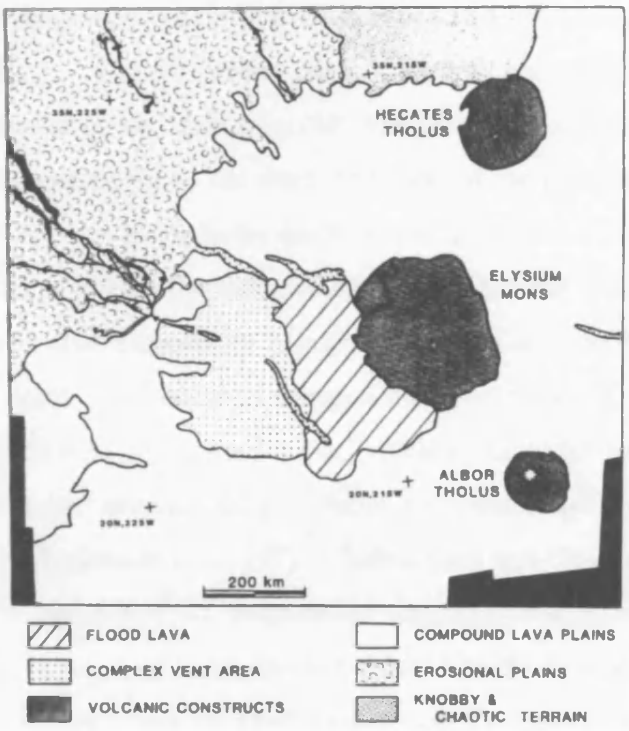

Figure 1.12: General geological map of the Elysium Montes and surrounding area (taken from the study by Mouginis-Mark et al., 1984). The black linear features marked with arrows are channels (suggested to be fluvial in origin), with the arrows marking the direction of flow. The features with hatched outlines are some of the Elysium Fossae.

The three major volcanic constructs are surrounded by lava flow fields, termed compound lava plains by Mouginis-Mark et al. (1984) (see Figure 1.12), and form the Ael_1 (volcanic plains materials) member of Greeley and Guest (1987) and the Ael_2 member (lava flows of latest widespread activity in the area) of Tanaka et al. (1992). These appear to surround and embay both Hecates Tholus and Albor Tholus, and can be seen to extend to the northeast, past the eastern flank of Hecates Tholus. These have been attributed to more than one phase of volcanism by Mouginis-Mark et al. (1984), who noted that much of the plains material has a strong affinity to the Elysium Mons volcano, while Tanaka et al. (1992), attributed it to vent eruptions later in the evolution

of Elysium Mons. An area to the south and southwest of Elysium Mons, adjacent to the volcanic construct, has been mapped by all workers as a younger flood lava unit. In places it can be seen to embay parts of the Elysium Mons construct (Tanaka et al., 1992). Further west still is an area of rough hummocky flows with many pit craters (Mouginis-Mark and Brown, 1981) that were the source for channels and sinuous rilles. This was termed the 'complex vent area' by Mouginis-Mark et al. (1984) (see Figure 1.12), who proposed that this was the site of a failed volcanic construct, perhaps due to high regional slopes. Greeley and Guest (1987) did not map this area separately from their member 1, and Tanaka et al. (1992) termed it Helr (rugged member) and interpreted it to be lava flows and eruptive vents that have been disrupted by steep topography, groundwater discharge and fracturing.

The volcanoes are all located on a regional system of WNW-ENE trending fractures and graben called the Elysium Fossae (refer to Figure 1.11). Most of these Fossae occur to the north and west of the Elysium Mons volcano, and can be observed to evolve towards the northwest into a series of branching channels. Most of the Fossae occur within the volcanic flow units, but the channels that lead from them occur within the area mapped by Mouginis-Mark et al. (1984) as erosional plains. This 'erosional plains material' was mapped by Greeley and Guest (1987) as their member 3 (Ael_3) which is interpreted to be volcanic material that has been extensively modified by fluvial, aeolian and periglacial processes, and is mapped as the 'coarse member' Aelc by Tanaka et al. (1992). Christiansen and Greeley (1981) proposed that this plains unit is composed of mega-lahar deposits, but Tanaka et al. (1992), suggested it was composed of easily eroded volcaniclastic deposits, not necessarily from lahars. It was also proposed by Christiansen and Greeley (1981) that many of the fossae were the source of intermittent parasitic eruptions, both of lava and of water or a mud/water mixture.

To the northwest of Hecates Tholus is an escarpment that marks the transition from the well-preserved lava flow fields in the south to an area of mesas and collapsed terrain. This collapsed terrain is called 'chaotic terrain' and was first described by Sharp (1973) (see Chapter 4), who interpreted ground collapse like this to have occurred due to the escape of melted ground-ice. Mouginis-Mark et al. (1984) found that there was no evidence for lava flows extending northward beyond or over the escarpment and concluded that collapse must have occurred after the emplacement of the lava flows.

The presence of chaotic terrain is often used as an indication of volatile presence on Mars.

1.32 Geological History of Elysium

Results from crater counting studies have been used in previous studies to give relative ages for the three volcanic constructs. Crater counting carried out by Plescia and Saunders (1979) indicates that the summit of Elysium Mons is older than the summit of Hecates Tholus, and that both volcanoes are older than Albor Tholus. However, in their map of the Elysium region of Mars, Tanaka et al. (1992) take Hecates Tholus to be the oldest construct, followed by Albor Tholus and then Elysium Mons. Although there is therefore some disagreement about relative ages, it is generally accepted that lavas from Elysium Mons buried and embayed the lower flanks of both Hecates Tholus and Albor Tholus. Plescia and Saunders (1979) and Neukum and Hiller (1981) both found evidence for re-surfacing events on Hecates Tholus, owing to a paucity of impact craters on the summit (see section 1.33), and this may represent some of the more recent activity in the region. Neukum and Hiller (1981) found evidence, using crater counting, that flank activity at Elysium Mons occurred a substantial amount of time after the summit was constructed, and that these lavas were emplaced over a time that spanned the period of formation of the knobby and chaotic terrain to the northwest of the area. This would appear to agree with the conclusions drawn by Tanaka et al. (1992), that flank eruptions occurred after the building of the main Elysium Mons summit region.

Mouginis-Mark et al. (1984) studied the relationship between volcanic and tectonic events in the region. Their work shows that most of the graben and fractures, both radial to and circumferential to the Elysium Mons edifice, were formed after the emplacement of the lava flow fields. However, image analysis carried out in the present study shows that the flood lavas to the west of the volcano (see Figure 12) have buried some of the graben or embayed the edges of some of these features, and the lavas also exhibit post-emplacement fracturing. This indicates that the emplacement of this flood lava unit occurred during or towards the end of the period of tectonic activity rather than prior to it. Activity to the northwest and west of Elysium Mons appears to have occurred later in the evolution of the volcanic field (Christiansen and Ryan, 1985),

when the Elysium Fossae were utilised as the source vents for volcanic flows as well as volcanic debris flows.

1.33 Characteristics of the Volcanoes

Elysium Mons is the largest of the three volcanic constructs shown in Figure 1.11, and the centre of the volcano lies at around 24°N, 214°W (146°E). In the past it has been proposed (Malin, 1977) that Elysium Mons was a composite volcano and could be compared to the terrestrial African composite volcano Emi Koussi. However, later measurements of the flank slopes (prior to MOLA) showed that they were not steep enough for Elysium Mons to be a composite volcano, and were more similar to the Hawaiian-type shields of Tharsis (Cattermole, 1996). Slope data produced in the present study using MOLA data also confirm this. Elysium Mons has a single, shallow (1-3 kilometres deep as measured by MOLA), central caldera, measuring ~13 kilometres in diameter that some have suggested was formed from a single collapse event (Mouginis-Mark and Rowland, 2001). Others such as McBride (1992) suggest that the slumping found in the caldera walls represents several collapse events. There are several channels leading from the edge of the caldera, thought to be lava channels (Mouginis-Mark and Rowland, 2001), and a series of chains of pits on the summit flanks to the west of the caldera. There are several examples in the Viking images of the summit showing short, narrow, sometimes levéed lava flows, otherwise the general appearance of the upper flanks is hummocky and lacking in clearly defined lava flows. Further down the flanks the hummocky appearance changes and more ridges are visible, some of which are composed of several aligned mounds, which may well be the surface expression of lava tubes (as observed at Alba Patera by Carr et al., 1977). Individual, long lava flows tens of kilometres in length can also be seen.

To the southeast of Elysium Mons lies the smaller volcano Albor Tholus, the remaining unburied flanks of which have a diameter of 160 kilometres x 150 kilometres. It has a larger caldera than that of Elysium Mons, measuring 35 kilometres by 30 kilometres, which may attest to the volcano having been larger in the past prior to burial of the flanks by lavas from other volcanic centres. The poor resolution (250 metres/pixel) in the Viking images of this volcano (as compared to that for the other two volcanoes) means that no lava flows are visible on the flanks of the volcano. However, Mouginis-Mark et al. (1984) propose that since there are no channels visible on the

flanks, it was probably formed by mostly effusive activity (Reimers and Komar, 1979; Mouginis-Mark et al., 1982). The only other features of interest here are the two graben that occur on the southwest flank of the volcano. They are generally circumferential to the volcano but the ends of each have been embayed by the compound lavas from Elysium Mons.

The last volcano to be described is Hecates Tholus, the most northerly of the three volcanoes in this area. Hecates Tholus reaches 6 kilometres (as measured by MOLA) above the surrounding plains, and has a diameter of 160 kilometres by 175 kilometres. The summit of the volcano is the site of a nested caldera complex measuring 11.3 kilometres by 9.1 kilometres. The most obvious characteristic of this volcano is that there are no visible lava flows on its flanks. Instead, the flanks are covered with many channels, the origins of which have been the subject of much debate. Reimers and Komar (1979) suggested that the channels were formed by pyroclastic flows, whereas Mouginis-Mark et al. (1982) showed that they could have been formed by fluvial activity. Plescia and Saunders (1979) showed that variations in numbers of superposed impact craters implied several resurfacing episodes on the flanks, and also noted that the western part of the summit showed a relative paucity of small impact craters. It was later suggested by Mouginis-Mark et al. (1982) that the western area of the summit is mantled by a relatively young pyroclastic fall deposit ~100 metres thick. Thus Hecates Tholus probably formed from a mixture of pyroclastic and effusive activity.

1.34 The Presence of Volatiles in Elysium

It is possible to infer the presence of surface water or near-surface ice by studying the surface geology of an area and trying to identify features that may have been influenced by the presence of water and/or ice during formation. Such features include: channels (Sharp and Malin, 1975; Baker, 1982), chaotic and fretted terrain (Sharp 1973a,b; Squyres, 1978; Lucchitta, 1984), debris flows and softened terrain (Carr and Schaber, 1977; Squyres, 1978; Lucchitta, 1984; Squyres and Carr, 1986), ephemeral lakes (Squyres, 1989; De Hon, 1991), ancient shorelines (Baker et al., 1991), glacial landforms (Kargel and Strom, 1990), thermokarst and periglacial features (Gatto and Anderson, 1975; Carr and Schaber, 1977), and volcano-ice interactions (Allen,

1979a). The occurrence of many of these features in one area would therefore suggest that there is/was a large amount of volatiles present under the surface in that area.

Numerous landforms that indicate the presence of water/ice have been identified in previous studies of Elysium by various groups, including the existence of chaotic terrain (Carr and Schaber, 1977), probable megalahar (mudflow) deposits (Christiansen and Greeley, 1981), outflow channels with multiple levels and streamlined islands (Baker, 1982), diverse impact crater morphologies (Hale, 1983), and a pyroclastic fall deposit on the summit of Hecates Tholus (Mouginis-Mark et al., 1982). In addition to this, Mouginis-Mark et al. (1984) and Mouginis-Mark (1985) found several other features within the Elysium region to support the hypothesis that there was extensive interaction between volcanic materials and a pre-existing water table or layer of ground-ice. These included meltwater deposits, possible pseudocraters, collapse features within troughs, and outflow channels.

It has therefore been suggested that there may be a layer of sub-surface ice underlying the Elysium Montes volcanic province (Mouginis-Mark, 1985; Cave, 1993). Volcano/ground-ice interactions are important because they provide a potential mechanism for the release of water to the surface and thus the production of the channels and other fluvial features observed in this area (and elsewhere on Mars). The presence of ground-ice/volatiles may also influence the type of volcanism in the area, since their interaction with magma/lava will produce explosive activity (Colgate and Sigurgeirsson, 1973; Allen, 1979), resulting in the deposition of pyroclastic materials. Thus the recognition and study of both landforms and resultant volcanic products from such interactions in Elysium would provide a useful basis for studies elsewhere on Mars where it is thought there may be a high level of sub-surface ice. Mapping and characterisation of both volcanic landforms and individual lava flows will be carried out in this study in an attempt to fulfil this aim.

1.4 Lava flow studies

The study of extra-terrestrial lava poses problems, not just because of the lack of rock samples to provide compositional data, but also because the flows are generally ancient. Any information regarding the physical properties of the lava or flow emplacement must be determined from the present day morphology of the flow. Often

the flows are heavily weathered, and source vents and the upper reaches of the flow can be hard to identify because they have been covered over by younger materials. On Earth it is possible to obtain relatively accurate data 'in-situ' regarding physical properties of active lava flows such as temperature, viscosity and gas content, and also to measure the changing morphology and dimensions of a flow as it develops over time. This allows geologists to determine how the rheology of a lava flow affects the morphology of the landforms it produces, and which physical properties have an important effect on flow behaviour. Using this knowledge, models of flow behaviour are produced which can be applied to flows for which the emplacement episode was not observed. These models can therefore also be applied to extra-terrestrial lava flows. A summary of the factors affecting flow of lava and the models developed to predict flow behaviour is given in this section.

1.41 Rheological Behaviour of Lava

The study of the behaviour of fluids is called rheology. Newton defined the law of liquid behaviour, which can be written as:

$$\text{Stress} = \text{viscosity} \times \text{rate of strain} \qquad (1.1)$$

The behaviour of a Newtonian liquid can therefore best be illustrated in a plot of shear stress versus rate of strain, where it is represented by a straight line passing through the origin (see Figure 1.13). The value of viscosity will be different for each liquid at a given temperature, and can be visualised as the amount of shear stress needed to produce a certain amount of strain, thus different fluids will plot with different slope values on the graph in Figure 1.13. A Newtonian fluid will flow even if subjected to small shear stresses.

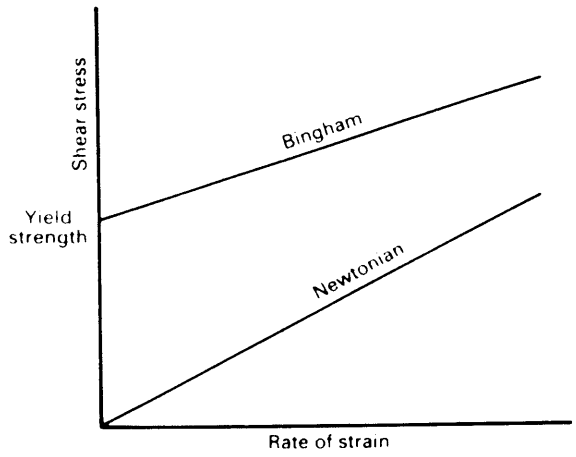

Figure 1.13: Plot to show the shear stress versus the rate of strain for both Newtonian and Bingham liquids, highlighting the difference between the two. This figure is taken from Cattermole (1996), and is after a similar one found in Hulme (1974).

In general as it is flowing, lava is cooling and crystallising. It is therefore a solidifying fluid - a mixture of molten rock, crystals and gas bubbles - so although it preferentially moves downhill and follows the topography of the surface on which it flows (like a Newtonian fluid), in other ways it will behave differently from a Newtonian fluid. For example, a lava flow may halt regardless of whether it is flowing on a steep or shallow slope when the rheological properties of the lava prevent further movement. This non-Newtonian behaviour was confirmed by observation of Etnean lavas (Walker, 1967; Robson, 1967), and Hawaiian lavas (Shaw et al., 1968), and in the study by Hulme (1974), and these studies show that natural lavas behave more like Bingham liquids. This means that they will flow like a Newtonian liquid (with a linear stress versus rate of strain characteristic), but only once a finite stress value has been achieved. Below this finite value, termed the 'yield strength' the lava flow will not advance. A Bingham liquid may therefore also be plotted on a graph of shear stress versus rate of strain, where it will be represented by a straight line that crosses the y-axis at the value of the yield strength, rather than through the origin as with Newtonian liquids (see Figure 1.13).

Hulme (1974) carried out a study modelling lava flows, which he found were best approximated to isothermal Bingham liquids in laminar motion. Hulme found that the morphology and dimensions of lava flows are primarily a function of the non-Newtonian character of the magma, rather than the effects of its cooling. He was able to show that when lavas move down slope, they assume a pre-determined constant width and depth, the reasons for which become clear when the way in which lava flows are emplaced is analysed. When lava is erupted it will move down slope, forming a flow that gets longer and wider. Excess hydrostatic pressure at the centre of the flow

provides the driving force for the lateral growth of the flow (see Figure 1.14). The height of the flow at the centre will decrease with the lateral spreading until there is an even thickness horizontally across the flow (no more hydrostatic pressure), and the shear stress at the base of the flow becomes equal to the yield strength. After this point the width of the flow will remain constant until the central thickness changes. Movement downslope can only continue if the shear strength at the base of the flow in that direction is greater than the yield strength. The shear strength is proportional to the depth of the fluid, so for a given slope there is a critical depth that must be exceeded before movement downslope can take place. The dimensions of the flow are therefore controlled in this manner.

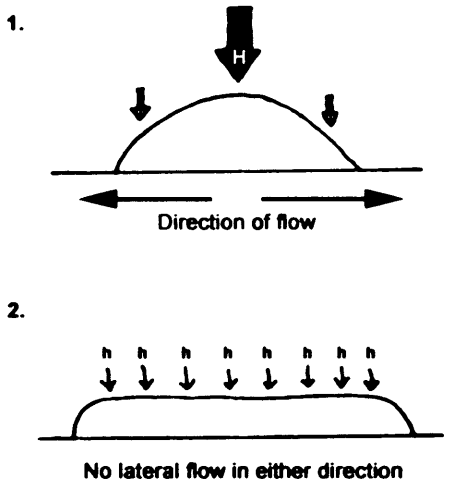

Figure 1.14: Diagram to demonstrate how and why flows spread laterally. In the first image the flow is thicker at the centre and thinner at the edges. The pressure due to the weight of the thicker area of the flow (H) will make the lava to move downwards and cause it to spread laterally. Where the thickness of the flow (h) is uniform (as in part 2 of the diagram), no extra weight is present at the centre of the flow so the flow does not spread laterally.

During emplacement there will be a section at each margin of the flow where the depth of the lava does not exceed the critical depth needed for flow movement. The lava here is static and cools, forming solid levées between which the molten lava flows in a channel. Using information about the development of these banks, Hulme produced a calculation that could be used to derive the yield strength of the lava. Depending on the data available, several equations can be used:

$$Sy = 2 * w_b * g * \rho * \sin\alpha^2 \quad (1.2)$$

$$Sy = \rho * g * \sin\alpha * H \quad (1.3)$$

$$Sy = \rho * g * H^2/w_f \quad (1.4)$$

where H is the flow thickness, w_f is the flow width, w_b is the levée width, g is the acceleration due to gravity, ρ is the density of the lava and α is the angle of the

underlying slope. Equations 1.2 and 1.3 were derived by Hulme (1974), and equation 1.4 is a derivative of the equation used for the study of the flow of glaciers (Orowan, 1949), which also show the behaviour of Bingham liquids (Johnson, 1970).

The model derived by Hulme (1974) and variations upon it have been used by many scientists to produce values for yield strengths of Martian lava flows and to use these values to infer lava composition (Hulme, 1976; Carr et al., 1977; Moore et al., 1978; Zimbelman, 1985; Cattermole, 1987). Several of these values will be used for comparison purposes later in this study, when discussing the results of the lava flow studies in this thesis. However, several authors (Moore et al., 1978; Crisp and Baloga, 1990b); Cattermole, 1996) have highlighted the fact that there are many errors involved in using this method to infer lava properties from the morphology of flow channels and levées. The flow dimensions and shapes of these features may change during the eruption and therefore the final shape and size may not reflect the initial conditions of the flow (Wadge and Lopes, 1991). In addition, changes that affect yield strength value will probably occur during flow emplacement, such as degassing, crystal growth and cooling, all of which contribute to an increase in yield strength, so that it will not be uniform throughout the history of a flow. Also, some workers have argued (Crisp and Baloga, 1990b) that cooling has a greater effect on the flow dimensions than was found by Hulme (1974). However, Hulme's method of determining yield strength is useful, if only to provide an approximate idea of the rheological properties of extra-terrestrial lavas. The yield strength can, in turn, be used to find the viscosity of the lava, using the following equation as defined by Hulme (1974):

$$\eta = F/E\,(g\rho)^3(Sy)^4/\tan\alpha \qquad (1.5)$$

where η is the viscosity, E is the effusion rate, g is the acceleration due to gravity, ρ is the density of the lava, Sy is the yield strength, α is the angle of the underlying slope, and F is a dimensionless parameter that is a function of the total flow width and the width of the levées. The effusion rate in a calculation such as this must be estimated from the flow length, according to the empirical method of Walker (1973). Although this method appears to have many errors, workers such as Schonfield (1979) were able to derive viscosities for Martian lavas from it.

1.42 Factors that affect Flow Dimensions

The dimensions and morphologies of lava flows are controlled by more than just the yield strength. Many physical processes occur during eruption which affect the flow including degassing, crystallisation, solidification, fracturing and shearing. Also, as will be discussed in Chapter 5, the eruption style and conditions, as well as the topography, may also partially control the final shape and dimensions. Walker (1973) was one of the first workers to notice the lack of any theoretical or empirical basis on which to predict the length of lava flows, and carried out a study to determine the most important factors affecting flow. He found that the major factor affecting the lengths of lava flows was effusion rate. Following this, other workers also found relationships between pairs of flow field characteristics, including flow field length and erupted volume (Malin, 1980; Lopes and Guest, 1982), and flow surface area and mean effusion rate (Pieri and Baloga, 1986). Other individual factors found to exert control on lava flow dimensions were: eruption viscosity (Nichols, 1939), channel pressure (Borgia and Linneman, 1990), and hydrostatic pressure gradients (Dalu et al., 1988). In all these cases, the effect of cooling is not thought to have a great effect on flow dimensions, since it is related to an outer crustal layer. However, Crisp and Baloga (1990b) found that it plays a more important role than this and developed a cooling-related model for the emplacement of lava flows that will be discussed in section 1.45.

1.43 Factors affecting magma discharge rates

Since effusion rate has been found to be one of the most important factors affecting the final dimensions of a flow, it is important to consider the factors affecting the rate at which magma can be discharged from a vent. The two most important factors affecting the magma discharge rate are the rheology of the magma (particularly the viscosity), and the size of the eruptive conduit. Generally the composition of Martian lavas is thought to be basaltic (Baird et al., 1976), or at least that the rheology of the lava is basalt-like (Cattermole, 1996), so discharge rates on Mars could be expected to be similar to those on Earth. However, vents and fissure widths on Mars are thought to often be much larger than those on Earth, perhaps as much as three times larger (Wilson and Head, 1983; Mouginis-Mark et al., 1984), thus magma discharge rates could have been much larger than those on Earth. It is important to note that in

nearly all the eruptions observed on Earth, discharge rates are highest during the early stages of activity (Thorarinsson, 1950; Cooke et al., 1976). The values obtained during modelling for effusion rate are only averages for the entire length of eruptive activity.

1.44 Factors affecting flow behaviour

The rheological properties of a flow will obviously affect the way a flow behaves during emplacement. One of the main ways to define flow behaviour is to determine whether it advances via laminar or turbulent flow, and this can be related to the Reynolds number. The Reynolds number is a way to determine the relative magnitude of the inertial and viscous forces affecting a mobile fluid. It is expressed as:

$$Re = \text{inertia forces/effective viscosity forces} = \rho U d_h / \eta_e \quad (1.6)$$

where ρ is the density of the fluid, U is the average velocity, η_e is the effective viscosity, and d_h is a characteristic length of the flowing body. In studies such as this one d_h is taken to be the hydraulic radius of the flowing material, which is given as:

$$d_h = 4 * (\text{cross-sectional area of flow/wetted perimeter}) \quad (1.7)$$

where the 'wetted perimeter' is a length measurement of the parts of the channel banks and base that are covered by the fluid as it flows. Since all the dimensions in equation 1.6 cancel each other out, the Reynolds number is a 'dimensionless number'. Generally, where Re is less than 2000, fluid flow is laminar, and above this flow is turbulent. Those flows with high viscosity, and therefore high yield strengths, show laminar flow. Flows may be turbulent if they are erupted on relatively steep slopes at high eruption rates (Head and Wilson, 1983), particularly if they also have low viscosity and low yield strengths. It is the turbulent flow of lava which is thought to have carved the sinuous rilles (see Figure 1.15) on the Moon (Hulme and Fielder, 1977; Head and Wilson, 1981), and also to be responsible for similar features on Mars. In fact, turbulent flow of lava may have been partially responsible for the large widths of the Elysium Fossae (Tanaka et al., 1992). This is because turbulent flows are thought to have enough energy to erode the ground on which they flow.

Figure 1.15: The channel-like features in this Apollo 15 photograph (AS15-2606M) are lunar sinuous rilles. The impact crater to the top right of the photograph is called Aristarchus and is ~40 kilometres in diameter. The scene is illuminated from the left.

The velocity, viscosity, density and effusion rate of the lava, as well as the slope upon which it has been emplaced, will all affect the type of flow that forms. For example, basaltic Hawaiian-type eruptions generally produce one of three types of lava flow: aa, pahoehoe and blocky, although many lava flows can be a mixture of these types as will be explained later. The pahoehoe flows develop continuous crusts and advance as a series of lobes and toes from the flow front, often being fed by tubes which transport the lava to the flow front. In contrast, aa lavas develop crust which is constantly broken and forms a rubbly flow top, and tend to advance using channels to transport lava from the source to the flow front. Blocky flows advance more slowly than the aa flows, and the crusts break into large blocks due to fracturing, as a result of their higher viscosities combined with occasional rapid flow.

Other morphological characteristics of lava flows that appear to be inherent from internal rheological properties are surface ridges. These can be seen to form on pahoehoe lavas giving a 'ropey' effect as a result of the contrast in viscosity between the hotter interior of the flow and its cooler upper surface. This is also true for more silicic flows, where pressure ridges (festoon ridges) form. Work has been carried out in the past to relate the spacing between these ridges to the viscosity of the lava (Fink and Fletcher, 1978; Fink, 1980; Theilig and Greeley, 1986). Values found indicated that viscosities were high and comparable to rhyolitic or dacitic flows (Fink, 1980), or trachytic flows (Zimbelman, 1985). However, the work of Theilig and Greeley (1986) on comparing Martian lava flows showing festoon ridges to basaltic Icelandic flows

showing similar ridges, did not find this. They concluded that the festoon ridges on the Martian flows examined could have been due to folding of the surface crust in basaltic lavas in the last stages of emplacement when viscosities were high, either due to cooling or to high-crystallinity lava being erupted under low temperatures. They found that festoon ridges are therefore not necessarily the result of silicic lava flows (see Theilig and Greeley (1986) for further details of their work on this).

1.45 Modelling lava flow growth

As discussed previously, the Bingham model of Hulme (1974) has been widely used by planetary geologists to determine the rheological properties of lavas. Wadge and Lopes (1991) used the model in their study of the distal lobes of lava flows. They proposed that the widths of the distal lobes are representative of the rheology of the lava, assuming that they represent the arrest of free-flowing isothermal Bingham fluids on a slope. They found a positive correlation between lobe width and silica content of lava flows and used it to investigate 20 flows on the flanks of Olympus Mons. When normalised relative to the widths expected on Earth, they were found to be equivalent to those expected for terrestrial flows with andesitic/basaltic silica contents.

The models of lava flow emplacement that have been discussed so far all assume that cooling is not an important control on flow dimensions, and that the flows are isothermal in cross-section. Other models have been produced however, which model the radiative cooling of lava flows in order to relate flow dimensions to eruption conditions. Pieri and Baloga (1986) proposed two models of radiative cooling for terrestrial lavas, one model where the flow was thermally well mixed, and a second where the flow was assumed to be "un-mixed", where there was a thermally homogeneous core covered by an infinitely thin crust. Radiation from the crust was characterised by a constant 'effective radiation temperature' that needed to be determined empirically. Cattermole (1987) applied these models to Martian flows, and calculated the effusion rates of several lava flows on Alba Patera, assuming a range of initial temperatures.

The approach by Pieri and Baloga (1986) was refined by Crisp and Baloga (1990a,b), who proposed a model where there was a finite crust thickness, and a partial exposure of the core to the surface. This is more representative of field observations, and was used by Crisp and Baloga (1990a) to calculate effusion rates of a flow on

Ascraeus Mons. However, the effusion rates are still subject to an error of an order of magnitude, since the model is dependent on parameters estimated from empirical studies of terrestrial lavas (such as the fraction of the surface of the flow that is exposed when the crust is cracked or overturns).

Using observations of the growth of lava flow fields, in conjunction with the model for radiative cooling produced by Crisp and Baloga (1990a,b), Kilburn and Lopes (1991) developed their 'flow growth model'. This relates measurable parameters of lava flows (maximum length and width, average thickness, and average angle of underlying slope) to the duration of flow emplacement. It is particularly applicable to extra-terrestrial lavas, since gravity and viscosity do not occur directly in the equation, and has been applied by Lopes and Kilburn (1990) to 18 flows on Alba Patera. However, the values they used for slope and flow thickness are only estimates. With MOLA, slope and flow thickness values can be obtained with greater accuracy, and therefore values for flow emplacement times and derived effusion rates will also be more accurate. It is therefore one of the aims of this study to use the flow growth model to obtain durations and other emplacement characteristics in conjunction with the MOLA data. A more in depth explanation of the flow growth model can be found in Chapter 5.

Determining the rheological characteristics of a lava flow simply from morphological information is not without error, as was shown by the work of Fink and Zimbelman (1985). Their work with lava flows in Hawaii showed that measurements of the thickness of lava flows could be incorrect without knowledge of pre-flow topography. For ancient flows for which previous topography is not known, or those flows for which vertical cross-sections are not available, thickness values obtained can differ greatly from the actual value. However, even though these errors do occur, the attempt to characterise the rheology and mode of emplacement of Martian lavas using models based on their morphology will still provide valuable information about them.

1.5 This Study

The data from MGS provide information that has long been lacking about the surface of Mars. The images from MOC have allowed smaller areas of the surface to be studied in greater detail, and enabled the search for small-scale analogues to terrestrial features. The MOC images have therefore been used in this thesis not just to aid the

mapping exercise where they have helped characterise terrain, but also to identify small-scale features that appear to be unique to Mars. Since this study is focused on volcanic processes, photogeological analysis of the MOC images has also been undertaken to provide information about the modification of volcanic features over time by studying several volcanic areas of varying ages, and this is presented in Chapter 3.

In Chapter 4 the MOC images and MOLA data have been used to produce a new map of the area around the Elysium Montes, since much geological activity has occurred here in the past. There is much evidence for volcano/ground-ice interactions in this area (Mouginis-Mark et al., 1984; Mouginis-Mark, 1985) and also to suggest that the flow of water produced channels to the west and north of the volcano complex. The presence of volatiles in the region, either as ice or liquid, may have had an effect on the production and emplacement of the lavas here. There is evidence for late stage explosive activity around the vent areas of both Hecates Tholus (Mouginis-Mark et al., 1982) and Elysium Mons (see Chapter 4), and also evidence for recent activity in the south east of the region near the Cerberus Fossae (Plescia, 1993; Burr et al., 2002; Hartman and Bermann, 2002). Combined with the theory of Hartmann and Berman (2000) that some of the volcanic surfaces in Elysium may be younger than 10 million years old, this makes Elysium an interesting volcanic area to study. Previous geological maps of Mars have been produced without the aid of MOC and MOLA data, so these have been used in conjunction with the previously existing Viking images to produce a map in this thesis. The MOLA data can be used to determine the heights and depths of topographic highs and lows, to give information regarding stratigraphic relations and to find thicknesses of individual units. It can also be used to produce profiles across features to show their morphology, and also to produce contour maps, which are useful during mapping projects. It is therefore hoped that the use of these new data will enable the production of a more detailed map than those made in previous studies.

As discussed in the last section, previous calculations of lava flow properties have relied on data that were only estimates and thus the results were subject to many errors. Prior to MGS the topography of Mars was only known to +/- 1 kilometre, thus making it impossible to gather information about the thicknesses of relatively small features such as individual lava flows, and meaning that regional slope values were inaccurate. Heights of features were calculated by measuring the widths of the shadows that they cast and using trigonometry to find a height value based on the fact that the angle of the incident sunlight was known. MOLA data can provide height values of

individual geological features to within 1 metre, so it is therefore ideal for the study of lava flows that sometimes only have a thickness of a few metres. Since Elysium was studied in the mapping section of this thesis, 24 of the simple lava flows in this area have been analysed. MOLA was used to produce longitudinal thickness profiles along the flows, to find the average thickness of each flow and also to calculate the underlying slope. Half of the flows were inferred to be aa and the 'flow growth model' of Kilburn and Lopes (1991) was used to find the flow durations and, in turn, the effusion rates and velocities of these flows. Since Kilburn and Lopes (1991) also applied their model to several flows on Alba Patera at a time when the slopes and thickesses had to be estimated, it was thought to be of interest to re-calculate the durations of these flows using the new MOLA values. The theory, methods and results of this lava flow study are presented in Chapters 5 and 6. It was hoped that any differences between results found for the flows would relate to differences between the two volcanic areas of Elysium and Alba, and that the results from Elysium would be useful in the analysis of the mapping carried out in this study.

2.0 Methods

All data used in this thesis required some manipulation or processing before they could be analysed and used to produce results. The methods that will be discussed in this chapter have been applied to all the data used throughout this thesis. The methods are intended to be general and often deal with the way in which the raw data has been processed. More specific methods for measurements and calculations made to produce results are discussed as appropriate within the four following chapters. Information concerning the manipulation of MOC and MOLA data is discussed in detail, as many researchers have not dealt with these new data before in depth.

2.1 Sources of Data

The three main sources of data that have been used in this work are the images from the Viking mission, the MOC images and the MOLA data from the Mars Global Surveyor mission. All these have been mentioned briefly in Chapter 1, but the way that each set of data were collected by the spacecraft, and the form of the data when available for use by the scientific community, will be discussed in this section.

2.11 Viking Images

2.11(a) Data Collection

Each of the Viking Orbiters had two cameras onboard which were incorporated into a visual imaging subsystem (VIS) that allowed larger format and higher resolution images to be taken than on previous missions. It also meant that the spacecraft could lay down swathes of pictures in an overlapping sequence in order to cover large areas of the surface. The two cameras took high-resolution images using slow-scan television framing. Each had a telescope that had a focal length of 475 mm and a 37 mm diameter vidicon which could scan 1056 lines by 1182 samples. The field of view of each camera was 1.54° by 1.69°, which meant that each pixel covered 16 μrad from orbit, and the cameras had been positioned on the spacecraft so that their fields of view overlapped. There were five colour filters on each camera and one clear one.

The Orbiters imaged the entire surface of Mars at a resolution of between 150 and 300 metres per pixel, and imaged selected areas of interest at a resolution of up to ~8 metres per pixel. The lowest altitude of each of the Orbiters above Mars during orbit (periapsis) was 300 kilometres, during which the highest resolution images were obtained. Further details about the Viking Orbiter cameras, the rest of the instruments onboard or about the mission itself can be found in the special publication of the Journal of Geophysical Research (volume 82, no. 28, 1977) that is dedicated to the scientific results of the Viking project, and more specifically in the paper by Snyder (1977) in the same volume.

2.11(b) Availability for Use

For the current study, Viking data was available in several different formats. All the negatives of the images taken by the Viking spacecraft were available for use, as well as the larger photographic prints that were produced from the negatives. Also available for use were the SCPs (Scanned Contact Prints), which are prints that have been printed directly from the negatives and thus show the best detail. There are two different SCPs for the same negative, one in rectilinear format and one in orthographic format. The rectilinear image shows the image in its original form, so some features such as impact craters or even larger ones like volcanoes appear stretched (due to the oblique angle of the camera on the spacecraft relative to the surface). The orthographic SCPs have been geometrically corrected to make the scene appear as it would if looking vertically from above. The brightness and contrast has already been adjusted in these orthographic images to enhance picture detail.

The individual low-resolution images were also pieced together by the Viking team to produce 'photomosaics' that cover the whole Martian globe. This global photomosaic was split up into Mars Chart areas to make it more manageable. High-resolution photomosaics, or MTMs, were produced for those areas where high-resolution imagery was available. Later, when the technology became available, all the individual images were stored on CD. Digital images of particular areas of the Martian surface were also pieced together on the computer to produce Mars Digital Image Mosaics (MDIMs), and these are also stored on CD.

The images were numbered according to which orbiter took the image and also according to the orbit number. On all the photomosaics there is a small 'blueprint' at

the bottom that shows the user the image numbers of the individual pictures that were used. Therefore if it is necessary to see an image in greater detail or to manipulate it on computer it is easy to find the desired image either in printed format or on CD. There are also global maps that show the location of the high-resolution images. Apart from the negatives, all the different forms of data were used for the work in this thesis.

The internet was also another good source of data. The Viking images were accessible on the NASA Planetary Data System (PDS) Map-A-Planet website (http://pdsmaps.wr.usgs.gov/), where it was possible to produce custom-made maps of the surface of Mars by specifying the desired area co-ordinates and other options. The maximum resolution for these maps was 64 pixels per degree, so they are not ideal for detailed work but useful if a quickly produced basic image was required.

2.12 MGS MOC Images

2.12(a) Data Collection

As mentioned in Chapter 1, the Mars Global Surveyor has three cameras: two wide-angle and one narrow-angle. The wide-angle cameras take global and regional images of the surface of Mars, with regional images having a spatial resolution and similar scale to the lowest resolution images that were obtained by Viking. The wide-angle cameras also have two differently coloured filters, blue and red, which can be merged to produce colour images of the surface. The narrow angle camera takes the higher resolution images. It can produce images with a resolution of 1.4 metres per pixel, although most images ranged between 1.4 to 5 metres per pixel generally. As discussed in Chapter 1, during the aerobraking phase the orbit was elliptical and at this early stage the mission scientists took images to test the capabilities of the camera. Once the circular orbit was achieved the 'mapping' phase of the mission began, and the highest resolution images were obtained.

The cameras were based on the 'push-broom' technique. This means that each camera has a row of detectors that each individually image the part of the surface they are positioned over. By the time all the detectors have acquired an image, the spacecraft has moved along over the surface of the planet a short distance and the detectors can all collect another line of data. In this way the image is acquired one line at a time,

'sweeping' over the surface of the planet. When all the lines of data are placed next to each other a whole picture of the area imaged is obtained.

The MOC wide-angle cameras were capable of viewing Mars from horizon to horizon and were designed for low-resolution global and intermediate resolution regional studies. Low-resolution observations could be made on every orbit during the Mapping Phase so that in a single 24-hour period a complete global picture of the planet could be assembled at a resolution of at least 7.5 kilometres per pixel. Regional areas (covering hundreds of square kilometres) could be imaged at a resolution of at least 250 metres per pixel at the nadir. The limb of Mars could also be imaged at vertical and along-track resolutions of at least 1.5 kilometres.

During the mapping phase the narrow-angle camera was used to produce images at 1.4 metres per pixel of areas ranging from 2.8 x 2.8 kilometres to 2.8 x 25.2 kilometres, the size of the area depending upon how much internal digital buffer memory was available. Also, lower resolution images (up to 12 metres per pixel) could be acquired by pixel averaging. These images could be much larger and at the lowest resolution could cover an area of up to 2.8 x500 kilometres. A summary of MOC specifications is given in Table 2.1.

Camera	Minimum wavelength (nm)	Maximum wavelength (nm)	Focal length (cm)	Aperture	F number	Resolution at 380 km orbit (metres/pixel)
Narrow-angle	500	900	350.0	0.35 m	10	1.5
Wide-angle (red)	600	630	1.1	1.7 mm	6.4	230
Wide-angle (blue)	420	450	1.14	1.8 mm	6.3	230

Table 2.1 Summary of MOC characteristics, modified from a table of performance parameters of the original Mars Orbiter Camera designed for the unsuccessful Mars Observer mission (Malin et al., 1992).

2.12(b) Availability for Use

In this study the MOC images were obtained via the internet, since the raw (unprocessed) MOC data available on CD required much processing before use. The MOC images can be downloaded from the MOC image gallery on the internet (at http://www.msss.com/moc_gallery/). At this site it is possible to pick the desired time period

when the images were acquired, the type of image required (regional or narrow angle for example), and also the Mars Chart area in which to search for images. Each Mars Chart area is then displayed as a low-resolution Viking map with the positions of the MOC images all being displayed as green rectangular boxes. The green rectangles are links that take the user to a page displaying a preview of the image, and a list of different versions of the image are offered for viewing. In general the images available are: a raw data file; a fast-downloading but poorer quality JPEG file that has been map-projected; a slow-downloading but best quality GIF file that has been map-projected; and a choice of non-map-projected JPEG and GIF files. During this study the high-quality GIF files were downloaded from this site and used for the photogeological analysis, although occasionally only the choice of a non-map-projected GIF file was available for download. Obviously all the images obtained from this site (other than the raw images) had been subjected to some processing by the MOC science team, and this had to be considered when analysing the images. The processing allowed better interpretation of the images and improved their appearance, but it did not allow rigorous radiometric, geometric or photometric rectification to be done to enable the quantitative interpretation of the data. Therefore, no measurements were made using the images.

When viewing the MOC images that are included in chapters within the present study, it is necessary to understand the processing techniques that are used by the MOC team. There are several artefacts in the images that need to be rectified by the MOLA Science Team to improve the appearance of the image and make it easier to analyse. Firstly, each of the detectors in the push-broom imaging system has a different response and sensitivity to the brightness of the scene being imaged. This leads to dark and light vertical streaks being seen in an unprocessed image. In order to correct this, it is first necessary to calculate the average brightness for each column in the image. Then each pixel in the column is divided by the average value for that column and then multiplied by the average of the scene as a whole. This method reduces much of the streaking, but occasional further streaking does occur and this is due to scene dependent brightness variations.

Another correction that has to be applied concerns the aspect ratio of the images. The down-track and cross-track pixel resolutions of MOC are slightly different, which leads to pixels that are rectangular on the surface rather than square. The reason for this difference is because the cross-track resolution is dependent on the altitude of the spacecraft and the camera focal length and pointing, whereas the down-track resolution

is dependent on the integration of the push-broom array and the relative velocity of the spacecraft as it passes over the surface of Mars. In order to make the pixels square (and therefore reduce the 'stretching' observed in the raw images) the images are re-sampled to make the cross-track resolution match the down-track resolution. A simple bi-linear interpolation method was used by the MOLA team to reduce the cross-track resolution, thereby resulting in fewer pixels.

Brightness variations due to solar illumination differences over the image array, and also large scene brightness variations due to surface albedo differences could be observed in many of the MOC images. This was rectified by passing a 301 x 301 high-pass boxcar filter over the data, and an average of the original scene and the high-pass filtered scene was used to produce the final image.

The images also had to be map-projected in order for features to have their true positions relative to each other (on the surface of the planet) and reduce any final stretching of the features on the surface. The position of the spacecraft at the time each image was acquired was always recorded and the MOC image team used this information to re-shape each image into a sinusoidal map projection. These images could then be more readily compared to the Viking images, although several different projections were used for the Viking data. Determination of the MGS spacecraft position, and how the surface positioning of data obtained by the instruments onboard was achieved, is discussed later in sections 2.13(a) and 2.23(a).

2.13 MGS MOLA Data

2.13(a) Data Collection

2.13(a)i Specifications of MOLA

The main components of MOLA are a laser transmitter, a 0.5 metre diameter telescope, a silicon avalanche photodiode detector (SiAPD) and a time interval unit (TIU). Specifications of MOLA are given in Table 2.2. The transmitter consists of a Q-switched chromium and neodymium-doped yttrium aluminium garnet (Cr:Nd:YAG) oscillator that is pumped by a 36 bar laser array. Each bar in the laser array is made up of around 80 aluminum gallium arsenide (AlGaAs) laser diodes. These produce lasing by optically exciting the Cr:Nd:YAG material. The laser is pulsed at a repetition rate of 10 Hz, controlled by the Q-switch. The pulses are emitted with ~8 nsecs full-width at

half the maximum amplitude (FWHM) at a wavelength of 1.064 μm. For a more detailed description of how the laser works see Abshire et al., (2000). Information regarding the design of the laser and a performance model are given in Afzal (1994), and details of laser calibration can be found in Afzal et al. (1997).

Parameter	**Specification**
Mass	28.8 kg
Power consumption[a]	34.2 W
Transmitter:	
Laser type	Diode-pumped, Q-switched, Cr:Nd:YAG
Wavelength	1.064 μm
Pulse rate	10 Hz
Energy[b]	48 mJ $pulse^{-1}$
Laser divergence	420 μrad
Pulse length	8 nsec
Receiver:	
Mirror	50 cm parabolic
Detector	Silicon avalanche photodiode
Field of view	850 μrad
Electronics:	
Microprocessor	80C86
TIU frequency	100 Mhz
Filter channel widths	20, 60, 180, 540 nsec
Data rate	618 bits s^{-1} continuous
Resolution:	
Maximum ranging distance[c]	787 km
Range resolution	37.5 cm
Vertical accuracy[d]	1 m
Surface spot size[e]	168 m
Along-track shot spacing	300 m
Across-track spot spacing[f]	4 km

Table 2.2 Specification for the MOLA instrument (taken from Smith et al., 2000).

[a] Includes replacement heat for temperature control

[b] At arrival at Mars; degrades with time

[c] Hardware limited

[d] Includes radial orbit error

[e] In 400-km-elevation mapping orbit

[f] Average at equator; varies with latitude

The laser detection system is composed of a 0.5 metre diameter gold-coated beryllium telescope, a 2.2 metre-wide optical band-pass filter which rejects solar background noise, and the SiAPD which accumulates backscattered photons. It also has the TIU, which is a binary counter that records the number of clock cycles between the sending of the transmitted pulse and the receiving of the returned pulse. The clock is an oven-heated crystal oscillator with a frequency of nearly 100 MHz. The final major component of the MOLA receiver is an 80C86 onboard computer that executes the flight software. Much of the information given in the next sections relates to the in-depth working of the MOLA instrument and details of its use. This is necessary to provide the reader with background knowledge needed when considering the results of this study and the errors inherent to the MOLA data.

2.13(a)ii How does MOLA work?

After over three years of successful data collection the MOLA instrument on the MGS spacecraft stopped working in June 2001. However, the following is a description of how the MOLA instrument worked and collected data during the MGS mission.

A laser beam is produced by the laser transmitter and a pulse of this laser beam is passed through a filter (called channel 0) which is used to stretch (increase the size of) the pulse so that it will trigger the MOLA detectors more easily. The transmitted pulse energy is then measured by the start pulse energy counter, which measures the energy of the laser pulse. The information concerning the energy value and the threshold value of the transmitted pulse is sent to the echo pulse detection system, and an impulse is sent to the TIU to start the timer. At the same moment the laser pulse is released and travels down to the surface of Mars. Since the energy of the laser pulse is related to the width of the pulse (see Abshire et al., 2000), the detection system will identify returned signals with this width. Although 'stretching' of the signal will occur before it returns to the spacecraft, the signal is passed through different filters that are designed to account for the types of stretching that may occur. The threshold value of the transmitted pulse is taken as the lowest energy value of the laser pulse. It is a fixed value and can only be changed by ground command. Since the design of the laser means that the laser energy decreases over time, it was necessary for the threshold value of the transmitted pulse to be reduced during the MGS mission, in line with changes in laser energy. The shape of the energy pulse is Gaussian (see Figure 2.1). This is important because the detection

system assumes the echo pulse will have this shape, and it is also necessary for some of the determinations of other properties of the returned pulse which will be discussed later. The detection system has a 'range gate' that represents an amount of time within which the return signal can be expected. This minimises the amount of noise from solar photons at about the same wavelength as the laser.

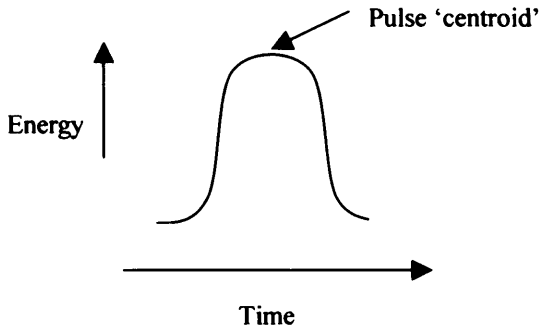

Figure 2.1: Illustration of a Gaussian trace, with the energy increasing to a maximum and then decreasing again at an exponential rate. Both transmitted and returned MOLA laser pulses have this characteristic shape, although the way in which the signal is stretched during the round-trip to the Martian surface will affect the impulse width of the returned laser pulse (see text). The pulse centroid is the point where the pulse reaches the maximum energy value.

The telescope focuses the returned laser signal onto the SiAPD detector. The energy from the received pulse is amplified and passed through four different filters. Each filter responds to a different impulse width and noise bandwidth, in order to account for the different ways in which the echo pulse may have been stretched on its journey between the spacecraft and the Martian surface, either by clouds or surface roughness. Each channel has a threshold setting which determines the minimum Signal to Noise Ratio (SNR) that is required for the channel to be triggered. The SiAPD detector outputs a voltage that is proportional to the amount of returned photons. This energy is passed through the filters and when it exceeds the value of the threshold setting a signal is sent to the TIU and the clock stops. A received impulse can trigger more than one of the filters but the signal which best fits the impulse response pulse width of the filter will have the highest SNR and will therefore pass through the filter more quickly and be the first to stop the TIU. It is the information from this signal that will be recorded for transmission back to Earth.

The onboard computer has an algorithm that independently and automatically adjusts the receiver threshold levels, based on statistics from the previous 14 seconds of

laser returns. This allows MOLA to maintain a false alarm rate of approximately 1% per channel. This is a self-adapting process that allows both strong ground returns and weaker atmospheric returns to be detected without modification from the MOLA science team. Also every 14 seconds, the laser fire time is compared to the MGS spacecraft time so that the location of the laser spot on the Martian surface can be reconstructed.

To obtain an unbiased time-of-flight estimate, the point at which the clock is triggered to start and stop should correspond with a specific point on each and every transmitted and received pulse. This point has been taken to be the pulse 'centroid' which is the point at which the energy reaches the maximum value. For symmetric pulses, such as that shown in Figure 2.1, the centroid is equivalent to the pulse midpoint time. Obviously, there will be a timing offset because the leading edge of the pulse will trigger the threshold value of the detectors before the pulse centroid point reaches the detector. There is also a small timing delay on the start and stop interpolators (0.25 of a clock period), as well as filter propagation delays and an instrument time bias that is due to electronics, circuitry and cables. These all contribute to an error in the time-of-flight measurement. Other MOLA measurement errors include a variance in the pulse width measurement at the threshold crossings, and a variance in the pulse area measurements. These errors have been measured and calculations developed to compensate for them. An in-depth discussion of these calculations can be found in Smith et al. (2000) and references therein.

The final accuracy of the surface height determination is controlled not only by uncertainties in time-of-flight measurements, but also by uncertainties in the spacecraft position, and the pointing angle of the laser beam. These errors are discussed in section 2.13(c) of this chapter. The MGS spacecraft has several sensors that enable the science team to work out the attitude of the spacecraft (the position of the spacecraft and the way that it is pointing relative to certain points in space). It has several sun sensors which give the attitude of MGS relative to the position of the sun, an Inertial Measurement Unit which can determine the yaw attitude of MGS, the Mars Horizon Sensor Assembly (MHSA) which determines the horizon as seen from the spacecraft (this provides an empirical nadir for pointing the science instruments), and a Celestial Sensor Assembly which provides attitude data based on the determination of positions of known stars. The IMUs are aligned along spacecraft fixed X,Y,Z axes and these use

the Earth Mean Equator and Vernal Equinox 2000 (J2000) as the standard reference system.

The vernal equinox is the intersection point between the ecliptic plane and the equatorial plane that the sun reaches in spring, and is used as the starting point for measuring angular distances along the ecliptic or the equator (see Figure 2.2). The ecliptic is a reference circle around the centre of the Earth, which is created by using the plane of the Earth's orbit. Two intersections occur between these two reference circles because the Earth is tilted, so the circle of the equatorial plane is at an angle to the circle of the plane of the Earth's orbit. There are two points (equinoxes) where this crossing of the two circles occurs, but due to gravitational effects (mainly from the Sun and Moon), the equinox points gradually shift along the celestial equator. A long-term effect called 'precession' causes the celestial poles to rotate around the ecliptic poles in a cycle of 26,000 years, which means that any co-ordinates given to celestial objects using this system are subject to change over time. Therefore, all such co-ordinates are given in terms of a date 'epoch'. The standard epoch at the moment is J2000, which is equivalent to noon on the first day of the year 2000.

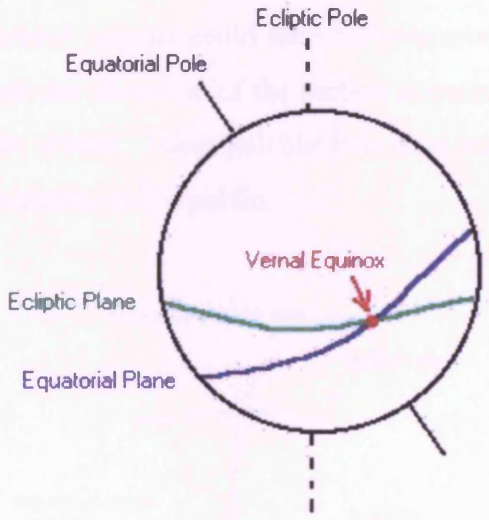

Figure 2.2: The point where the ecliptic plane (green) crosses the equatorial plane (blue) is called an equinox. The vernal equinox occurs in spring and is used as a reference point to determine planetary co-ordinates. Due to precession (the long-term movement of the equatorial pole around the ecliptic pole, the position of the vernal equinox gradually moves. A specific date (or epoch) is used so that the position of the vernal equinox at that time can be used as a reference point.

The science instruments have a co-ordinate system which defines the mounting of the instrument with respect to the X,Y,Z axes of the spacecraft. A series of matrix calculations relate the instrument fixed co-ordinates to the inertial J2000 co-ordinates so that it is possible to tell which way the instruments are pointing. Data obtained by MGS was initially referenced to this internal co-ordinate system, but by adopting appropriate values for the orientation of Mars, as defined by the International Astronomical Union

(IAU), and the International Association of Geodesy (IAG) (Seidelmann et al., 2002), these co-ordinates could be converted into planet-fixed co-ordinates of latitude and longitude. The co-ordinate system (latitudes and longitudes) used by MOLA is different from that used in previous missions like Viking, and will be discussed later in section 2.23(a).

The elevation of each MOLA laser 'footprint' is determined by interpolating the orbital trajectory of the spacecraft to the time of the laser measurement. This allows the distance between the spacecraft and the Martian centre of mass to be obtained. The range R_{Mars} from MGS to the Martian surface is related to the time of flight t_{opt} of the laser pulse by:

$$R_{Mars} = \frac{Ct_{opt}}{2} \tag{2.1}$$

where C is the vacuum speed of light. The difference between the value for the radial distance to the spacecraft from the planetary centre of mass and R_{Mars} provides the radius of Mars at the location of the laser footprint on the surface (see Figure 2.3). Areoid heights could then be compared to the radius value obtained for the laser spot and the elevation of the surface covered by the footprint could be calculated relative to the areoid. These calculations were made by the MOLA team and the data then made available to the public.

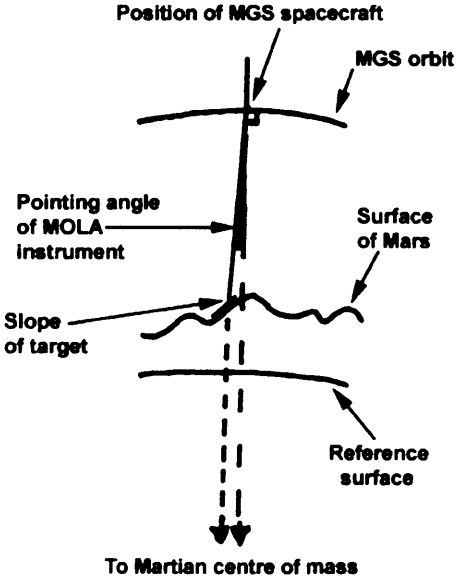

Figure 2.3: A simplified illustration of the geometry of the MOLA instrument as it makes measurements. Errors inherent in the positioning of the MGS spacecraft, and the pointing angle of the MOLA instrument are discussed in the text.

The slope of the sampled ground surface, as well as the roughness of the ground, have an effect on the precision of the MOLA range measurements. In the MGS mapping orbit, the sampling rate of the instrument (one pulse every 10Hz) and the laser beam divergence (420 μrad) lead to a laser footprint size on the Martian surface of ~168 metres with shot-to-shot spacing of ~300 metres (see Table 2.2). Clearly then, the way in which the roughness of the terrain changes over this area will have an effect on the way the width and shape of the laser pulse has been spread in time, and will also affect the precision of the MOLA range measurements, with greater slopes leading to a less precise range value. The precision of the MOLA range measurements is around the limiting resolution of 37.5 cm on smooth, level surfaces with low slopes, and can increase to ~10 metres on rougher surfaces with slope values of up to 30° (Gardner, 1992; Abshire et al., 2000).

As previously mentioned, the backscattered laser pulse can be used in ways other than determining the elevation of the surface covered by the laser spot. It can also be used to determine the way the relief varies over the target area (often called 'footprint scale slope' or 'root mean square' (RMS) roughness. The width of the returned laser pulse can be used to determine this, and can be measured in two ways.

Firstly, a coarse estimate can be found from the matched filters (channels 1 to 4). These have been designed to identify specific types of returned signal (see Table 2.3). The filter that best fits the shape of the returned signal gives some indication of the conditions on the ground. For example, channel 1 would be triggered by a laser footprint that covers smooth terrain, but if the terrain was hilly and the ground height over the footprint area varied by 27 metres or more then it would trigger channel 3 and be described as rough. However, this only gives a crude estimate of the roughness of the terrain. A more accurate measurement can be made by using the difference in times between when the leading and trailing edges of the returned pulse cross the detection threshold, which is a measure of the optical pulse width. The pulse spreading contains contributions from both the shape of the sampled area and the roughness of the terrain. In most areas of Mars the spreading of the optical pulse is affected more by the roughness of the optical terrain than by the local slope (Garvin et al., 1999). Where this is true it is therefore possible to derive roughness by correcting the returned pulse for local slopes determined from MOLA ranging.

Characteristic	**Channel 1**	**Channel 2**	**Channel 3**	**Channel 4**
Description	**Smooth**	**Moderate**	**Rough**	**Clouds**
Channel width, nsec	20	60	180	540
Terrain height variation within footprint, m	3	9	27	81
Footprint-scale surface slope, deg	1.0	2.9	8.6	24.2

Table 2.3 MOLA matched filter characteristics, showing expected terrain type for each filter taken from Smith et al. (2000).

2.13(a)iii How does MOLA tell the difference between clouds and the ground?

Clouds are difficult to detect because they are diffuse targets. However, one of the matched filters in the MOLA detection system (see channel 4 in Table 2.3) is specifically designed to detect the backscattered signal reflected by clouds. Also, the fact that MOLA has an adaptive detection threshold that keeps updating every 14 seconds enhances their probability of detection.

The range gate of the detection system usually works within values which only usually allow clouds within 20 kilometres of the surface to be detected, since anything further away from the surface than this will arrive back to the spacecraft sooner than expected (outside the range gate) and be discounted. If a cloud falls within the range gate of the MOLA instrument, has sufficient opacity and produces enough backscatter, then an atmospheric reflection will be registered. MOLA ground and non-ground returns are semi-automatically classified by a tracking algorithm contained within the software onboard MGS, and then manually edited once the data are returned to Earth (Neumann et al., 2003). Often the atmospheric returns can be determined by comparison with the recent history of ground returns since the atmospheric returns will register at several km higher than the recent ground returns. For particularly dense clouds, such as those found over the poles, MOLA sometimes lost its lock on the

surface and tracked clouds instead (Zuber et al., 1998c; Neumann et al., 2003). Returns were deemed to represent reflective 'clouds' when either three or more non-ground triggers were detected within 0.5 seconds of each other, or when six or more were detected within a six second timescale (representing about 20 kilometres on the ground), since the probability of these groups of data occurring by chance is less than 0.001% (Smith et al., 2000). Reflective clouds on channels 1 and 2 are categorised as "sharp" because the returned pulse has not been distorted and stretched much, while returns from channels 3 and 4 with wide returned pulse widths are "diffuse". "Sharp" cloud fronts have mainly been observed around the flanks of the southern polar cap (Neumann et al., 2003).

Non-reflective clouds can also be detected, and are characterised by groups of two or more shots in a two second time window that do not trigger any of the filter channels. Alternatively they can be detected using the average reflectivity-transmittance product (which is also used to determine the surface reflectivity and is discussed in the next section).

2.13(a)iv Surface reflectivity and atmospheric opacity

Surface reflectivity and atmospheric opacity are other properties that can be measured by MOLA. The surface reflectivity can be measured by comparing the energies of the transmitted and received laser pulses. In practice the reflectivity value contains contributions from the reflectivity of the terrain and the opacity of the atmosphere. Therefore, if independent measurements of the atmospheric opacity can be obtained, such as from TES, then the surface reflectivity can be better constrained. In the same way, if independent estimates of the reflectivity of terrain in areas that MOLA has ranged can be obtained, then the MOLA reflectivity measurement can be used to provide an estimate of the 1.064μm opacity of the Martian atmosphere (since 1.064μm is the wavelength of the transmitted laser pulse). These properties are not used during this study but it is important to understand everything about the MOLA instrument at a level that provides background knowledge of how the instrument works and the ways in which it can be used.

2.13(b) Availability for use

The MOLA data can be downloaded from the internet or accessed on CD. The raw engineering and science data are contained in the Aggregated Experiment Data Records (AEDRs) and are stored in the same time ordered series in which the data were collected by the MOLA instrument. The data that were used in this study to produce individual MOLA orbit profiles were stored in PEDRs (Precision Experiment Data Records). The MOLA data in the PEDRs have been corrected by the MOLA Team using information about the position of the spacecraft relative to Mars (the collection of this data was described in section 2.13(a)ii). The PEDRs contain information regarding instrument science data, spacecraft location, estimates of the planetary radii and elevations relative to the areoid. Any instrument delays have also been accounted for and, as the mission continued, greater knowledge of the errors in the instruments was established so that better corrections could be made. The processing software used to generate the MOLA PEDRs was updated as better orbit information became available during the mission, particularly with respect to the type of gravity model used. Although PEDRs produced with different versions of the processing software have only minor differences, it is important to note that different versions exist, particularly for the benefit of this study since the research in this study was carried out using data that had been processed with several different versions of the earlier PEDR processing software.

A PEDR produced during the Mapping Phase of the MGS mission is a large binary file containing one day's worth of data collected by MOLA. This means that it will often contain data from more than one orbit, and that the number of orbits in each file will vary between PEDRs. They are identified by the orbit number + 10000, so for example, the topography profile produced during orbit number 146 will be found in the PEDR AP10146L.B, with L signifying the software processing version and B indicating that it is binary file. L is the latest software processing version (earlier versions being signified by letters found earlier in the alphabet), and uses the latest GMM-2B gravity model. Since the MOLA laser stopped working on 30th June 2001, all the data have now been processed and older data have been re-processed with version L of the software so that a complete set of PEDRs with a consistent processing history is now available. This was not available during the time the research in this thesis was carried out.

Two other forms of data are available for use. One set is the 'gridded' data or Gridded Experiment Data Record (GEDR), which are large files in which many MOLA tracks have been compiled together to produce a global 'mesh' or grid of topography data. The orbit of MGS is polar so the descending limb of the orbit will produce a MOLA ground-track which is angled and looks diagonal on a flat map of the surface due to the rotation of the planet as MGS travels above it. On the ascending limb, the rotation of the planet will cause the ground-track to have a completely opposite angle (see Figure 2.4a on the following page) so when the ground-tracks from the ascending and descending orbits are all compiled together they cross to form a grid (see Figure 2.4b). The gridded data were used in this study because they are useful for creating contour maps and shaded topography images that can be used for mapping. There have been several versions of the gridded data, because as more MOLA data were collected a more detailed topographic grid could be produced. Grids are available at 1, 2, 4, 8, 16, 32, 64 and 128 pixels per degree resolution. The lower resolution grids are available as a single file that covers the whole surface of the planet. However, those files with greater spatial resolution have become large (requiring over 100Mbytes of computer memory) and they have had to be split up into several files, each of which covers just a part of the Martian surface.

The last MOLA data set produced was the Spherical Harmonics Aggregated Data Record (SHADR), which can be used for gravity modelling of the planet. This data set contains planetary radius values from the EGDRs that have been transformed into spherical harmonics, and can be used to provide absolute radius from the centre of mass of Mars in metres. The SHADR were not directly used in this study.

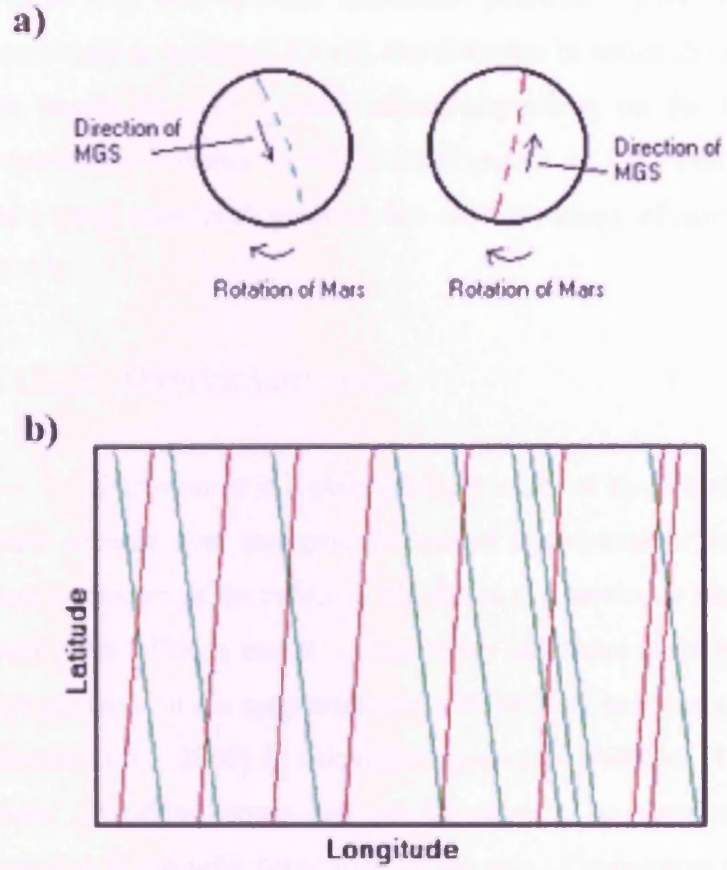

Figure 2.4: (a) The apparent direction of the ground-track of MOLA on the surface of Mars changes as MGS orbits, according to whether MGS is moving towards the north or the south poles. This means that the ground-tracks can be compiled to produce a grid of data, as the ground-tracks will cross each other as shown in (b).

Figure 4(b) also demonstrates the fact that global coverage by MOLA is not uniform, with some areas having more ground-track coverage than others.

2.13(c) Major corrections applied to MOLA data

2.13(c)i Orbit Determination

The position of the MOLA ground-track on the surface of Mars was precisely calculated by the MOLA team using the NASA GSFC GEODYN/SOLVE programmes (Rowland et al., 1993; McCarthy et al., 1994). GEODYN numerically integrates data from the spacecraft concerning its position relative to Mars with a model of the forces acting on the spacecraft by using a Cowell predictor-corrector model. The force modelling uses a spherical harmonic representation of the Martian gravity field, and takes into account point mass representations for the Sun and other planets in the solar system (except Pluto). The programme also estimates solar radiation pressure, measurement and timing biases, and tracking station co-ordinates. The accuracy of the laser footprint location in latitude and longitude is limited (as it was for the final accuracy of the surface height values) by the knowledge of spacecraft pointing (see

Figure 2.3) and absolute spacecraft position. Even with all the onboard sensors mentioned in section 2.13(a)ii, the direction in which the spacecraft is pointing can only be known to 1 to 3 mrad which, depending on the height of MGS above Mars, represents a distance of 400 to 2000 metres on the surface of the planet. The absolute horizontal spacecraft position has an uncertainty of around 100 metres (Smith et al., 2000).

2.13(c)ii Altimetric Cross-overs

A cross-over is a place on the surface of the planet where the ground-track of an orbit crosses over the ground-track of a previous orbit. This provides two sets of measurements of the radius of the planet at a particular location on the surface, one from each orbit. This is useful because there are errors in the gravity field model used in the computation of the spacecraft orbits which lead to radial errors of between 3 to 5 metres (Smith et al., 2000) in calculated spacecraft position. Cross-over observations easily show up orbital errors and can be used as an observation of the spacecraft radial position in the orbit determination process. Cross-overs can improve orbit calculations as well as providing information into dynamic processes on the planet, such as the changing topography due to seasonal removal/deposition of ice at the polar caps. Thus, as the mission progressed and more cross-overs occurred, calculations of spacecraft position improved and less error was involved in the calculation of the MOLA footprint elevations.

2.13(c)iii Overall errors

The accuracy of estimates of global topography, produced using the GEDRs, have errors inherent from the radial orbit that have a value of 0.85m RMS (Lemoine et al., 2001). There is also an instrument error of 3 metres RMS (Abshire et al., 2000), and an areoid error of +/- 5 metres RMS (Lemoine et al., 1999, 2001; Smith et al., 1999a). However, the inclusion of altimetric cross-over values has reduced these errors so that there is only a mis-match of +/- 0.96 metres for the topography at cross-over locations (Neumann et al, 2001), and therefore this represents the accuracy of global topographic models. Overall, using geolocated positions of MOLA footprints on the Martian surface (Rowlands et al., 1999; Smith et al., 1999b), the locations sampled by MOLA

are known to a horizontal position of +/- 100 metres and vertical positions are known to the accuracy of the global topographic model (~1 metres) (Smith et al., 2000). Other larger errors in the horizontal location are introduced by conversion between the MOLA co-ordinate system and the Viking co-ordinate system (this will be discussed later in this chapter), which reduce the significance of the smaller errors discussed above.

2.2 Manipulation of data

Details of the errors that were present in the data before they became available for use by researchers and the methods that were used to correct for them have been mentioned in the previous section. This section deals with the ways in which the data used in this project could be manipulated in order to make it easier to work with and analyse, and discusses the techniques used to achieve this. Any difficulties faced or further errors that were introduced during this manipulation are also discussed in this section.

2.21 Viking Images

2.21(a) Use of software

The digital Viking images stored on CD can be manipulated using a computer. Two main programmes were used in this study to do this. Viking images are saved as image files (with file extension IMG), which can be accessed using software called Nasaview. They can then be converted into GIF files for viewing in other software applications. These IMG files have been processed and map projected but the brightness and contrast of the images have not been adjusted. As a result, when they are viewed in a software application such as Adobe Photoshop (which is a programme specifically designed for the manipulation of images), many of the digital Viking images appear dark and it is difficult to determine any detail. In Photoshop both the brightness and the contrast can be adjusted. Increasing the brightness immediately lightens the whole image, and changing the contrast allows the user to make surface features in the images become more visible. Levels of brightness and contrast can be changed to highlight different features, particularly if the features are particularly bright or dark, or if they are faint in appearance.

Another useful feature of Photoshop is the ability to alter the magnification of the image. It is possible to 'zoom-in' on an image to see individual pixels if required, and is a good tool to use when examining small-scale features or surface textures of areas within an image. It is also possible to use other functions in Photoshop to join two or more images together. Although some MDIMs have been produced, sometimes there are no or only partial MDIMs covering the area of interest. In these cases a photomosaic of individual digital images must be pieced together instead. This can be easily achieved with the 'cut', 'paste', and 'layering' functions of Photoshop.

2.21(b) Errors and difficulties

2.21(b)i Digital data

Sometimes artefacts can be viewed in the digital images. They often occur as darker 'rings' or circular spots, which at first may be interpreted as buried impact craters, but as they look similar in all the images they can be easily identified as artefacts that were introduced either when the image was obtained or during processing. These artefacts can be ignored during analysis.

The joining of individual digital images, as mentioned previously, can rectify the lack of coverage of some areas in the MDIMs. However, there are some problems that may be encountered when attempting this. Firstly, the brightness and contrast of each original image varies from every other image so that when joining images it is sometimes found that the area near the edge of one image may be noticeably darker or lighter than the brightness of the next image. Careful adjustment of brightness and contrast means that a compromise between the colours of the edges of both images may be found but the effect cannot be eliminated completely. Also, the scale and spatial resolution of the individual images differs due to variations in spacecraft height and positioning, so some features such as impact craters do not fit together well at the edges of images. In some cases it is possible to adjust the size of one of the images to fit, but often the only way to solve this is to use a 'best-fit' method and try to find the closest fit possible.

Sometimes, during the collection of image data by Viking, parts of the data were lost. This is referred to as data that has 'dropped out'. It means that when some of the images are loaded up from the CDs they either contain black stripes all along them or

they are speckled in appearance with numerous small black spots. The dark areas are places where data are missing, but they can be corrected with a computer algorithm that interpolates the data in the image, thus filling in the gaps. During this study it was found that these corrected images were present in hard-copy photomosaics. However, the individual images corresponding to those used in the hard-copy photomosaics had not been corrected and when analysed in Photoshop the dark lines make it difficult to make any further interpretations. A complete list of Viking images, along with their pixel sizes and location on the planet, is available on the internet (ftp://nssdc.gsfc.nasa.gov/pub/planetary/viking/). This list could be used to find an alternative image of the same area that had not been used in the photomosaics and which often had less data missing.

2.21(b)ii Printed material

Obviously it is not possible to manipulate any of the hard-copy Viking material unless it is first scanned onto a computer. However, it is important to understand the limitations of these data because they have been used in the present study. Again, as with the digital images, there are artefacts inherent from the image processing techniques that are visible as rings or circles. These can be ignored once recognised.

The Viking photomosaics have co-ordinates on them and so are useful when trying to determine the positions of the MOLA tracks. The Viking Orbiter images all have varying resolutions according to spacecraft height, positioning and even the amount of dust in the atmosphere at the time. As such, it often happens that a line of images that have been pieced together on the photomosaic suddenly become joined to an image with lower resolution and therefore less detail. This means that some features, such as the lava flows, become hard to identify in the lower resolution images. Occasionally it is possible to find alternative images of the same area, or to find a digital version of the image used in the photomosaic and adjust the brightness and contrast to make the feature more visible. At other times it is possible to look at the SCP of the image, which has been produced from the negative, as often features are more easily visible in these. The individual Viking images also had varying scales, which means that in some places on the original photomosaics the edges of some of the images do not fit correctly. Sometimes, in comparisons between the photomosaics and the SCPs or individual digital images, small impact craters or other features have been omitted if the

images do not fit together properly. When analysing features in the photomosaics, these omissions and mismatching images can be overcome by observing the area in question in all the data formats available. It can however pose greater problems for the fitting and analysis of MOLA topographic profiles, as some features that are present in the profiles may not be visible in the images or may have different dimensions because some of the image has been omitted.

2.22 MOC images

2.22(a) Manipulation of images

As all the MOC images are digital, the manipulation of the data in Photoshop is an important part of the analysis process for using these images. All the techniques mentioned in section 2.21(a) regarding Photoshop can also be applied here. Indeed, the magnification tool is of particular use, because the high-resolution narrow-angle camera images allow small features (several pixels in size) to be analysed.

When a feature of interest had been a particular scientific target for the MOC science team, several images were taken close together, sometimes overlapping. However, no MOC image stereo pairs were produced. Generally the positions of the MOC high-resolution images are evenly distributed over the entire surface of the planet, covering about 1% of the surface. Therefore, it is rarely possible to create a mosaic of these images using Photoshop.

2.22(b) MOC footprints

An image 'footprint' is the term given to the area covered by the image. As the MOC narrow angle images cover only a small area (a few kilometres wide by several or tens of kilometres long) it was often difficult to recognise which particular area of the surface had been imaged. In order to make narrow-angle MOC image analysis meaningful, it was necessary for the MOC image team to produce a map (displayed on the internet as discussed in section 2.12(b)) to indicate the positions of the MOC footprints. A Viking base map of each Mars Chart area has been used for this, since no photomosaics of the MOC wide-angle images had been produced towards the start of the mission. However, these maps do not show much detail of the Martian surface

features in each MC area. It was therefore necessary during this study to transfer the MOC image positions shown on the internet onto a sketch map (produced from Viking photomosaics) of any area of interest so that analysis using higher resolution Viking photomosaics in combination with the higher resolution MOC images could take place. However, it could be difficult to transfer the MOC image positions because the differences between MGS and Viking co-ordinate systems (see section 2.23(a)) and map projections meant that the MOC images had to be drawn at an angle onto the Viking base map. This was made easier because the position of each narrow-angle MOC image is often indicated on a wide-angle MOC context image. However, where positions of footprints were not shown on a context image, or the context image was poor and did not show the position clearly, it was more difficult to sketch the correct narrow-angle image position. On the MOC image internet site, the co-ordinates of the centre of each image were given, which helped placing each footprint into the correct position on the base map.

2.22(c) Errors and difficulties

In Photoshop the high-resolution MOC images were too large to view in entirety at a magnification suitable for viewing individual geological features. Owing to the fact that a relatively small area of the Martian surface is shown in these images, difficulty could arise in interpreting some of the features viewed. Constant reference to Viking context images was necessary, and comparisons had to be made to other MOC images showing similar features. Difficulties also arose during printing the MOC images in their entirety at full pixel size (actual size). Reduction of the image size resulted in features becoming less defined, and faint surface textures disappeared completely in the print-out. Printing out a representative area of the image at full resolution allowed the surface texture or feature of interest to remain easily recognisable and thus enabled further analysis.

Many MOC images have a lined or streaked effect that is due to the resonance of the spacecraft. It was worse in some images than others, but did not make analysis difficult because it could be ignored. Also, there could be large areas of data missing which meant that some areas of the surface in the footprint were missing in the image and could not be analysed. These areas are rarely imaged twice during the MGS

mission so usually, if the feature was of interest for the present study, it had to be analysed from the Viking images.

One last problem was that the wide-angle MOC images generally did not show features in similar detail as the Viking ones. Therefore, even though the MOC science team had used a wide-angle image for context to show the position of a narrow-angle one, Viking images were often used within this study to provide context and to help determine the nature of surface textures and features observed.

2.23 MOLA data

2.23(a) Co-ordinate systems

The manipulation and use of the MOLA data is complicated by the fact that, since the Viking-era, the co-ordinate systems used by project scientists have changed. The fact that MGS data have a different co-ordinate system from Viking data makes the process of matching up the two data sets problematic. MGS uses the areocentric co-ordinate system (Davies et al., 1994), whereas Viking uses the areographic system. Both use the centre of mass as the origin, latitude is measured from –90 degrees at the south pole to +90 degrees at the north pole, and longitude extends from 0 to 360 degrees from the prime meridian. However, there is a difference in the way the latitude is calculated. Areocentric latitude is defined by the angle between the equatorial plane and a vector extending from the origin of the co-ordinate system to the relevant point on the surface (see Figure 2.5(a)), whereas the areographic latitudes are defined by a vector normal to a reference spheroid surface (see Figure 2.5(b)). The reference spheroids used were different for both missions, thus explaining the differences in latitude values obtained. Each latitude can be converted into the other using equation 2.2.

$$\text{Tan}\,(l_c) = (1\text{-}f) * (1\text{-}f) * \tan\,(l_g) \qquad (2.2)$$

Where: f = flattening (MGS value)

l_g = areographic latitude

l_c = areocentric latitude

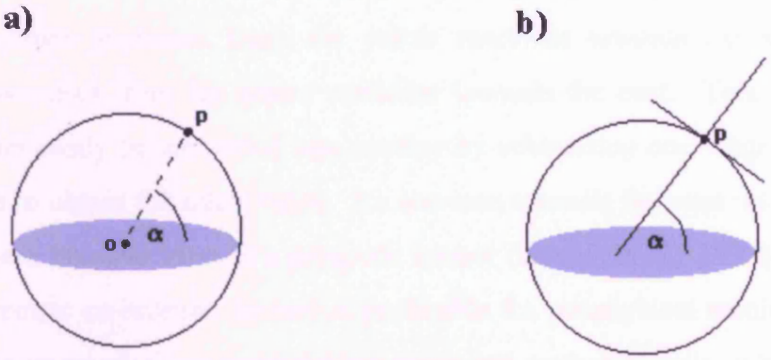

Figure 2.5: **(a)** areocentric latitude is defined as the angle (α) between the equatorial plane and the line from the centre of the body (o) to a given point (p); **(b)** areographic latitude is defined as the angle (α) between the equatorial plane and the normal to a spheroidal reference surface at the given point (p).

The reference spheroid is the standard sphere used to produce all co-ordinate values. The values used to produce the reference spheroid in both systems are given in Table 2.4. A value for flattening is used in the calculation of the reference spheroid and the need for this value can be explained in the following way. As a planet rotates, its mass will be redistributed slightly due to the forces acting on it caused by the spin. The equator of the planet will bulge outwards and the poles will flatten to compensate, meaning that the planet is no longer a perfect sphere. This is what is referred to as 'flattening'. The value of flattening for MGS is calculated as 1 – the ratio of the polar radius to the equatorial radius, which yields the value given in Table 2.4.

	MGS	**Viking**
Equatorial radius	3397 km	3393.4 km
Polar radius	3375 km	3375.73 km
Flattening	0.0064763	0.0052083

Table 2.4 Values used to produce the reference spheroid for Mars for the MGS and Viking missions.

During the Viking era, the prime meridian (the line of zero longitude) was positioned so that it crossed through the crater Airy (de Vaucouleurs et al., 1973). Later, better imaging of the crater showed a smaller ~500 metre crater inside Airy,

called Airy-0, and so the prime meridian for the MGS mission has been chosen (Duxbury et al., 2002) to cross through this smaller crater.

The differences between MGS and Viking regarding longitude are that the Viking longitude increases from the prime meridian towards the west and MGS longitude increases from the prime meridian towards the east. This means that one longitude can easily be converted into another by subtracting one longitude value from 360 degrees to obtain the other value. An increase towards the west was chosen during the Viking-era because Mars is a prograde rotator (Davies et al., 1994). However, the MGS areocentric co-ordinate system is preferable for geophysical studies where values for elevation or gravitational potential are generated mathematically, which explains the switch from areographic to areocentric for the MGS mission. Nevertheless, even though now new global data sets are being displayed on maps using the areocentric system, prior to MGS the areographic system was standard for the cartography of Mars. This means that the conversion of co-ordinates from MGS to Viking is necessary if MOLA data (and other MGS data) are to be used with older maps, images and other previous work.

On top of the conversions already mentioned, further corrections need to be carried out when converting MGS co-ordinates to Viking co-ordinates. Even after using the calculation given (equation 2.2), there is still a small discrepancy in latitude of around +/- 0.1 of a degree (about 6km on the surface) between MGS and Viking co-ordinates. When calculating the longitude there is an additional eastward offset of the Viking co-ordinates relative to MGS co-ordinates. The size of this offset ranges from 0.1 to 0.3 of a degree, which corresponds to a distance of up to ~20 kilometres on the surface. A first-order correction for this is to add 0.2 degrees east longitude to the MOLA co-ordinates in order to allow for comparisons with Viking data. Further positioning of the ground-track is necessary when fitting the MOLA data to features observed in the high-resolution Viking images, as will be discussed in a later section of this chapter. There could be several reasons for this residual offset between MGS and Viking. There could be a drift of the prime meridian due to uncertainties in the Martian rotation period. There may also be errors in the Viking spacecraft orbital position that propagated through the image processing (Smith et al., 1998). However, the main reason is probably due to a change in the IAU co-ordinate system. The geodetic constants that were used in the MOLA investigation are different from those that were used for Viking. Also, these geodetic constants have been changing as the MGS

mission has progressed owing to constant improvement of the system using new data. At the start of the MOLA investigation the geodetic constants assumed were based on the IAU 91 reference system (Davies et al., 1992), but this changed to IAU 2000 much later in the mission, and final version PEDRs have now been calculated using this system (Smith et al., 1999a).

2.23(b) Production of orbit profiles

As previously mentioned in section 2.13(b), the PEDR MOLA topography data are stored in time-ordered series on CD. The data are stored as large (~1MB in size) binary files containing continuous strings of data from successive orbits. It is therefore necessary to break down these large files into individual files each containing a single orbit, before they can be plotted meaningfully. A computer programme called 'splitorb' can be used to do this. It has been written by the MOLA science team specifically for use with the MOLA data. It is designed to run in Interactive Data Language (IDL), which is a complex piece of software that is designed to create and run programmes written in this specific computer programming language. The Splitorb programme reads one of the large binary files, splits it up into individual orbits, and writes them as smaller individual files into a specified directory on the user's computer. A single orbit is defined as a ground-track starting at the south pole (-90 degrees latitude) travelling up to +90 degrees (the north pole) and down the opposite side of the planet to the south pole again.

Once the individual orbit files have been written they can then be plotted as graphs. To do this there is a separate programme, Mprof, that is also written in IDL by the MOLA science team, which can read the smaller single orbit files and plot the information as a graph (see Figure 2.6). Once this has been done it is possible to click and drag with the mouse in order to highlight an area on the profile on which to 'zoom-in' and see more detail. It is possible to keep magnifying the view until the individual data points (individual MOLA footprints) are visible as points on the screen. After using the mouse to click and drag a highlighted box around the desired area of the profile, it is then possible to save the selected area to a separate file. This new file contains the areocentric co-ordinates of each data point in the selected area, as well as the elevation of each point. The user can then open the new file in a spreadsheet, such

as Microsoft Excel, in order to view the data and manipulate it to produce graphs for analysis.

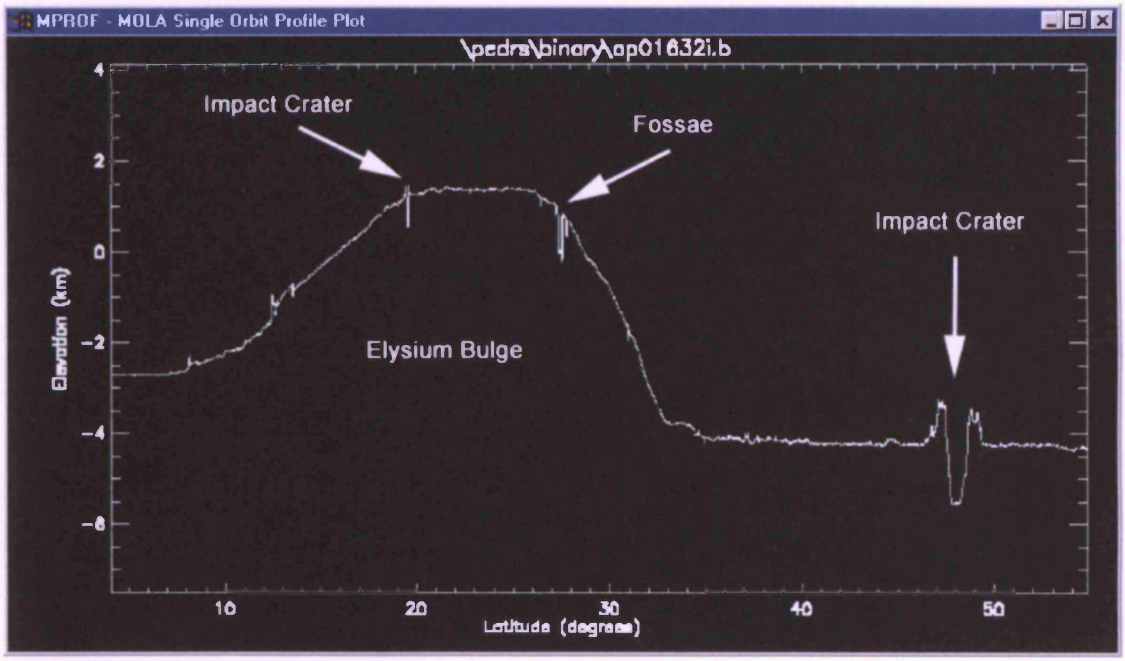

Figure 2.6: Plot of MOLA data produced in IDL using the programme Mprof. The plot shows part MGS orbit number 01632. The area covered in this plot is part of Elysium. The Elysium bulge is clearly visible, as are some of the Elysium Fossae (labelled). Two prominent impact craters can also be observed.

2.23(c) Determining the positions of MOLA ground-tracks

2.23(c)i Finding orbits in a specific area

Obviously, when studying a particular area on a planet, it is only necessary to have data just for that area, particularly when dealing with a data set that is as large as that produced by MOLA. It would therefore be useful to have a computer programme that searches through all the MOLA data and makes a list of only those orbits covering the area within co-ordinates specified by the user. At the start of this study programmes that did this were not readily available. However, eventually the programme Molacov became available. It runs in UNIX and allows the user to remotely access a database containing data from all the MOLA orbits ever produced. It scans the data for only those co-ordinates specified by the user and then produces a list of all the orbit numbers

of interest. Clearly this greatly speeds up the process of producing useful orbits for analysis.

2.23(c)ii Mapping of orbits

When using MOLA to study particular features in an area, it is necessary to know the position of the ground-track as accurately as possible. Once the data from the orbits covering the desired area of Mars have been obtained (as outlined in the previous section), the co-ordinate values for each separate orbit can be viewed in Excel. In this study, the areocentric latitude values in the file produced by Mprof were converted to areographic using equation 2.2, and areocentric longitudes were subtracted from 360° to give an approximate areographic longitude. These converted co-ordinates could then be drawn onto a tracing paper overlay on top of the photomosaic of the area of interest, to give an approximate position of the orbit ground-tracks. Once all ground-tracks were drawn, the tracing overlay could be shifted by 0.2° eastwards as a first order correction for conversion from MGS longitude to Viking longitude. This improved the approximate positioning of the ground-track to within +/- 0.1° longitude. If specific features on the image were being studied then it was easier at this stage to see which orbits were most likely to cross the feature once the orbits were accurately fitted. This was important because the profiles of those orbits that crossed the feature of interest needed to be printed out to scale, so to save time it was necessary to know which orbit profiles would be useful, and which ones were no longer of interest. Only once the profiles were printed out could the orbit ground-tracks be correctly positioned, as explained in the next section.

2.23(c)iii Matching profiles to photomosaics

The desired orbits were plotted in Excel, with latitude on the x-axis and elevation on the y-axis. The length of one of the ground-track tracings was measured and the x-axis was enlarged to match this length. This allowed for features to be easily seen when the print-out of the profile was laid next to the corresponding ground-track tracing. The scale on the y-axis was exaggerated to make features obvious enough to be readily identifiable. If the profile had been printed out to scale then it would not have

been possible to see some of the smaller topographic features. However, if the scale was exaggerated too much then it became difficult to fit parts of the profile to features observed in the image. This was because some features in the topography profile could not be observed in the image (due to the limit of the resolution), and sometimes shadows in the image contorted the way features appeared so that they did not seem to fit the topographic profile. It was found that a vertical exaggeration of between x10 and x20 was a suitable amount to allow the profiles to be matched up with the images easily. It was difficult to measure the exact lengths of the graphs in Excel so they were imported into Photoshop and the lengths of the axes were changed there before the profile was printed out.

Once a profile was printed out it was laid next to the corresponding ground-track tracing and then shifted around (usually to the east and to the north slightly) until features on the print-out matched those observed in the image. Useful features for matching up profiles were impact craters, graben or channels, as these were obvious in both the topographic profiles and the images. Sometimes no easily recognisable features were present in the profiles, particularly if the area measured by MOLA was smooth, and they were difficult to position accurately. It was therefore usual to find three or four profiles with recognisable features that could be fitted first, in order to obtain a value by which to shift all the ground-tracks so that they were then in their correct positions on the image. Once the ground-tracks were in the correct positions it was usually easy to see the less obvious features like thin lava flows, even in the smoother profiles. Nearly all the ground-tracks in a specific area, such as within the space of one high-resolution photomosaic (5° square), needed to be shifted by the same amount. Occasionally one or two needed to be shifted further as they were still found to contain features that did not fit the photomosaic. The amount the ground-tracks needed to be moved by overall (before first-order corrections) was found to range between 0.15° and 0.3° longitude, and this value varied at different locations around the planet. It was also found that the latitudes were still mismatched even after converting them using equation 2.2. Usually profiles needed to be shifted upwards relative to the Viking photomosaic by a value of $< 0.1^{\circ}$. After determining where a particular feature of interest was on the printed profile (and therefore on the graph in Excel) it was possible to go back to the data in Excel and start to analyse it

2.23(d) Gridded data

The individual profiles were not the only way the MOLA data could be used for analysis. As mentioned in section 2.13(b) all the MOLA profiles can be combined to produce a 'grid' of data that can be used to produce Digital Elevation Models. A programme called Gridview was written specifically by scientists in the USA for the viewing and manipulation of the gridded data in IDL. It can be used to produce shaded topography, and gives the ability to change the lighting conditions and colour shading to alter the view, to produce contour maps and also to produce topographic profiles (although these are not as highly detailed as those produced by Mprof), amongst other tools. IDL can also be used to produce Digital Elevation Models using MOLA, although the programme 3DEM can also be used to do this too, more easily and with better results. A Digital Elevation Model (DEM) is a virtual view of a landscape where the computer plots the data three-dimensionally so that it is possible to visualise the landscape. It is possible to exaggerate the scale of the elevation to make smaller scale features more obvious. Clearly, when mapping an area, particularly one that is too remote for fieldwork, tools like these are highly valuable. The EGDRs (or 'gridded data' have also been shaded by MOLA scientists to produce shaded topography images of all the Mars Chart areas, and these are also useful for mapping and understanding the geology of Mars. They are available to download from http://valles.wr.usgs.gov/mcmolashaded/.

2.23(e) Errors in results produced using MOLA data

The error inherent from spacecraft positioning uncertainties and instrument delays means that the horizontal position of MOLA footprints on the surface is known with an accuracy of +/- 100 metres. However, further error is introduced when the ground-track is drawn onto the tracing overlay, since the starting and finishing co-ordinates of the ground-track can only be drawn with a ruler, the smallest accurate measurement being +/-0.5 mm on the tracing (~250 metres on the surface). After this there is also the shifting of the ground-track tracing to fit features observed in the images to those observed in the profile, as this is done by eye there will be a further error of +/- 0.5mm. The total horizontal error therefore is +/- 600 metres.

The vertical accuracy is ~1 metres, which means that the position of the MOLA footprint in relation to the centre of mass of Mars is known to within 1 metres. However, since MOLA is being used in this study to measure elevations of features relative to each other, rather than in order to obtain heights, depths and thicknesses of features, it is more important to consider the precision of the MOLA measurements. Also, regional errors in vertical accuracy over relatively small areas such as those considered in this study will not vary greatly and can therefore be considered to be constant. As mentioned in section 2.13(a)ii, MOLA has a precision of 37.5cm on smooth, level surfaces, which means that if a MOLA footprint landed on exactly the same place on low slopes (several degrees) on the surface of Mars it would return two values that were within 37.5cm of each other. On steeper surfaces with slopes of ~30^{o} the precision could change to ~10 metres. In this study slopes rarely exceed 3^{o}, so it is assumed that the MOLA data points used for analysis in this study are precise to 37.5cm. In which case, the maximum error on a height or thickness measurement (between two MOLA points) is taken to be +/- 37.5cm.

3.0 Narrow-angle MOC Image Analysis

3.1 Introduction

One of the main aims of the MOC image analysis was to observe small-scale features and textures in the images that could be related to those found on Earth. This should provide information regarding the type of environment present, and the processes that were occurring when these features formed. This was intended to aid the mapping of Elysium, as presented in Chapter 4. A particular emphasis is placed on periglacial features, since these will indicate the presence of ground-ice and would be an important finding for both the mapping and lava flow studies presented in this thesis. The surfaces of lava flows were also analysed because this may indicate the style of flow emplacement and complement the lava flow study that is described in Chapters 5 and 6. In the highest resolution images it is possible to resolve features such as boulders that are tens of metres in diameter, so it was expected that many interesting geological features would be found within the mapping area in this study.

Several different types of features are analysed that, collectively, highlight the geological processes occurring in the areas discussed in this chapter. Image analysis was carried out to a greater extent in the Elysium mapping area because analysis of images of this area should help to characterise units and thus enhance the information gained from the mapping, as well as indicating the positions of some of the less obvious unit boundaries. Since the main emphasis of this study is on volcanic processes, a section of this chapter has been devoted to the volcanic features observed. During image analysis it was found that lava flows in older areas have been highly modified over time and so the flows found on the flanks of several Martian volcanoes of varying ages were studied to determine how lava flows become modified over time on Mars. Also during image analysis much evidence was found to support the idea that many different surface processes still occur on Mars and so features that show this have been discussed.

3.2 Methods

The main method used in this chapter was photogeological analysis. This is the method used to study the geology of a region that is inaccessible for

fieldwork, it is therefore a useful technique for terrestrial geologists in addition to being an important tool for planetary geologists (Wilhelms, 1990). It is the method used to determine the number and characteristics of units present in that area. It involves studying images of the surface of the area of interest to look for features and surface textures that will help to piece together the geology of the area. In this study there were several different types of images available, and these were all used during the mapping carried out during this study (see Chapter 4). The focus of this chapter is the MOC images, which can be used to analyse smaller-scale features with widths of several metres. In many cases it was possible to find images of terrestrial features that looked similar to those features found in the images of Mars. These 'terrestrial analogues' are of great use in studies of this kind. If the process for the formation of a certain terrestrial geological feature is known, then if a feature looking similar to this is found on another planet it is possible to infer the same mode of formation for that feature. In this way, the geological history for a remotely-sensed area can be determined. In this study aerial photographs of various volcanic, periglacial and desert features were available for comparison with the MOC images, since it was thought that these were the most likely features that would be observed. Terrestrial analogues for observed Martian features have been included wherever possible. In addition to this, it was also useful to produce sketch maps of several of the MOC images, as this helped to highlight and identify the presence of many different features and evidence for different processes occurring in an image. Where terrestrial analogues were not found, suggestions for the formation of the observed features have been put forward.

3.3 Volcanic Features

Analysis of the high-resolution MOC images shows that the scale is not sufficient to expect to see detailed surface textures of lava flows such as rubble on the surface of aa flows, or the ropy appearance of pahoehoe flows. However, initially it was thought that analysis of these images would reveal decametre-scale features associated with lava flows (such as tumuli, inflation pits and rises if they are present) and should clearly show channels and levées even on lava flows smaller than those studied in Chapters 5 and 6. It was also expected, particularly in Elysium and at Alba Patera (as mentioned in the previous chapter), that lava/ice (water) interactions might be visible, such as pseudocraters and also deposits formed by explosive activity.

Unfortunately, further analysis showed that the level of dust cover on the Martian surface greatly exceeded the expectations of the author and further reduced the potential to see small (on a scale of several metres) surface features. Little evidence for small-scale surface features other than channels and levées was found, although possible pahoehoe inflation features were observed in places, as detailed later on in this chapter. The substantial dust cover was found to be more marked in the more ancient areas of Mars, or where there has been extensive explosive volcanic activity. It was therefore expected that dusty deposits would modify the appearance of the lava flow surfaces and so the MOC images were analysed to determine the scale of modification/erosion, and their changing appearance over time. This was carried out by making comparisons between Hecates Tholus, Elysium Mons, Alba Patera, and Olympus Mons, which have volcanic surfaces of varying ages, as will be discussed later. During analysis of the images it was also found that some of the unit boundaries could be identified, and this information was used to refine the maps that are presented in Chapter 4.

An analysis of the flows from four different Martian volcanoes is now given. The different volcanoes studied were Hecates Tholus, Elysium Mons, Alba Patera and Olympus Mons. The different ages of the volcanoes and their positions on the surface of Mars are given in Figure 3.1. The analysis starts with Olympus Mons since this is the youngest of the four volcanoes and all features observed here were more easily recognisable since they have undergone the least modification.

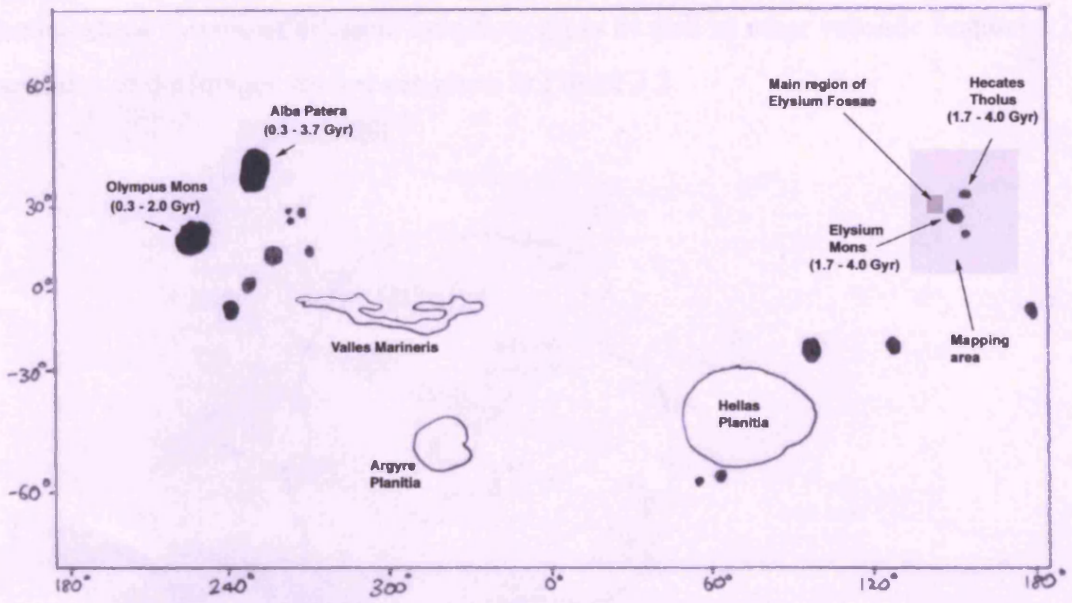

Figure 3.1: Sketch map of Mars showing the positions of the volcanoes studied in the image analysis section of this thesis. The age of each of the volcanoes is given in Gyr. The other major volcanic centres in Mars are shown as unlabelled shaded features. The two shaded rectangular areas in Elysium show the position of the main mapping area (see Chapter 4), and the area covered with the highest density of Elysium Fossae.

3.31 Olympus Mons

The volcano Olympus Mons is a vast edifice that rises 23 kilometres above the surrounding plains and 27 kilometres above the zero elevation level (as measured by MOLA during this study), and has a diameter of around 600 kilometres (Cattermole, 1996). It is surrounded on all sides by a scarp that can reach up to 6 kilometres high in places (as measured by MOLA also during this study), and outside the scarp is a region of blocky and ridged terrain that has been termed the 'aureole'. The formation of both the scarp and the aureole has been a subject of much debate since they were observed in the spacecraft images and various mechanisms for the formation of these features have been put forward, involving volcanic, tectonic or mass wasting processes (Carr, 1973; King and Riehle, 1974; Blasius and Cutts, 1976; Harris, 1977; Hodges and Moore, 1979; Lopes et al., 1980; Morris, 1982; Francis and Wadge, 1983; Tanaka, 1985). It is the youngest of the volcanoes that will be discussed in this chapter, and as such it is expected that MOC images of this volcano should show the highest numbers and clearest images of lava flows, compared to MOC images of the flanks of the other

volcanoes studied. Indeed this was found to be true, and the images studied in this section show a range of different lava flow types as well as other volcanic features. The positions of the images studied are given in Figure 3.2.

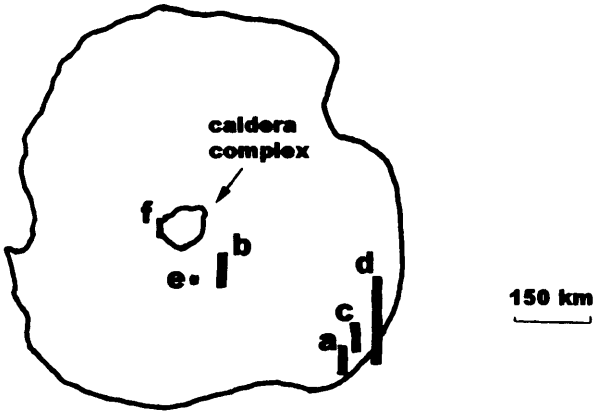

Figure 3.2: Sketch of Olympus Mons showing the general shape and size of the volcano, and the position of the central caldera complex. The green rectangles represent the areas covered by high-resolution MOC images where **a** is the position of MOC image M15-01548, **b** is the position of M08-00065, **c** is M07-02112, **d** is M04-01222, **e** is SP1-20806, and **f** is SP2-35605.

Some MOC images of the summit of the volcano showed areas covered by well-defined sheet flows. The sheet flow shown in Figure 3.3 appears to have been erupted from a summit vent on Olympus Mons, the vent having long since been destroyed by a caldera collapse event. Slightly further out from the caldera complex however, yet still on the summit of the volcano, there is a lack of well-defined lava flows. The surface appears to be heavily mantled with dusty materials, and in places shows many aligned ridges. Analysis of the surface textures of the summits of the other volcanoes mentioned all display areas covered by aligned ridges similar to those found on Olympus Mons and also a similar level of mantling by dusty deposits. It is curious that the summit region of Olympus Mons should be appear to be mantled by as much loose, dusty material as the other volcanoes discussed when Cattermole (1996) states that there is no evidence for the presence of pyroclastic deposits anywhere on the shield. Also Olympus Mons is thought to be younger than the other volcanoes in this section (Plescia and Saunders, 1979; Neukum and Hiller, 1981) and should therefore show a sparser

covering of aeolian materials if the deposition rate is constant for the surfaces of all the volcanoes. The lava flows are more easily observed further out from the summit towards the middle flanks and particularly near the basal scarp. It seems unlikely that deposition of aeolian deposits would preferentially occur at higher elevations, particularly as the summits of the larger volcanoes often lie above the global dust storms or are the first places to emerge from them (as shown in the Mariner 9 image, Figure 1.3). One possible explanation for the large volume of material observed on the summit of Olympus Mons in this study, is that the caldera collapse events that occurred after the extrusion of the summit lavas may have mobilised much loose material that has been deposited on the main summit area.

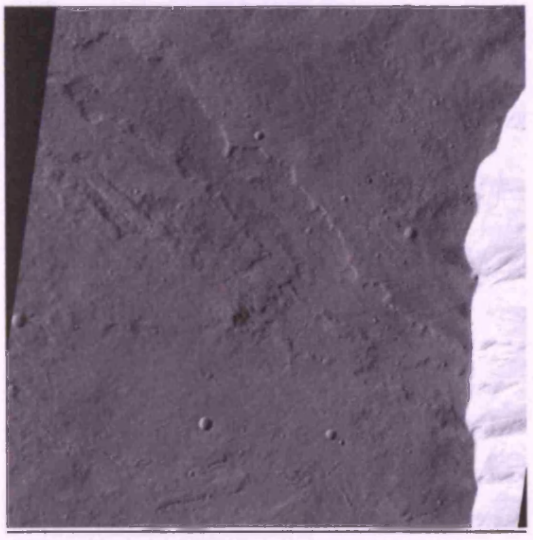

Figure 3.3: Part of MOC image SP2-35605 of the western edge of the Olympus Mons caldera complex. A sheet lava flow can be seen to have flowed diagonally from right to left across the image. The bright feature to the right-hand side of the image is the edge of the caldera, the cliff-face can just be seen, and it is clear that this flow was emplaced before the collapse of the caldera, since it continues from the very edge of the caldera. The area shown in this image is 7.86 kilometres in width.

One image of the outer summit/upper middle flank area shows a channel feature that appears to have a source depression (see Figure 3.4). This is similar in appearance to terrestrial volcanic craters that are the source for lava flows (see Figure 3.5). Analysis of the image in Figure 3.4 shows that the channel appears to have levées along either side. Since the surface texture of the area shown in this image is dominated by raised linear features, it is postulated in this study that they may therefore be older, partially buried levées from channels emanating from volcanic craters. Such linear features may be the precursor to the lines of ridges observed at the older volcanic sites of Elysium Mons, Hecates Tholus and Alba Patera.

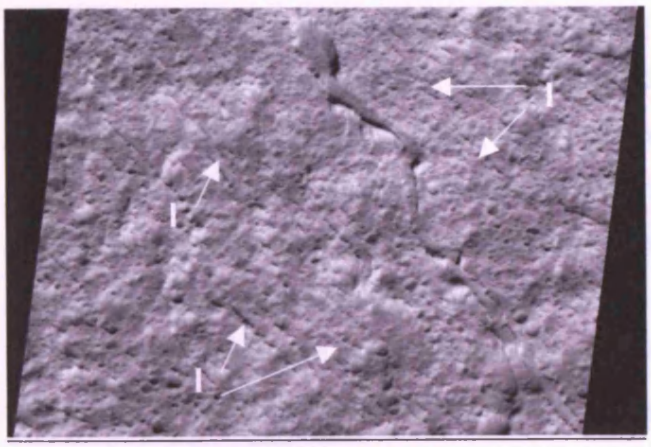

Figure 3.4: MOC image SP1-20806 showing a channel feature that leads from an elliptical depression towards the top of the image. Many linear features can also be observed in this image (l), and may be ancient buried versions of the prominent channel feature discussed above. This image is 2.53 kilometres in width, north is towards the top, and the scene is illuminated from the lower left.

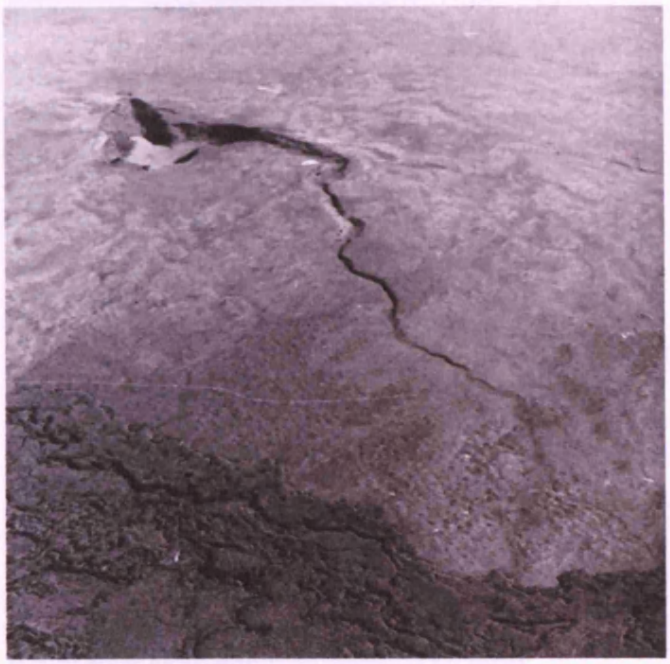

Figure 3.5: Oblique aerial photograph of Bear Crater and associated lava channel, part of the Bear Butte shield volcano, Idaho. The crater is 60 metres deep, and the whole feature bears a striking resemblance to the feature found on the upper flanks of Olympus Mons. Photo is taken from Greeley and King (1977).

The middle flanks of Olympus Mons seem to be characterised by compound flow fields rather than the individual simple flows found close to the caldera. Many of the images are similar to the images of compound flow fields observed on the upper flanks of Elysium Mons shown later in this chapter. Figure 3.6 shows a typical example of the appearance of the flows found on the middle flanks of Olympus Mons. Many of the flows have levées or clearly defined boundaries. It is proposed in the present study that over time these features become buried by aeolian materials and then partially eroded by the wind. It is likely that, subsequent to this modification, they form the typical linear features, hummocky texture and aligned hills seen in many of the images of the surfaces of the other volcanoes studied in this chapter. It is proposed that owing to the relative youth of Olympus Mons compared to other large volcanic edifices on

Mars (see Table 1.2, Chapter 1), it is possible to see the surface texture before much burial and erosion has taken place. Further evidence for this is seen in Figure 3.7, which shows a high-resolution MOC image of the surface of Olympus Mons near the basal scarp that reveals partially buried lava flows. The levées of the flows are still visible, but other parts of the flows have been buried and some yardangs are starting to form. Yardangs are streamlined hills that are formed by wind erosion of less resistant areas of rock (see Figure 3.33). Since they are one of the major features visible on the flanks of the older volcanoes, their formation is discussed later in this chapter.

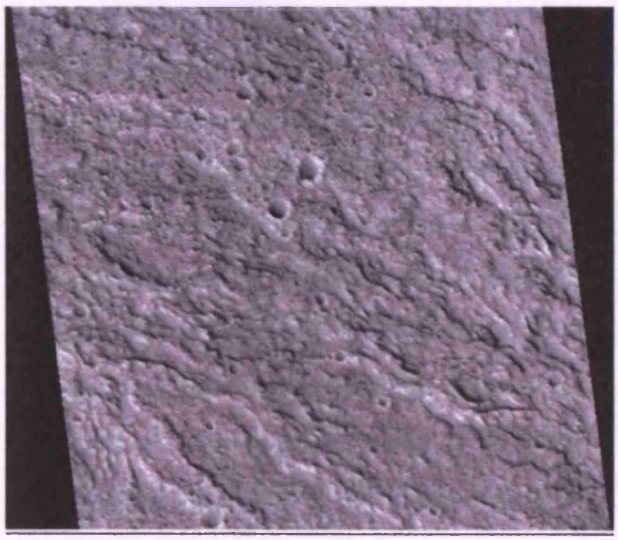

Figure 3.6: Part of MOC image M08-00065, which is a sample of the middle flank of Olympus Mons. It shows some levéed flows within a compound flow field. Flows found here are similar in appearance to those found on Elysium Mons, particularly around the summit. The flows are heavily cratered with impacts and are not so clearly defined as those found close to the caldera or out near the basal scarp of the volcano. This image is 3.03 kilometres in width, and north is towards the top and it is illuminated from the lower left.

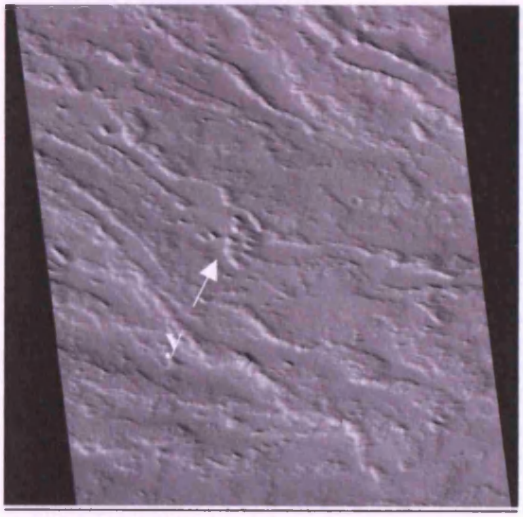

Figure 3.7: showing part of MOC image M07-02112. The dust-filled channels of lava flows are visible. In some cases only the tops of the levées remain uncovered. These levées could be the precursor to linear features and hummocky terrain visible on the flanks of the older volcanoes. An area of yardang-like features has already formed in the centre of this image (**y**). The image width is 3.03 kilometres, north is towards the top, and is illuminated from the lower left.

Individual lava flows are more numerous in these images than in the images taken of any of the other volcanoes in this chapter. This is probably best illustrated in the images taken of the area around the basal scarp of Olympus Mons, where the flanks of the volcano abruptly change into the surrounding plains. Lava flows traverse the scarp and flow from the lower flanks of the volcano out onto the surrounding plains. Perhaps owing to the differing underlying slopes here, several types of lava flow are observed, and flow fields here are different to those found on the middle flanks of the volcano. Figure 3.8 shows an example of the many narrow, levéed flows found in this area, some of which flow along the top of ridges that have built up. Where lava flows move onto the shallower slopes of the surrounding plains they tend to spread out, and sometimes the channels disappear in favour of flat-topped sheet flows. In places flows appear to become thicker and wider, and exhibit pressure ridges along their surfaces (see Figure 3.9), which look similar to more silica-rich, viscous flows on Earth, such as those found at Big Glass Mountain in the USA (see Figure 3.10). It has been proposed by several planetary geologists that such flows are the result of rhyolitic, dacitic or trachytic flows (Fink, 1980; Zimbelman, 1985; see Chapter 1), and they have attempted to determine the viscosity of the lava using the spacing of the festoon ridges on the surface (Fink and Fletcher, 1978; Fink, 1980; Theilig and Greeley, 1986). However, according to the work of Theilig and Greeley (1986), as discussed in Chapter 1, such flows do not necessarily have these compositions, and thus these MOC images do not prove that the lavas of Olympus Mons were more evolved than those of the other volcanoes discussed here.

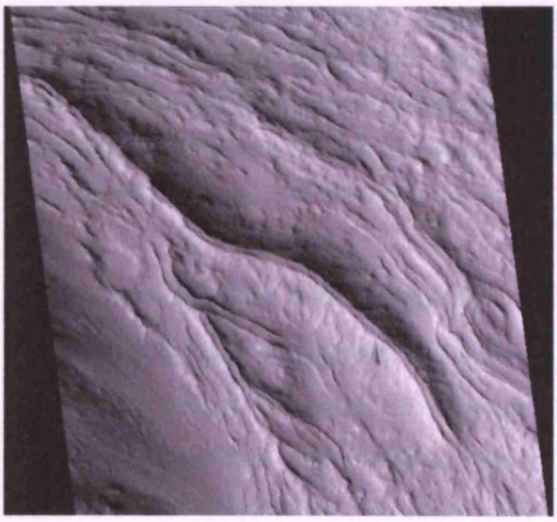

Figure 3.8: Part of MOC image M15-01458 showing lava flows on the Olympus Mons south east basal scarp. The image shows many narrow levéed lava flows, the most obvious having flowed on top of a ridge, the direction of flow being from top left to bottom right in this image. The image is 2.26 kilometres in diameter, north is towards the top, and is illuminated from the lower left.

Figure 3.9: Shows part of MOC image M04-01222 of large, thick lava flows at the base of the Olympus Mons basal scarp. They appear to have flowed with central channels, but also show festoon ridges where pressure against forward movement of the flow has forced the lava to 'fold' into arcuate ridges. The direction of flow is from left to right, and north is towards the top. This image is ~2 kilometres across the top.

Figure 3.10: Aerial photograph of Big Glass Mountain, California, USA. It is a rhyolite obsidian flow complex exhibiting steep flow fronts, rugged relief surfaces, stubby flows and festoon ridges. This is typical of terrestrial silicic block flows. There is some similarity between these flows and some of those found at the base of Olympus Mons, such as those shown in Figure 3.30, indicating that the Martian flows may also have a silicic composition (see text). Image is taken from Greeley and King (1977). This image covers an area of approx. 3.75 kilometres across.

As mentioned at the beginning of this section, many different explanations have been given for the formation of the basal scarp around Olympus Mons and for the surrounding aureole material. It is thought that the scarp face transects a broad pedestal of pre-shield material, about which little is known (Cattermole, 1996). An image of the scarp face was analysed in this study, and it was found to exhibit layering of rock units

(see Figure 3.11). The material appears to be easily erodible because scalloped sections occur that appear to be the source of aprons of loose material directly below. This layering may just have been formed from the build-up of different lava flows. However, one of the ideas for the formation of Olympus Mons is that it grew as a composite volcano, with alternating lava and ash deposition (King and Riehle, 1974). This could explain the layering seen, with each layer representing a different eruptive event, as well as explaining the easily erodible nature of some of the materials that are producing the apron of loose material observed in the image, and perhaps closer to the summit. Alternatively, gravity-assisted rockslides have been invoked for the production of the Olympus Mons scarp and aureole (Lopes et al., 1980), which would require facilitation of movement by the presence of a ground-ice layer in the pedestal of pre-shield material. This would involve the pedestal material being made of brecciated or porous material (Cattermole, 1996) such as volcanic ash or tuff. The nature of the layering in the MOC image in Figure 3.11, as well as the easily erodible nature of the material would seem to fit this theory. Since substantial pyroclastic activity is thought to have occurred during the formation of Alba Patera (Mouginis-Mark et al., 1988; see Chapter 1), Olympus Mons may have had a similar history. Therefore, although some previous workers such as Cattermole (1996) discount substantial pyroclastic activity at Olympus Mons, the evidence observed in the high-resolution MOC images indicates that pyroclastic activity has occurred here in the past. This would therefore be responsible for the formation of the more easily erodible layers observed in the walls of the scarp and also for the ease of formation of yardangs, and it would help to explain the presence of much 'dusty' material on the flanks of this relatively young volcano.

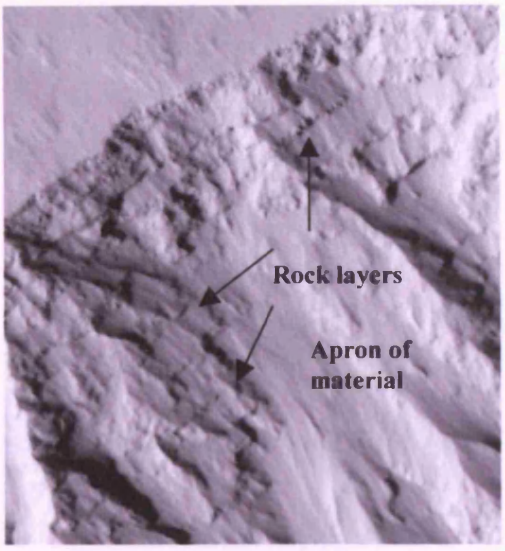

Figure 3.11: Part of MOC image M07-02112 showing an area of the basal scarp of Olympus Mons. Several layers of rock units, each approximately tens of metres thick, can be observed in the walls of the scarp. Material appears to be quite easily erodible since an apron of loose material descends from the layers in the centre of the image. The image is ~1.5 kilometres across, and north is towards the top.

3.32 Alba Patera

Alba Patera is thought to have had a long geological history that started before the growth of both Elysium Mons and Hecates Tholus (Plescia and Saunders, 1979; Neukum and Wise, 1976; Hartmann, 1978; Neukum and Hiller, 1981; Scott and Tanaka, 1980,1986; Cattermole, 1990), and the eruptive episodes occurring at the summit of this volcano are thought to have occurred after effusive activity (though not explosive activity) at both Hecates Tholus and Elysium Mons ceased (Neukum and Hiller, 1981). Therefore, even though it is older than Olympus Mons high-resolution MOC images of the summit should still reveal relatively fresh-looking lava flows amongst other surface textures. Several images that are representative of the surface textures observed here are discussed in this section, and the positions of the areas imaged are shown in Figure 3.12.

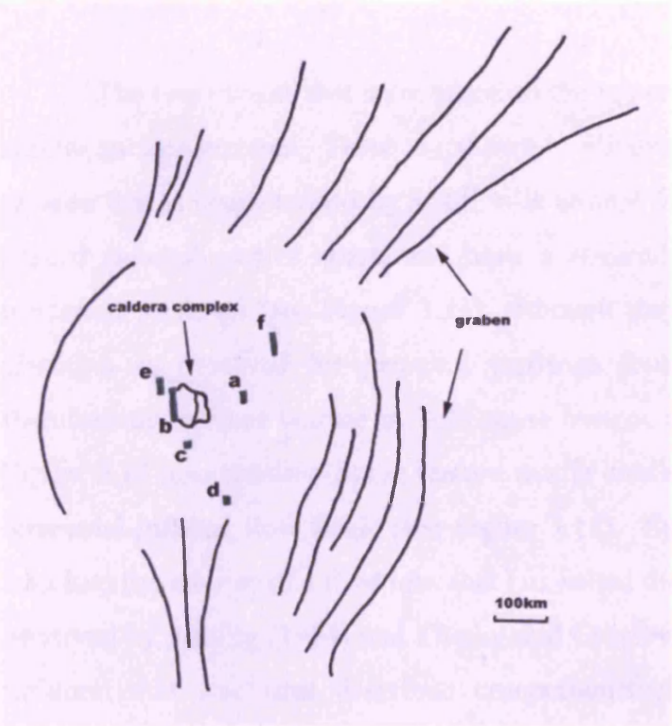

Figure 3.12: sketch of Alba Patera showing the general shape of the volcano, positions of the major graben system surrounding the summit, and the position of the central caldera complex. The green rectangles represent the areas covered by high-resolution MOC images where **a** is the position of MOC image M13-01041, **b** is SP2-46804, **c** is SP1-21004, **d** is M04-00803, **e** is M08-06317, and **f** is E10-02733.

Surprisingly, no clear images of individual lava flows were found, and the images reveal surfaces covered with much loose material and which are similar in appearance to those images found of the summit areas of Olympus Mons and the older volcano Hecates Tholus. The image of part of the caldera (Figure 3.13) shows a 'hilly' appearance inside the depression of the caldera (similar to a texture observed at Hecates Tholus), and then a hummocky texture of the surrounding flanks, possibly due to dunes or yardangs.

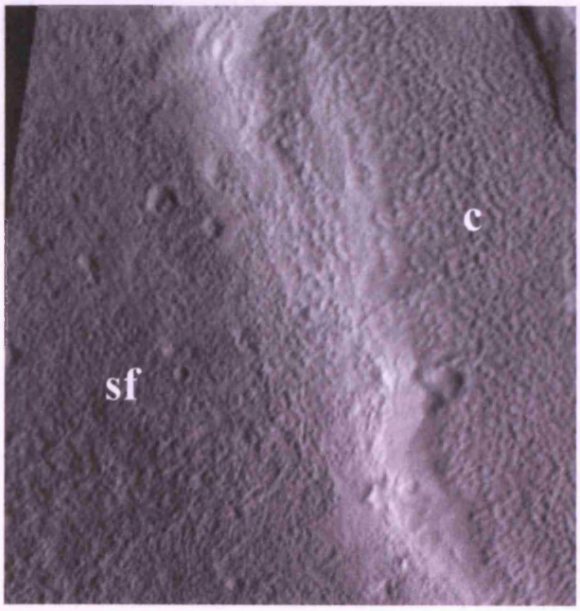

Figure 3.13: Part of MOC image SP2-46804 showing the western edge of the caldera complex on Alba Patera. It shows similar hummocky material in the caldera to that found in the caldera (**c**) of Hecates Tholus, and also yardang features outside of the caldera on the summit flanks (**sf**), as also observed in the MOC images of Hecates Tholus. The image is approximately 2.3 kilometres across.

The two images that were taken on the upper western flanks of the volcano have similar surface textures. These are shown in Figures 3.14 and 3.16. Both images show an area that is characterised by small hills around 50 metres in length, that are closely spaced (several metres apart) and have a streamlined appearance similar to that of terrestrial yardangs (see Figure 3.33), although they are not aligned in one particular direction as observed for potential yardangs found at Hecates Tholus. Although therefore the surface texture in both these images is probably due to aeolian activity, Figure 3.14 also shows a linear feature that is similar in appearance to ridges found in terrestrial inflated flow fields (see Figure 3.15). Such ridges form by the injection of lava into the interior of a flow lobe that has halted due to cooling of the flow margins, as observed by Theilig (1984) and Theilig and Greeley (1986), during the process of flow inflation that was later described comprehensively by Hon et al. (1994). Thus, depending on how much aeolian material is thought to be present here, it is possible that these images are showing possible inflated flow surfaces. It has been inferred by Mouginis-Mark et al. (1988) that this volcano did undergo pyroclastic activity at some time in it's evolution, and these types of events may account for a large volume of loose or easily erodible material in this area.

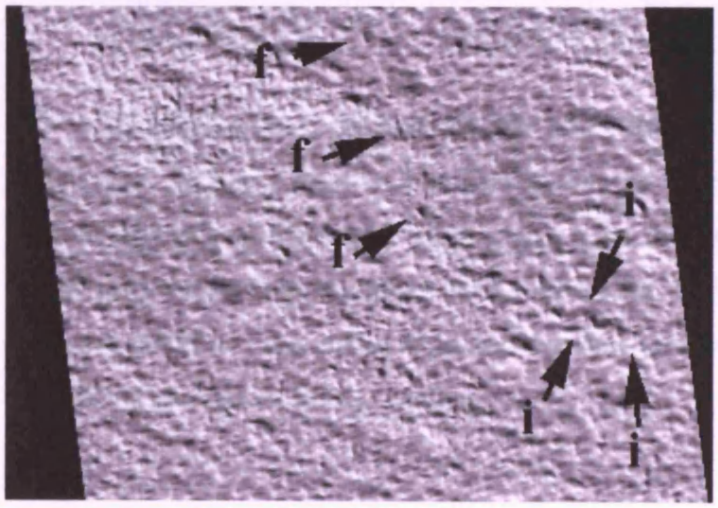

Figure 3.14: Part of MOC image M08-06317 showing linear arrangements of hummocks similar to those seen on the summit of Hecates Tholus. These hummocks may be the result of wind erosion of soft deposits (deflation), but the aligned feature indicated by **f** (fissure) and **i** (inflated ridge) may have volcanic origins similar to the terrestrial inflated ridge shown in Figure 3.19. Image width is 1.58 kilometres. The scene is illuminated from the lower left.

Figure 3.15: Part of the Wapi flow field in Idaho. This flow appears to have undergone inflation after initial emplacement, to form pressure ridges **(r)** and plateaus **(pl)**. Image width is 1.3 kilometres, and is taken from Greeley and King, 1977. The scene is illuminated from the top right.

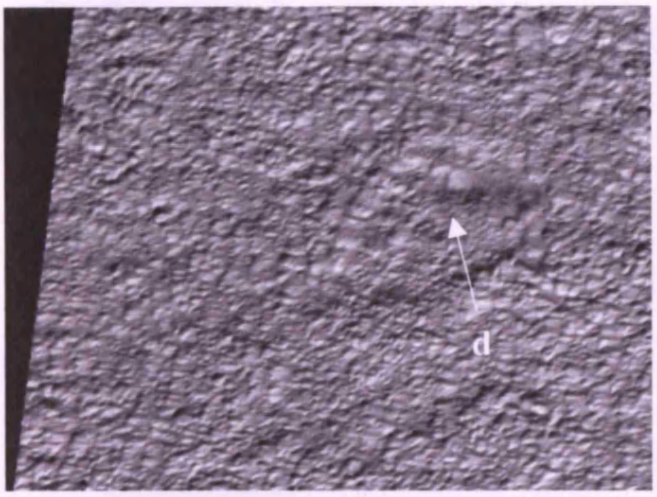

Figure 3.16: Part of MOC image SP1-21004. This image shows part of the upper flanks of Alba Patera (see Figure 3.16 for position). It shows more hummocky terrain that are possibly deposits of dusty material. Part of the area (centre right) looks as though it may be filling a depression **(d)**. Max width at bottom of the image ~1.1 kilometres. The scene is illuminated from the lower right.

Further out from the summit, the MOC images of Alba Patera show a 'pitted' appearance. There is an overall surface texture of muted aligned small hills but within this are depressions filled with what appear to be yardangs (see Figures 3.17 and 3.18). These depressions may represent places where the surface materials are softer, or less well consolidated. This pitted appearance is also seen at the summit of Hecates Tholus, particularly in and around the caldera.

Figure 3.17: Part of MOC image M13-01041 showing the two textures typical of many of the MOC images of the outer summit area of Alba Patera. A typical linear- ridged surface texture can be observed, interspersed with depressions displaying a pitted appearance. The image width is 1.5 kilometres across at the bottom. Loose, dusty material is visible in the prominent crater to the bottom right.

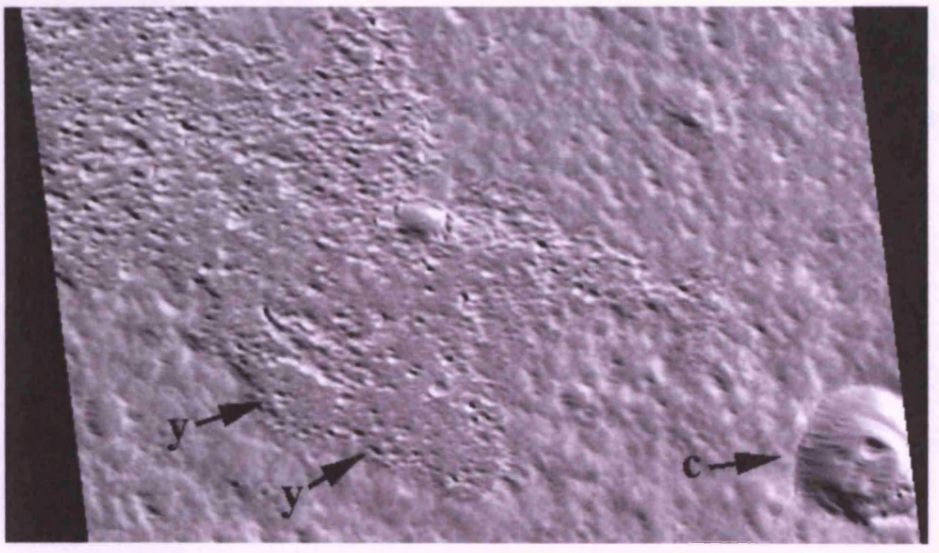

Figure 3.18: Part of MOC image M04-00803 of the southern outer summit area of Alba Patera. It shows a depression, similar to the ones shown in Figure 3.21 that are at a lower resolution, filled with what appear to be yardangs (y), due to their alignment and typical streamlined appearance. The floor of the impact crater (c) to the right also exhibits several large yardang features, the largest of which is ~60 metres in length. Total image width is 1.57 kilometres.

Since many well-defined lava flows can be observed on the summit of Alba Patera in the Viking images, it is surprising that few lava flows were found in the MOC images of this area. However, one of the few images studied that did show a lava flow is shown in see Figure 3.19. It shows part of the outer summit area of the volcano, and appears to show the boundaries of a lava flow, and also a sinuous rille feature. This lack of lava flows in the MOC images may indicate that only large lava flows several to

tens of kilometres in both width and length are now visible on the upper flanks of this volcano. Larger flows would not be visible in a single high-resolution MOC image unless just the boundary of a flow was captured, and may explain why none were found. This does not necessarily mean that only large lava flows were erupted from the central vents of Alba Patera, but may indicate that any smaller flows have since been obscured by younger, probably aeolian, materials.

Figure 3.19: Part of MOC image E10-02733 showing possible flow edges or boundaries (b), and a sinuous rille-type feature (s). The underlying 'aligned ridges' surface texture is still present, and there is still much loose material present as evidenced by the deposits in the impact crater in the centre of the image. This image is 3.33 kilometres in width.

The surprising finding that the summit region of Alba Patera has a higher dust cover than expected, may indicate that pyroclastic activity was a common process at this volcano and produced much fine-grained material. This corresponds with the suggestion of Mouginis-Mark et al. (1988) that anastamosing channels on the flanks of this volcano were incised into unconsolidated material that was formed by pyroclastic events.

3.33 Elysium Mons

Several MOC images of Elysium Mons have been included in this section to highlight the typical surface textures and features that were observed in this area during this study. A map of the positions of the MOC images used has been given in Figure

3.20. Elysium Mons is inferred (both in Chapter 4 of this study and by Tanaka et al., 1992) to be younger than the oldest volcano analysed in this study, Hecates Tholus. However, the surface of the summit flanks is older than that of the two previously discussed volcanoes. It is therefore expected that surfaces will appear fresher than at Hecates Tholus but that the lava flows observed will be significantly buried and eroded compared to those at the two younger volcanoes. Since lava flows were observed in the Viking images of this volcano it was expected that many would be visible in the high-resolution MOC images.

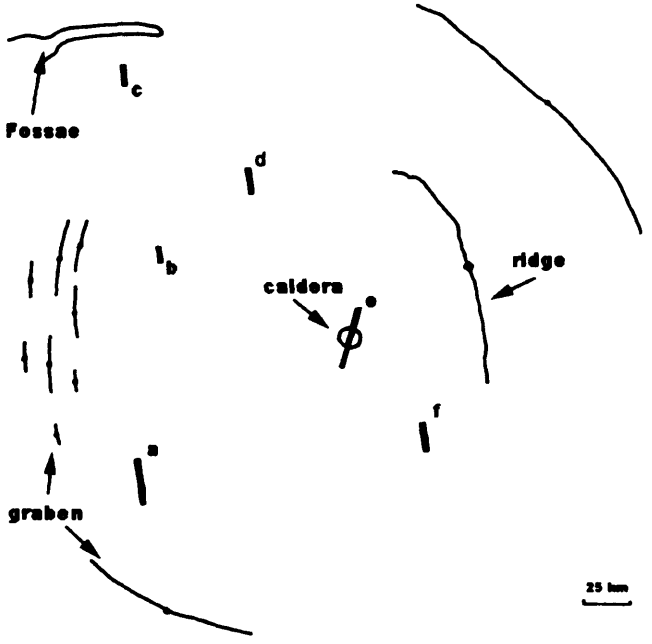

Figure 3.20: Sketch of Elysium Mons showing the general shape of the volcano, positions of the major graben and ridges on the flanks, and the position of the central caldera complex. The green rectangles represent the areas covered by high-resolution MOC images where **a** is the position of M03-05365, **b** is SP2-54804, and **c** is M03-05367, **d** is SP2-51204, **e** is SP2-40303, and **f** is M15-01676.

Despite the evidence in the wide-angle MOC images that Elysium Mons underwent late stage explosive volcanism (see Chapter 4), there is less aeolian material present at the summit than would be expected. MOC image analysis shows that Hecates Tholus has a larger volume of aeolian deposits on the summit and flanks than is present on Elysium Mons.

Close to the summit a surface texture was observed that appears to be characteristic of many of the MOC images of Elysium Mons (see Figure 3.21). The uneven boundaries of this material, as well as the irregular depressions within it, led to a comparison being made between this material and the appearance of inflated pahoehoe fields on Earth (see Figure 3.22). The presence of these features on Mars is further supported by the observation of potential inflation ridges on the flanks of Alba Patera

(see Figure 3.14). Although the large, flat-topped pressure plateaus observed to occur in pahoehoe fields on Earth (Theilig, 1984; Theilig and Greeley, 1986; Hon et al., 1994) are not present in the MOC images, this may be due to a difference in the inflation mechanism on Mars (Walker, 1991).

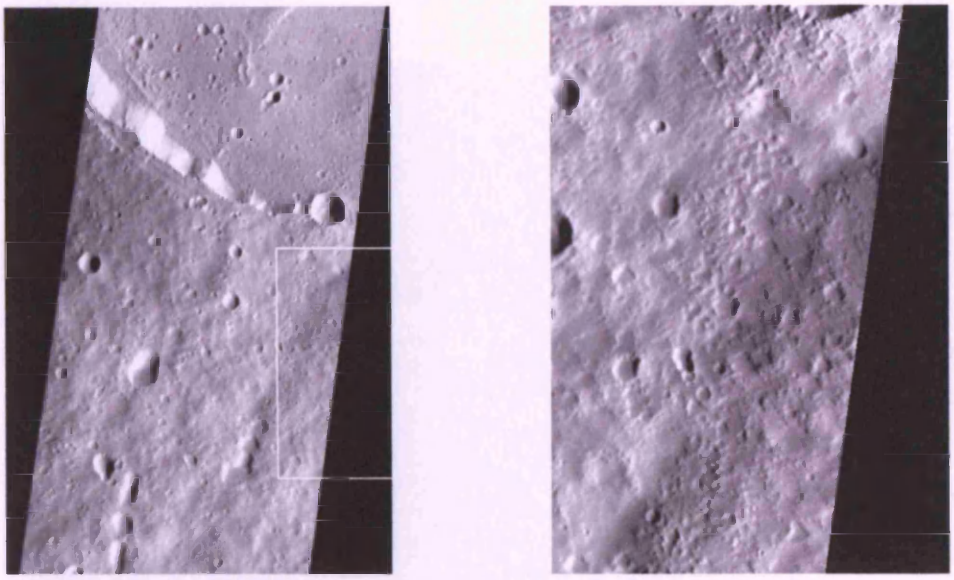

Figure 3.21: Part of MOC image SP2-40303, which crosses the caldera and upper flanks of Elysium Mons. The white rectangle in the left-hand image shows the position of the close-up view shown in the right-hand image. A lava flow surface texture that is typical of the summit region of Elysium Mons can be seen in the right-hand image, and has been compared in this study to those textures found in inflated basalt pahoehoe lava flows fields. The width of the entire image (left) is 5.34 kilometres, and north is towards the top.

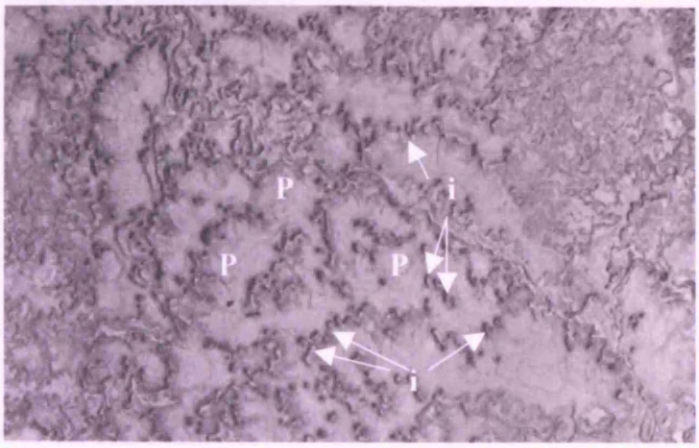

Figure 3.22: Aerial photograph of an area of pahoehoe flows on the Eastern Snake River Plain, Idaho. The area shows the typical appearance of inflated pahoehoe, and inflation pits (**i**) and raised pressure plateaus (**p**) can be observed. The area of the photograph is 2 kilometres by 1.3 kilometres. Photo is U.S Geological Survey Photograph GS SWEZ 6-80, September, 1971.

This typical 'inflated pahoehoe' texture continues further down to the upper and also middle flanks of Elysium Mons. Further down the flanks the texture becomes more

eroded and also increasingly covered in aeolian materials. Figure 3.23 shows the typical appearance of this surface texture further down the flanks, and also highlights the large number of craters found on the flanks of Elysium Mons. Many of these are probably impact related, but those that appear to coalesce (as in Figure 3.21) may be volcanic in origin (Mouginis-Mark et al., 1984; Mouginis-Mark and Rowland, 2001).

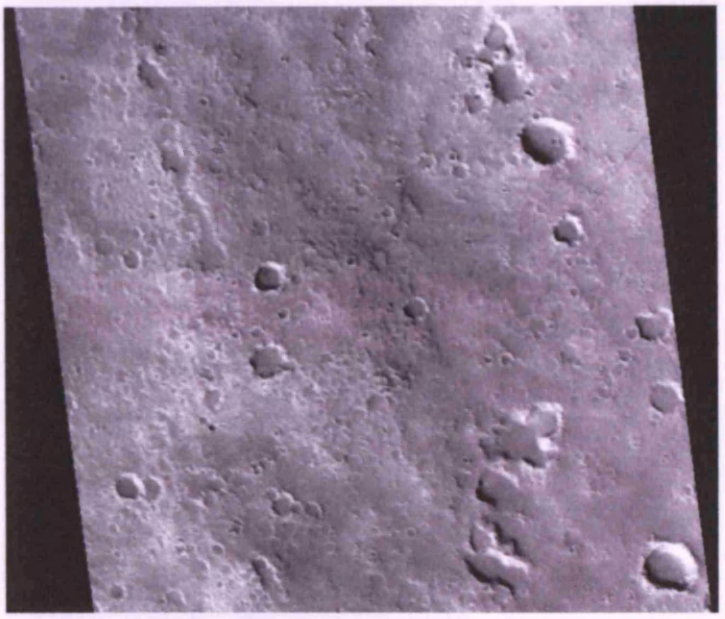

Figure 3.23: Part of MOC image M15-01676, taken on the middle south east flank of Elysium Mons. It shows a surface texture similar to that found at the summit (Figure 3.21) but appears more eroded and is superposed with more craters. Many are probably impact related but some, like several in this image, coalesce and may be of volcanic origin. This image is 3.07 kilometres wide and north is towards the top.

Figure 3.24 shows an area of similar flow texture to that shown in Figures 3.21 and 3.23, at a similar distance from the summit as the area shown in Figure 3.23. However, the area in Figure 3.24 appears to have been highly modified by aeolian materials through erosion, burial by deposits or both. Some of the surface material appears to have the streamlined form of yardangs. The boundaries if the flows are indistinct and they may have been mantled by aeolian materials, and therefore be partly covered in dunes. For comparison, an example of an area where aeolian materials have covered inflated pahoehoe flow fields on Earth is given in Figure 3.25.

Figure 3.24: Part of MOC image Sp2-51204 showing the edges of older, more buried lava flows. The surface texture has been highly modified by the wind and is reminiscent of the dunes and yardangs seen on Hecates Tholus. However, this image may also be showing inflated lava flow fields that have become covered with loose material. The image is illuminated from the left, is 2.26 kilometres wide and north is towards the top.

Figure 3.25: Aerial photograph of pahoehoe basalt flows of the Eastern Snake River Plains, covered with streaked deposits of wind-blown particles. The area of the photograph is about 2.5 kilometres by 3.6 kilometres, north is towards the top. Photo is U.S Geological Survey Photograph GS SWEZ 1-233, October, 1971.

Further from the summit, many individual lava flows are visible in the MOC images, and several examples are given in Figures 3.26, 3.28 and 3.29. The surface texture of these flows is muted by the high levels of aeolian material present here, as evidenced by the accumulation of loose materials in impact craters and the partial burial of features. However, as detailed in the fractal work of Bruno et al. (1992) and Bruno (1994) the shape of the boundaries of the flows, as well as evidence for flow in central channels (Kilburn and Lopes, 1991) indicates that these flows are probably aa flows

(see chapter 5 for further discussion of the shape of flow boundaries). Figure 3.27 shows a typical basaltic aa flow in Hawaii, and the boundaries of this flow, particularly on the right-hand-side look similar to those observed in the MOC images included in this section.

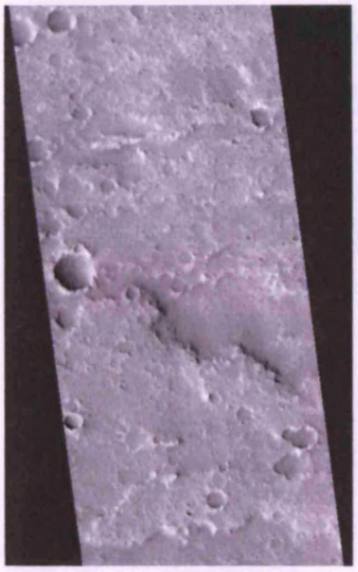

Figure 3.26: Part of MOC image M03-05365 taken on the lower south west flanks of Elysium Mons. Part of a lava flow is visible in the bottom half of the image, and an older lava flow field can be observed towards the top of the image. Channels visible in the older flow field could possibly be central channels although a fluvial origin cannot be disregarded. There are many impact craters that have been modified and eroded. A substantial volume of dusty material is present, which covers up any small scale features that would be useful for analysis (such as aa flow surface textures for example). The image is 1.54 kilometres across and north is towards the top.

Figure 3.27: Oblique aerial photograph of an aa flow in Craters of the Moon National Monument, Idaho. The boundary on the right-hand side of the flow is typical of an aa flow since although it deviates from a straight line at this scale, it will appear more linear at a greater scale, unlike pahoehoe flows which tend to have boundaries that are more fractal in nature (see Chapter 5 for an explanation and also Bruno et al., 1992). The road to the left of the lava flow shows the scale. Photo taken from Greeley and King, 1977.

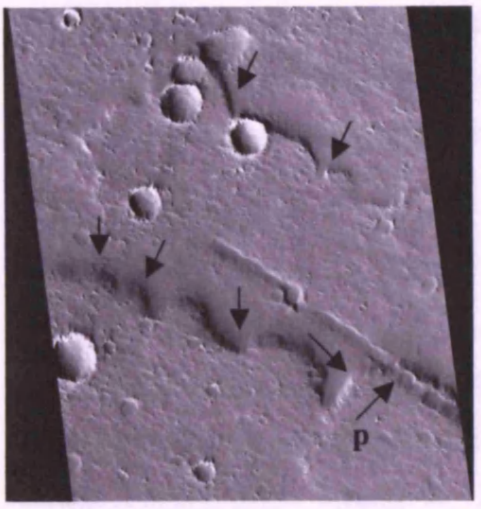

Figure 3.28: Part of MOC image M03-05367 showing a buried lava flow. Part of a lava flow is visible at the bottom of the image and what appears to be an older, buried flow occurs towards the top of the image (flow boundaries shown by arrows). Collapse of the surface along an underlying fault or lava tube has occurred subsequent to the emplacement of the younger flow, producing the collapse pits that are visible in the bottom right-hand corner of the image (p). The image is 3.09 kilometres across and north is towards the top.

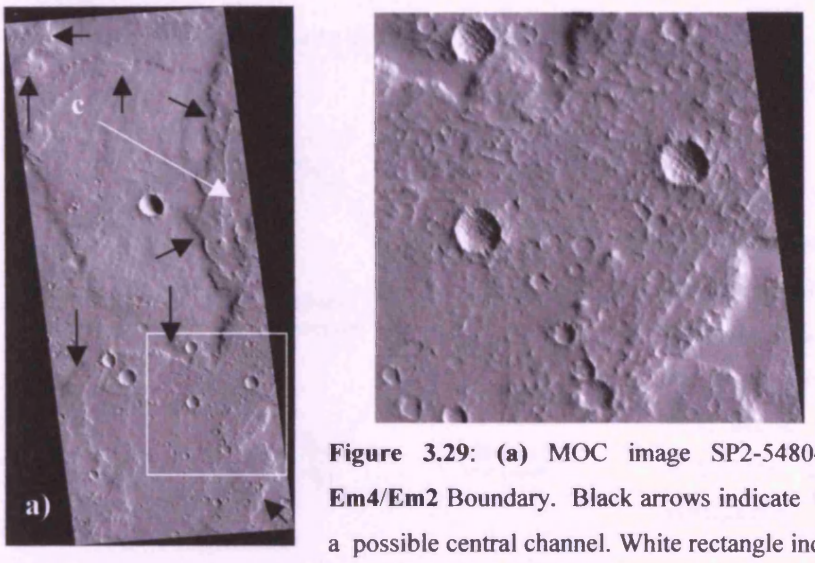

Figure 3.29: **(a)** MOC image SP2-54804 showing lava flows near **Em4/Em2** Boundary. Black arrows indicate the edges of flows, c indicates a possible central channel. White rectangle indicates position of (b); **(b)** is a close up of the surface of the lower flow, showing linear features (l) which may become eroded to produce the hills and yardangs visible in images of older flows. Note the dunes inside the craters indicating the presence of dusty material that is probably covering up small-scale surface textures. The total image width is 3.74 kilometres, north is towards the top.

Analysis of the images in this section shows evidence for the presence of both pahoehoe and aa, and therefore suggests that both types of flows are present in Elysium. However, no features were found that looked similar to the potential inflated ridge feature found at Alba Patera. The lava flows observed are not as numerous as was expected considering the number of lava flows observed in the Viking images. However, they are as eroded and buried by 'dusty' materials as expected at the start of analysis. One part of the image analysis that is surprising is that the summit of Elysium Mons is not as mantled by fine-grained material as expected. As is discussed in Chapter 4, there is a dark, 'dusty' deposit that can be observed on the summit of Elysium Mons

in the wide-angle MOC images, which should mean that much unconsolidated material is visible in high-resolution MOC images of the summit of Elysium Mons. This is, however, not evident in the images analysed in this part of the study.

3.34 Hecates Tholus

The general morphology and characteristics of Hecates Tholus have been discussed in Chapter 1, and specific features of the volcano are discussed in Chapter 4. However, MOC image analysis has revealed small-scale details of the surface of Hecates Tholus. Three images of Hecates Tholus have been presented here, which highlight the main surface textures observed in the MOC images of this volcano. The positions of the images are given in Figure 3.30.

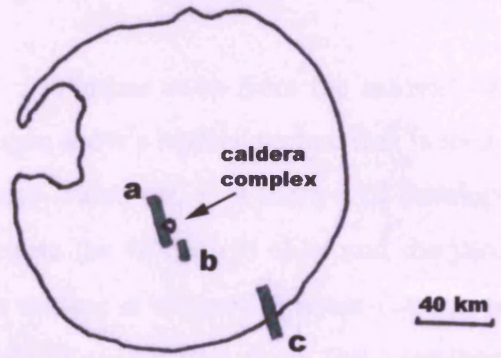

Figure 3.30: Sketch of Hecates Tholus showing the general shape of the volcano and the position of the central caldera complex. The green rectangles represent the areas covered by high-resolution MOC images where **a** is the position of M18-01860, **b** is M09-03953, and **c** is M03-04750.

As discussed in Chapter 1, Hecates Tholus is thought to have undergone late-stage explosive activity near the summit (Mouginis-Mark et al., 1982), and thus any MOC images of the summit area would be expected to show large amounts of loose material. Figure 3.31 shows part of the caldera of Hecates Tholus, and highlights the large amounts of aeolian deposits observed here. The depression of the caldera appears to have a hilly surface texture that may possibly be dunes or yardangs, but may also be the higher standing points of lava flows that have been buried by substantial volumes of aeolian material. The presence of lava flow levées may have initiated the formation of yardangs, since they may channel the wind. The surface of the surrounding flanks has a smoother appearance, which could indicate that the surface is more heavily covered

with loose material than the area inside the caldera. It is possible to observe the presence of small dunes/hills ~30 metres across on this surface.

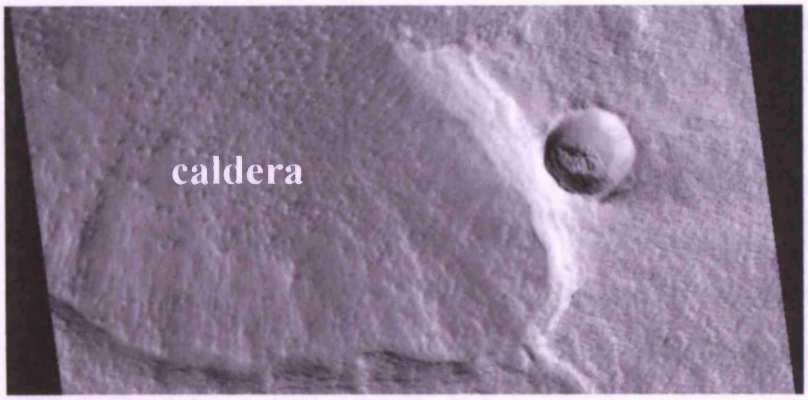

Figure 3.31: Part of MOC image M18-01860, showing small hills in the caldera, and mantling by loose material on the summit slopes. A deposit of aeolian material is clearly visible in the impact crater towards the right-hand side of this image. Image width is 3.13 kilometres, north is towards the top.

Further away from the summit, on the upper flanks of the volcano, the MOC images show a surface texture that is seen on the flanks of each of the volcanoes in this study. However, it is more well-developed on Hecates Tholus, which is likely to be because the volcano is older and the yardangs/dunes have had a longer time to form. The surface is covered in linear features that are possibly aligned dunes, or may be the result of eroded lava flows that have been subsequently, at least partially, covered in dusty materials. This typical appearance is shown in Figure 3.32, which also shows several impact craters with deposits of loose material in the base of each, and thus shows the continued presence of loose material further away from the summit. If caused by the deposition or removal of material by the wind, the alignment of these features testifies to the presence of prevailing winds on Mars, occurring over a long time period. The erosive action of prevailing winds occurring over long time periods on Earth often results in the formation of yardangs (see Figure 3.33). A yardang is formed when softer materials are stripped away by the wind to leave a streamlined hill of more resistant rock (Whitney and Dietrich, 1973; Breed et al., 1989). Greeley and Iversen (1985) state that although yardangs can form in any type of rock, most are found in slightly compacted, fine-grained sediments. In his study of Martian yardangs in the Tharsis region of Mars, Ward (1979) stated that the yardangs present in this volcanic area were likely to be composed of ignimbrites, highly porous lava flows or mudflows.

Other common yardang lithologies seen on Earth are lake-bed silts and clays. At Hecates Tholus ashy materials from an explosive deposit would be easily erodible, and could thus explain the features seen and the volume of loose material present.

In many of the images of the flanks of the volcanoes that have been discussed so far, it has been suggested that the 'hilly' areas, and areas of aligned hills could either be dunes or yardangs. One way to determine the difference between the two would be to determine the prevailing wind direction, since yardangs generally form parallel to the wind, and dunes form at right-angles to the prevailing wind direction (see section 3.6 for a more detailed discussion of dune formation). In some cases it is not possible to discover the prevailing wind direction. However, in some of the images it is possible to infer it from the position of aeolian deposits within impact craters. For example, in Figure 3.32 the deposits within the craters are situated in the southern part of the craters, indicating that the prevailing wind is blowing from the north. Since the linear features are oriented in a north-south direction, this implies that the linear features observed here are yardangs and not dunes.

Figure 3.32: Part of MOC image M09-03953 showing a typical surface texture on the upper south east flanks of Hecates Tholus. Linear features are a series of aligned yardangs, their initial formation perhaps due to the erosion and burial of lava flow levées. The image width is 3.12 kilometres, north is towards the top.

Figure 3.33a: This image (left) shows a yardang in southern Egypt. It is 2 metres high, and the blunt side faces the direction of the prevailing wind. (Image taken from El-Baz and Maxwell, 1982)

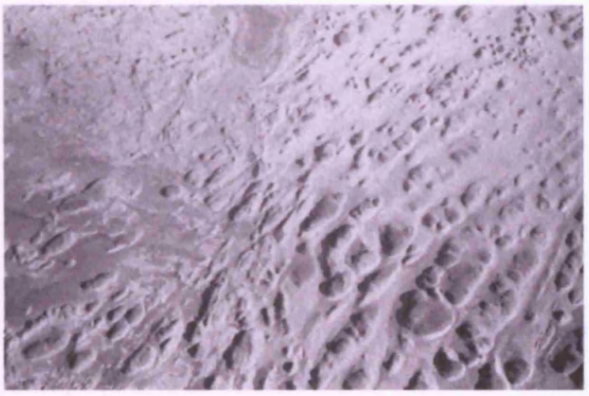

Figure 3.33b: This image (right) shows an air-view of a limestone plateau between Kharga and Asyut in Southwest Egypt. Many yardangs and troughs can be seen here that are nearly all aligned with the prevailing northerly winds. The photo is taken from El-Baz and Maxwell, 1982, and shows an area 1.5 kilometres across at the base of the photo.

Hecates Tholus can be characterised by the numerous channels that are carved into the flanks of the volcano. Both Plescia and Saunders (1979) and Mouginis-Mark et al. (1982) observed that there was not only a paucity of impact craters near the summit, but also a lack of channels. Although Reimers and Komar (1979) deemed the channels to have been formed due to density currents, Mouginis Mark et al. (1982) thought that the anastamosing appearance of many of the channels implied a fluvial origin. High-resolution images gained by MOLA do not help to resolve this issue, since no evidence for any kind of flow or deposits from flow, are visible in the base of the channels, even where there is little cover by aeolian deposits.

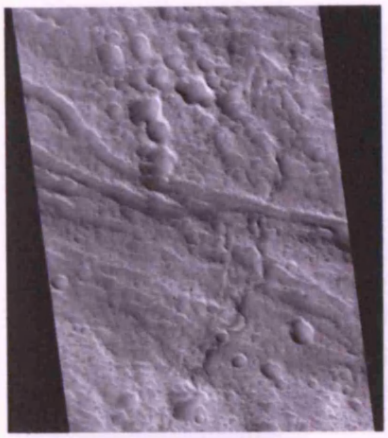

Figure 3.34: Part of MOC image M03-04750, which covers part of the lower south east flanks of Hecates Tholus. Crossing the centre of the image from left to right are two channels which converge in the centre of the image to continue as one channel. A ridge or scarp feature crosses the image at right-angles to the main channel. Craters observed in this image may be impact or volcanic in nature. There is little dust cover at this distance from the summit, even in the base of the channels. The image width is 3.11 kilometres, and north is towards the top.

There is much evidence for erosion here as shown by the likely presence of yardangs. There is also much evidence to support the theory that the summit of Hecates Tholus (if not everywhere on the volcano) is covered with materials that are the result of pyroclastic activity and explosive eruptions, since the volcano is heavily mantled with 'dusty' material. In many places the 'hilly' texture observed here is proposed in this study to represent the remnants of buried and eroded lava flow levées. Evidence for this was found in the images of the flanks of Olympus Mons where the levées were starting to erode or be covered in mantling material to give them a similar appearance to the features observed on the older volcanoes.

3.35 Unit Boundaries

In some of the MOC images it was possible to see where boundaries occurred between units. This was particularly helpful in the Elysium mapping region, especially where boundaries were not clear. Thus, although the small-scale appearance of the lava flow surface was not visible, the MOC images were still useful during the mapping of Elysium. Two examples of unit boundaries are shown in this section. The first is the boundary between Hecates Tholus and the surrounding (**Em 5**) plains (see Figure 3.35, and Chapter 4 for explanation of the mapping units). In Figure 3.34 the boundary is distinct since the plains unit in the lower half of the image clearly overlaps the channelled flanks of Hecates Tholus.

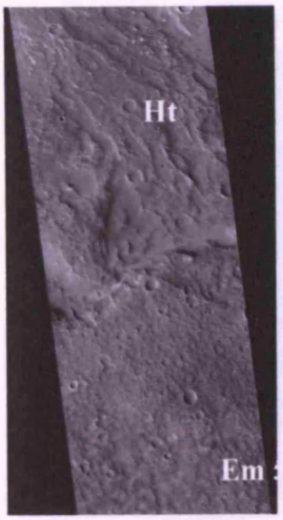

Figure 3.35: Part of MOC image M03-04750, showing the contact between Hecates Tholus (Ht) and the surrounding plains (mapped in this study as the Em 5 unit). The plains can clearly be seen to overlap the flanks of the volcano and are thus the younger unit here. The difference in texture is quite obvious since Hecates Tholus is covered in many channels. This image was taken at the base of the south east flanks of Hecates Tholus. North is towards the top and the image is 3.11 kilometres in width.

Figure 3.36 (below) gives an example of the boundary between the lava flows of the vent flows unit (**Vf**) and the start of the northern ice-rich plains (unit **Txp**), see Chapter 4 for a description of these units. The boundary is not distinct in the Viking image (Figure 3.37 a), but in the MOC image in Figure 37 (b) it can clearly be seen that the rougher lava surface grades towards the north into a smoother, yet fractured surface.

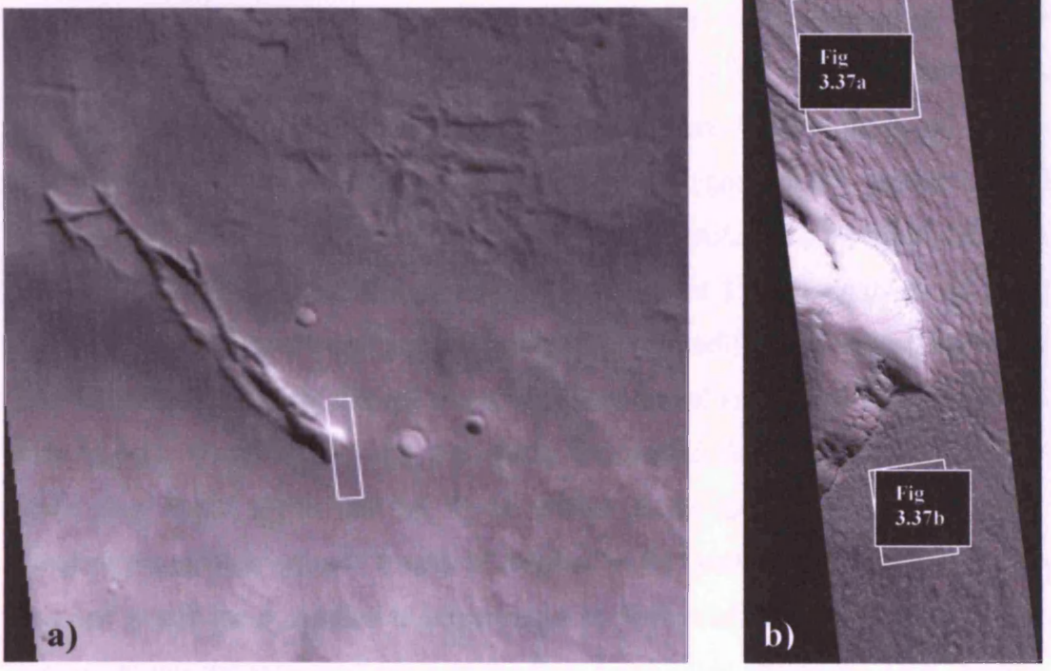

Figure 3.36: (a) MOC context image M09-06067 of the plains to the north of Elysium Mons. The feature shown is a graben complex, and the area to the top right of the image is part of the chaotic terrain and modified plains region mapped in Chapter 4. The white rectangle shows the position of Figure 3.37 (b). North is towards the top of this image and the resolution is 3.06 metres per pixel. **(b)** Part of MOC image M09-06066 showing the boundary between the Elysium Mons lavas and the northern ice-rich plains. The white boxes show the positions of Figures 3.37 (a) and (b).

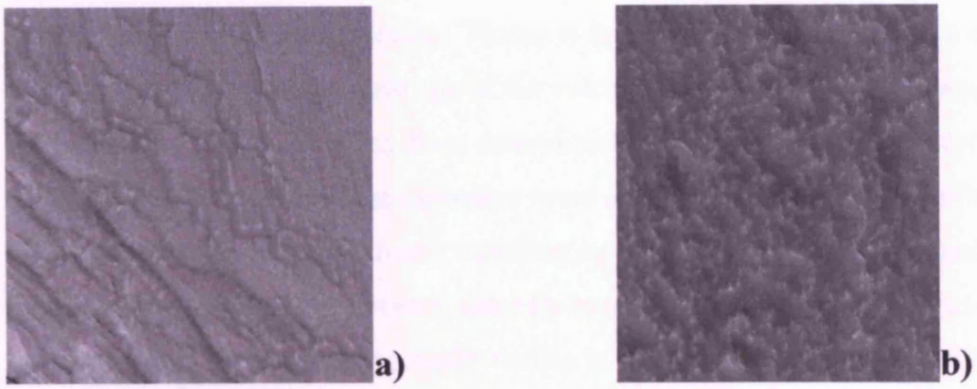

Figure 3.37: (a) Part of the ice-rich plains identified in the mapping study. Note the smooth texture and surface fracturing, perhaps related to the graben complex to the bottom left of this image; **(b)** Part of the lava fields associated with Elysium Mons. The texture of this area is hummocky and ridged, suggesting that the lavas here have been modified over time, perhaps by wind erosion.

This section of the study shows that although the MOC images were not always useful during the analysis carried out in this study, they could sometimes help to determine the positions of boundaries in the mapping exercise, even if only approximately. The MOC images have also helped to characterise some of the terrain observed in the mapping study, and in this section it has been possible to compare features observed on both Hecates Tholus and Elysium Mons with those observed on two relatively younger volcanoes. This has been particularly useful since it has highlighted the fact that on the flanks of each of the volcanoes a typical 'aligned hills' texture has been observed (like that shown in Figure 3.32). Analysis of the surface texture of volcanoes of varying ages, and therefore modification stages, has shown that this characteristic texture may be the result of the burial and erosion of channelled flows with levées. If this is the case then since channelled flows are a characteristic of aa flows this would mean that aa flows appear to be the dominant lava flow form. However, a surface texture found in several areas (particularly near the summit) on Elysium Mons looks similar in appearance to terrestrial inflated pahoehoe flows. In contrast to this the shapes of some of the flow boundaries imaged by MOC further down the flanks of Elysium Mons appear to look like terrestrial aa flows. These findings support further evidence presented in Chapters 5 and 6 which shows that the presence of both aa and pahoehoe at Elysium is likely.

Many of the MOC images of the flanks of all the volcanoes show that they are covered in dusty deposits. Hecates Tholus is heavily mantled by loose material as had been expected given the relative age of the volcano and the implied explosive history of the construct. Although it has been determined during the mapping of Elysium Mons that there had been a late-stage explosive event at the summit, the images of the summit of this volcano do not show heavy mantling by loose deposits here. Instead the lower flanks are found to exhibit greater cover by loose materials. It had been expected that individual lava flows would be easily visible in the MOC images of this volcano since many could be observed in the Viking images. However, there are surprisingly few in the MOC images. This is also true for MOC images of the summit of Alba Patera. Clear images of individual lava flows were expected here, not only because lava flows were visible in the Viking images of this volcano, but also because it is relatively younger than both Hecates Tholus and Elysium Mons and thus flows should be better preserved and less covered by loose deposits. The MOC images show Alba Patera to be heavily mantled with loose materials and no clear lava flow fronts are visible.

The volcano that has the most well-defined lava flows in the MOC images, as well as the most diverse array of lava flow types, is Olympus Mons, the youngest of all the volcanoes discussed here. Sheet flows have been found on the edge of the caldera, volcanic craters and lava channels have been observed, compound channelled flow fields are present on the middle flanks and individual channelled flows are visible on the lower flanks and crossing the basal scarp. Where lava flows traversed the scarp and flowed onto the shallower slopes surrounding the main volcanic edifice, the flows appear to thicken and exhibit festoon ridges. Olympus Mons also exhibits mantling by loose materials. This is particularly noticeable at distances of tens of kilometres out from the caldera, but is less obvious at distances closer to the basal scarp. Layering of materials is found to occur in the walls of the basal scarp, and is probably related to different eruptive events during the history of the volcano, some of which may have been pyroclastic given the easily erodible nature of the materials in the MOC images.

3.4 Periglacial Features

Evidence has been found for the presence of water and/or ice in the past history of the Elysium region of Mars, not only in previous studies of the region as discussed in Chapter 1, but also in both the mapping exercise in this study and in the new data from the more recent Mars Odyssey mission (Head et al., 2003). The image analysis of the north of the Elysium mapping area that was carried out in this study has shown further evidence for the presence of ice in this area. The geological features present in this area that are associated with, or formed by, the presence of ice on or in the ground will be discussed in this section. Analysis of these features is useful because they help to confirm the results of the mapping carried out in this study.

In the higher latitudes on Earth there are areas where only the top ~1 metre of soil thaws in the summer months, and the ground below that is permanently frozen. Such freezing and thawing every year causes characteristic patterns to occur in the ground surfaces, and this environmental setting is termed 'periglacial'. When parts of features formed in periglacial conditions start to erode, they form what are termed 'thermokarst' features, and are often, although not necessarily, caused by a change in environmental conditions. Much of the northern part of the mapping area, and that area covered by the Elysium lava flows studied in Chapters 5 and 6, is in the mid-latitudes of Mars and so it might be expected that periglacial conditions are present there, or were present in the past. Periglacial features expected to be observed in the MOC images of the northern part of the mapping area might include pingoes, polygonal terrain and cracking/fracturing of the ground, mass movements facilitated by ice (a process otherwise known as gelifluction (Washburn,1979)), and striped or other patterned ground, as well as the erosional remains of such features.

In many of the images of the plains to the north of Elysium Mons, where the Elysium Rise meets the start of Utopia Planitia, many features were found that were similar in appearance to features characteristic of the presence of ground-ice on Earth. In Figure 3.38(c), some parallel ridges are visible to the right of the large mesa. These may indicate that flow of material has occurred here, facilitated by ice, or may be the erosional remains of an ice stream similar to those proposed in some Martian valley systems by Lucchitta (2001).

However, the most common feature was a pitted surface appearance that was quite different to the pitted surface texture found on the flanks and within the calderas

of the volcanoes that was discussed in section 3.3 and which was attributed to dunes and yardangs. Figure 3.38 shows several examples of this pitted texture, some found on the plains, and others within the chaotic terrain region to west of Hecates Tholus. In some cases the pitted texture lies within depressions, such as in Figures 3.38(a) and (b), but in other cases the texture occurs on top of mesas and higher standing ground as well as on the surrounding plains. In Figure 3.38(b) the texture can be seen to terminate abruptly at one particular elevation all along the base of the surrounding higher standing ground. The height at which this texture terminates could indicate the top of a ground-ice layer, but alternatively it could show that these features are actually aeolian in nature, and that wind activity ceases to have the same effect above this height. Even with the high resolution available in the narrow-angle MOC images, it is not possible to definitely state whether these features are formed by the action of wind or ice. However, in conjunction with the other types of features found here, it is thought in the present study that they are ice features, perhaps similar in places to terrestrial relic or fossil pingos (see Figure 3.39). Many of the features appear to be rounded or oval in nature, as is particularly noticeable in Figure 3.38(b), which would be the expected appearance of fossil pingoes (Flemal, 1976; De Gans, 1988; French, 1996). On Earth this would suggest the presence of a periglacial setting in the area in the past, so it seems likely that the presence of such features on Mars would represent this also. The rounded nature of some of the features may be indicative of other periglacial processes, such as the formation of sorted circles, which have a border of stones surrounding finer material (Washburn, 1956), and are common on shallow slopes. The sizes of these features on Earth rarely exceed several metres, and would therefore not be resolved fully in the MOC images if the equivalent features were of a similar size on Mars.

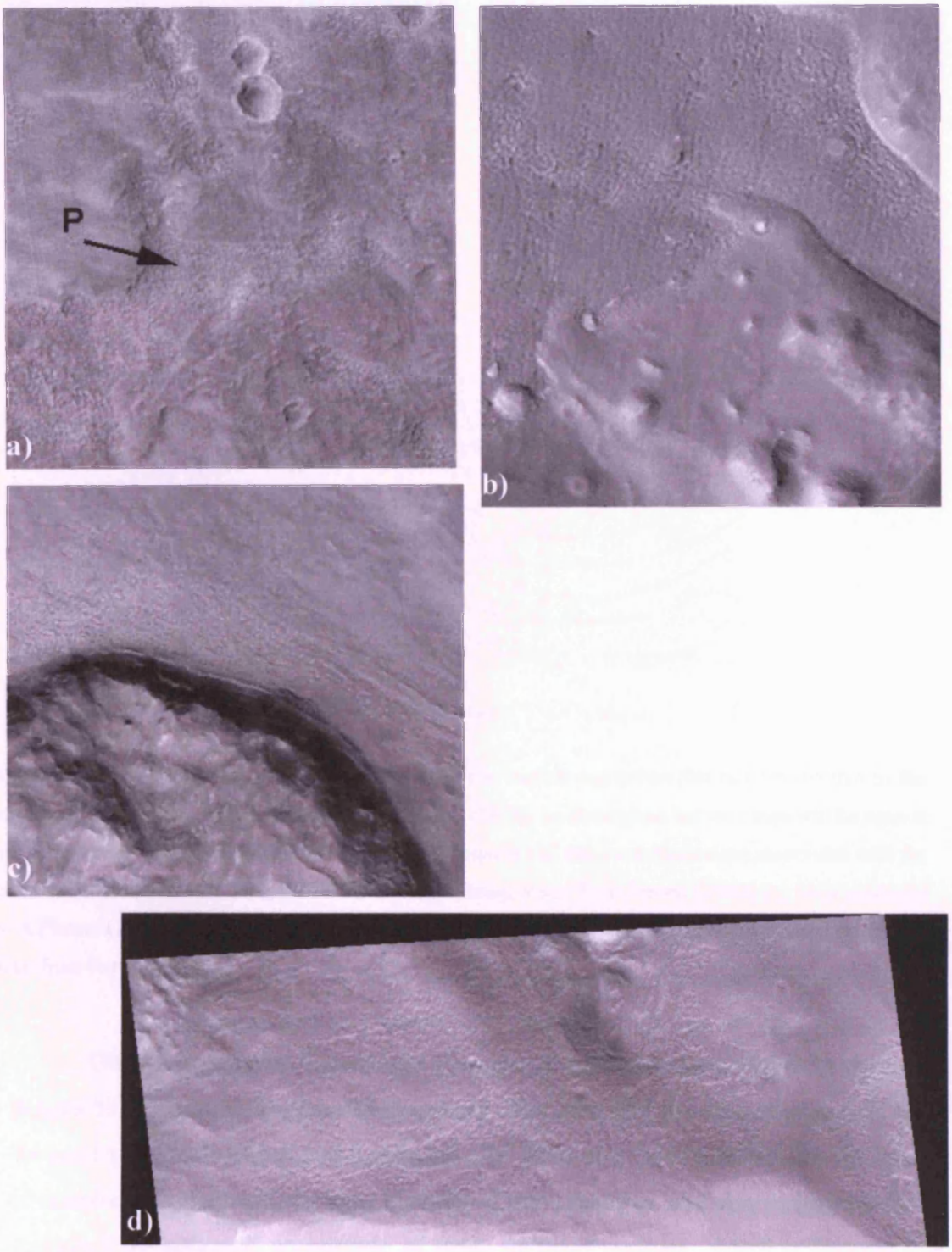

Figure 3.38: **(a)** Part of image M2301395 showing pitted terrain on the northern Elysium plains west of Hecates Tholus; **(b)** part of image M0304232 showing pitted terrain near the chaotic terrain west of Hecates Tholus **(c)** part of MOC image M1001149 showing pitted terrain near the transition between the Elysium rise and Utopia Planitia; **(d)** part of MOC image M1100836 also showing pitted terrain around the transition between the Elysium rise and Utopia Planitia.

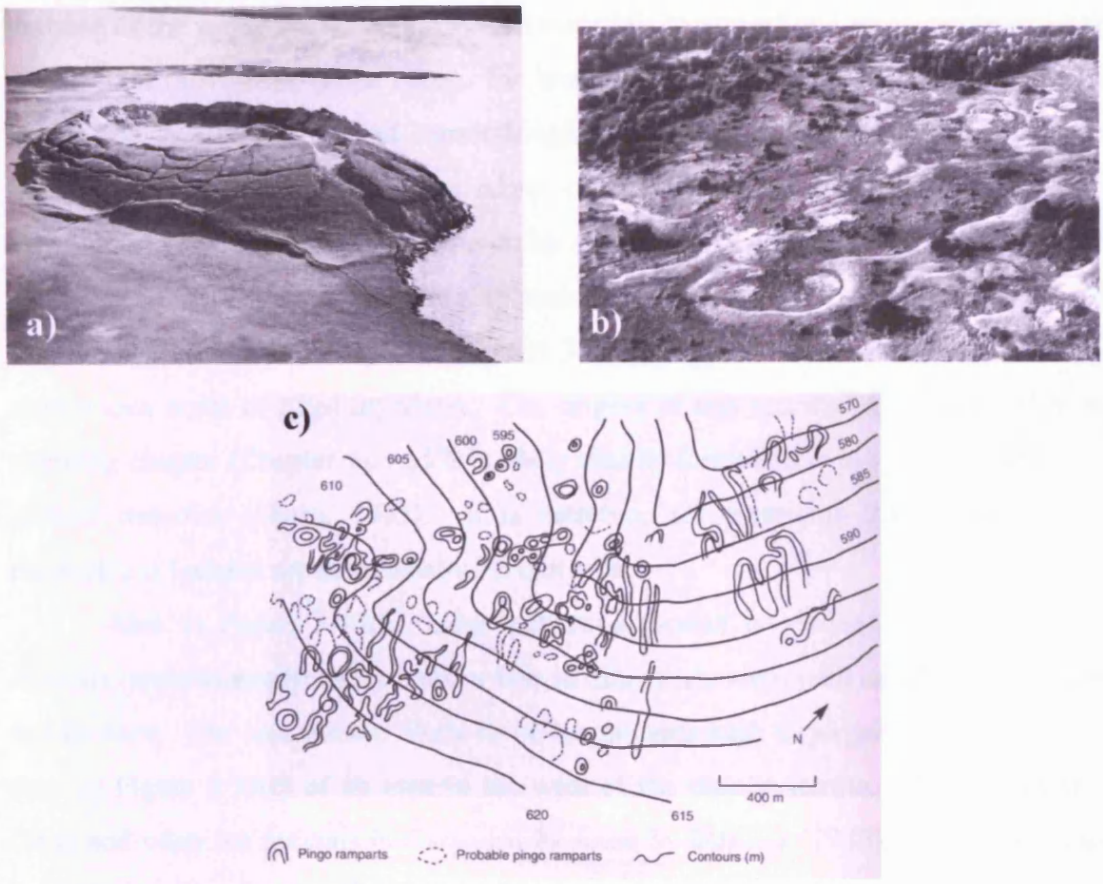

Figure 3.39: (a) image of a pingo with a characteristic central depression that has formed due to the thawing of the ice core. Image taken from Washburn, (1979), no scale given but the pingo will be several tens of metres in diameter; **(b)** Oblique air view of ramparts and enclosed depressions associated with the formation of frost mounds. Vegetation shows scale. Image taken from French (1996); **(c)** Map produced by A.Pissart (1965) of frost mound ramparts in the Brackvenn, Hautes Fagnes region, Belgium (image taken from French, 1996).

Other features that indicate the presence of ground-ice are visible in the MOC images that have been analysed in this study. For example, the flow of materials from the crest to the base of isolated mesas and cliff faces may be responsible for the aprons of material found around the base of some of these features, and also may produce the smoothed or 'softened' appearance of many of these surfaces. Martian features that appear to have been 'softened' have been studied by Carr and Schaber, (1977); Squyres, (1978); Lucchitta, (1984) and Squyres and Carr, (1986) and are thought to be related to the presence of ground-ice. Flow of materials from higher to lower elevations may be facilitated by the presence of ground-ice, either because melting of the ice provides water that reduces internal friction and cohesion and thus promotes flow of materials (gelifluction, for example see Washburn, 1979), or because repeated freezing and

thawing of the surface material allows the materials to expand and settle producing a net downwards movement (frost creep, for example see French, 1996). Figure 3.40(a) shows the apparent flow and 'smoothing/softening' of a higher standing block of material down into a valley. The edges of flow lobes are visible and indicate the direction of flow, which has been shown by an arrow on the image. Figure 3.40(b) also shows smoothed material, where higher standing blocks appear to have merged into the surrounding area. The images in Figures 3.40 (a) and (b) show parts of the chaotic terrain area north of Elysium Mons. The origins of this material are discussed in the mapping chapter (Chapter 4), and it is likely that its formation is highly associated with ground water/ice (Sharp, 1973). It is therefore not surprising that periglacial and thermokarst features are associated with this area.

Also in Figure 3.40(b), more patterned ground is visible, and several small mounds (approximately 100 metres or less in diameter), some with small central craters, can be seen. The mounds are likely to be ice mounds such as pingos, and more can be seen in Figure 3.39(c) of an area to the west of the chaotic terrain. The formation of these and other ice mounds is discussed in detail by Mackay (1986), but can generally be thought of as the growth of an underground ice core, which pushes up the ground surface to produce a mound or conical feature. Often, when the ice melts, the centre of the mound collapses, leaving a central crater surrounded by ramparts (Washburn, 1979) (see Figure 3.39a). The features in Figure 3.40(b) may look similar to impact craters but the size of the central crater compared to the total diameter of the feature seems too small for this to be the case. Also, the ramparts appear to be too high relative to the size of the central depression and they do not grade away into the surrounding surface as is typical of impact ejecta unless it has been highly eroded. The rim-to-floor depth of simple bowl-shaped craters similar in appearance to the features shown in Figure 3.40b, is generally ~1/5 of the rim-to-rim diameter of the crater, and the rim height is ~4% of the diameter according to Melosh (1989). The features in Figure 3.40 (b) appear to have depths and rim heights that exceed these proportions. Figure 3.40(c) shows part of a feature that is thought to be volcanic in origin according to the present study (see the Volcanic Ridge Feature in Chapter 4), but despite this, possible pingos and pitted and patterned ground, and ground cracking occur on the surface here, indicating that (if the subsequent features were formed by ground-ice) water or ice must have entered the ground here after the volcanic mound was formed. Previous studies have indicated that the 'Volcanic Ridge Feature' is very similar in appearance to the terrestrial moburg

(hyaloclastite) hills and ridges of Iceland that form during subglacial eruptions (Moore, 1982). If this were the mode of formation of the feature then ice and ground-ice would already be present to allow for the subsequent formation of periglacial surface features.

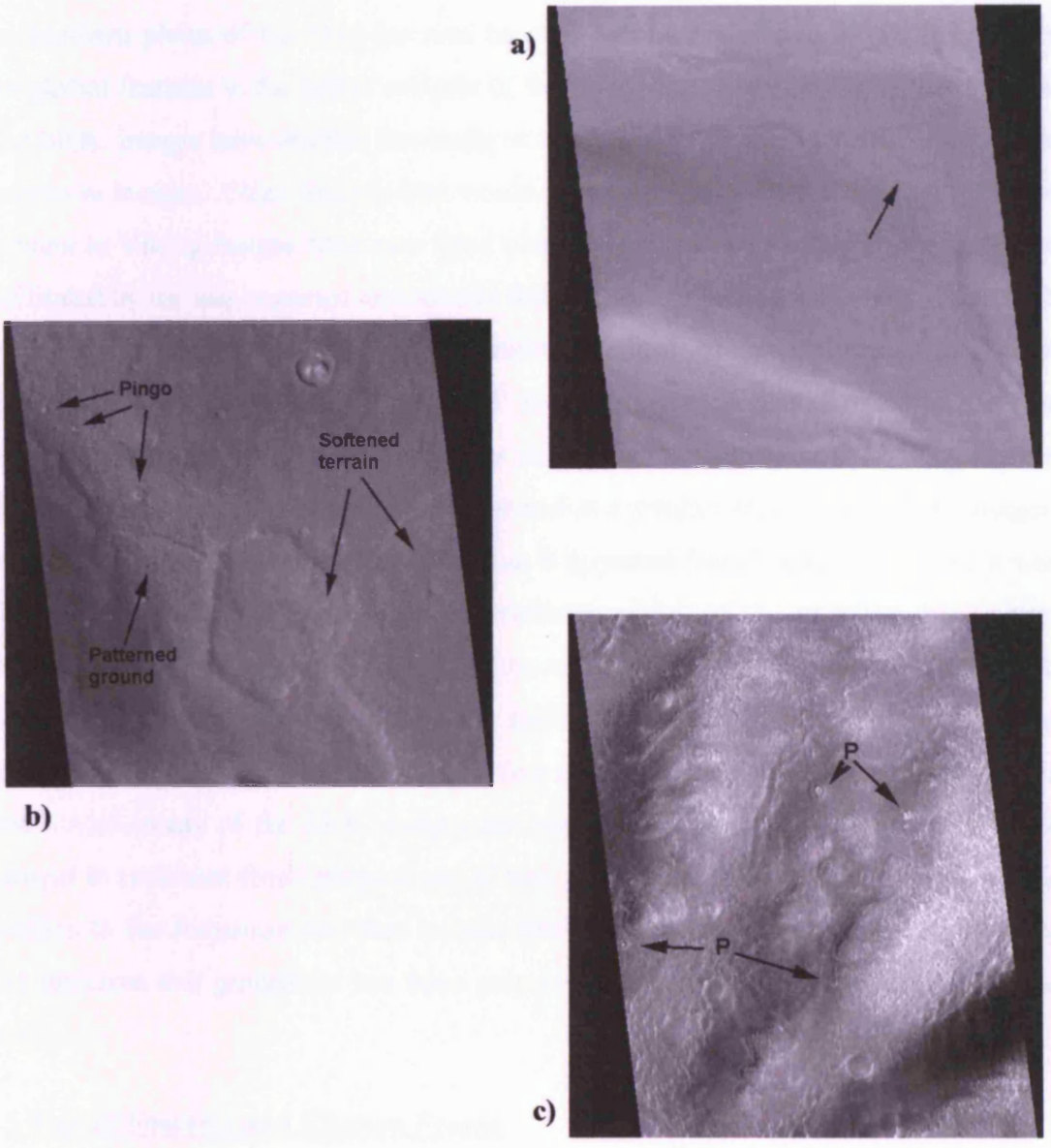

Figure 3.40: (a) Part of MOC image M0905164 showing part of the chaotic terrain north of Elysium Mons. Flow of the higher standing ground (in the direction of the arrow) has occurred, potentially facilitated by the presence of ground-ice; **(b)** Also showing part of MOC image M0905164, further to the north of the area shown in Figure (a). This shows patterned ground, possible pingos and softened terrain, all typical indicators of ground-ice; **(c)** Part of MOC image M2200153 showing the northeastern edge of the 'volcanic ridge' described in Chapter 4. Three ridges can be observed in this image and in the depressions between these several circular features can be observed (p) that are similar in appearance to terrestrial pingos.

In the Viking images of the mapping area it is possible to see features and surface textures that indicate the presence of ground-ice, such as chaotic terrain, the possible moberg features and the patterned ground near these features (see Chapter 4). Much of the MOC analysis concerning periglacial features was done using images from the northern plains of the mapping area because this area exhibited the most potential periglacial features in the initial analysis of the mapping area using the Viking images. The MOC images have enabled the study of smaller scale features by providing higher resolution images. Other features that would have been expected but were not possible to view in Viking images have now been observed. Evidence for the flow of material facilitated by ice was expected and several features were observed that showed this such as the ridges in Figure 3.38(c). The formation of 'aprons' of material around mesas and hills, particularly those that are 'softened' in appearance, is also characteristic of the presence of ground-ice. Although this has already been observed in the Viking images of the mapping area, it has now been observed at a smaller scale in the MOC images. This process is therefore more common than it appeared from Viking data, since it was observed in many MOC images of the northern plains of the mapping area. Other features observed in the MOC images of the northern plains of the mapping area look similar to terrestrial pingoes. Since on Earth these are formed in the presence of ground-ice, if these are Martian pingoes then they indicate the presence of ice in this area. Also, many of the MOC images analysed exhibited a 'pitted' texture. This is thought to represent fossil pingoes and if they have been identified correctly then this testifies to the formation and then subsequent modification of pingoes in this region, and indicates that ground-ice has been present in this area for a substantial period of time.

3.5 Fluvial Features and Elysium Fossae

Chapter 4 presents much evidence that both lava and water emerged from the Fossae, and the vents and ridges associated with them. It is therefore of interest to analyse some of the products associated with the Fossae, as well as to study the floors of the channels, the Fossae and the channels leading away from the Fossae to try to find out more information about the type of material present and the way it was emplaced. Mapping of these features indicates that material flowed along them in the past, therefore it might be expected that some evidence would be found for scouring and the layering of deposits both in the fluvial channels and in the Fossae. As is discussed in

Chapter 4, the materials emerging from the Fossae are expected to be fluvial sediments and also eroded and broken lava materials, and potentially also explosive deposits from water/lava interactions. Evidence that there was fluid flow through the fluvial-like channels would provide more indication that these channels were indeed carved by water or a fluid acting like water.

During the mapping carried out in the next chapter, several different units were found within the materials erupted from the Fossae. At the outer edges of the Fossae Materials was a unit that was designated as unit **Dr** (Disrupted flows). This unit was thought to have been formed either by the settling-out of sediment from a sediment-laden fluid, or from the remnants of lava/sediments that were left after further eruptions from the Fossae. This material could either then be lava flow material or could be possible fluvial deposits, perhaps from a sediment-laden flow such as a lahar. Indeed, the presence of lahars in this area is inferred by Christiansen and Greeley (1981). Figure 3.41(a) shows the surface appearance of one of these deposits and indicates that this may indeed be deposits of water-borne sediments since both narrow channels and ripples (similar to those caused by the rise and fall of tides on a beach on Earth) can be observed.

In the mapping chapter it is suggested that the inner areas of the Fossae Materials (unit **Ffr**) represent rock that has been broken up or fractured by the flow from the Fossae. Therefore MOC images of the area should show fractured terrain, and perhaps also sedimentary deposits depending on the type of flow erupted. Figure 3.41(b) is one example of the images that cover areas of unit **Ffr**. In the Viking images **Ffr** has a rough surface texture. The MOC images of areas of this unit show that the rough appearance of the unit in the Viking image is due, not only to isolated blocks, but also to many dunes. No fractured materials are visible, neither is there evidence in these images for the remnants of the flow of lava from the Fossae. However, all features in Figure 3.41(b) are aligned in the same direction, which could be the result of streamlining by flow of a liquid, therefore the original suggestion for the formation of this unit is still valid.

Analysis of Viking images shows that closer to the Fossae many channels have formed. Figure 3.41(c) is a MOC image of an area close to the Fossae where the units of the Fossae Materials are present. It is clear from Figure 3.41(c) that flow of a sediment-laden fluid (thought in this study to be water), has occurred, since there are many small channels (many of which are anastamosing), much dark material that could

be sediments, and also the emplacement of dark material mostly at the outer edges of curves in channels. Since the energy of a flow is lessened at bends in channels (due to friction) it is interpreted that these deposits are the results of deposition from the sediment-laden fluid, forming point bar deposits similar to those observed on meandering streams on Earth, as shown in the work of Schumm and Kahn (1972) and Dietrich and Smith (1984).

In Figure 3.41c the smaller channels associated with the Fossae could be observed. However, in many cases these feed into the larger channels that are postulated in this study to have eroded sedimentary and volcanic materials and thus form the **Ffr** and other fractured Fossae Materials units. If these channels were formed by the flow of water then it might be expected that deposits of sedimentary material or erosional patterns indicative of the flow of water would be visible in the base of the channels. If the channels have been incised by the turbulent flow of lava, then erosional patterns might also be expected, but it might also be possible to see some evidence for the flow of the lava on the walls of the channels, since the rise and fall of the level of the lava would leave different levels of solidified lava on the walls. Figure 3.42(a) shows part of one of the larger channels (Hrad Vallis) that leads away from one of the Fossae. It shows a high level of scouring, the presence of streamlined islands, several different ground levels (that were also observed on a larger scale in the Viking images by Mouginis-Mark et al., 1984), and numerous different paths of smaller channels within the larger one, which may represent changing flow rates over time. Many small channels are visible crossing the ground surface next to the larger channel. These may have fed into the channel, or could have been formed during the start of flow from the Fossae before the main channel became established. No evidence for the deposition of sediments can be observed in this image, and as the area shown is situated near the suspected source fossa it suggests that this area of the channel underwent a high level of erosion from high-energy flows, probably water. This image shows evidence for a liquid (suggested in this study to be water, see Chapter 4) flowing over the surface here for a substantial period of time, since it takes time for fluvial channels to become established.

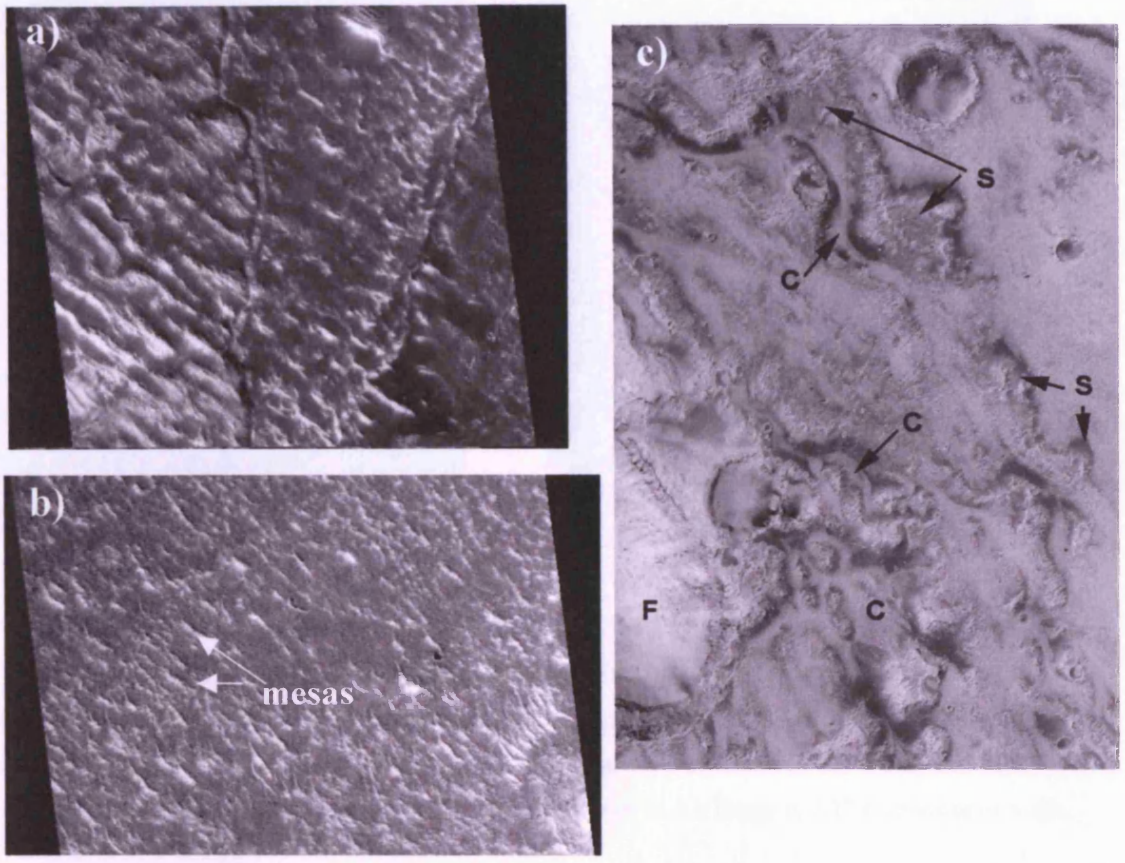

Figure 3.41: (a) shows part of MOC image M11-00169 of part of the Fossae Materials mapped as the **Dr** unit. Narrow, sinuous channels can be observed and features that appear to be similar to terrestrial ripple marks, although on a larger scale, can also be seen. The image is 1.55 kilometres in width; **(b)** part of MOC image M09-00366 of part of the fossae flows mapped as the **Ffr** unit. Many aligned dunes can be seen, but there are also many isolated mesas ~50 metres in width and ~100 metres in length, that appear to be aligned in a similar direction to the dunes and may be erosional remnants of volcanic materials. This image is 1.56 kilometres in width, north is towards the top; **(c)** part of MOC image M22-02332 showing channels and probable sediments erupted from the Fossae. Part of one of the Fossae (F) can be seen, (c) indicate small channels, and (s) highlight patches of potential fluvial deposits. This image is 3.12 kilometres in width and north is towards the top.

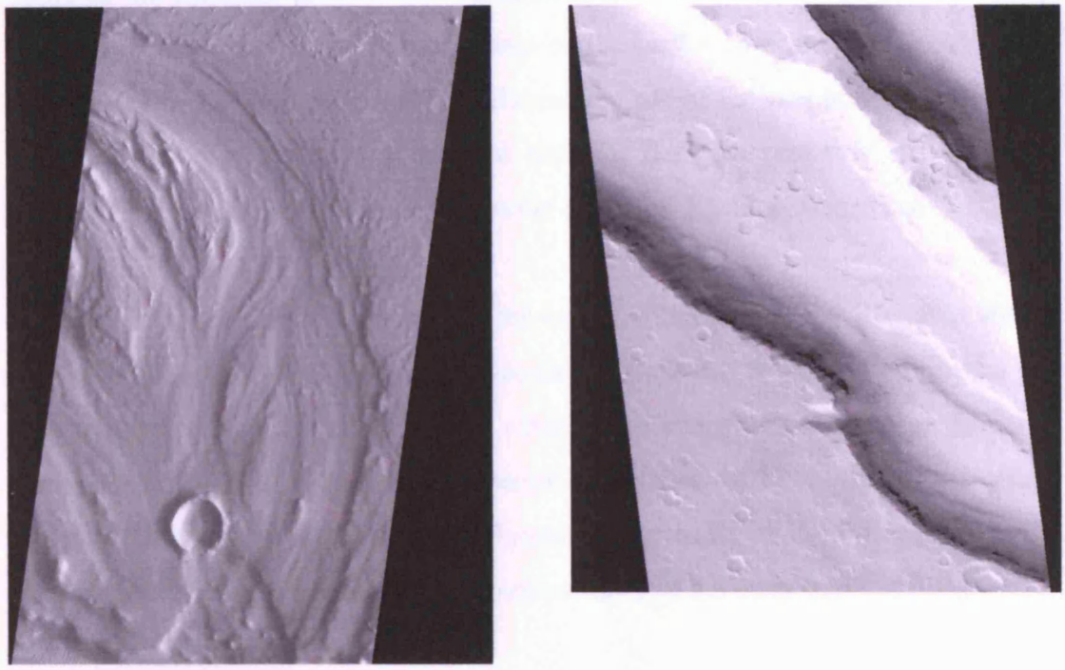

Figure 3.42: (a) Part of MOC image SP2-43904 showing erosional features within the channel of Hrad Vallis. North is towards the top of this image and flow within the channel occurred from bottom to top in the image. The image is 4.85 kilometres in width; **(b)** Part of MOC image M13-02010 showing part of one of the Elysium Fossae. A smaller channel can be seen on the floor of the fossa, and layering of material can be seen in and close to the walls. The area shown in this image is 2.88 kilometres in width.

Figure 3.42(b) shows the floor of one of the Elysium Fossae. The floor of the fossa is flat and fairly smooth which is typical of the Fossae, but the presence of a superimposed, narrower channel can be observed on the floor of the fossa, which grades away into the base of the main fossa. Several layers can be observed towards and within the wall of the fossa, one of which is most likely to be a layer of bedrock, but several that could either be less prominent bedrock layers, or could have formed from flow (probably of lava) within the channel. The differing appearances of Figures 3.42(a) and 3.42(b) leads to the suggestion that either the fluids that flowed through them were different, or that the mode of flow was different. As discussed, a turbulent, high-energy flow was probably necessary for the channels in Figure 3.42(a), but a slower flow may have been responsible for the appearance of the channel in Figure 3.42(b). Differing levels of dust deposition may also be accountable for the different appearance of the two channels.

Much of the MOC image analysis of the fluvial features aided understanding of some of the mapping units described in Chapter 4. Ripples on potential flood plains, and the apparent deposition of sediments on the banks on channels appear to testify to the flow of water/mud within the northwestern part of the mapping area. Some MOC images show the presence of aligned features that are probably the result of uni-directional flow, though whether the mode of their formation was wind or liquid is still unclear.

The bases of both fossae, and the larger of the potentially fluvial channels were analysed using the MOC images. Evidence for flow was found in both cases, though it was clearer in the fluvial channels where high-energy flows appear to have been channelled for a relatively long time period. Evidence for flow within the Fossae is not so clear, although potential layering found on the walls of the Fossae, as well as the smoothness of the bases points to the laminar flow of a slower moving fluid.

3.6 Aeolian Features

The action of the wind is one of the major forces modifying the surface of Mars at present (Cutts and Smith, 1973), so the study of aeolian features is important to this study. Until the high-resolution MOC images were returned, the scale of the dust cover on Mars was not fully appreciated. A discussion of the aeolian features observed in the MOC images analysed must therefore be included in this study. The way in which the wind has modified volcanoes and associated products has been discussed in section 3.3, but the more widespread features are discussed here. Features expected to be resolved in the MOC images are not only dunes, but also ripples, which occur on a much smaller scale, as well as yardangs, and the deposition of aeolian materials in depressions and as wind streaks behind objects. It may also be possible to see contacts between materials where the wind is gradually stripping away easily erodible material.

3.61 Erosional Processes

When wind moves across a surface, the kinetic energy of the wind is transferred to the surface through shear stress. Strong winds have greater kinetic energies than weaker ones and can therefore move or entrain more particles. The mechanism of particle transport by the wind is discussed by Livingstone and Warren (1996) and given a planetary context by Greeley and Iverson (1985). Due to the lower atmospheric pressure on Mars, the wind speeds must be an order of magnitude higher to initiate

particle movement (Sagan, 1973). This led early workers to propose that abrasion of the Martian surface by the bombardment of windborne particles would be an efficient process on Mars, since the particles would bombard the surface with greater speeds than on Earth (Sagan, 1973; Greeley et al., 1982). Viking results showed that although wind erosion occurs on Mars, it did not occur to the extent expected (Arvidson et al., 1979), and Greeley et al. (1982) attributed this primarily to the relative paucity of the 'sand-sized' particles (~100μm) that are required for abrasion of surfaces under Martian conditions. Greeley et al. (1982) found these sand-sized particles to be quickly reduced to silt or clay-sized particles in the Martian aeolian regime. They also found, via wind-tunnel experiments, that the 100μm particle size was the optimum size for entrainment by the wind, with smaller and larger grain sizes needing stronger winds before grain movement took place. Therefore if fewer 100μm sized grains are present on the surface of Mars, then fewer can be entrained to cause erosion of rock surfaces. The reason why larger particles need stronger winds to be entrained is because there is a larger mass for the wind to move. In the case of the smaller particles there are cohesive electrostatic forces holding the grains together that must be overcome before movement of individual grains can occur. This minimum force required to move a particle of a given size is termed the threshold shear force of the particle.

Although erosion caused by the wind was not found to have occurred at the large rates expected, Mariner 9 and Viking images still showed evidence for wind erosion since the equatorial regions exhibited yardangs, pits and grooves (McCauley, 1973; Ward, 1979; Ward et al., 1985), and wind-eroded pits were found in the polar regions of the southern hemisphere (Sharp, 1973b). Analysis of the MOC images in this study has shown that erosion of surface layers by the wind is a continually re-occurring feature within the MOC images of the Elysium mapping area. In some places, especially around Hecates Tholus, it implies the presence of soft, easily eroded material. This could be partially consolidated aeolian deposits, fluvial deposits, or volcanic deposits that are either loose, like ash, or partially consolidated such as ignimbrites or lahar deposits. In places weaker material becomes stripped away (a process called deflation) leaving more resistant areas of rock and streamlining them to produce features similar to terrestrial yardangs (see Figure 3.43a).

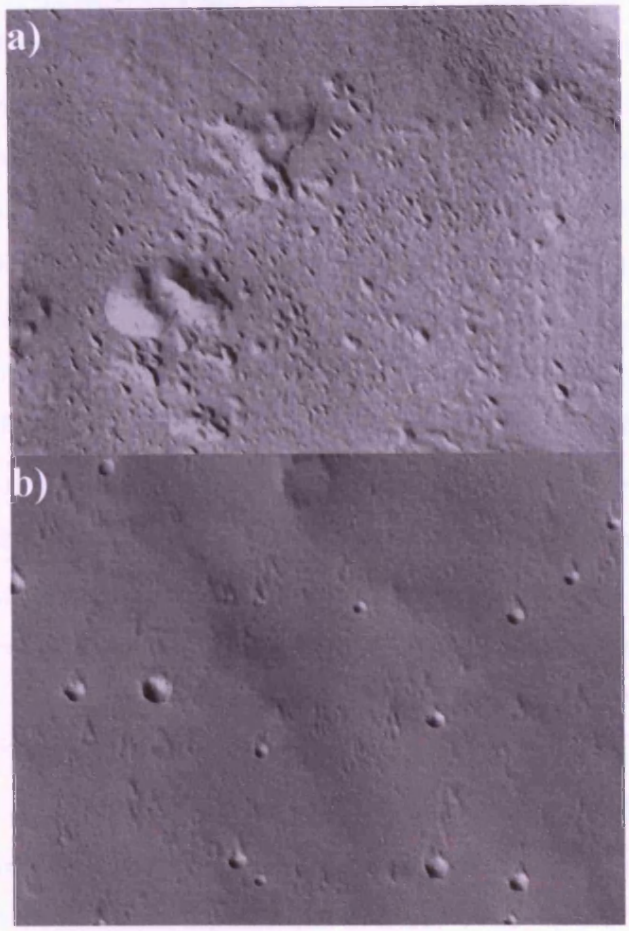

Figure 3.43: (a) Part of MOC image M03-01763 of an area within the depression on the northwestern flank of Hecates Tholus. The teardrop-shaped features are streamlined hills (yardangs), formed by the erosion of surrounding softer materials by prevailing winds. North is towards the top of the image, and the image width is ~1.05 kilometres; **(b)** part of MOC image M07-04049 showing an area on the flanks of Ceraunius Tholus. The triangular-shaped features occurring behind the impact craters are probably remnants of material that has been protected from the wind by the rims of the craters. Some of the features may be features similar to terrestrial barchan dunes. This image is ~2.7 kilometres in width, north is towards the top.

In other places deposition can be seen to be the most recent surface process dominating the mapping area, since many of the MOC images analysed in this study show substantial surface dust cover. It is generally agreed that the globally-averaged dust deposition rate on Mars is between 1 to 10 μm yr-1 (eg. Wells et al., 1984; Hartmann, 1999; Thomas et al., 1999; Burr et al., 2002). However, dust deposition may occur preferentially in some areas of Mars as shown in the regional dust-deposit model (Christensen, 1988), where it was calculated that dust is largely deposited between latitudes of 0 and 60° at an average of 4.6 x 10-3 $g.cm^{-2}.yr^{-1}$. According to Greeley et al. (1992), this deposition rate could produce the present equatorial and temperate aeolian deposits in 10^5 to 10^6 years. Therefore, it is likely to take a substantial amount of time to deposit the quantities of dust observed in many of the MOC images analysed in this study, and many of the surfaces can be inferred to be ancient. In other places, enhanced deposition or apparent deposition rates are observed, perhaps due to the positioning of an area of higher elevation that allows material to avoid being stripped

away, or encourages deposition of sediments (see Figure 3.43b). Often this type of deposition leads to the formation of wind streaks behind topographic obstacles. The formation and subsequent migration of these features is documented by several researchers including Sagan et al. (1973), Thomas et al. (1981), Thomas et al. (1984) and Lee (1984). The faster emplacement of 'dusty' deposits can occur via explosive volcanic eruptions, which can emplace large volumes of loose or partially consolidated material onto a surface in a short amount of time. The model produced by Mouginis-Mark et al. (1988) for the dispersal of pyroclastic particles falling from plumes shows that mm-sized particles will commonly be carried 100 kilometres downwind from the vent, and that 50μm diameter particles may travel up to 1000 kilometres. Therefore those deposits occurring far from the vent may not immediately appear to have been produced via volcanic eruption. Thus the volume of aeolian deposits in an area cannot be used alone as an indicator for the age of the underlying surface.

3.62 Small-scale processes

Perhaps the most important finding in this study regarding the analysis of aeolian deposits in the MOC images is the fact that, in addition to the large scale erosional and depositional features seen in the Viking images, there are numerous smaller scale aeolian bedforms and features. Figure 3.44(a) shows an area dominated by hills and shallow valleys. Loose material in this region has been laid down as dunes or ripples that have formed perpendicular to the wind direction. The dunes/ripples in Figure 3.44(a) generally range in size between ~25 and ~50 metres wide. On Earth ripples are in the range of a few centimetres to tens of metres wide, and dunes are larger, having widths of 1 to 500 metres. The sizes of the Martian features observed in MOC image SP2-43904 therefore span the size range where the features may be ripples or dunes. It would be interesting to find out whether the features were dunes or ripples because the distinction between dunes and ripples is not only one of size, but also mode of formation.

The mechanism of dune formation is not well understood although several workers have tried to document the process (Bagnold, 1941; Knott, 1979; Warren and Knott, 1983; Kocurek et al., 1992). It can generally be thought of as the accumulation of sand-sized sediment in and around obstacles or depressions, which in turn trap more particles that continue to build the dune. Whereas dunes are composed of similarly

sized particles, ripples appear to form where there is a mixture of different grain sizes. The formation of ripples may therefore be related to the way in which the wind shears across an interface between materials of different densities. The formation of both ripples and dunes is explained in detail in Livingstone and Warren (1996). Although both ripples and dunes do migrate, where dunes may move by up to a metre in a day during windy conditions (Hunter and Richmond, 1988), ripples can take less than ten minutes to reach equilibrium with new wind conditions (Seppala and Linde, 1978). Thus, depending on wind speeds, the bedforms in the region shown in Figure 3.44(a) may be constantly shifting and dynamic. It is also possible that these features are megaripples, which can take centuries to form and then remain in the same state for centuries. However, they generally form from coarser grained sediments which are unlikely to be common on Mars according to the work of Greeley et al. (1982) as discussed previously, and also from initial Mars Exploration Rover results, which seem to show that drifts of loose material in the landing site area are commonly fine grained particles (see http://marsrovers.jpl.nasa.gov/home/).

Most ripples form at right-angles to the direction of the wind that formed them, whereas dunes tend to show more varied forms. The features in Figure 3.44(a) have formed at right-angles to the wind direction and clearly show that the winds were diverted along the valleys and between the hills. This is particularly well demonstrated in the area towards the top left of the image where the winds have travelled around the hills, causing the orientation of the ripples to constantly change and form radially around the hills. Due to the size and shape of these features it is proposed in this study that they are ripples. If this is correct then they indicate a dynamic environment in the area shown in Figure 3.44(a), and also testify to the presence of a mixture of grain sizes.

It would be expected that where the energy of the wind drops on Mars, materials carried by the wind would fall out, since this is what is observed to occur on Earth (Owen, 1964; Bagnold, 1941; Wilson, 1971; Fryberger and Ahlbrandt, 1979). Figure 3.44(b) indicates that this is indeed the case. It shows a graben that becomes progressively deeper and wider from the left-hand side of the image to the right and exhibits a sudden steep decrease in elevation towards the right-hand side of the image. Orientations of small dunes or ripples on the floor of the graben suggest that the wind was channelled along the graben (since they formed perpendicularly to the trend of the graben). The wind strength, and therefore energy, will decrease when it encounters a drop in elevation and so material entrained by the wind will fall out of suspension and

be deposited on the lee of the slope (Hoyt, 1966; Anderson, 1988). A fan of material can be seen on the floor of the graben, presumably produced by the fall-out of materials entrained in the wind. This study shows that, although atmospheric pressure on Mars is much lower than on Earth, small-scale aeolian processes on Mars appear to be similar to terrestrial ones.

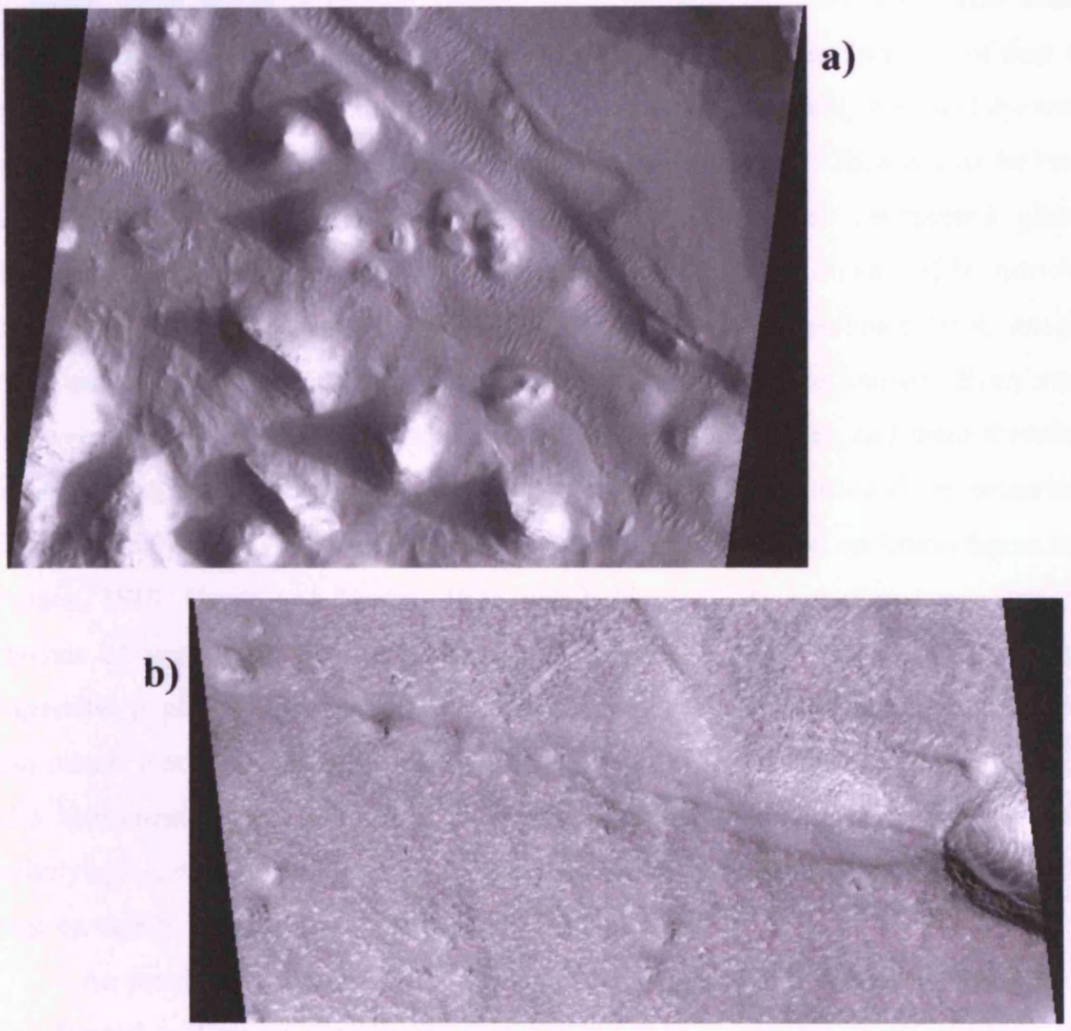

Figure 3.44: **(a)** Part of MOC image SP2-43904 showing part of the northern Elysium plains. It clearly shows that the wind is diverted around the small hills, since the direction of the ripples in the channels and valleys between the hills changes direction following the path of the wind. This image is 4.85 kilometres in width and north is towards the top; **(b)** Part of MOC image M03-04232 showing an area near the chaotic terrain west of Hecates Tholus. It is evident that the graben in the image has channelled the wind from left to right, since,where the elevation decreases, the wind loses energy and dusty material has dropped out to produce the fan effect seen on the floor of the graben at the right-hand-side of the image. The image is 3.13 kilometres in width and north is towards the top.

3.63 Dunes

Prior to the MGS mission it was obvious that dunes formed on Mars since they could be seen in the Mariner 9 and Viking images (eg. Cutts and Smith, 1973). Dune fields usually appeared as dark patches of material, since the resolution of most of the images was not good enough to resolve dunes that were only several metres in diameter. However, some higher resolution images were available in which individual dunes could be resolved. In addition to this, the fact that there was a large amount of dust on the Martian surface, and the fact that aeolian processes were probably the most dynamic process occurring on Mars at present, were also known prior to MGS, since as far back as in 1954 de Vaucouleurs observed Mars from Earth and interpreted global obscurations of major albedo features on the surface of Mars to be caused by massive dust storms. However, it was not until MGS sent back the high-resolution MOC images of the surface, that the extent of the dust cover on the surface was known. Even areas that were sparsely covered with impact craters in the MOC images, and were therefore thought to be relatively young, were usually covered with mantling dusty materials. This is not surprising given the extent of the dust storms observed on Mars (Sagan and Pollack, 1969; Capen and Martin, 1971, 1972; Hess, 1973), but does mean that the analysis of small-scale surface features and textures is made more difficult, if not impossible in places, since they have been covered in dust. The extent of the dust cover also means that spectral studies of the surface, such as that carried out with the MGS TES instrument, mainly send back chemical compositions of the dust cover, not the underlying bedrock, except in those places where bedrock is exposed with a spatial area large enough to be resolved by the instrument in question.

As previously discussed, the ripples occurring in Figure 3.44(a) were likely to have formed as the wind carrying the particles has been channelled along a feature, and therefore to a small extent their formation has been controlled by topography. The formation of dunes can also be controlled by topography. Those that are not controlled by topography can be termed 'self-accumulated' (Pye and Tsoar, 1990) and several examples of these self-accumulated or 'free' dunes have been found in the high-resolution MOC images analysed in this study. The features are larger than those observed in Figure 3.43(a), and they have also been found to take on different shapes. This is probably primarily due to different wind directions and wind strengths as

explained in the study by Fryberger and Dean (1979), who showed that, in general, dunes could be classified by the wind regimes that form them.

Some examples of features that are possibly barchan dunes have been shown in Figure 3.43(b), although as mentioned in the previous section these features may also have resulted from deposition or the protection from erosion of softer sediments behind the rims of impact craters. Barchan dunes are a type of transverse dune, which means that they have slip faces (the slope at the front of the dune) that face in roughly the same direction and they are characterised by net sand transport normal to their crest (the top of the dune that is normally the point of maximum height). Barchans are crescent-shaped dunes that generally form isolated ridges and are often found on firm, coherent surfaces such as desert pavements (Livingstone and Warren, 1996). Since there has been much speculation, particularly regarding the panoramic scenes returned by the Viking Landers, that many of the plains of Mars might be desert pavements (eg. El-Baz and Maxwell, 1982), the presence of barchan dunes may be expected. The possible presence of barchan dunes in the Hellespontis region of Mars (47.5° S, 331°W) was suggested by Cutts and Smith (1973) in the Mariner 9 images. In general these dunes form from unimodal wind regimes (Fryberger and Dean, 1979).

Further types of dunes are shown in Figure 3.45 (a) and (b), where many dunes of the same kind have formed together to produce dune fields. Small dunes that are between <10 metres to ~35 metres across are shown in Figure 3.45(a). These do not appear to be long and narrow like ripples, so it is assumed in this study that they are dunes. In places the material in the area shown in Figure 3.45(a) has formed into longer transverse dunes that are occasionally overlain by the smaller dunes. As with the barchan dunes, the ones in this image have been formed by one prevailing wind direction. The smaller dunes in this image appear to be a different shape to the larger transverse dunes, but they are barely at the resolution of the image and the shape of the small dunes can be distinguished.

When an area is exposed to winds coming from several different directions over time, the dunes tend to form into a star shape (see Nielson and Kocurek, 1987, and a review by Lancaster, 1989). Star-shaped dunes were found in the mapping area, within impact craters that were superimposed on a lava flow (see Figure 3.45b). These dunes are more likely to be examples of 'controlled' dunes rather than free ones, and the relatively sheltered nature of this setting may be one of the reasons that these dunes were able to form, since once they had descended into the bowl of the impact crater the

winds would have been diverted from the regional wind regime. Star-shaped dunes were not observed in any of the other MOC images analysed, not even within impact craters in other areas.

The occurrence, type and size of wind-blown dunes will vary depending on the geological setting of the area, and may thus be able to aid geological analysis of the Martian surface. Greeley et al. (1992), found that Viking data showed that most dunes on Mars have a morphologic similarity to terrestrial barchan and transverse dunes. Although the presence of very fine-grained material has been shown in the 'drifts' of material analysed by the Mars Exploration Rovers (as mentioned earlier), Greeley et al. (1992) suggested that the presence of these types of dunes made it likely that the dunes were composed of sand-sized materials, as they would be on Earth. Linear dunes are formed when there is a wide unimodal or a bimodal wind regime (according to the work of Fryberger and Dean, 1979), and are characterised by the fact that sand transport is parallel to the crest of the dune. This type of dune was not observed in the MOC images analysed in this study, and testifies to the presence of narrow unimodal wind regimes that produce transverse and barchan dunes. It would therefore appear that star-dunes are produced where topography has an influence on diverting the regional wind regime. Where one dune type is superimposed on another type (as possibly shown in Figure 3.45b), this can be termed a 'complex' dune field pattern (McKee, 1979; Breed and Grow, 1979). When this occurs on Earth it may mean that the larger dunes have adjusted to a complex wind regime and then been overlain by smaller dunes that have adjusted to a more recent wind pattern.

The erosional and depositional features observed and documented in previous studies using Mariner 9 and Viking data, were also visible in the MOC images. However, smaller scale processes were also visible and are important because they show that despite the differences in atmospheric pressure and gravity, the aeolian processes occurring on Mars are similar to those observed on Earth. Potential ripples were observed in the MOC images, as well as the channelling of the winds by even relatively small depressions or topographic highs (only tens of metres in elevation). Different types of dunes were observed, most showing narrow, unimodal wind regimes, although some, such as the star dunes observed in Figure 3.45(b) formed in conditions where the regional wind regime is diverted by topography. Complex dune fields have been observed where one type of dune is superposed on another and indicate changing wind patterns. This shows that Mars is more dynamic than is indicated by the presence

of aeolian features that show areas of the surface that is dominated by the unidirectional flow of winds for long periods of time, such as yardang fields as discussed at the beginning of this section.

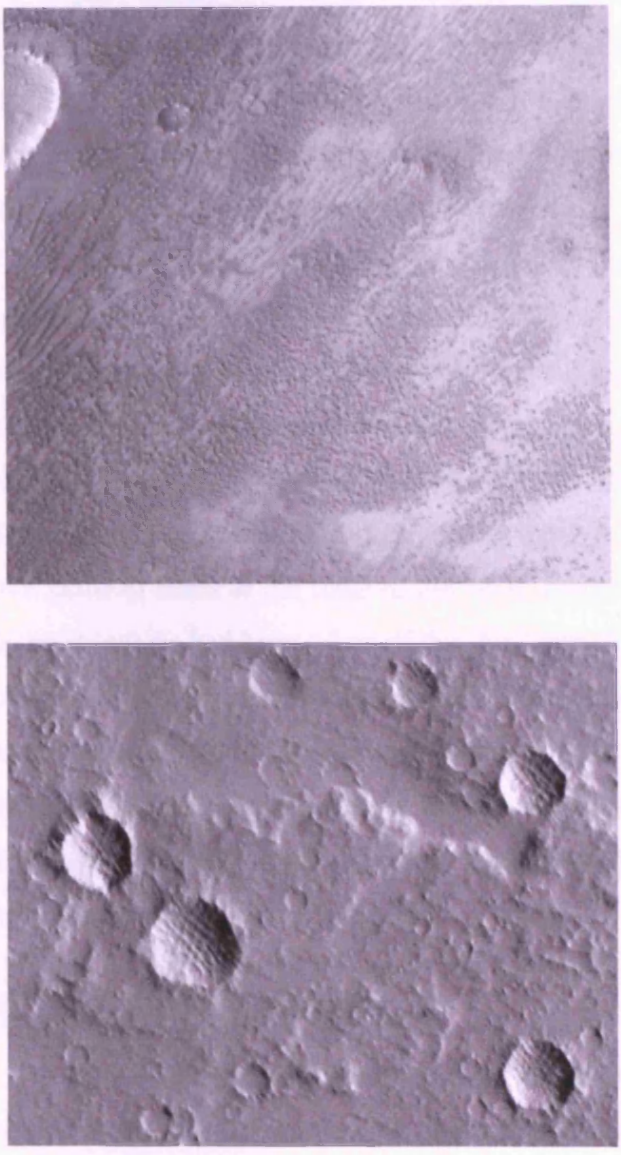

Figure 3.45: (a) Part of MOC image M07-01588 showing dune fields on the flanks of Arsia Mons. On the left of the image the dunes are long and linear, but further towards the centre the dunes are smaller and occur in patches. The image is 2.92 kilometres across, and north is towards the top; **(b)** Part of MOC image SP2-54804 showing dunes within craters emplaced on a lava flow from Elysium Mons. The dunes appear to be similar to terrestrial star-shaped dunes, implying several different prevailing wind directions. This image is 3.74 kilometres across and north is towards the top.

3.7 Impact Cratering

Impact cratering is another important process that has constantly been shaping the surface of all of the rocky bodies of the solar system, both in the past and also at present (Melosh, 1989). The study of the morphology of impact craters on Mars has shown that it has a diverse array of crater types, and these have been attributed to many different factors including differences in target strength, depth of excavation, the presence of near surface volatiles and environmental conditions (Carr et al., 1977a;

Mouginis-Mark, 1979; Bridges and Barlow, 1989). Since impacts can penetrate into deep subsurface rock layers, it was hoped that some interesting layering may be present in some of the crater walls, as well as in the floors of the freshest craters. Analysis of the impact craters showed more than just layering within the walls of craters. The images also showed different ways in which the impact craters were modified, as well as insights into the formation processes of Martian impact craters. Given the large numbers of impact craters present in the MOC images, a discussion of the analysis of these features is given in this section.

At the higher resolutions of the MOC images, large numbers of small impact craters were visible. The percentage of the surface that is covered with small (100 metres or less in diameter) craters is surprisingly high in some parts of the mapping area, particularly in areas covered by lavas, such as the caldera of Elysium Mons (see Figure 3.21). It is therefore proposed in this study that many of these small craters found in volcanic areas are volcanic in origin. It is difficult to distinguish between the two kinds of crater at the scale of the MOC images, although it may have been easier to do so if images had been taken of the 'Flo' unit discussed in the mapping chapter, since proposed explosive craters in this unit were at the limit of resolution for the Viking cameras, and would have been visible in pictures taken by MOC. It is, of course, also possible that these craters could be secondary craters that formed as a result of the break-up of larger impacting bodies. Neither origin can be proved or discounted using MOC.

3.71 Impact cratering processes

Some of the images analysed in this study give insights into crater formation processes on Mars. For example, the collapse features observed on the west and north-western flanks of Hecates Tholus have an ambiguous origin (see Chapter 4). Tanaka et al. (1992) suggested that the features were volcanic in origin. Analysis in this study of high-resolution MOC images of this area of Hecates Tholus have led to the suggestion that the features are actually degraded impact craters. MOC images of the walls of the depression show that sections of the wall of the depression are layered, and some layers appear to decrease in thickness as distance from the centre of the depression increases (see Figure 3.46a). As an ejecta blanket from an impact crater is expected to thin as it moves outwards from the centre of the impact (Melosh, 1989) then it is possible to suggest that the materials observed in the exposed walls of the flanks in Figure 3.46(a)

are impact ejecta materials. However, it is also true that emplacement of the material by an explosive volcanic event may have a similar effect and thus cannot be ruled out. The material appears to be easily erodible, as shown in Figure 3.46(a) which shows the base of the depression, but partly welded or loose relatively fine deposits would be expected for both mechanism presented here. See Chapter 4 for further discussion of this.

Many impact craters on Mars have ejecta blankets that appear to have flowed either during or immediately after formation (Carr et al., 1977a). This implies that the impactor landed in a region rich in ground-ice, which fluidised the ejecta, allowing it to flow. Other features associated with this flow-like ejecta appearance such as central pits (Smith, 1976; Wood et al., 1978) and double and multiple lobate ejecta (Greeley et al., 1980; Mouginis-Mark, 1981a; and Barlow and Bradley, 1990) have been used as evidence that subsurface volatiles were involved in the formation of impact craters with this appearance. The presence of craters with this morphology is widespread on Mars (Allen, 1979; Mouginis-Mark, 1979), and MOC images of some of these craters within the mapping area were analysed in this study. This allowed the appearance of the craters and associated ejecta to be observed at a resolution of only a few metres. Analysis of these images has shown that the ejecta of these craters has a characteristic 'jumbled' or irregular appearance, and that this was found in many of the images analysed. There was no obvious evidence for flow on a small scale, and instead the material has a chaotic appearance. Figure 3.46(b) shows an example of one of these impact craters and the characteristic 'jumbled' ejecta material. The floor of the crater also appears to have experienced the flow of some material, potentially ejecta that slumped into the base of the crater. The base of the crater shows apparent flow from north to south in Figure 3.46b, forming a 'banded' appearance.

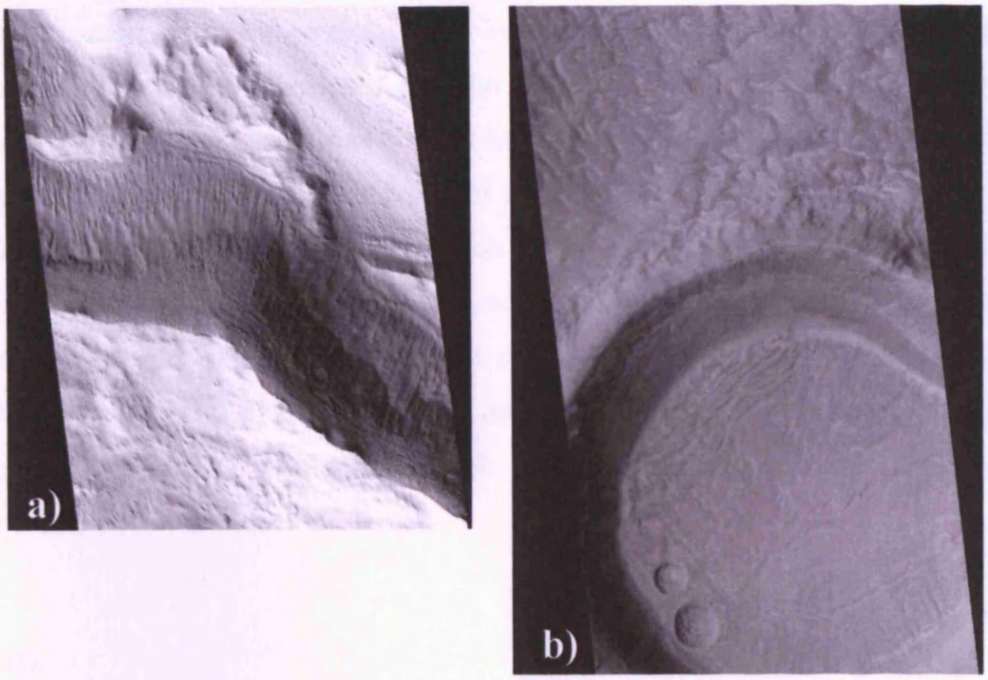

Figure 3.46: (a) showing part of MOC image M03-01763, of the southern wall of the depression situated on the north-western flank of Hecates Tholus. Several different rock layers can be seen in the wall of the depression, one of which seems to decrease in thickness from one side of the image to the other, and may represent a layer of impact ejecta. North is towards the top, and the image is 3.13 kilometres across; **(b)** showing part of MOC image M22-02410 of an impact crater on the plains north of Elysium Mons. Layering of materials is visible in the wall of the crater, and materials on the crater floor appear to have flowed and produced flow-banding features. The ejecta seen to the north of the impact crater in the image has a jumbled appearance that is typical of ejecta blankets seen on the northern plains in the mapping area. North is towards the top of the image, and the image is 3.15 kilometres.

3.72 Impact Crater Modification

Study of the MOC images has shown that impact cratering on Mars is an important geological process that still occurs on Mars today, at least within the areas studied, as shown by the numerous fresh-looking craters observed in many of the images analysed. However, image analysis carried out in this study has also shown that the older impact craters have undergone much modification due to a number of processes. The images in Figure 3.47 show some of the ways in which impact craters can be modified on Mars. Aeolian activity probably has the biggest effect on the appearance of impact craters, since crater materials can be stripped away by the wind leaving blocky, blunt-edged crater rims (see Figure 3.47d), or can bury the craters and

ejecta blankets (see Figure 3.47a) with loose, dusty material. Burial of craters by volcanic products such as lava flows also occurred in the past (see Figure 3.47b). Modification by fluvial processes has been seen to occur, particularly in the Viking images of flooded terrains on Mars, but high-resolution MOC images of the Martian surface have shown that it was not just liquid water that has affected impact craters. It appears that in some areas the floors of impact craters have rebounded over time (see Figure 3.47(c). They have an appearance similar to some of the impact craters observed on the icy moons in the outer solar system (see Figure 3.48). One theory is that the materials in the bases of these impact craters on the icy moons are thought to have flowed to allow the floors to rebound and in some cases for a weaker ice layer to be uplifted to form a central peak (Schenk, 1993). Modelling of crater relaxation in a

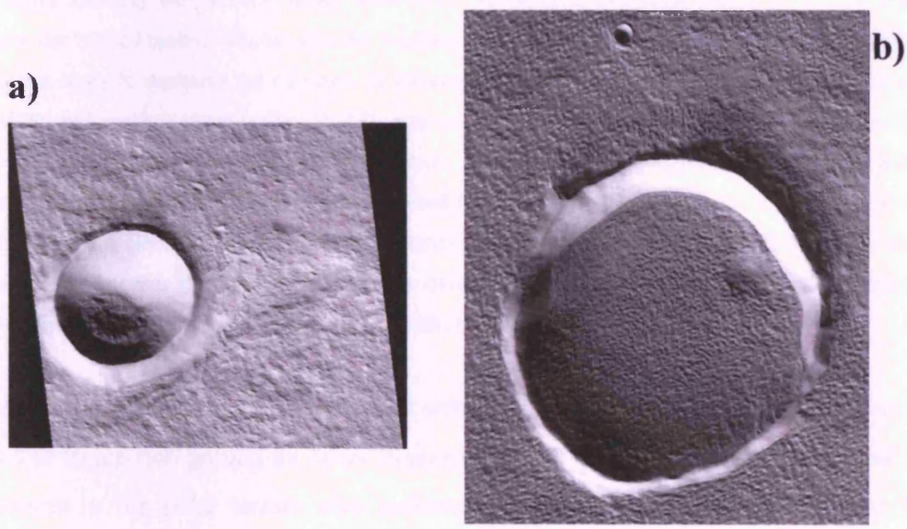

Figure 3.47: (a) part of MOC image M10-01500, showing an impact crater on the flnaks of Hecates Tholus. This bowl-shaped crater is ~1.1kilometres in diameter, and the base of the crater appears to be filled with a deposit of dusty material. Ejecta from this impact is hardly visible, and must have been removed by erosion or buried by other materials. North is towards the top; **(b)** part of MOC image E09-02627 showing part of the summit region of Alba Patera. The larger crater towards the bottom part of the image is ~3 kilometres in diameter, and appears to have been filled by a large amount of material. It may have been flooded by lava from the volcano, since there is a breach on the rim of the crater on both the left and right-hand sides. North is towards the top.

c)

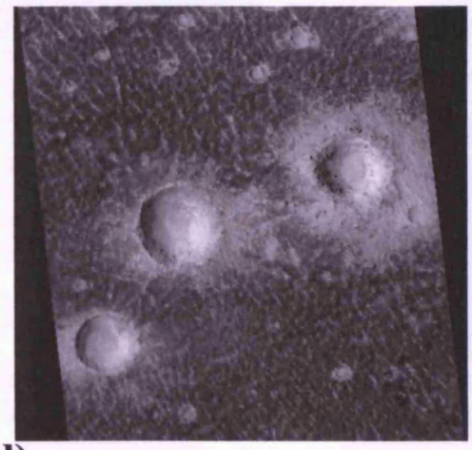

d)

Figure 3.47: (c) part of MOC image M07- 03645 showing an area of the plains north of Elysium Mons, near the 'ribbed mound' discussed in the mapping chapter. The circular features in this image are thought in this study to represent the remnants of ice-modified impact craters. The image is 3.14 kilometres in width, and north is towards the top; **(d)** part of MOC image M22-01769, showing an area within the 'rough flows' (**Frf**) unit near the Elysium Fossae. The surface texture appears to be platy and the material is dark. Where impact craters have punctured the surface, the brighter underlying material has been thrown out as ejecta on top of the darker material. The impact crater on the right of the image may be the oldest one because it is not as pristine as the others and the rim is starting to be eroded into blocks and boulders. The image is 2.36 kilometres in width and north is towards the top.

viscous medium overlying a rigid substrate has shown that a similar effect should occur in ice-rich ground on Mars (Squyres, 1989). Recent studies of 'softened' impact craters in the polar terrain also indicate that ice-rich ground facilitates the flow of materials (Turtle et al., 2001). Therefore it is proposed in this study that the presence of water-ice within the ground has facilitated the gradual 'flow' of the material within the impact craters imaged in Figure 3.47(c). Over time this has allowed the ground to rebound to compensate for the loss of the overlying ground layers.

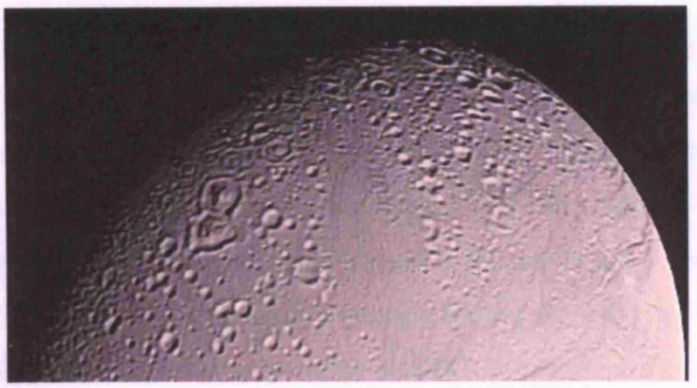

Figure 3.48: High-resolution photomosaic of part of the northern hemisphere of Enceladus (a small icy moon of Saturn). Central peaks in the centre of the impact craters towards the top and left of the image may either have be volcanic edifices constructed from ice, or may be due to the rebound of the crater floors, facilitated by the presence of ice. Enceladus has a radius of 249 kilometres and the images used to produce the photomosaic were taken by Voyager 2, courtesy of the Jet Propulsion Laboratory, NASA.

Analysis of impact features using the MOC images has been interesting because it has highlighted the fact that impact craters can be modified in many different ways and testifies to the fact that many different geological processes have occurred in the mapping area over time. In this study impacts have been modified by infilling both by aeolian deposits and by lava flows, and also by the action of wind and ice. Layering observed within the flanks of Hecates Tholus has potentially uncovered a section through the ejecta deposit of an impact. This has shown that a typical thinning of the ejecta with distance from the centre of the impact has occurred as it does on Earth and in laboratory experiments simulating impact processes.

The most interesting part of the analysis into impacts carried out in this study was the study of the rampart craters that show ejecta that has apparently flowed. Where it may be expected that the high-resolution MOC images of such ejecta would show evidence for flow, the MOC images actually show that the ejecta is in the form of jumbled blocks of material. Such impacts are thought to have occurred in ice-rich ground, as discussed previously. Those impacts analysed in this study that show rebounding of the floor of the crater are also thought to have formed in ice-rich ground although they do not exhibit lobate ejecta. They provide further evidence that ground-ice is or was present in the mapping area.

3.8 Conclusions about the surface of Mars

The MOC images have revealed much about the surface of Mars, with particular reference to the surfaces in the mapping area of this study. The MGS MOC instrument was the first instrument to give scientists the chance to resolve surface features that are only a few metres in size, and thus it has allowed a greater insight into the geology of specific areas. Not surprisingly, aeolian processes are the most dynamic and frequently occurring processes on the planet at present, and this is shown with the abundance of erosional and depositional features presented and discussed in this chapter. Importantly to this study, the erosion and burial of features via wind-blown materials is the major modification occurring to lava flows on Mars at present. In many places only the levées of the oldest flows remaining above a blanket of loose deposits, and form a characteristic, linear type of surface texture on several of the volcanoes studied. Except at Olympus Mons where many of the flows are still very well preserved, most of the flows analysed in this chapter and in Chapters 5 and 6 have been modified by dust cover so that it remains difficult, even with the higher resolution images, to gain information about small-scale surface textures such as the ropy texture of pahoehoe, or the rubbly flow tops expected of aa flows. Also, the high levels of dust mantling on Olympus Mons and Alba Patera (which both have surfaces that are relatively young compared to the two other volcanoes studied) suggest that much of the material is the result of pyroclastic activity. Other images showed evidence for the presence of both aa and pahoehoe flows, both at Elysium Mons and at Alba Patera. This is important because the presence of both is implied using other techniques in the lava flow studies chapters. No evidence was found to either prove or discount the presence of volcanic craters in the Elysium volcanic units.

The modification of impact craters by aeolian processes includes burial of the floors of channels and fossae by aeolian materials, which made it difficult to study any flow that may have occurred through these features but some evidence for fluid flow was still visible. Small scale (tens of metres in size) aeolian and periglacial features have been observed in this study using the MOC, and all have highlighted the many similarities between Martian and terrestrial geological features and processes. The presence of periglacial features is evidence for the presence of ground-ice in Elysium in the past and perhaps also in the present. This is important because the analyses carried out in this section of the study agree with the results of the mapping

exercise in the next chapter, where it is found that the presence of ground-ice was likely to have influenced the formation of units in the area north of Elysium Mons.

4.0 Geological Mapping

This chapter aims to outline the methods that were used during the geological mapping research that was carried out in this study. It also presents the results that were obtained from the mapping, and discusses how they determine more about the geological history and major geological processes affecting the Elysium region, which was the chosen area of interest. The results of previous studies concerning the geological history and mapping of Elysium have been outlined in Chapter 1. The results of this present study were produced using both previously and newly available imagery, as well as the new topography data from MOLA, and therefore highlight some new aspects of the geology of this region that were previously unnoticed. More specifically it was the aim of this study to use the MOLA data and MOC images to gain more information regarding the formation and evolution of the Elysium Fossae. A second major aim of this mapping study was to use the new data from MGS to re-map the area of interest in order to highlight features and processes that had not been observed previously. The MOC images have been used to show small-scale surface details that help to provide information regarding geological processes occurring in the chosen area.

4.1 Methods of Geological Mapping

4.11 Aims

The production of the maps in this chapter was based on images of the surface, and topography data. Due to the lack of compositional data for the rocks observed in Elysium, the maps produced in this study aim to show not only different rock types, but also different geomorphologies. The geomorphology of the region not only gives insight into which rock units are different from others, but also shows how the area has changed throughout time, and what processes were involved in this change. Two maps were produced in this section of the thesis. One is a sketch map that is designed to give an impression of the overall geology and history of the area of interest and the immediate area surrounding it. The second is a more detailed map that is intended to show some of the more complex history of the region to the north and west of Elysium

Mons, where previous studies have indicated that there has been extensive fluvial and volcanic activity and interaction (as explained in Chapter 1).

4.12 Boundaries and choice of units

In the maps presented in this chapter, an area of the surface that had a particular texture or was covered in particular types of features was designated a Geological Unit. Each Geological Unit represents a particular rock type and is unique, having particular characteristics. Sometimes a rock type is inferred by the way in which it has been laid down and subsequently modified. Units are therefore also used to infer the geological history of the area. Two areas that are of the same rock type but which have been modified in different ways are designated as two separate units but will be related stratigraphically (since they will have been laid down in the same period of time) and in the way that they are named. Naming of the units was carried out according to which part of the area the material occurred in (such as whether it made up part of the plains or part of a volcanic construct). The unit name also often included a particular feature that was characteristic of the unit, such as ridges or lava flows.

Boundaries of the units indicate where one unit ends and another begins, and can often show the relationships between units (see section 4.13). They were identified where the characteristic features or surface texture of a unit ceased to be present. Other indications that a boundary between two units was present are changes in density of surface impact craters (due to differing ages of the units); cross-cutting relations of surface features; and superposition of younger units on top of older ones.

4.13 Ages of Units

In this study, only the relative ages of units have been given, since it was the overall history of the area and the processes that occurred in it that were of interest and not the absolute ages of the units. Estimates of the absolute ages, produced by Plescia and Saunders (1979) and Neukum and Hiller (1981), of the surface materials in the Elysium area have been discussed in Chapter 1. The relative ages found in this study were produced from observation of features in the images, and were determined mainly by using the density of impact craters, by using cross-cutting relationships between units, and by superposition of rock units.

Since the end of the period of heavy bombardment by impactors early in the history of the solar system, the rate of impact cratering on Mars has remained relatively steady (Chapman, 1974; Chapman and Jones, 1977; Tanaka, 1986), so it would follow that the longer a material has been exposed on the surface of a planet such as Mars, the more impact craters it will accumulate. This is one of the main foundations of the studies of absolute Martian ages as discussed in Chapter 1. Thus, it was sometimes possible to see areas in the images where one area of the surface was more covered with impact craters than another. This was particularly obvious where there were many larger impact craters, since the larger impacts (over 100 kilometres in diameter) occur less frequently (Strom et al., 1992) and therefore are another indication that the unit where they occur is old. Generally then, where a more heavily cratered area lies next to a less cratered area, this can be used to define a boundary between units and shows which unit is the older one. Those areas with a relatively higher number of large impact craters can be inferred to be some of the oldest units in the mapping area. However, although rates of resurfacing due to weathering are not as high as those on Earth, impact craters do become filled in by dust and can be flooded and in-filled by lava flows, so this method of defining relative ages is not without its limitations.

Geological features such as graben, ridges and even lava flows can be sometimes be used to determine the relative ages of several units using the principles of cross-cutting relations. For example, if a graben cuts across several units but one of the units has embayed and filled the graben then this unit will be younger than the graben and hence younger than the other units that are cut by the graben. In cases where it is possible to see where one unit has been emplaced on top of another, the principles of superposition can be used to determine relative ages. In this study it has been assumed that the topmost unit is the youngest and therefore a stratigraphic history for all the units can be inferred. Even if units are not adjacent to each other, it is possible to say which of the two is the oldest because of the way they have been emplaced relative to other units with clear stratigraphic relations. The MOLA data were useful in this respect because they could be used to show whether a unit was emplaced on top of another, and could also be used to provide a thickness value for each unit.

4.14 Image Analysis

Mapping the surface of planets other than the Earth must be approached in a different way to conventional terrestrial mapping because it is rarely possible to obtain field data or samples from the area of interest (except for selected areas on the Moon). Planetary mapping involves using data that has been collected remotely, to infer something about the composition, formation and subsequent modification of the materials in a selected area of a planetary surface. Photogeology is one of the main methods used in these cases and the theory and use of this technique has been described by Wilhelms (1990). An outline of the methods of photogeology is given in Chapter 3 (section 3.2). There were several sets of images that could be used for photogeological analysis in this study. The Viking photomosaics and individual prints could be used to observe larger scale features and surface textures. The new Mars Orbiter Camera (MOC) images, could be used to analyse smaller-scale features with widths of several metres.

Apart from the images, topography data, gravity and spectroscopic data available, it is also possible to relate what is observed in all the remotely sensed data, to terrestrial data (terrestrial analogues) and thus find similarities that might help to explain what is being observed on the surface of the planet of interest. When a terrestrial analogue could not be found, a mode of formation had to be constructed using information known about the surrounding geological environment (such as likely rock type, the presence of water/ice or volcanic flows, and other environmental conditions). Some of the features observed would be characteristic of a surface material and would lead to the material being mapped as a geological unit.

4.15 Analysis of MOLA data

The ability to use MOLA was a key element to the mapping in this study, since detailed topographic knowledge was not available during previous mapping studies. The shaded topography images, like the one used to produce the sketch map of Elysium in this study, made many units stand out more obviously than they did in the images, and the relationships between units became more obvious, particularly concerning the 'fossae materials' (see section 4.3). Contour maps were used to give a general

impression of the relationships between features in the area, and to highlight those areas with particularly steep or shallow slopes.

MOLA profiles were used in a number of ways. As mentioned previously, they were used to determine whether a unit was overlying another if it was not clear from the images, and could be used to determine thickness values for units where it was thought to be important. If it was not clear how a feature formed then a profile could often be obtained that crossed the feature. This could be used to provide information regarding the nature of a feature, how it was formed and how it related to the surrounding area. MOLA profiles could also be used to show the shape of a feature, this was found to be particularly useful when applied to features such as volcanic edifices. Profiles across larger features could be obtained using IDL (as outlined in Chapter 2) and could be used to determine slopes.

4.16 Errors and difficulties

One of the major difficulties with the mapping carried out in this study was the fact that there were virtually no compositional data available for the materials in this area at the time of study. There are limited compositional data from the MGS Thermal Emission Spectrometer (see section 4.8), and also from the Viking Landers, Pathfinder and the Martian meteorites, but these provide general data that are not specific to Elysium. More recently, field data from the Mars Exploration Rover 'Spirit' have shown evidence that basalt and also andesite are present in Gusev crater (Squyres et al. 2004b). Gusev crater is in the Elysium Basin south east of the mapping area and therefore it is possible that these types of rocks are present in the mapping area. In Chapters 5 and 6 some inferences are made about the lava that formed the extensive lava flows in the Elysium region, using information gained from lava flow modelling. Knowing how the units were emplaced, either from information from modelling or from mapping and image analysis, allows for the inference of composition, and this is discussed in section 4.3.

A major potential error concerns the analysis of Martian features using terrestrial analogues. Some terrestrial geological features can be formed by two or more different geological processes. This means that if analysis of a feature is based heavily on this kind of data, the conclusion obtained about the formation of the Martian feature could be wrong. This is particularly well exhibited by certain periglacial features. Periglacial

features are formed in areas where the top few metres of soil are frozen in the winter, but thaw during the summer months leaving a permanently frozen layer several metres below the surface. Hexagonal patterns can form in these conditions, induced by the action of the freezing and thawing of the ground. However, similar patterns can be formed in places where there is no water or ice at all due to desiccation of the ground (Washburn, 1956). The danger in this analysis is that in one case there is plenty of water present (as ice or melt-water), and in the other there is none at all. Clearly then, the analysis of features must be supported by evidence from the surrounding area too.

4.2 Physiographic Setting of Mapping Area

A shaded MOLA topography image (created by the MOLA Science Team) of the whole area of interest is shown in Figure 4.1. It covers an area bounded by the co-ordinates 5 – 40° latitude and 130 – 170° East longitude (190 – 230° West longitude). In the middle of the mapping area is Elysium Mons, which is accompanied by two further volcanoes Hecates Tholus and Albor Tholus, which lie to the north and south of Elysium Mons respectively. Elysium Mons reaches a height of over 13 kilometres above the Mars Mean Datum (MMD), with the steeper part of the cone rising ~11 kilometres over the surrounding area. The other two volcanoes are less high, with Albor Tholus having a maximum height of just over 3 kilometres above MMD, and Hecates Tholus reaching a height of around 4 kilometres above MMD.

The region has numerous graben, some seemingly circumferential or radial to Elysium Mons. Those that are tens of kilometres in length and width are termed Fossae. Most Fossae also have characteristic flat floors. The three volcanoes are positioned on top of and, in most cases, surrounded by a large, low dome of material that covers a roughly circular area of ~1500 kilometres in diameter. To the north and west of this the ground steadily decreases at a slope of around 2° into the Utopia Basin, until it descends to an elevation of 3 kilometres below MMD (as measured by MOLA). Many fluvial channels and lava flows extend from the north and western edge of the dome of volcanic material down into the Utopia Basin. To the north east of the volcanic dome and the volcanoes, is a region of plains and heavily cratered mountains. Similar mountains are found to the south of the volcanoes and dome, and to the southeast is a

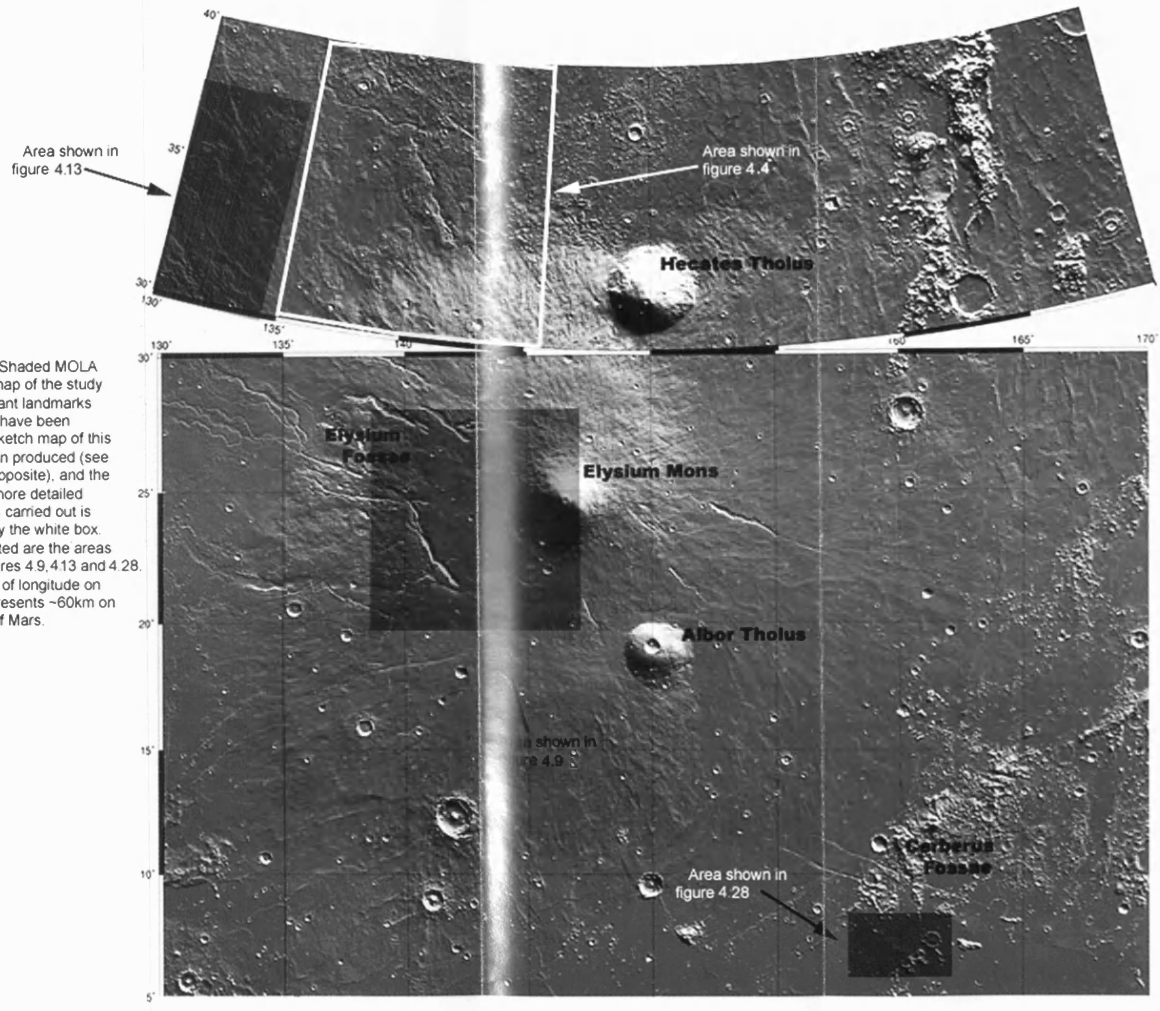

Figure 4.1: Shaded MOLA topography map of the study area. Important landmarks and features have been labelled. A sketch map of this area has been produced (see Figure 4.2 opposite), and the area where more detailed mapping was carried out is highlighted by the white box. Also highlighted are the areas shown in figures 4.9, 4.13 and 4.28. Each degree of longitude on this map represents ~60km on the surface of Mars.

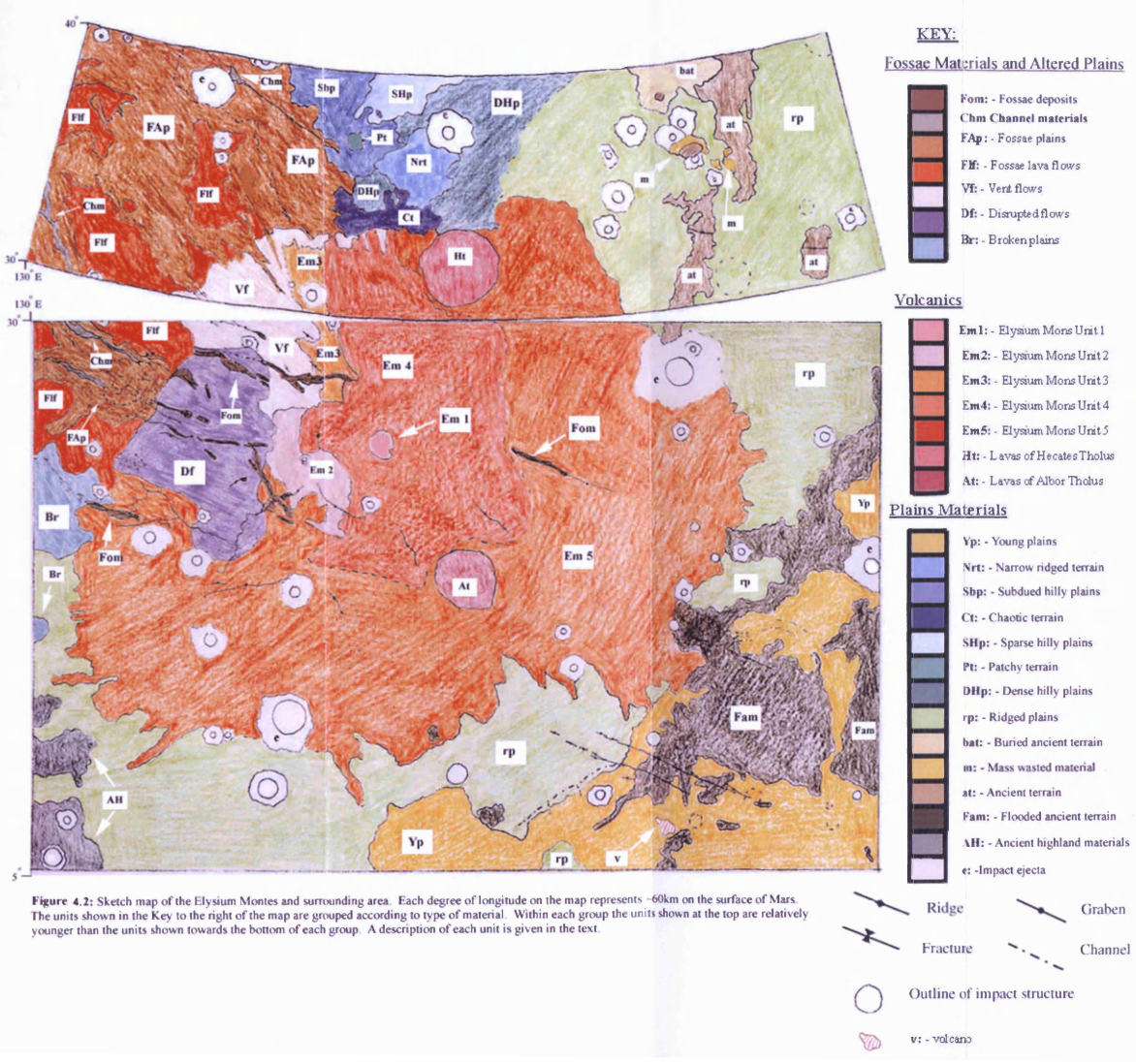

Figure 4.2: Sketch map of the Elysium Montes and surrounding area. Each degree of longitude on the map represents ~60km on the surface of Mars. The units shown in the Key to the right of the map are grouped according to type of material. Within each group the units shown at the top are relatively younger than the units shown towards the bottom of each group. A description of each unit is given in the text.

series of graben called the Cerberus Fossae which appear to have been the source of major resurfacing in the south east area (Plescia, 1990, 1993; Tanaka et al., 1992; Hartmann and Berman, 2000; Keszthelyi et al., 2000; Burr et al., 2002.

4.3 Mapping Units

The sketch map showing the area of interest in this study is shown in Figure 4.2. In the following section the units shown on the map will be discussed. It was found that the units could be divided into three groups: Volcanics; Plains Materials; and Fossae Materials (see Figure 4.3). Since the main aim of this study is to discover more about the processes occurring on and in relation to the major volcanoes in this region, the units that were formed by or had an effect on the development of Elysium Mons and Albor and Hecates Tholi, will be discussed in more detail. Since most of the Elysium lava flows that were studied in Chapters 5 and 6 are situated to the north west of Elysium Mons, as well as this being the area where much of the volcano/volatile interaction and fluvial activity occurred, this area has been mapped in more detail (see Figure 4.4). Many of the units in this area north west of Elysium Mons are discussed in detail because they provide an insight into much of the activity that has occurred in the mapping area.

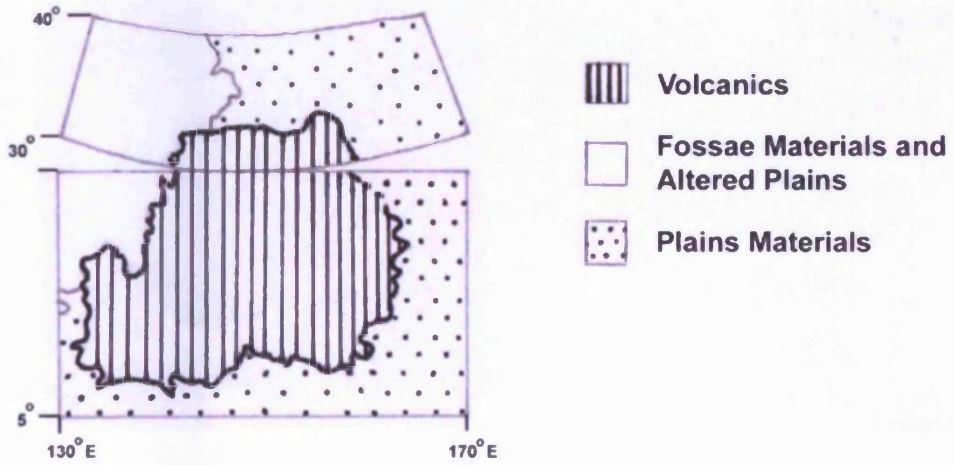

Figure 4.3: General sketch map of the Elysium mapping area, showing that it has been divided in this study into three main types of materials.

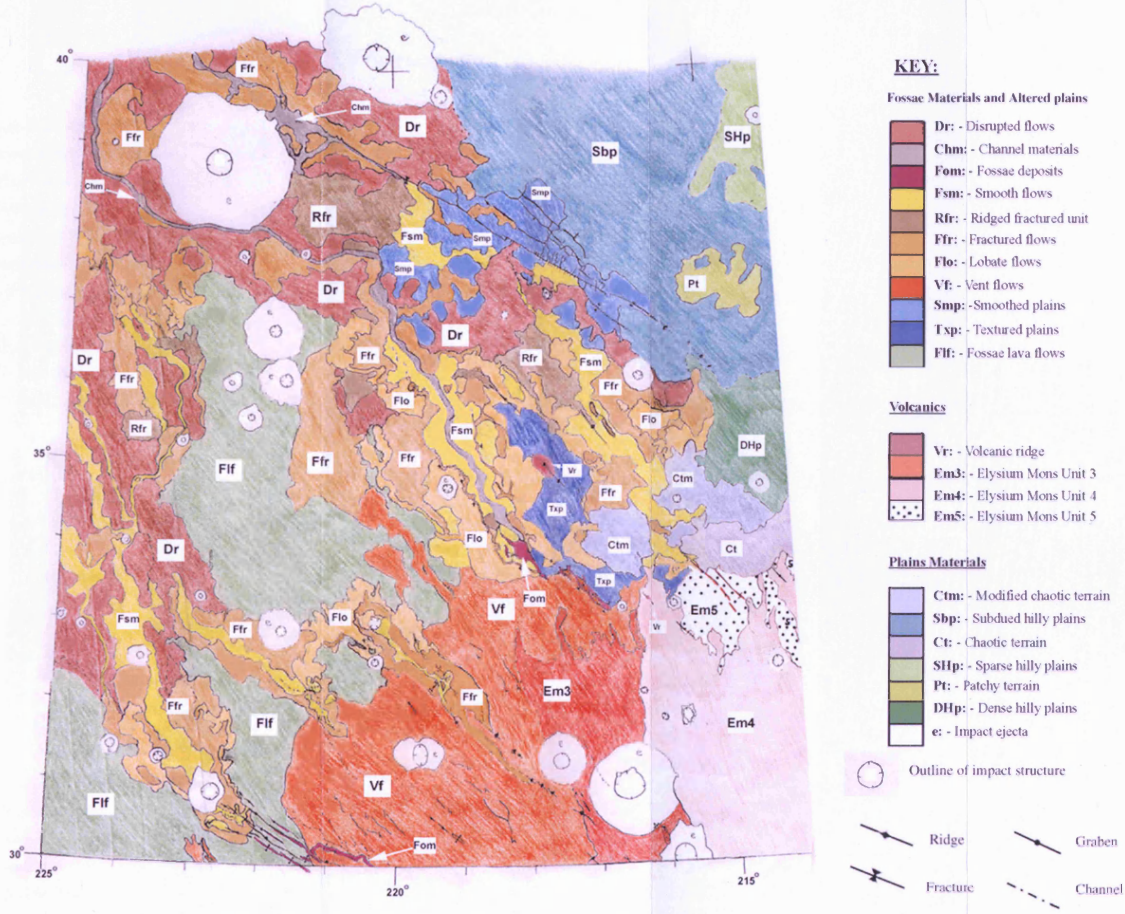

Figure 4.4: Part of a detailed map produced of the north of the main mapping area (figures 4.1 and 4.2). The part shown here covers the north-western part of the sketch map area and shows more detail of the area surrounding several of the Elysium Fossae. As in figures 4.1 and 4.2, each degree of longitude on the map represents ~60km on the surface of Mars. The units are grouped in the Key to show type or origin of material, and in each group the units are positioned according to relative age, with the youngest at the top and the oldest at the bottom. The units are individually described in the text.

4.31 Volcanics

This section deals with the central part of the map in Figure 4.2, which is covered by the main central vent volcanism that has occurred in the mapping area. These units are: **At** (Albor Tholus), **Ht** (Hecates Tholus), **EM 5** (Ancient Lava Flows), **Em 4** (Elysium Mons Main flows), **Em 3** (Channel Flows), **Em 2** (Young Flows), and **Em 1** (Explosive Deposit), and have been highlighted in Figure 4.5 for ease of discussion. Initial examination of the contour maps produced using the MOLA data, as well as initial analysis of MOC images, indicated that the volcanic evolution of the area had not been as simple as it has been presented in previous studies. Not only did it appear that Elysium Mons had grown and evolved on top of a larger, older volcanic edifice, but also that it had undergone late-stage explosive activity at the summit, perhaps similar to that which occurred at Hecates Tholus.

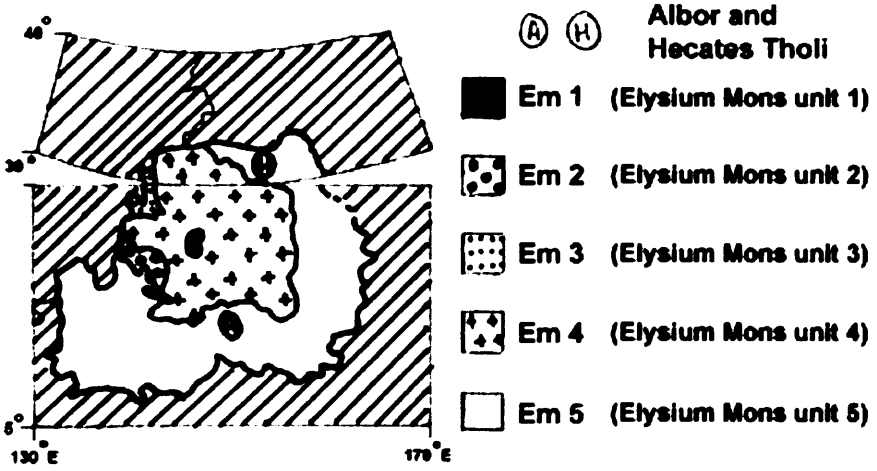

Figure 4.5: Sketch map of the mapping area showing the relative positions of the units grouped as 'volcanics'.

Albor Tholus and Hecates Tholus (At & Ht)

The boundaries of these units are distinct, and both volcanoes appear to have been surrounded, and in places embayed, by unit **Em 5**, suggesting that they are older than **Em 5**. A contour map of the region created in IDL with MOLA data shows clearly how the material of the **Em 5** unit, flowed around both Albor Tholus and Hecates Tholus (see Figure 4.6). The flanks of Albor Tholus exhibit a hummocky texture, and also exhibit ridges towards the base of the flanks that are radial to the caldera. The ridges and hummocks could be the surface expression of tube-fed flows. There appear

to be several pits on the flanks (perhaps formed by collapse over a lava tube), particularly at the base to the northeast and to the south of the caldera, where a chain of coalescing pits forms part of one of the graben that are present on this part of the volcano. These graben or fractures run almost concentrically to the caldera (see Figure 4.1), but do not continue to occur on the surrounding **Em 5** unit, so could have been formed in the late stages of the formation of Albor Tholus. The contact between **At** and **Em 5** is not as distinct to the southeast of Albor Tholus, and shows that the direction of the flows that surrounded it was from northwest to southeast, both due to the position of the contours, and also due to the position of flow fronts visible in the images of the area. One large graben cuts both **At** and **Em 5**, and must have formed after the emplacement of **Em 5** in this part of the mapping area. The graben trends in the same northwest-southeast direction as most of the Elysium Fossae.

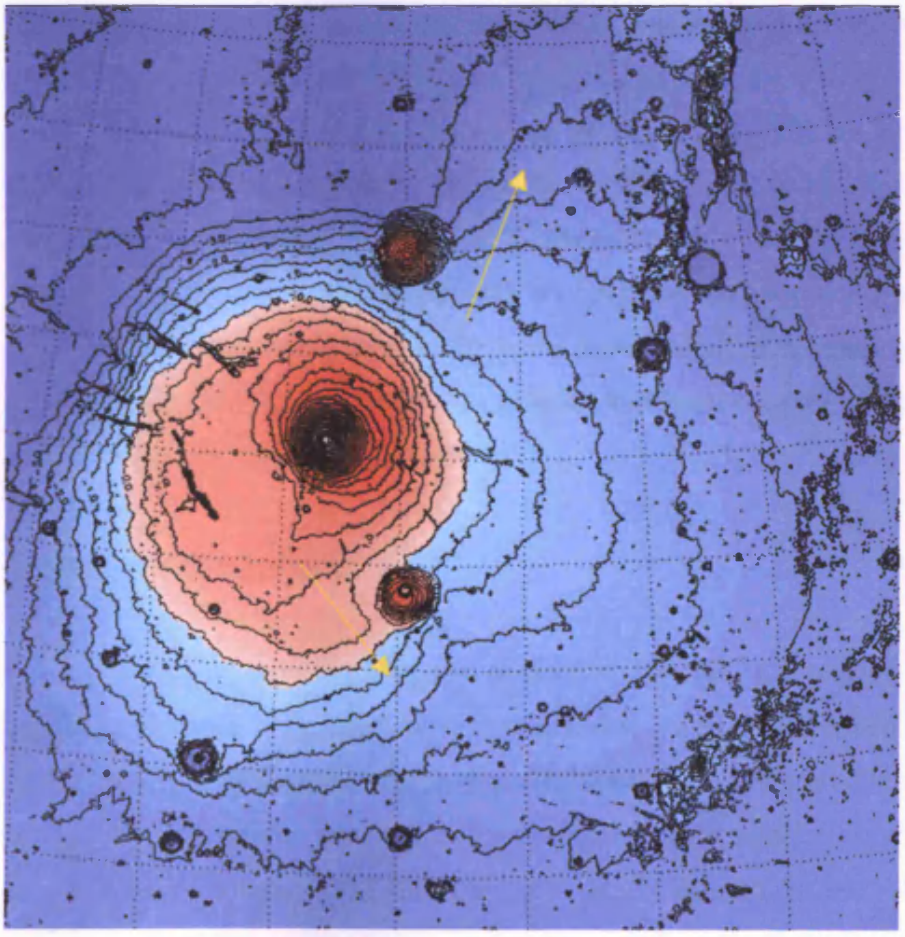

Figure 4.6: This contour map covers the entire area shown in the sketch map (Figure 4.2). The orange and red areas show higher elevations, and the contours clearly show the constructs of Elysium Mons and Albor and Hecates Tholi in the central area of the map. The blue areas on the map represent lower elevations, and several large impact craters can be observed, some with central peaks. The contours indicate the general flow pattern of lavas, the yellow arrows highlight where the flows have wrapped around Hecates Tholus to the north, and Albor Tholus to the south. Area shown is ~2250 kilometres in width, the contours are at 0.5km intervals.

The flanks of Hecates Tholus are also hummocky, like those of Albor Tholus, but do not exhibit the ridges of Albor Tholus. Instead they are characterised by many sinuous channels of a few hundreds of metres in width. Previous studies have suggested that these channels were formed by water, others have suggested that they were formed by density flows, either base surges or nuees ardentes, as discussed in Chapter 1. MOC images show that there are dunes in the base of impact craters and along the base of channels (see previous chapter). Higher up the flanks closer to the summit, there appear to be fewer channels, and the hummocky texture becomes the dominant surface feature. Analysis of both Viking and MOC images shows that the surface of Hecates Tholus is covered with fine-grained deposits. The surface material does appear to be made of easily erodible material, since yardangs can be seen to have formed near the summit (as discussed in Chapter 3). Since evidence has been found for a pyroclastic-fall deposit on the summit of Hecates Tholus in a previous study (see Chapter 1), the fact that much of the summit appears to be mantled by a dusty, easily erodible deposit provides more evidence for the pyroclastic-fall theory.

As in the case of Albor Tholus, one side of Hecates Tholus faced away from the direction of flow of unit **Em 5**. But unlike at Albor Tholus, **Em 5** did not completely surround Hecates Tholus, leaving the northern flanks to border onto the Dense Hilly Plains. On the western flank of Hecates Tholus there is a large depression measuring 30 x 46 kilometres, which appears to have been embayed by materials from **Em 5**. Analysis using MOLA data show that actually this is not the case. The formation of this feature will be discussed in section 4.4.

Elysium Member 5 (**Em 5**)

This unit covers an extensive area of around 1.2 million kilometres^2, and surrounds several of the other volcanic units that are being described in this section. It is characterised by long lava flows that can be several hundreds of kilometres in length, many of which can be seen to flow around previously existing structures (see Figures 4.1 and 4.6). Although the flows are not clearly defined in the Viking images, it is possible to see many flow fronts and parts of individual flows in these same images. The unit surrounds Hecates Tholus and Albor Tholus, and Elysium Mons has been emplaced just off-centre on top of it (this is clearly shown on the contour map in Figure 4.6). There are many large impact craters (~20 – 25 kilometres in diameter) in this unit,

most with the ejecta still present, and some of the Elysium Fossae occur here too. **Em 5** appears to have been emplaced as a roughly circular dome of lava flows, parts of which have now been modified into other units or have been buried by younger units, thus implying that it is ancient relative to all the other central vent volcanics described in this section. The slopes on the flanks of this lava pile are shallow, at around 1-2°. It is proposed that this unit is an Ancient Volcanic Edifice (AVE) that formed when central vent volcanism became prevalent after the emplacement of the Ridged Plains unit (**rp**). The AVE may have started to form at around the same time as Hecates Tholus and Albor Tholus, but activity at the vent feeding the **EM 5** flows is proposed to have continued after activity at Hecates Tholus and Albor Tholus ceased. The major evidence for this is that the AVE is significantly larger than Hecates Tholus or Albor Tholus, and also many of the **Em 5** flows can be seen to wrap around these two structures as shown in Figure 4.6. Several fossae occur in this unit, and since **Em 5** is older than the rest of the volcanics described in this section, the formation of the fossae may have started early in the history of this region once central vent volcanism had commenced.

Elysium Mons Main Flows (**Em 4**)

This unit corresponds to the region on the shaded MOLA topography map (Figure 4.1) where the Elysium Mons edifice can clearly be seen to rise above the surrounding **Em 5** unit, and includes the main bulk of flows from the central vent area, which extend to the north of the volcano, just to the west of Hecates Tholus. The contour map also clearly shows that **Em 4** has been emplaced on top of **Em 5** (the AVE) in the DEM of the area shown in Figure 4.7. It has numerous well-defined and well-preserved lava flows, the best examples of which can be found to the north of the volcano. Higher up the flanks, closer to the caldera, there are not only individual lava flows but also many ridges, which may be the surface expression of tube-fed lava flows. Pit craters occur, many in groups as chains, or along graben, and also some sinuous channels are present that may have been produced due to erosion by fluid lava. There are many graben in this unit that appear to be concentric to the caldera, also one prominent ridge occurs ~ 70 kilometres to the northwest of the caldera. These features all cut through the flows on which they occur and must have formed after the flows were emplaced, perhaps formed by local stresses due to the immense weight of the

volcanic pile. Some of the graben have been termed 'fossae' in previous mapping, although they do not exhibit the extreme widening and flat floors of those fossae that occur in **Em 5**.

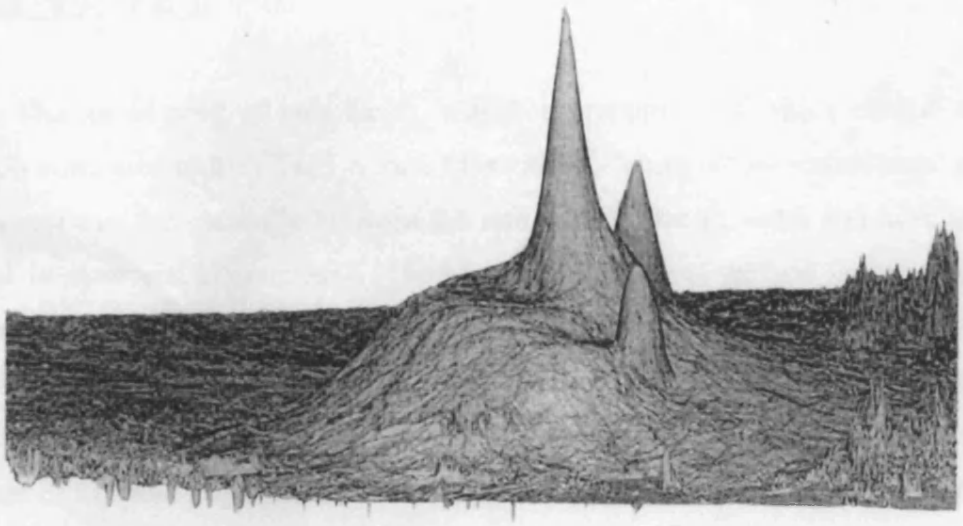

Figure 4.7: A shaded DEM of the major volcanoes in the mapping area of this study. The view is looking north across Albor Tholus, Elysium Mons and then Hecates Tholus, which is partially obscured behind Elysium Mons in this image. The way lavas from other volcanoes have surrounded Albor Tholus is clear, as is the way that Elysium Mons is offset on top of a larger mound of material. The flat area to the left of the Elysium Mons main edifice is where the Em2 unit is located, and a bulge of material on the right-hand flank of Elysium Mons can also be observed. The vertical exaggeration of this DEM is ~40 x.

The boundaries of this unit with **Em 5** at the eastern and southern extents are not clear, since the flows from Elysium Mons gradually grade into the surrounding flows from **Em 5**. Therefore, although some of the material of this unit may extend outside the boundary shown on the map, the boundary is intended to denote the bulk of the Elysium Mons main flow material as it appears on the shaded MOLA topography image. To the west of the unit there are several graben which are, again, concentric to the caldera. They must have formed during the emplacement of this unit, since they cut most of the unit material, but there is at least one flow that has travelled over the graben. These graben are buried to the north by the **Em 3** unit, and to the south by the **Em 2** unit, thus implying that **Em 3** and **Em 2** are younger than the Main Elysium Mons flows

(**Em 4**). The emplacement of **Em 4** on top of **Em 5**, means that **Em 4** is younger, and the fact that the caldera of Elysium Mons is offset from the centre of **Em 5**, implies that there may have been a shift in vent activity here, as discussed in section 4.6.

Channel Flows (**Em 3**)

This is an area of lava flows, a higher proportion of which exhibit central channels compared to the other Elysium Mons flows. There are numerous small graben in this unit that are generally between 0.5 and 1 kilometre in width and have lengths ranging from several kilometres to ~100 kilometres. Many of the lava flows in this unit are single flows, rather than being part of a large compound flow field. This unit appears to have flowed into one of the Elysium Fossae (see Figure 4.8), so the unit must postdate at least some of the Fossae. It also buries part of the graben system that lies to the west of Elysium Mons within the **Em 4** unit, and thus postdates this feature and **Em 4**. This unit is interpreted to be one of the younger flow units erupted from Elysium Mons. Since the unit cannot be traced back to the caldera, it seems likely that **Em 3** flows were erupted from vents in the flanks of the volcano, which could have been similar to the small graben observed in this unit. Some of the flows in this unit have been studied in Chapter 5, and analysed using MOLA data.

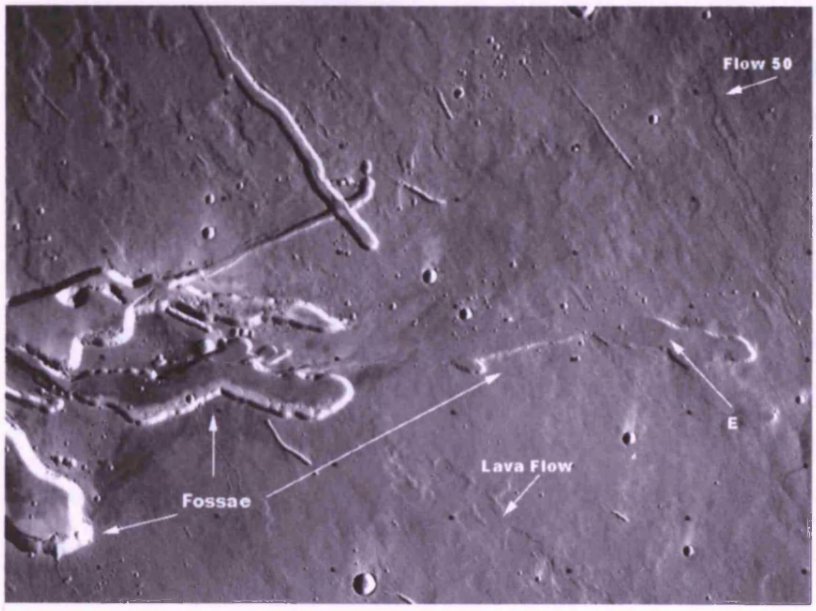

Figure 4.8: Part of Viking image 541A45 showing part of several fossae to the north west of the main edifice of Elysium Mons. Several individual lava flows can be observed, and flow 50 from the lava flow studies section of this thesis has been identified. E denotes the edge of a flow that is thought to have embayed one of the fossae here. It has been interpreted to be material from the **Em3** unit (see text). This image shows an area that is approximately 140

Young Flow (**Em 2**)

This is a smooth, flat area with slopes of <<1°, as proved by analysis of MOLA data. It has fewer impact craters than all the surrounding units, and has distinct boundaries because of this. It can be seen to embay the southwestern edge of the **Em 4** unit, and to have flowed into and along the graben in the western part of the **Em 4** unit (see Figure 4.9).

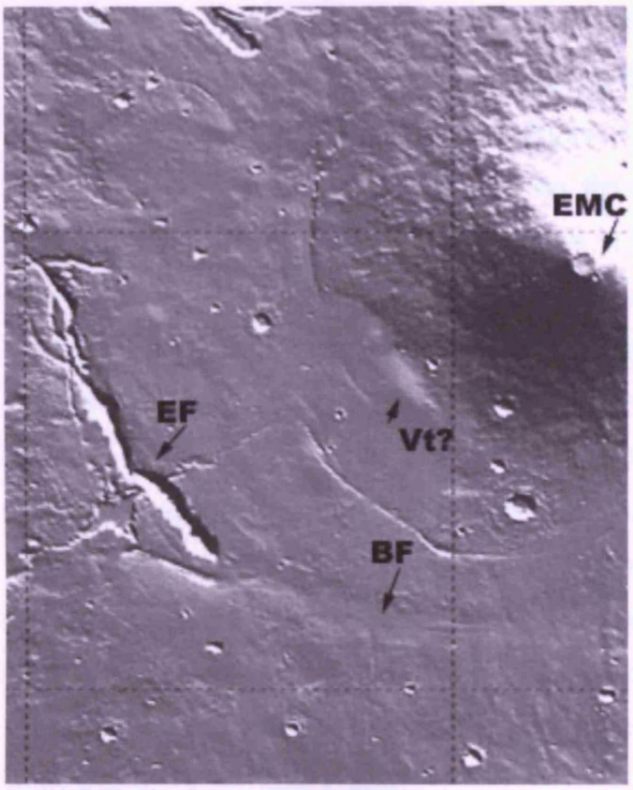

Figure 4.9: A close-up of the shaded MOLA topographic map shown in Figure 4.1. EF indicates one of the large graben, called fossae, that occur in this area. The fossae may have continued further to the southeast. A depression (indicated by BF) continuing to trend from the fossae can clearly be seen using the topography data. This may represent a buried fossae system, potentially buried by the flows from **Em2**. EMC indicates the Elysium Mons caldera. Vt? Shows a raised area that may have been one of vent areas for the Em2 flows that flooded the area to the southwest of the main Elysium Mons edifice. This image is ~420 kilometres across.

Although difficult to see in the Viking images, it is clear in the shaded MOLA topography (Figures 4.1 and 4.9) that this unit has filled a depression that may at one time have been part of the fossae system that can be seen to the northwest in this area. Many other graben that occur within this unit have been embayed at the ends by the **Em 2** material, although some must be younger than **Em 2**, since they have not been filled by the material at all. Although no flow fronts are visible in this unit, it is interpreted to be recent flood lavas that have filled a previously existing depression in the flanks of Elysium Mons (see section 4.6 for discussion of this). There is a higher standing area surrounding a small graben (Vt? in Figure 4.9), which could have been one of the vents for the flood lavas that comprise this unit. MOLA profiles across this potential vent

show that the feature reaches a maximum elevation that is ~100 metres above the surrounding area.

Explosive Deposit (**Em 1**)

Only just visible in the Viking photomosaics, but easily seen in high-resolution MOC images, is unit **Em 1**, which is a dark, dusty deposit that has been emplaced on the summit area of Elysium Mons. It appears to have been ejected radially (but with the bulk of the material having been deposited to the east) from a chain of pits that are present to the west of the caldera (see Figure 4.10). The margins of the deposit are feathered and a material-free 'shadow' on the side of an impact crater near to the caldera indicates the direction of the blast (S in Figure 4.10). A material-free shadow such as this means that the material must have been emplaced as a type of flow. The feathering at the edges of the deposit, combined with the dusty appearance of the deposit have caused it to be inferred in this study to be the result of late-stage explosive activity, the source of which is possibly from the collapse pits close to the caldera. Emplacement by pyroclastic flow may explain the lack of symmetry of deposited material around the source pits. The dusty deposit must be relatively recent since it has not been obscured by aeolian materials, or been eroded away. This eruptive event may be similar to that which occurred at the summit of Hecates Tholus and therefore shows that the later stages in the life-span of a Martian volcano may be dominated by small-scale explosive volcanic events.

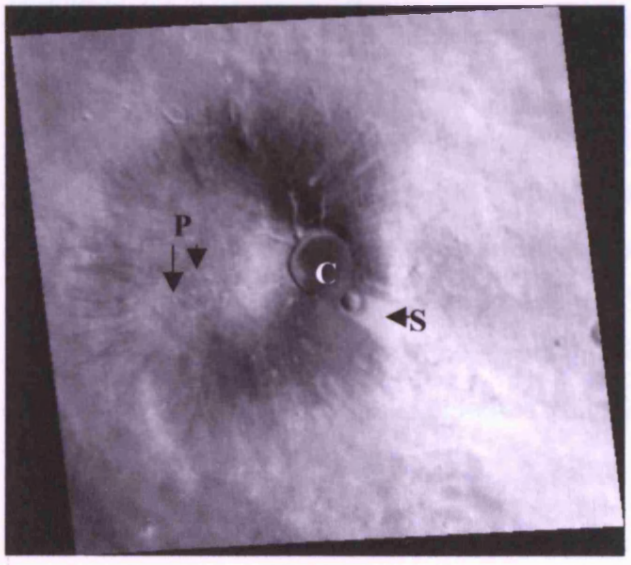

Figure 4.10: Part of MOC image M17-00297 showing the summit of Elysium Mons. The caldera is labelled **C**. The dark deposit discussed in text is very obvious in this image. It covers the summit but is offset to the left slightly, which would point to the chains of pits (**P**) observed to the left of the caldera being the likely source of the deposit. A deposit-free 'shadow' (**S**) can also be observed where the material was deflected by the rim of a crater near the caldera. This image is ~130 kilometres in width, and north is towards the top.

4.32 Fossae Materials and Altered Plains

Previous geological studies of this region of Elysium (Mouginis-Mark et al., 1984; Mouginis-Mark, 1985) have shown that material has been erupted from many of the Elysium Fossae (see Chapter 1). Careful analysis of Viking, MOC and MOLA data during this study provided further evidence of this, and also enabled more of the geological history of these materials to be determined. Mechanisms of formation for many of these units have been determined using the new data, and where appropriate, thicknesses of the units were calculated. Initial analysis of the shaded MOLA data (see Figure 4.1) indicated that several emplacement events occurred on the plains northwest of the Elysium Fossae, and mapping carried out in this study enabled the source, likely type of material present and emplacement mechanism to be inferred. Therefore the units described in this section are thought to be the materials that were erupted from the Fossae (the **Fossae Materials**), as well as those surrounding plains units that have been altered by the flow of these materials (the **Altered Plains**). A basic sketch map of these two groups of units is given in Figure 4.11.

Since the **Fossae Materials** comprise several different units, some of which cover relatively small parts of the mapping area, they have been grouped together in the sketch map in Figure 4.11 where they are represented by the area labelled Fm. In the larger sketch map in Figure 4.2 the Fossae materials are subdivided into units **Flf** (Fossae Lava Flows), and **FAp** (Fossae plains). Unit **Flf** is thought to be a single rock unit in this study, but in the more detailed map in Figure 4.4 the smaller units within **FAp** are shown. They are: **Flo** (lobate flows); **Fsm** (Smooth Flows); **Ffr** (Fractured Flow); **Dr** (Disrupted Material); **Rfr** (Ridged Fractured Material), **Fom** (Fossae Base Material).

The units **Txp** and **Smp** occur within the Fossae Plains unit in Figure 4.2, since they were too small to map separately on the sketch map, but are actually members of the **Altered Plains** assemblage and will be discussed in the **Altered Plains** section. The rest of the **Altered Plains** units are shown on Figures 4.2, 4.4 and 4.11 and are: **Br** (Broken plains); **Df** (Disrupted Flows); **Vf** (Vent Flows); **Txp** (Textured Plains); **Chm** (Channel Materials), and **Smp** (Smoothed Plains).

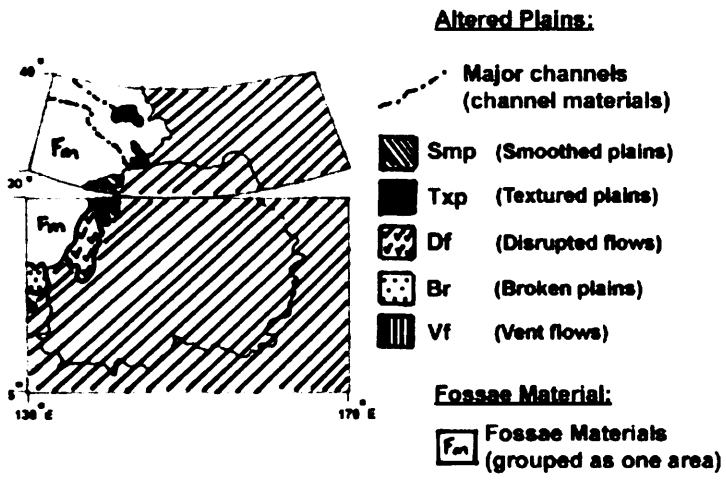

Figure 4.11: Sketch map of the mapping area showing the relative positions of the units grouped as 'altered plains'. The fossae materials have been grouped as a single unit in this diagram since they cover small areas as individual units.

4.32 a) Fossae Materials

Fossae material is a term that is applied in this study to all the material that appears to have been discharged from the Fossae, or features associated with the Fossae. There are several units that are classified as Fossae material, some are flow units, some are fractured and eroded units, and some are sedimentary/depositional units

Fossae Lava Flows (**Flf**)

The Fossae Lava Flow unit comprises large numbers of long (several hundreds of kilometres), wide (up to 40 kilometres) flows that appear to have erupted from the Fossae from analysis of the shaded MOLA topography image. The unit is mottled in appearance with lighter and darker patches, in both Viking and MOC images, with impact craters in the MOC images seen to penetrate through the surface to lighter-coloured materials beneath (see Figure 4.12).

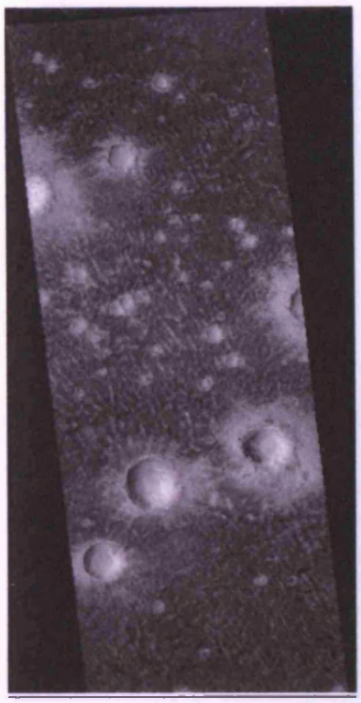

Figure 4.12: Part of MOC image M22-01769 showing an area of the Fossae Lava Flows Unit, several hundred kilometres to the west of Hecates Tholus. The impact craters visible in this image have clear ejecta blankets and appear to have penetrated through to brighter material beneath the darker surface covering. The surface deposit here appears to have a platy texture. It is hard to determine whether this is an effect of aeolian activity or of the way in which the material was emplaced. Platy lava flow textures have been found in MOC images on other areas of Mars (Keszthelyi et al., 2000). This image is 2.36 kilometres in width and north is towards the top.

A study of the MOLA shaded topography image shows that unit **Flf** is overlain by other Fossae Material units, and was therefore probably the first material to be erupted from the Fossae. The overlying materials appear to have been eroded and then further flows emplaced on top, and this sequence has occurred several times, as can be seen in a close-up of the shaded MOLA topography image (see Figure 4.13). Therefore, as suggested previously by Christiansen and Greeley (1981), Christiansen and Ryan (1985) and Russell and Head (2001) it is proposed in this study that the Fossae erupted both lava flows and sediment-laden water, and this is further proved by the study of each of the Fossae Materials, as will be discussed in this section. However, this study also highlights evidence that the Fossae alternately erupted this material to produce the surface morphology observed in the shaded MOLA map, part of which is shown in Figure 4.13. It appears that the lava and water were erupted at different times on several different occasions to produce layering of deposits observed in the shaded MOLA map. This has not been shown in previous studies. The mottled appearance of the **Flf** unit could therefore be due to the presence of fluvial sediments as well as aeolian materials. It is noted at this point that the Fossae extend down from the flanks of the older volcanic dome (AVE) represented by unit **Em 5**, onto the flatter floor of the surrounding plains, but material was not discharged from the Fossae until the point where the Fossae cross this boundary. The significance of this will be discussed in section 4.6.

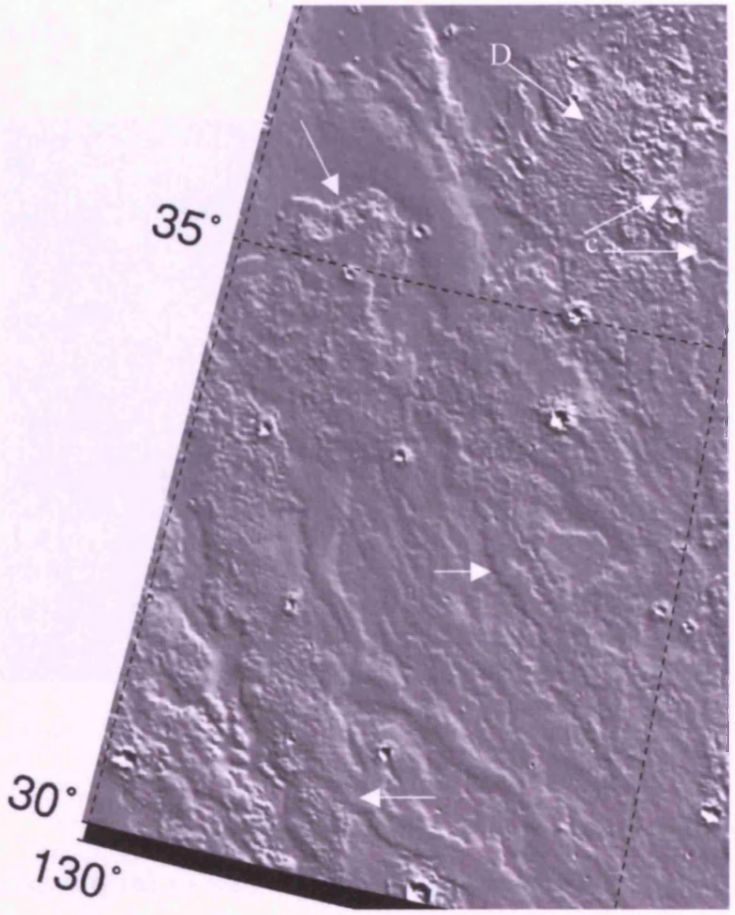

Figure 4.13: A close-up of part of the northwestern region of the shaded MOLA topography map shown in Figure 4.1. This area shows materials which are proposed in this study to have been erupted from the Fossae. The arrows show areas where overlapping layers of materials can be seen, thus indicating that several separate eruptive events occurred from the fossae. **D** highlights a potential delta feature that occurs at the termination of several channels, **c**. This may be where sediment carried in the fluid within the channels was deposited once the channels debouched onto the surrounding plains. One degree of longitude in this image is ~60 kilometres in length.

4.32 b) Fossae Plains (**Fap**)

On Figures 4.2 and 4.11 this unit is mapped as a group of units. Figure 4.4 displays each individual unit, and these are discussed below.

Lobate flows (**Flo**)

This unit is characterised by mainly being composed of long (up to several hundreds of kilometres in length), lobate sections, which range between several kilometres and tens of kilometres in width. They have characteristically smooth looking surfaces and many a 'pitted' texture. The source of this material appears to be the Fossae, or ridges associated with the Fossae. MOLA contour maps show that the **Flo** unit was emplaced as a flow that travelled in the direction of the regional slope and

Viking images indicate the topographic control displayed by the flow unit (see Figure 4.14).

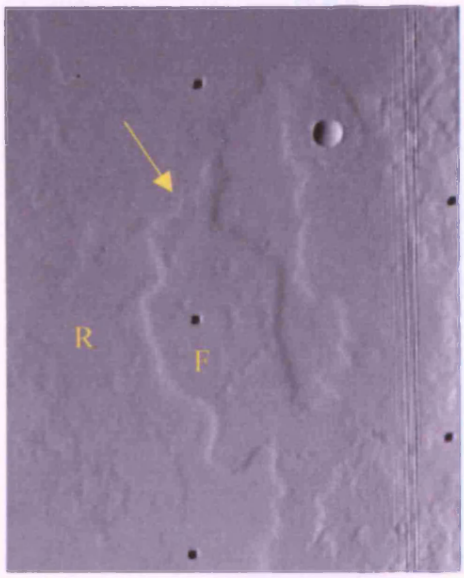

Figure 4.14: Part of Viking image F541A08. The left-hand side lobe of this **Flo** unit (F) can be seen to have stopped short of the adjacent boundary of an **Ffr** unit (R). The **Flo** unit may have flowed around the **Ffr** unit, or the **Ffr** unit has flowed down an incline that the **Flo** unit could not climb, thus indicating topographic control. The **Flo** unit can also be seen to terminate at the scarp formed by the boundary of another unit (arrowed). Also note the pitted appearance of the **Flo** unit. Black spots are artificial additions to the image. Area shown in image is 40 kilometres across.

The resolution of the images is too low for the pits to be clearly visible (see Figure 4.14) so they might be impact craters, but it may also be possible that they are phreatomagmatic explosion craters (such as those shown in Figure 4.15). Phreatomagmatic explosions occur when hot volcanic material comes into contact with water, rapidly heating the water and causing it to turn into steam. The formation of water into steam involves rapid expansion under the surface of the flow, causing the explosive nature of the escape of the steam, and forming the explosion craters. On Earth, craters formed in this way are a few tens of metres in diameter (Fisher and Schmincke, 1984), so if they were a similar size on Mars it would not be possible to resolve them in the Viking images available of the mapping area, and it therefore seems likely that they may be visible as small, unresolved 'pits', like those seen in Figure 4.14. No MOC images of this unit were found, which is unfortunate as explosion craters, if present, would have been visible in them. Terrestrial phreatomagmatic explosion craters often form when water gains access to layers of ignimbrites (or pumice-flow deposits as they are also known) that are still hot from eruption, so it is possible that the **Flo** unit could be an ignimbrite. However, similar features occur on lava flows where the lava has flowed over a source of water. In this case rootless cones are formed, and these have a similar appearance to phreatomagmatic explosion craters.

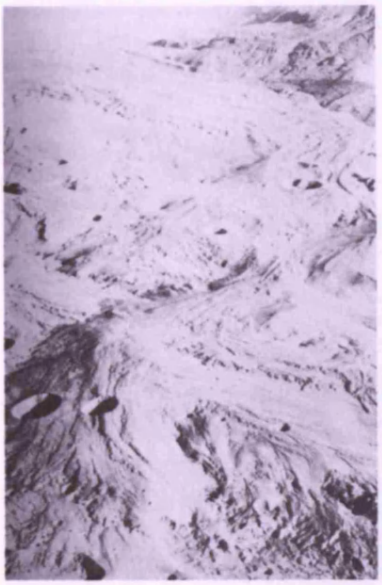

Figure 4.15: Image shows phreatic explosion craters in pumice flow deposits at Mount St Helens. Craters are approximately 5-25m in diameter. (Taken from Cas and Wright, 1987).

The **Flo** material near the source of the flows also has many small channels within it that are visible in Figure 4.16. These channels can be several hundreds of metres up to several kilometres in width and are several kilometres in length, and they appear to have channelled water that emerged from the fossae/graben and ridge sources of the **Flo** material. In many places on the map the **Flo** unit seems to be the boundary for the rest of the fossae materials, particularly in cases where the fluid flow has subsequently occurred from the Fossae. Even where the **Flo** unit does not completely surround the other Fossae Materials, it is usually distributed around the edge of the fractured units of the Fossae Materials. It is therefore inferred in this study that the centres of the fossae flows became broken up because fluid (possibly water) flowed through the centres of the Flo material, eroded channels and broke up the underlying material. Water may also have escaped from underground through areas in the **Flo** unit, which helped contribute to the formation of the central channels, and would have been responsible for the break up of the surrounding material. The release of this water must therefore have occurred after **Flo** was laid down. The formation of an underground hydrothermal system underneath the Elysium volcanoes is a possible source for the water that is suggested to have flowed through the **Flo** unit (this is discussed in further detail in section 4.6).

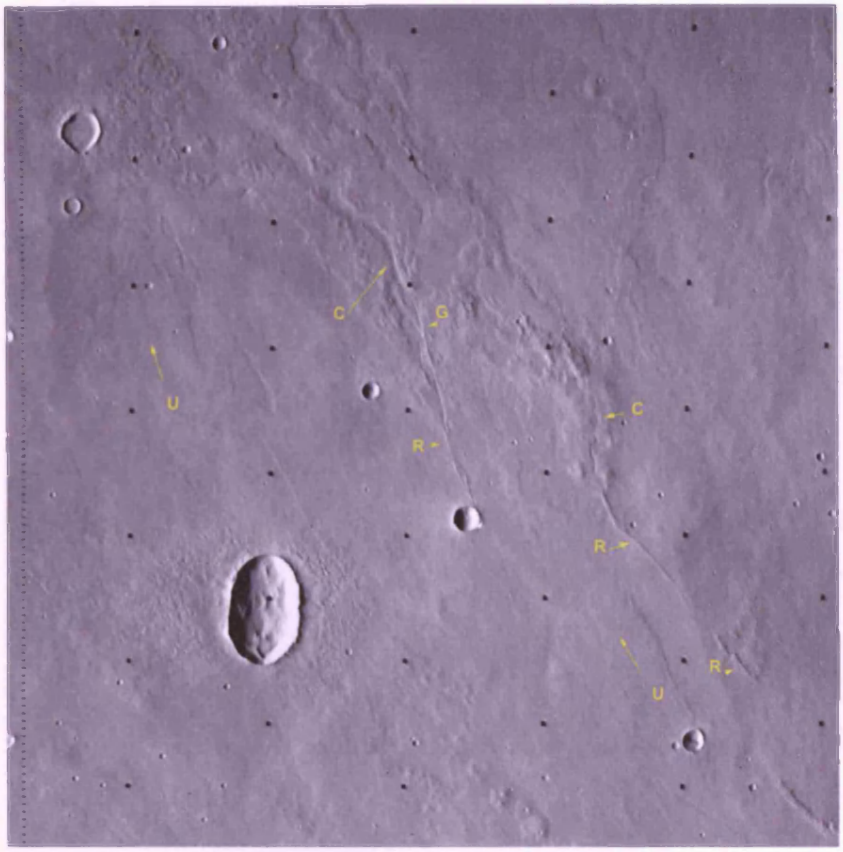

Figure 4.16: Part of Viking image 541A25 showing the sources for some of the Flo materials. The ridges (**R**) are the sources for three flows, the flows with an unknown source (**U**) have an arrow indicating the direction of flow, and two of the channels (**C**) that have formed at the end of ridges and graben (**G**) have been marked.

If the **Flo** unit was emplaced first, and then subsequently modified by fluid to form the other units in this section, then presumably it would stand above the rest of the surrounding units. The MOLA profile in Figure 4.17 shows that this is the case, and calculations show that the average thickness of the **Flo** material is ~30 to 40 metres. **Ffr** is a thinner unit 20-30 metres in thickness, and **Fsm** is in a depression between these two previous units and is thought to represent the base of one of the channels formed in the **Flo** and **Ffr** units.

It is therefore inferred in this study that the **Flo** unit is composed of material that was emplaced as a flow that was topographically controlled. It has a pitted appearance that, considering the number of pits, is unlikely to be due to impact craters and is more likely to represent explosion craters, where the hot volcanic **Flo** material was emplaced on top of water or ice-rich ground. Given the evidence for ice in this part of the mapping area (indicated by the presence of chaotic terrain, unit **Ct**, and textured ground, unit **Txp**, as well as in the MOC images in Chapter 3), this seems a likely explanation. The **Flo** material surrounds much of the rest of the Fossae Material units that will now be discussed in this section, and is inferred in this study to have been eroded to produce

the **Rfr** unit. **Flo** must therefore be composed of a material that can be eroded easily, and is of volcanic origin, such as either ignimbrites or friable lava.

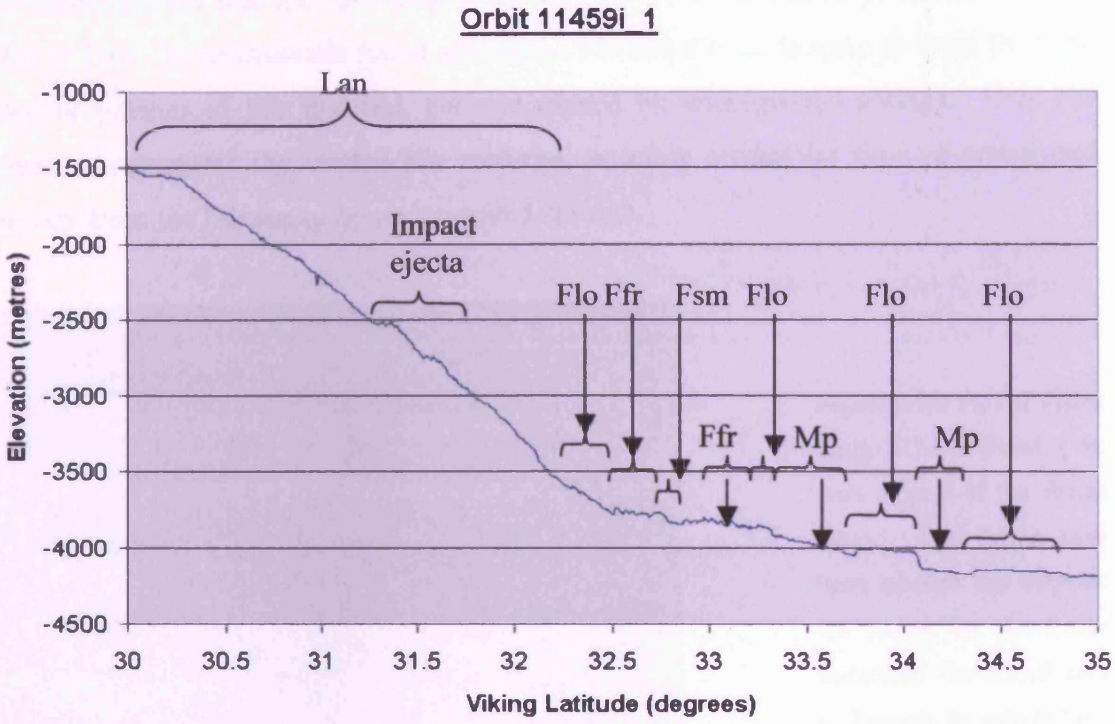

Figure 4.17: MOLA profile across fossae materials. Values of the height of the **Flo** unit above the Fossae Lava Flows (**Flf**) unit were measured on either side of the unit and measurements were found to be ~30-40 metres high.

Fractured Flow Unit (**Ffr**)

This unit is characterised by areas of irregular depressions within the **Flo** material, and may be **Flo** material that has been broken up and eroded. It is therefore probably the same material as **Flo**, but the difference in appearance has been identified as a separate unit in order to indicate the geological events and processes that have occurred in this area. The typical surface appearance of **Ffr** is shown in Figure 4.18.

The **Ffr** material is rarely found on the edges of the flows of the fossae material and, as mentioned in the previous section, is often bounded by areas of **Flo** material. Study of the geological map shows that **Ffr** is generally found in between the **Flo** and **Fsm** units, with **Flo** being on the outside of the main flow, and **Fsm** composing of the central channel. It can also be found to border the larger channels (**Chm**) further to the

north, and other areas of what is thought to be water/fluid modified material. Sometimes instead of patches of material, the **Ffr** unit forms narrow channel-like erosional features that lead into larger patches of **Ffr** or other units of eroded material (**Rfr** or **Dr**). Some channels found within the **Flo** and **Ffr** units seem to issue from the edge of patches of **Ffr** material, perhaps caused by underground springs. Unit **Ffr** therefore represents the eroded **Flo** material, possibly eroded by flow of water/mud directly from the Fossae, or by underground springs.

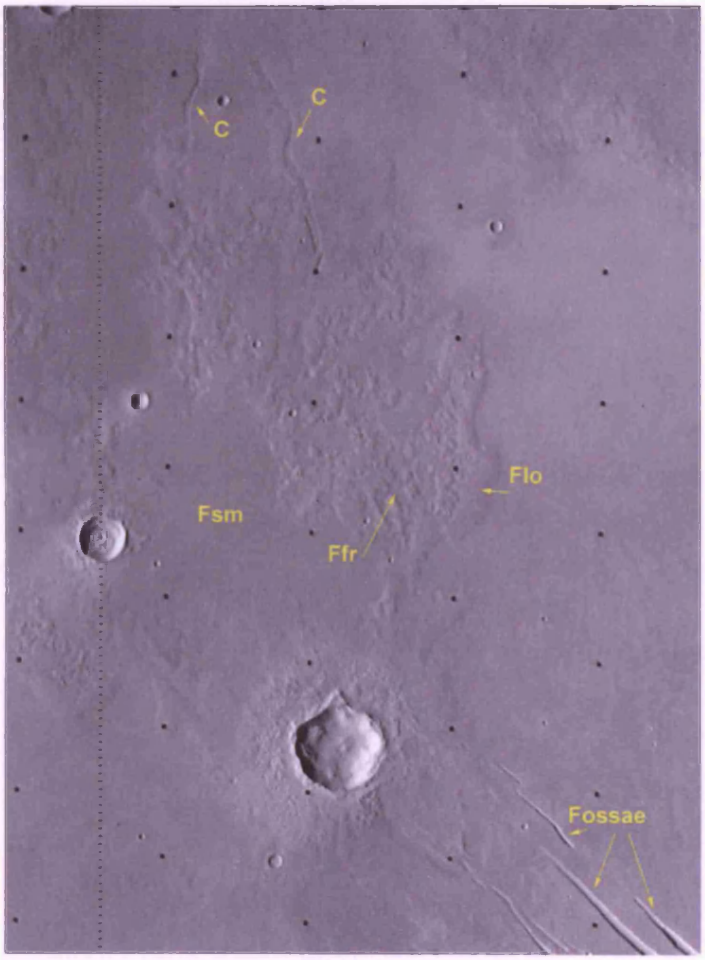

Figure 4.18: Part of Viking image 541A23 showing the start of one of the fossae flows. The fossae have been labelled and they are the source for the fossae materials. The smooth area of **Fsm** can be seen to form a central patch of material, and the **Flo** unit can be seen to occur along the right hand edge of the fossae flow. The **Ffr** unit is found between these two units and two channels that appear to have flowed from the **Ffr** unit are labelled (**C**).

MOLA profiles across the **Flo** and **Ffr** units show that the surface of the **Ffr** unit is irregular with series of peaks and troughs, and it is sometimes difficult to distinguish between the pitted areas of **Flo** and the fractured surface of the **Ffr**. Depressions within the **Ffr** are much lower than the height of the **Flo** unit, with values for the average depth of the depressions being ~15 metres. The high-standing points are at a similar height as the height of the **Flo** unit, and this supports the idea that **Ffr** is in fact eroded **Flo** material.

Smooth Flow Unit (**Fsm**)

The **Fsm** unit is characterised by a smooth appearance that is sometimes mottled with darker patches of material, and it often appears to have a channel-like form (see Figure 4.19). Analysis of the photomosaics and MOLA shows that this unit appears to be flat, and shadow analysis, cross-cutting relations and MOLA profiles show that the **Fsm** unit appears to have a lower elevation than any of the other Fossae Materials. Some of the areas of **Fsm** are wide, with values of around 20 kilometres although one area measures 40 kilometres across. The wider stretches of **Fsm** tend to occur closer to the Fossae, which are thought to be the source of the materials that formed the **Fsm** unit, and the more channel-like, narrower stretches start to occur several hundred kilometres away from the source.

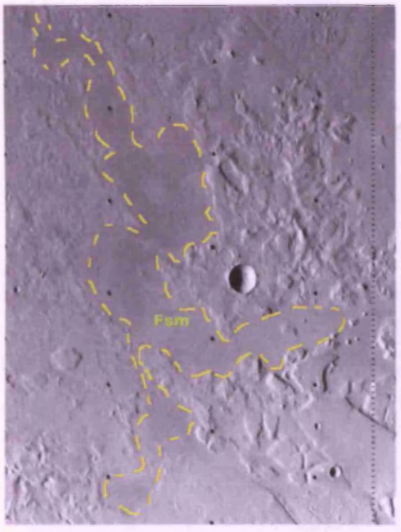

Figure 4.19: Part of Viking image 541A12 showing an area of the Fsm unit (boundaries denoted by dashed yellow line). Note the smooth, mottled appearance of the unit.

As explained earlier in this section, the **Fsm** unit could represent areas carved out by water released from the Fossae. Some of areas of the **Fsm** unit seem to start from small channels within adjacent units. This unit is usually found next to areas of fractured ground such as the **Ffr**, **Rfr**, **Dr** units, providing more evidence for the water erosion theory. The mottled patches on the surface of this unit could represent aeolian material, or sedimentary deposits laid down during the flow of water over the surface when the channels were created.

Fossae Material (**Fom**)

This is a Fossae Materials unit that is characterised by being the material that covers the insides of the Fossae structures. The interpretation in this study is that the Fossae have been formed tectonically and then enlarged, first by the flow of lava through them, and then by the release of water, and that this sequence happened several times. So the Fossae should be layered with a number of deposits, and these are collectively termed the **Fom** unit.

Although evidence from the Viking images (Mouginis-Mark, 1985) and MOLA data points towards material having flowed from the Fossae, MOC images show that there is little evidence of flow within the channels, or from the edges (see previous chapter). However, not all of the Fossae were imaged by MOC, and this result shows that not all Fossae were the source of eruptions, and that any evidence of flow may have been covered up by aeolian material.

Ridged Fractured Material (**Rfr**)

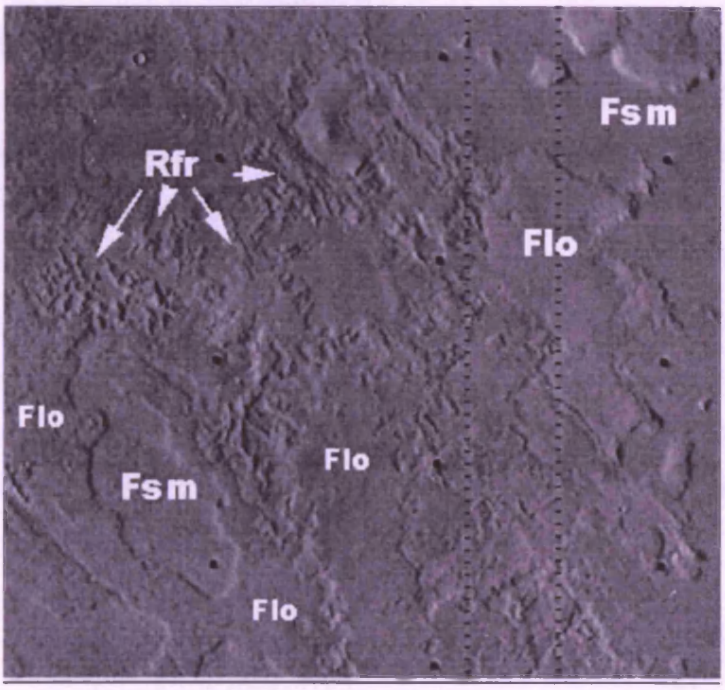

Figure 4.20: The typical ridged surface texture of the Rfr unit highlighted in part of Viking image F541A11. North is towards the top of the image and the image width is approximately 80 kilometres. Other geological units mapped in this study have also been highlighted.

This unit is similar in appearance to the **Ffr** unit by being broken up and fractured, with many depressions. However, the fracturing appears more aligned than in the **Ffr** unit, sometimes forming ridges of material 1 kilometre or less in width and up to

5 kilometres long, and sometimes occurring as smaller, angular patches of blocks (see Figure 4.20). The exception is that there is one large ridge in this unit that is 55 kilometres long and up to 4 kilometres in width. The **Rfr** unit does not occur as close to the Fossae as many of the other Fossae Material units, but does tend to occur next to areas of **Ffr**. The **Rfr** unit may have formed with this more structured appearance because there may have been some tectonic influence in its formation. It is possible that the same erosional process that formed the **Ffr** unit also formed the **Rfr** unit. The areas of **Rfr** could have been previously faulted so that the fracturing followed this trend when the surface was being eroded. Further evidence for this may be the fact that sometimes the **Rfr** unit seems to extend from the ends of surface faults and graben.

Disrupted Material (Dr)

Much of the material making up this unit is chaotic and irregular and has the appearance of a mixture of **Flo** and **Ffr**, with blocks (500 metres across or less) of broken, fractured material that, in places, appears to have flowed. The areas of this unit that are close to the **Smp** unit (Smoothed Plains Material) have lobe-shaped edges that appear to have flowed around higher standing ground (see Figure 4.21). Further to the north and to the west of the map the **Dr** unit borders the **Fsm** unit, or the **Ffr** units that surround **Fsm**, thus leading to the proposal that the formation of **Dr** is related to the presence of water, since **Fsm** is interpreted to have been formed by the flow of water. The images of these areas further north and west are at lower resolution in the Viking images so the unit forms blocky areas that appear smoother. The **Dr** unit is interpreted to have formed by the disruption of **Flo** material as it was emplaced. Intermittent eruptions of **Flo** material from the Fossae, or water interaction and/or erosion, may have been the cause of the irregular, blocky appearance of this unit.

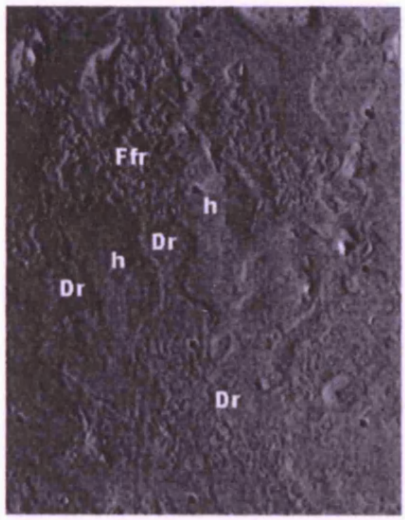

Figure 4.21: Part of Viking image 541A11 showing a typical area of unit **Dr**, the disrupted material. This image shows where **Dr** appears to have flowed between two higher standing areas (**h**), and displays the typical smoothed blocks of the surface appearance of this unit. The more angular blocks of the **Ffr** unit have also been highlighted.

4.32 c) Altered Plains Materials

The previous section presented evidence for the flow of water in the northwest region of the sketch map in Figure 4.2. It seems likely that this water was able to erode and affect the rock units in the immediate region. It is proposed in this study that the Textured Plains (**Txp**), Smoothed plains (**Smp**) and Broken Plains (**Br**) have all been affected by the outflow of water once it has flowed at least several tens of kilometres from the source. The Disrupted Flows (**Df**) and Vent Flows (**Vf**) occur closer to the Fossae and are thus thought to have been altered by both water and lava erupted from these features.

Smoothed Plains Materials (**Smp**)

This unit has a hummocky appearance with the most characteristic features being smooth, rounded hills that occur singly or in groups, each hill being several kilometres in width. It occurs approximately 200 kilometres away from the Fossae, and lies next to other Fossae Material units, particularly the **Fsm** unit, and it also borders the **Sbp** (Subdued Plains) unit. A major feature of the **Smp** unit is that it almost totally surrounds the start of a large fracture complex over 280 kilometres in length, which widens further to the northwest. There is evidence for the outflow of water at this point since the northern end of the fracture is eroded and a channel leads away from the fracture down the regional slope. Therefore, there is much evidence for the presence of

water here, and it is therefore inferred in this study that this unit may previously have been a Hilly Plains unit that was eroded by the flow of water from the Fossae and the fracture system to form the smoothed unit observed now.

Channel Materials (**Chm**)

The **Chm** unit represents the materials left in the major channels that were formed by the long-term flow of water. Prolonged flow of water is deemed necessary in the formation of these channels because they have incised into the floor of the plains, and do not exhibit flash-flood features such as those in Chryse Planitia, but rather indicate that flow was steady and small in volume. If the flow of water was responsible for the production of the channels then one might expect the floor of each channel to be layered with fluvial sediments. In fact, as the floors are seen to be covered with dunes of aeolian material in the MOC images, it is not possible to determine whether layering is present. The source for most of the channels are the Fossae, although for one channel it is a large fracture system, and occasionally several areas of **Fsm** unit will merge to form one well-defined channel. One of the Elysium Fossae is the source for the channel called Hrad Vallis. This channel extends for over 200 kilometres in the mapping area, and continues off the northwest edge of the map in Figure 4.4. Further analysis of images just outside the mapping area in conjunction with shaded MOLA data shows that this channel extends for several hundreds of kilometres down the regional slope into the basin of Utopia Planitia. If there were no other sources of water further along the route of the channel then there must have been a large volume of water available at the Fossae for a substantial period of time to form this channel.

Textured Plains (**Txp**)

This unit is characterised by a smooth surface with no hills which exhibits an unusual patterned texture. In places, the pattern is like a series of ridges, but elsewhere it is a 'herring-bone' pattern (see Figure 4.22). The unit occurs around the edges of some of the Fossae, including the Fossae that are the source for Hrad Vallis as discussed in the previous section. Patterned ground also occurs in other areas of Mars, such as Isidis Planitia and Utopia Planitia. These areas have coalescent cratered cones and ridges, which may be volcanic in origin (Hodges and Moore, 1994; Frey, 1986),

although their formation by ground-ice has not been discounted (Rossbacher and Judson, 1981; Grizaffi and Schultz, 1989). Lucchitta et al. (1986) support the idea that other ridges in northwest Utopia Planitia form like ridge features in Antarctica, where ice streams converge and produce a ridge that runs along the base of a shallow depression. However, the ridges in **Txp** do not exhibit summit craters, nor are they surrounded by depressions, so they must have formed by a different process.

The **Txp** unit exhibits some surprising features apart from the patterned ground. In the centre of the area denoted as **Txp** is an unusual ridge-like feature (unit **Vr** in Figure 4.4). This is discussed in section 4.4. Also, the MOC images show that many of the impact craters in this area have a peculiar appearance. The bottom of each of the craters appears to be rebounding. The impact craters here are discussed in Chapter 3, where it is explained that this unfamilar appearance may be related to the presence of ground-ice. Therefore, it is thought in this study that the Textured Plains unit has been formed by periglacial activity, which created the patterned ground surface. This contradicts Mouginis-Mark (1985) who suggested that it was a sediment flow deposit, and that the ridges observed were due to settling of the deposit.

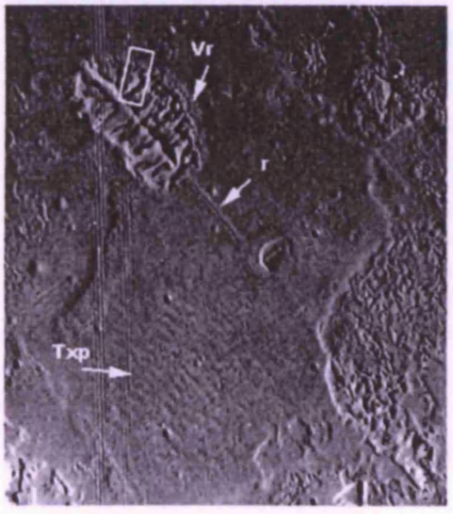

Figure 4.22: Part of Viking image F541A12 showing the 'ribbed' volcanic ridge (Vr) to the top left, and the textured plains (Txp) in the lower central part of the image. A long, narrow ridge that appears to be related to the volcanic ridge is also indicated (r). Many of the features in this area have been attributed by the author to the presence of ground ice (see text), particularly the patterned ground of the Txp unit. North is towards the top of the image, which is ~70 kilometres across. The white rectangle indicates the position of the image shown later in Figure 4.38.

Broken Plains (**Br**)

This unit occurs in the western part of the mapping area (Figure 4.2), near the ridged plains (**rp**), where some of the Fossae debouch, forming several channels that cross this unit. The author suggests that the channels carried material from the Fossae across the plains, and that they are fluvial owing to their meandering, and dendritic

appearance. The characteristic feature of this unit is that the surface material here has been broken up, much like the Chaotic Terrain (**Ct**) but into smaller blocks. It appears that the ground here has broken along previously existing fault lines, since there appears to be a regular pattern to the shapes and positions of the blocks. It is proposed in this study that the ground has been broken and eroded by the materials flowing from the Fossae. The erosion of the surface material was possibly enhanced by a sapping process that caused the ground to collapse along pre-existing faults.

Disrupted Flows (**Df**)

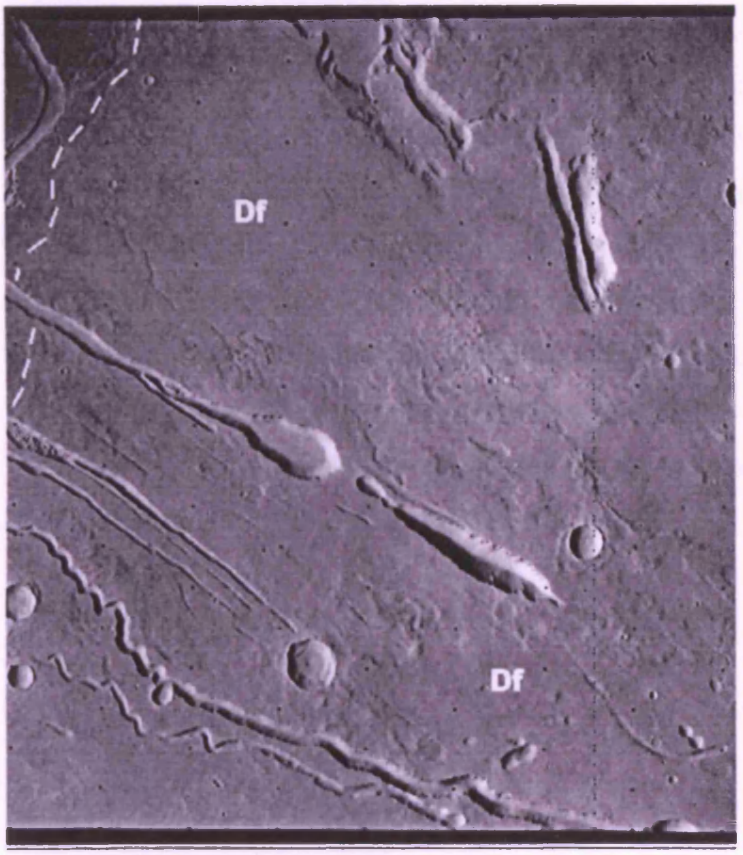

Figure 4.23: Part of Viking image F541A37, showing an area of Fossae (linear, often flat-floored depressions) surrounded by the Disrupted Flows unit (**Df**). The typical rough, often blocky, surface appearance of this unit can be observed. The white dashed line in the top left of the image indicates a boundary between **Df** and another unit. North is towards the top of the image, and the width of the image is ~160 kilometres.

This unit is characterized by lava flows that have rough-looking, irregular margins (see Figure 4.23). Some appear to have been broken up into blocks and many flows are interspersed with small graben and channels. The graben are ~200-300 metres in width and the channels are ~500 metres across. Both the graben and the channels can be tens of kilometres in length. This unit surrounds the majority of the Elysium Fossae. Mouginis-Mark et al. (1984) suggested that this area had been created by the flow of lava from many vents that had not managed to build up into a volcano due to steeper

slopes than in the rest of the region. They termed it the 'complex vent' region. MOLA studies show that slopes here are steeper than those of the surroundings, with values of up to 2° as opposed to <<1° for other areas at a similar distance from the summit of Elysium Mons. Although this is considered a low slope value for lava flows on Earth, on Mars this slope value may have been great enough to considerably affect flow behaviour, as is indicated by the study of some Martian lava flows in chapters 5 and 6. Thus it is possible that the lava flows may have flowed in a turbulent rather than a laminar manner. The turbulent flow of lava can mean that the lava has enough energy to erode the surface over which it is flowing, as suggested by Hulme and Fielder (1977) and Head and Wilson (1981). Greeley et al. (1998) found unequivocal evidence for thermal erosion at Mount St Helens (USA), and they showed that erosion was enhanced in areas of locally steep slopes, possibly as the result of localised turbulence. If steeper slopes are the reason that the rilles and enlarged fossae are present in the **Df** unit, then it shows that a small increase in slope had a great effect on volcanic processes occurring in this area.

It is suggested here that this unit was formed by lava flows that were erupted from the Fossae and emplaced on top of the older **Em 5** unit. The flows were possibly turbulent in nature having been emplaced on relatively steep slopes. Subsequently the flows have become broken up and eroded by the repeated flows of water/ water and mud mixtures, and by lava from the Fossae.

Vent Flows (**Vf**)

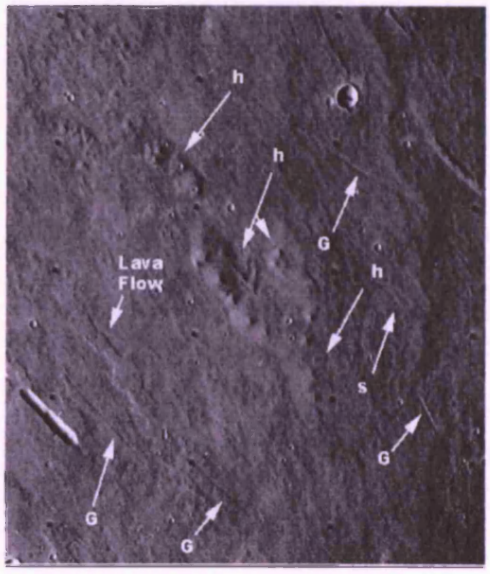

Figure 4.24: Part of Viking image F541A24 showing an area of the Vent Flows (**Vf**) unit. Typical characteristics of this unit such as the chains of hills (**h**), small graben (**G**) and narrow channel-like features (**s**) have been highlighted. These chains of hills may be related to features seen on Earth (Greeley and King, 1977). The lava flow indicated in this image is one of the flows that have been analysed in the present study using MOLA. In this image north is towards the top and the image covers an area ~70 kilometres across.

This unit is characterised by having more single, easily identifiable lava flows than any of the other volcanic units in the mapping area. It exhibits many small graben and narrow fossae, and many small sinuous rilles and channels, all only a few hundred metres in width but varying in length from several kilometres to tens of kilometres. It is also characterised by having many chains of small hills (each hill being 2 kilometres across or less), and many small ridges (see Figure 4.24). Some of the ridges seem to be associated with the Fossae and are the source of flow material. Those lava flows that are visible have rough, irregular edges that may have been eroded. The chains of hills look similar to terrestrial rootless vents. These are formed where the roofs of lava tubes rupture during active flow and lava spills from the rupture to produce a "rootless" vent that creates small domes (Greeley and King, 1977). It is suggested that lava in this area was either erupted from flank fissures or within tubes, some of which subsequently ruptured to produce the chains of hills visible now. Some of the numerous small graben in this area may have been exploited as vents. Eruption of lavas from the Fossae may have added to the flows in this area and disruption of the flow surfaces by the release of water from the Fossae may have eroded some of the lava flows.

4.33 Plains Materials

Many of these materials are thought to be ancient, and are said to have formed during the Noachian period of Martian history according to previous mapping studies (Scott and Allingham, 1976; Greeley and Guest, 1987; Tanaka et al., 1992). This is because the surfaces covered by these materials display many large impact craters 70 kilometres or more in diameter), they have been heavily modified by erosion, and many of the units in this section have been embayed or overlain by other units. They can generally be divided into two categories: **Highland Materials** and **Hilly Plains**, and these are shown on the sketch map in Figure 4.25. Many of these units provide information about the earlier geological history of this area, formation mechanisms for several of the units have been inferred, and the presence of ground-ice both in the past and present in this area has also been inferred. Other units in this section are found to be some of the youngest units in the mapping area, and analysis of the MOLA data has improved knowledge of the extent of some of the units and their stratigraphic relations.

The presence of a small, relatively young volcanic construct in the southeast of the mapping area has been confirmed.

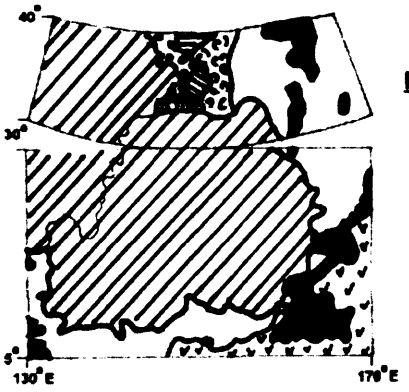

Highland Material:

Highland Materials grouped as a single unit

Hilly plains:

Sbp (Subdued hilly plains)

SHp (Sparse hilly plains)

Nrt (Narrow ridged terrain)

Rp (Ridged plains)

DHp (Dense hilly plains)

Other:

Ct (Chaotic terrain)

Yp (Young plains)

Figure 4.25: Sketch map of the mapping area showing the relative positions of the units grouped as 'hilly plains'. The highland materials have been grouped as a single unit in this diagram since they cover small areas as individual units.

4.33 a) Highland Materials

On Figure 4.25 the units that are grouped as **Highland Materials** are: **AH** (Ancient Highland Materials), **Fam** (Flooded Ancient Material), **at** (Ancient Terrain), **m** (Mass Wasted **at**), and **bat** (Buried Ancient Terrain). Although they are all Martian highland materials, they have been eroded and modified so that it is not possible to discern whether the units are related. Therefore they have been mapped separately as shown in the sketch map in Figure 4.2.

Ancient Highland Materials (AH)

This unit is smoother than the other highland materials, but maintains a characteristic 'dimpled' appearance, particularly in the MOLA shaded topography (see Figure 4.1). It has some large mountains and hills that are 10 – 20 kilometres across, and due to its softened appearance it looks as though it may have been the result of a collapse from material further southwest of the mapping area. It stands 600-800 metres above the surrounding plains and appears to be ancient due to the relatively high numbers of large impact craters (~70 kilometres in diameter) that are present compared

to other places in the mapping area. It seems to be related, at least in appearance, to other highland materials further south of the mapping area that form part of the north-south divide termed the 'dichotomy'.

Flooded Ancient Material (**Fam**)

This material has many large impact craters (~50 kilometres) and also several faults oriented northwest-southeast. It has been flooded and embayed by the unit **Yp**, which will be discussed later. The surface of this unit is covered by many hills that are 4 – 5 kilometres in diameter, and where it has been flooded by **Yp**, it is almost completely covered so that only the tops of the hills are exposed. The faults running through this unit trend in the same direction as the Elysium Fossae and this may be a regional trend created by the same tectonic forces.

Ancient Terrain (**at**)

This ancient highland material has been flooded by the plains unit **rp**. It is more prominent and higher standing (1 – 2 kilometres above the surrounding plains) than the other highland units described in this section, and comprises part of the Phlegra Montes mountain range that occurs at the eastern edge of the mapping area. There are some large impact craters (30 - 40 kilometres in diameter) in this material, some of which have been partially flooded, and there are also several large graben that can be up 100 kilometres in length and up to 20 kilometres in width. Some of the graben have also been flooded by **rp** and it is possible in several cases to see graben in different parts of the unit that were probably one feature until they were separated due to flooding by **rp**. This unit appears to have been a mountain complex in the ancient highlands. Many of the margins of this unit show evidence of mass wasting, by having a 'skirt' of smooth material that appears to have flowed outwards from the base of the unit. This mass wasted material has been termed unit **m**. Where this unit is lower standing (1 kilometre or less), more of it has been flooded by the lavas of **rp**, and the surface has a more softened appearance. This buried unit has an irregular, undulating appearance and may have undergone mass wasting before burial by lava. Where this occurs the rocks are termed 'buried ancient material' (**bat**).

4.33 b) Hilly Plains Units

The Hilly Plains Units shown in Figure 4.2 and 4.25 are: **rp** (ridged plains), **DHp** (Dense Hilly Plains), **Nrt** (Narrow Ridged Terrain), **SHp** (Sparse Hilly Plains), **Sbp** (Subdued Hilly Plains), and **Pt** (Patchy Terrain, which covers an area that is too small to show in Figure 4.25). Analysis of the images has shown that these plains are younger than the ancient highland materials because they embay the highland materials in places. However, they are older than most of the other units in the mapping area because they are overlain by many of them. These Hilly Plains Units are presented here as early flood lavas that embayed and covered the highland units before the onset of central vent volcanism.

Ridged Plains (rp)

This unit is characterized by north – south trending wrinkle ridges which are sometimes interspersed with southwest – northeast trending ridges that give the surface of this unit a patterned appearance (see Figure 4.26). There are several large flow fronts which lead to the inference that this unit was emplaced as large sheet flows erupted from large fissures. The flows have been distorted by faulting as well as by the ridges that characterize them. Interspersed occasionally within this unit are mesas of material, many of which are about 2 kilometres across although larger ones have been found to be 4 kilometres across. The mesas may be remnants of ancient highland material that has been overlain by the **rp** unit. The edges of the flow fronts have a rough, uneven appearance, and may possibly have been eroded. The unit is covered by many large impact craters, most of which measure 20-25 kilometres in diameter, but some are up to 80 kilometres in diameter. The largest of the impacts do not have any trace of an ejecta blanket. It is presumed in this study that the ejecta have been eroded away or overlain by the lavas of **rp**. This unit was presumably laid down as flood lavas and then subsequently subjected to the compressional forces that formed the ridges.

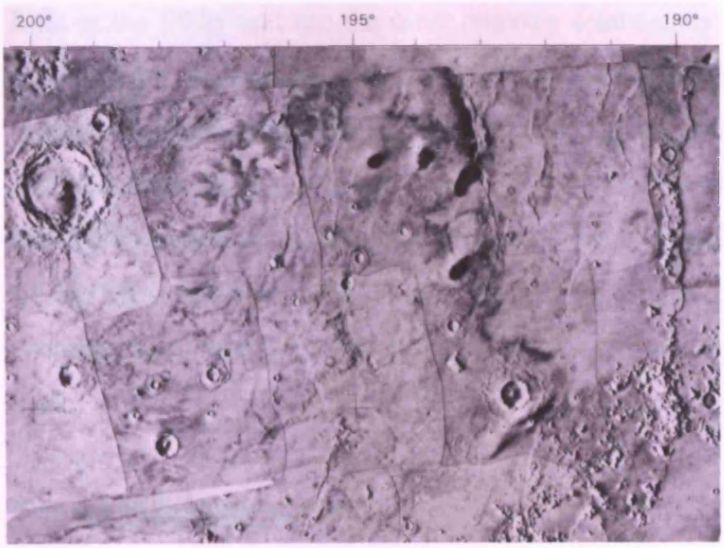

Figure 4.26: Part of Viking photomosaic of the MC15 Elysium Quadrangle. This shows a typical area of the **rp** geological unit mapped in this study. The area covered in this image is ~600 kilometres in width, and is bounded by the co-ordinates 189.5 to 200.5 degrees W longitude, 24 to 30 degrees N latitude. Individual ridges can be up to 15 kilometres in width and tens of kilometres in length. All the ridges in this image appear to trend NE-SW.

Dense Hilly Plains (**DHp**)

This unit characteristically displays knobs or hills of 1 kilometre or less in width, on top of a smooth, flat (low slopes of around 1°) plains surface. As the name suggests, the Dense Hilly Plains unit is characterised by hills close together and often less than 1 kilometre apart. The hills become smaller but more numerous towards the east of the map where this unit has a boundary with the **rp** unit. The **DHp** unit gradually grades into the **rp** unit since it is probably an erosional unit that composed of **rp** which were broken up by the action of ice, water or wind, or maybe a combination of these. In Chapter 1 it was suggested that ice or water was present in this area at some stage in the past. Further evidence to support this view has been provided by analyses of Viking and MOC images in Chapter 3 and is also given later in this chapter.

Sparse Hilly Plains (**SHp**)

This unit occurs to the west of **DHp**, and the two units grade into each other, so that they are probably related. The hills are larger here (between 1 and 2 kilometres) but do not occur so close together as in **DHp,** being spaced up to 10 kilometres apart. The hills have well-defined edges. Further west this unit grades into the Subdued Hilly Plains (**Sbp**). This unit displays hills of a similar size to those of the **Shp** but with a more rounded appearance and their bases appear to have been affected by mass-wasting or flow of their constituent material. One interpretation is that the more sharply defined

hills in the **DHp** unit are the most recently formed, the hills further west become more modified by wind or ice so that they become more subdued looking, or are eroded away completely leaving sparser plains. An area of the plain that is completely devoid of hills has been mapped separately as Patchy Terrain (**Pt**). This is probably related to the other hilly plains units, and may be an area where conditions favoured complete erosion of the hilly material. The Patchy Terrain may have been an area where the original material that eventually formed the hilly plains was less resistant than the surrounding rock.

Narrow Ridged Terrain (**Nrt**)

This unit occurs to the southwest of the Dense Hilly Plains unit but north of the Chaotic Terrain Materials (**Ct** in Figure 4.2). Some hills (that measure ~2 kilometres across) exist within this unit, but the unit is characterized by many ridges, some of which occur in what appear to be depressions that were too small to be visible in MOLA profiles. Several of the ridges also border the depressions, or seem to occur next to lines of hills. They also exhibit flow of material around the edges of the ridges. This flow of material is here ascribed to the action of ground-ice, particularly given their proximity to the Chaotic Terrain Materials, which are also thought to owe their formation to ground-ice (see later in this section). The formation of the ridges may have been facilitated by the presence of ice, perhaps within a compressional regime.

Two further units need to be mentioned in this section because of their relationship to the rest of the units, but neither of them fits into the two general categories above. Firstly there is the Young Plains unit **Yp**, which occurs next to both an ancient highland terrain unit and the ridged plain unit but which is much younger than either of them (Plescia, 1990, 1993; Tanaka et al., 1992; Hartmann and Berman, 2000; Keszthelyi et al., 2000; Burr et al., 2002). It appears to have been erupted from several of the fissures (some of which are the Cerberus Fossae), which cut across the **rp** and **FAm** units, and actually represents a number of units that could be mapped at a smaller scale. It is composed of both volcanic materials and sedimentary materials, since both flow fronts and fluvial channels can be observed in the Viking images. These are particularly noticeable in the shaded MOLA topography. The unit has flooded and embayed parts of the **Fam**, and flowed around impact craters and covered up all the associated ejecta. It has also left some 'ghost craters' where the **Yp** material

has flooded into the impact craters and almost completely submerged it, except for the highest standing parts of each crater rim. There are few impact craters, which implies that the unit is relatively young. Previous work on this part of the mapping area was mentioned in Chapter 1, and evidence for recent lava flows and water was found in these studies (Berman and Hartmann, 2002; Burr et al., 2002.). As in these studies, this unit is interpreted here as young volcanic plains that have been modified by fluvial activity.

One observation that provides evidence that this area has been volcanically active is the presence of several small volcanoes, one of which lies in this mapping area and is shown by feature **v** on Figure 4.2. These were visible in the Viking images and were suspected of being volcanic in origin (Plescia, 1990), but since they have low relief it is only now that MOLA has provided detailed topographic data that the true extent of the flows from these volcanoes can be seen (Figure 4.27). MOLA profiles show that the volcano in Figure 4.5 reaches 110 metres above the surrounding plains, that the flanks have slopes of ~0.3°, and that the depression that probably marks the vent of the volcano is 10 metres deep. Although this area is of interest because more recent volcanism has occurred here, it will not be discussed in any greater detail because this study is primarily concerned with the larger volcanic constructs such as Elysium Mons.

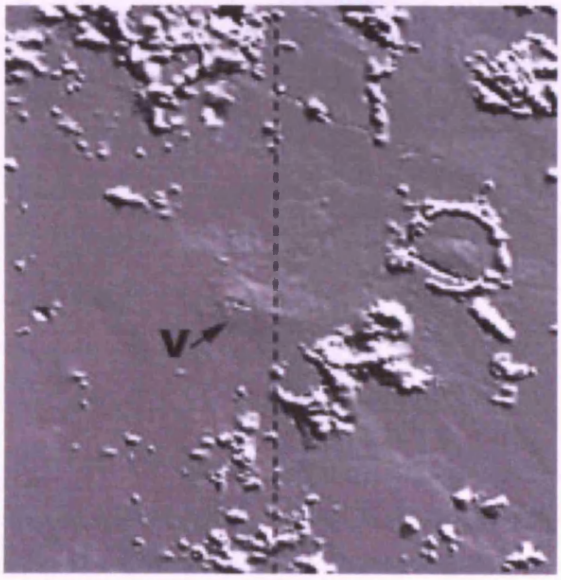

Figure 4.27: This is part of the shaded MOLA base map shown in Figure 4.1. The feature 'v' is thought to be a small volcano that is relatively young compared to the surrounding plains. An apron of flows can clearly be seen around an elongated vent, which may be a fissure created by the collapse of several pits, as can just be seen in the image. This image is ~300 kilometres across, so that the volcano, including main flows, is about 150 kilometres in diameter.

Chaotic Terrain (**Ct**)

Another unit that needs to be discussed at this point is the Chaotic Terrain. It is shown as unit **Ct** on Figure 4.2, and in more detail on Figure 4.4, where it is split into

two units: Chaotic terrain (**Ct**), and Modified Chaotic Terrain (**Ctm**). Chaotic Terrain is the geological unit that has formed immediately north of the volcanic pile on which the three major volcanoes in this mapping area are situated. Unit **Ct** is therefore positioned at the base of the lava slope formed by this large volcanic edifice, and to the north the unit grades into the hilly plains. Much of the surface of the Chaotic Terrain has been highly fractured into large mesas that can range in diameter between 1 kilometre and 10 kilometres across, and they form a characteristic 'honeycomb' appearance (see Figure 4.28). Some of the fractures/depressions between the mesas appear to be aligned and several can be seen to extend onto unbroken ground. This led Mouginis-Mark (1985) to postulate that lines of structural weakness may have played an important part in the formation of this unit. These aligned structures do not appear to line up with regional tectonic fracturing and faulting, which trends in a northwest-southeast direction as can be seen on Figure 4.2. The larger mesas tend to occur near the southern edge of the boundary. Further north and west in the chaotic terrain unit, there are areas of smoother ground where the mesas have a sunken appearance, as if they had melted into the surrounding surface, and these areas have been mapped as Modified Chaotic terrain (**Ctm**).

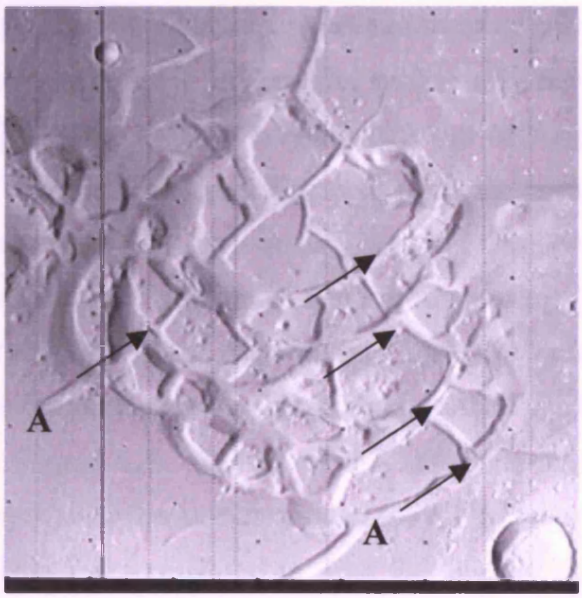

Figure 4.28: Example of chaotic terrain showing fractures/depressions extending onto unbroken ground (**A**) and a directional trend to the fracturing (indicated by the arrows). Both of these characteristics may imply a localised tectonic influence in the formation of chaotic terrain. The arrangement of mesas in this image is an example of the characteristic honeycomb appearance of chaotic terrain. This image is ~35 kilometres across and is illuminated from the upper left-hand side.

The general theory for the formation of chaotic terrain involves the melting of a subsurface ice layer (likely to be water but possibly carbon dioxide) and the subsequent escape of the melted substance onto the surface. The overlying rock mass then collapses because it is no longer supported (Sharp, 1973). Carr and Schaber (1977) proposed that in this particular case underground heating by magmas of the Elysium volcanoes, and over ground heating from the Elysium Mons lavas, melted subsurface water ice. The water that was subsequently produced escaped to the surface, and the overlying surface could not support itself and collapsed, forming the sets of fractures and mesas characteristic of chaotic terrain. This is also the formation mechanism preferred in the present study. The influence of underlying structural weakness may have initiated their formation and contributed to the aligned fractures observed in the images of the chaotic terrain (Mouginis-Mark, 1985). In their study of long Elysium Mons lava flows, Mouginis-Mark and Yoshioka (1998) found evidence that at least some of the Elysium Mons lavas (from unit **Em 3** in this study) had flowed onto ground that subsequently collapsed to form Chaotic Terrain. This shows that formation of the Chaotic Terrain occurred after at least part of the northern area of unit **Em3** was emplaced.

In this study it is suggested that the process of forming chaotic terrain may have worked in a similar way to sapping, so that the surface may have started to collapse from the northern edge of the original surface first, and collapsed back towards the south until it reached its current position. This means that mesas further to the north are more degraded and eroded possibly because they are older and have been eroded by the water that was discharged by the collapse of mesas further south. It has been suggested by Mouginis-Mark et al. (1984), that fluid released from the formation of the Chaotic Terrain might have flowed north and been discharged via the large fracture visible to the west of the **Sbp** unit (Figure 4.2). Release of this meltwater may also have been the source of water responsible for the modification of the Hilly Plains Units. Also, the fact that ice underlay materials that collapsed to form the Chaotic Terrain means that ice might also have underlain the materials that were originally eroded to form the Dense Hilly Plains, and therefore provides a formation mechanism for **DHp**. No evidence for fluid flow in the depressions surrounding the mesas of the Chaotic Terrain was found in the MOC images, however, because the depressions had been filled with aeolian material (as shown in Chapter 3).

4.4 Features of interest

In addition to the well-preserved lava flows surrounding the Elysium volcanoes, there are many other interesting features in the Elysium region. These include the Elysium Fossae; the calderas and morphologies of the volcanoes; the collapse feature on the north-western flank of Hecates Tholus; and the unusual ridges found in the northwest of the mapping area that were earlier termed 'volcanic ridge features'. These features have all been highlighted in Figure 4.29. Since one of the aims of this study was to obtain more information about the formation of the Elysium Fossae and the role that they played in the evolution of the area, they have been analysed using the new MGS data. Analysis of the other features mentioned above has also given insight into the evolution of the mapping area, particularly with regard to the levels of ice and water that were present in the past.

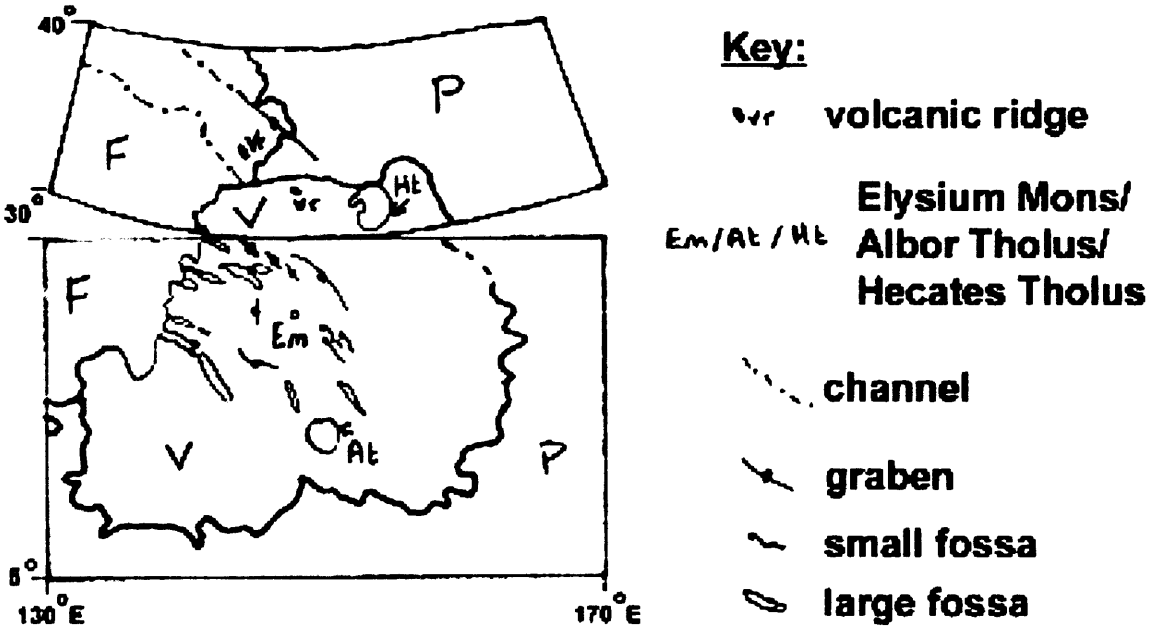

Figure 4.29: Sketch map of entire mapping area showing the positions of the major geological features in the area. These features are discussed in the text.

4.41 Elysium Fossae

One set of features near Elysium Mons that is of interest is the Elysium Fossae, and as the previous section has shown, the Fossae have had a great influence on the

geology of the region. Previous work has shown that they comprise linear troughs that are thought to be collapse features, probably related to the regional tectonics of Elysium Planitia, as they are typically orientated to within 15° of being radial to the summit of Elysium Mons (Mouginis-Mark, 1985). Their precise location was perhaps controlled by concentric fractures associated with loading of the region by Elysium Mons (Hall et al., 1984). Even though they are probably tectonic in origin they seem to have been modified by fluid flow and mass wasting. Generally the floors of the troughs are smooth and flat, there is a small head tributary, and the distal end of the trough is usually open and broadens out. Mouginis-Mark (1985) found evidence for the burial of lava flows at the distal ends of some of these troughs, showing that material did flow out of them. The cross-cutting relations of the Elysium Fossae, show that some parts of the troughs were formed after others, and there is also evidence that some parts of the Fossae have undergone more modification than others. Other Fossae walls display slumping, and there are mesas within the Fossae some of which have a streamlined appearance (see Figure 4.30).

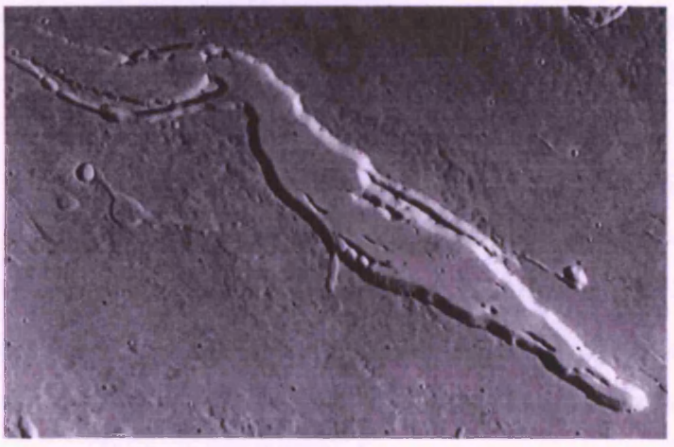

Figure 4.30: Part of Viking image F541A24, showing a large example of one of the Elysium Fossae. This example measures ~20 kilometres (at the widest point), and exhibits several linear ridges on the floor, which were probably formed either during the flow of a liquid contained within the fossa as it formed, or from gradual slumping of the walls of the fossa. It may have been a combination of both of these. North is towards the top of this image.

Given the evidence above, it seems likely that the Fossae initially formed as narrow fractures or graben. Indeed, some of the Fossae still resemble ordinary graben. A mechanism must be found to produce the present appearance of those Fossae with wide flat floors, and there are several possibilities, the first of which involves lava. Flow of lava from Elysium Mons could have been channelled through the Elysium Fossae while they were in their initial graben stage. Since the angle of slope in this area is relatively steep compared to the surroundings (as discussed during proposals for the

formation of unit **Df**), the angle of the slope could have caused the flow to become turbulent, thus giving the lava enough energy to incise the walls and floor of the trough (Hulme, 1973, 1982; Carr, 1974, Wilson and Head, 1980; Head and Wilson, 1980, 1981; Greeley et al., 1998). The second possibility is that the flow remained laminar but at a rate which melted the walls and floor of the trough and carried these extra materials downhill with the rest of the flow (Carr, 1974).

An alternative mechanism for the modification of these troughs is the flow of water. A possibility is that there was, and still could be, ice under the surface in this region (as shown in both previous work and in the present study). The radial nature of many of the troughs means that a sub-surface fracturing regime may have been present that was exploited by magma to form dykes. Therefore the graben and Fossae are (or were originally) the surface expressions of the dykes. The intrusion of the dykes would have heated the surrounding ground, which would have provided the heat to melt the ground-ice. In this way a large volume of melt water could have been produced and stored underground, where it can potentially remain in a liquid form for several millions of years (McKenzie and Nimmo, 1999). Therefore, pressure could have built up underneath the ground surface until sudden release of the water occurred into the graben. Such a flood would have eroded many of the graben making them longer and wider and in some cases forming the present-day Fossae features. This formation mechanism would explain the deposits on top of the lava flows at the distal ends of the troughs. Some evidence of scouring or a water-carved channel might have been expected at the ends of the troughs, and this has not been found. However, this may be because much of the water had evaporated upon reaching the end of the troughs. This may also explain why the troughs seem to grade away into the surface at the distal ends.

However they were formed, it appears that the Fossae were later reactivated and used as the source vents for further lava flows and fluvial activity (as has been discussed in the previous section). A model for the source of the lava and water is discussed in section 4.6.

4.42 Volcanic Calderas:

The ancient volcano represented by unit **Em 5** does not have a visible caldera, and presumably it has been covered by later lava flows from Elysium Mons. The calderas of Elysium Mons, Hecates Tholus and Albor Tholus are all visible and will be briefly

discussed as they are of importance to this volcanic study. The surface textures of parts of all three volcanoes are analysed in detail in the previous chapter (Chapter 3).

4.42a) Elysium Mons

The caldera of Elysium Mons is approximately 13 kilometres in diameter, and the study of several MOC images shows that it has undergone several collapse events. There must have been at least five different events because in MOC image M18-01756 (see Figure 4.31) it is possible to see four different benches on the caldera wall. These benches are unlikely to have formed by slumping of the caldera wall (Mouginis-Mark and Rowland, 2001), and therefore are probably caldera collapse events. The shape of the caldera today is circular, which suggests that hardly any migration of the magma chamber occurred over the evolution of the shield, and that the circular shape of the caldera was sustained.

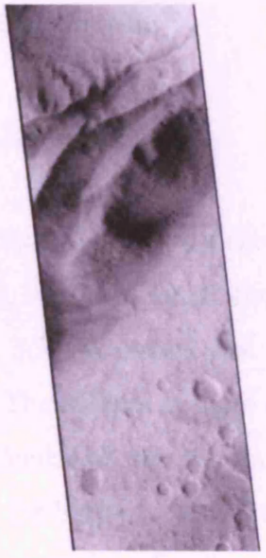

Figure 4.31: Part of MOC image M18-01756, of part of the northwestern edge of the Elysium Mons caldera. At least four different benches can be seen in the wall in this image, thus implying several collapse events. The base of the caldera can be seen in the lower half of this image. The base of the caldera is covered with many small impact craters of varying sizes, and also many wrinkle ridge features, which often join up into loops. One of these wrinkle ridges can be observed in the lower right-hand corner of this image. This image is 1.16 kilometres across, and north is towards the top.

Analysis of MOLA data shows that the caldera dips to the east, with a 350 metre scarp on the west and north walls (as measured by MOLA). There is no scarp at all on the eastern wall, which ends suddenly where the sloping surface of the eastern flank begins. There is a marked difference in elevation between the north/west of the caldera and the east/south caldera walls (as can be observed in Figure 4.40a), and this is owing to uneven collapse of the volcanic cone.

The MOC images have also revealed that the surface of the caldera harbours some unusual features. There are some ridges on the surface that are similar to wrinkle ridges in appearance and they are unusual because they join up at the ends into loops (see Figure 4.32). The areas inside the loops often look as though they are depressions, although they are too small for this to be checked using MOLA. It is possible that these features formed by ponding of lava within the caldera, where the cooling lava may have formed these loops and depressions as it solidified. The fact that the caldera of Elysium Mons is shallow, particularly on the eastern edge where it appears to meet the flanks with no discernible scarp, could be an indication that it was once deeper (Mouginis-Mark and Rowland, 2000). It may have been infilled with lava at some point after the collapse that formed the caldera, and thus provided the environment for the looped ridges to form. Lava inflation and subsequent collapse can occur in calderas on Earth and forms circular depressions bounded by ridges (A. Duncan, personal communication). However, it is unlikely that the formation of the ridges observed in the MOC images was via this mechanism because the wrinkle ridges seen are more irregular than circular.

4.42b) Albor Tholus

Albor Tholus has a caldera that measures 35 x 30 kilometres (Mouginis-Mark et al., 1984), which is much deeper that that of Elysium Mons. It reaches a maximum depth of 3.5 kilometres and almost reaches the same elevation as the surrounding surface. The caldera is large compared to the size of the edifice itself which suggests that the flanks of the volcano have been substantially buried, thus providing further evidence for burial by **Em 5** and **Em 4** lavas. Images of the caldera show that there were two episodes of collapse, one measuring 10 x 14 kilometres, and a larger one measuring 32 x ~20 kilometres. The smaller collapse section occurs to the north of the main caldera, and is 300 metres deeper than the larger, main caldera. It is probably the youngest collapse event as the entire outline of the smaller caldera is visible within the larger one and to judge from MOLA profiles the caldera complex does not appear to have subsided as a whole as might have been expected if the larger collapse event was younger.

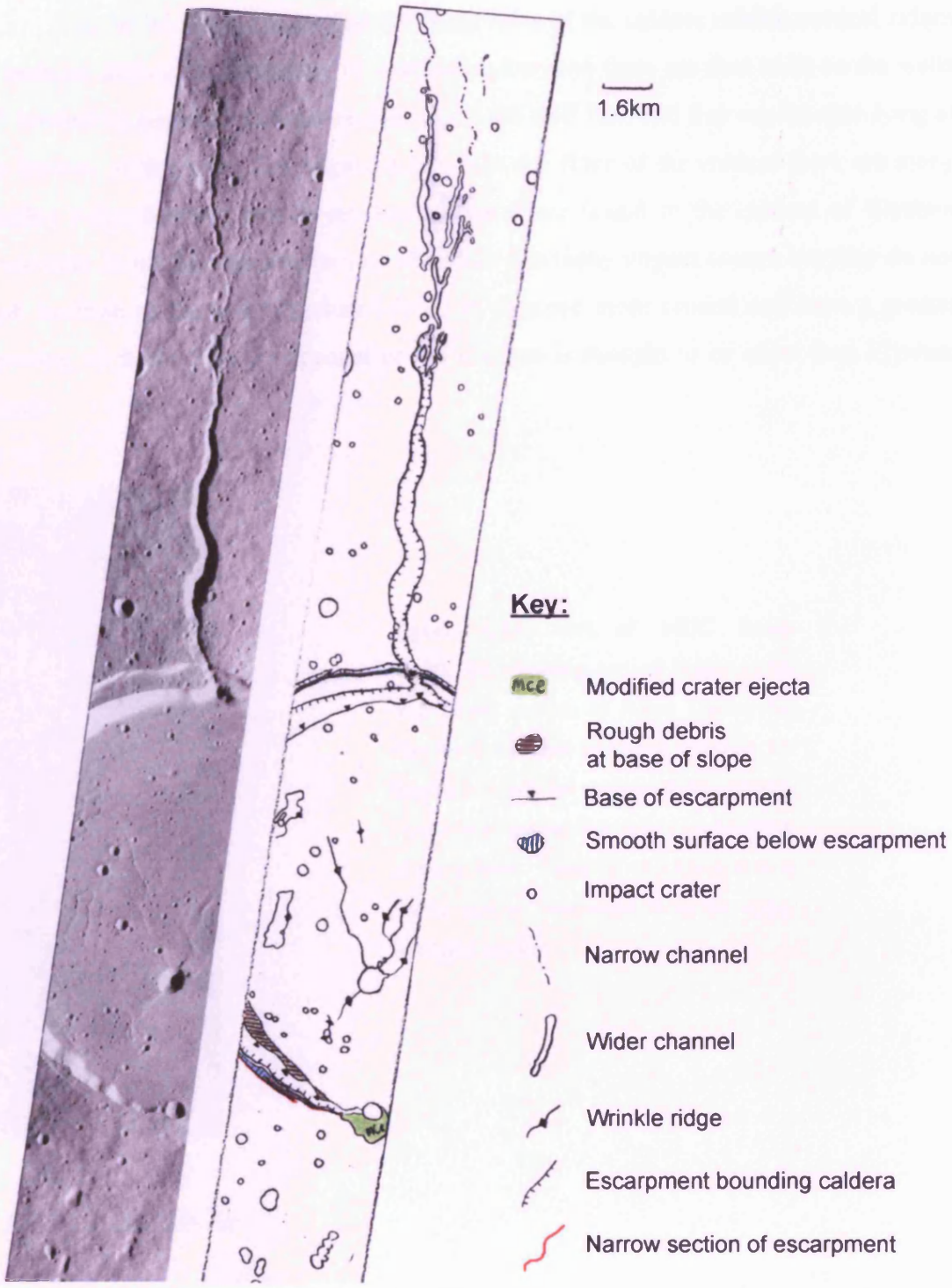

Figure 4.32: The image on the left is part of MOC image SP2-40303, showing a traverse along the central section of the Elysium Mons caldera. The image on the right is a sketch map of the MOC image. Note the 'loops' of wrinkle ridges, and the many small craters superimposed on the otherwise smooth-looking surface of the base of the caldera.

The MOC images show that the steep sides of the caldera exhibit vertical ridges of bedrock that could potentially be exposed dykes, and there are dust trails on the walls left behind by boulders that have rolled down the cliff face and that can be seen lying at the bottom of the walls (see Figure 4.33). On the floor of the caldera there are many wrinkle ridge features, which are larger than those found in the caldera of Elysium Mons and do not join up into loops. The floor has many impact craters but they do not look as fresh as those on Elysium Mons, as they are more eroded and have a greater covering of dust. This is expected as the volcano is thought to be older than Elysium Mons.

Figure 4.33: Part of MOC image M0001780, showing vertical ridges in the wall of the caldera of Albor Tholus that may be dykes that served as conduits for magma to reach the surface of the volcano. Notice also the wrinkle ridges on the floor of the caldera. Image is ~1.5 kilometres in width, and is illuminated from the upper left-hand corner.

4.42c) Hecates Tholus

The caldera of Hecates Tholus is shallow like that of Elysium Mons, having a depth of 200 metres. It is small compared to the size of the volcanic edifice, with a width of ~6 kilometres. Analysis of MOC images has shown that there have been at least four collapse events. MOLA profiles only show two of these clearly, with the floor of the south and southwestern part of the caldera being 75 metres deeper than the north/northwestern part.

High-resolution MOC images show that there is a large volume of dusty material covering the summit and caldera. There are impact craters that are almost buried, and many others have dunes and depositional materials on their floors. The surface has three major textures (see Figure 4.34). There are smooth areas with an undulating surface texture, which look as though underlying features have been buried by dusty material. Other areas are characterized by being covered by many small mounds that are sometimes aligned in a ridge-like fashion and may be dunes. Some other areas of the caldera are covered with many short (20 metres in length), linear features, all trending in the same direction, as though controlled by the wind direction. These are possibly small yardangs, formed by wind erosion of soft, dusty deposits. All the images of Hecates Tholus analysed in this study reinforced the theory that this volcano underwent at least one late-stage explosive event, as proposed by Mouginis-Mark et al. (1982).

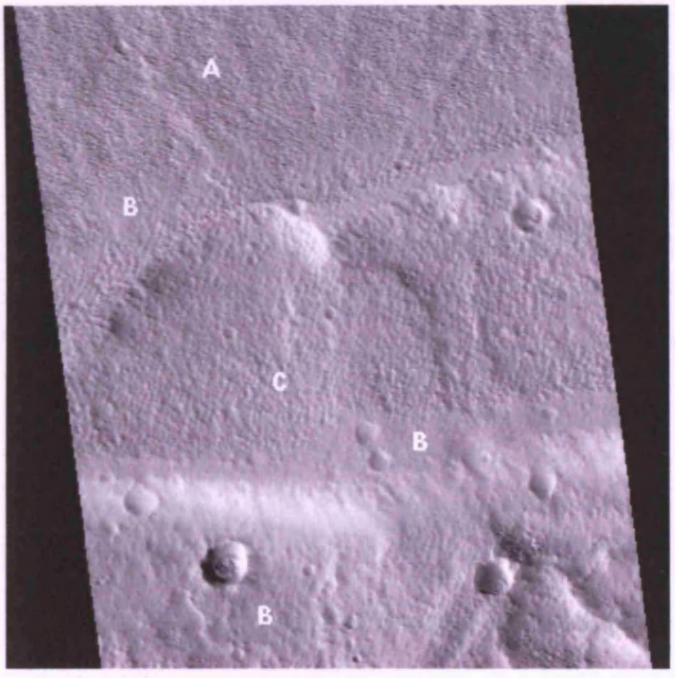

Figure 4.34: Part of MOC image M03-03180, showing part of the northern edge of the caldera of Hecates Tholus. The three distinctive surface textures found on the summit of this volcano have been identified. **A** indicates short, narrow linear features; **B** indicates smooth, dusty terrain; and **C** indicates larger, rounder mounds which are sometimes aligned. Since Hecates Tholus is thought to have undergone an explosive event in the latter stages of eruption, much of the material here is likely to be pyroclastic and thus easily eroded. Different surface textures here are therefore probably due to aeolian activity, with some areas subject to deposition, while others were undergoing erosion by prevailing winds. In this image north is towards the top and the image is 3.12 kilometres across.

4.43 Slopes of the Volcanoes

Early analysis of images from Mariner 9 indicated that the slopes of Elysium Mons were relatively steep on the upper flanks (with values of around 10°) compared to other Martian shield volcanoes, and became shallower towards the lower slopes. The shape of the volcano, and the implied steep slopes led Malin (1976) to make a comparison between Elysium Mons and the African composite volcano Emi Koussi, as discussed in Chapter 1. The new slope values from MOLA data are lower.

Kallianpur and Mouginis-Mark (2001) carried out a survey of the mean slope values of several volcanoes using MOLA data. They found that between 50 and 90% of the surface of Elysium Mons has an average slope of just over 7°. The top 10% and the lower 50% show significantly shallower slopes. Individual profiles carried out in this present study show that the angle of slope varies on the flanks of the volcano but shows similar values to those obtained by Kallianpur and Mouginis-Mark (2001), see Figure 4.38a for a typical profile across the volcano.

Elysium Mons is a shield volcano, so that the summit area and upper flanks are less steep than the lower parts. On the dome shaped volcanoes Hecates and Albor Tholus the upper flanks are steeper than on the lower flanks. From individual profiles the lower flanks of Hecates Tholus have slope angles of around 2°, and the upper flanks have slopes that are around 7.8° to 4.0°. MOLA measurements for the lower flanks of Albor Tholus had slopes of around 1° or less, and the upper flanks ranged between 5° and 6°.

4.44 Hecates Tholus Collapse Feature

On the lower part of the western flank of Hecates Tholus, on the border of the volcano with the surrounding plains, is a large depression measuring ~40 kilometres in length by 20 kilometres in width (see Figures 4.2 and 4.29). The floor of the depression appears to be flat and analysis of the Viking images suggested that it had been embayed by **Em 5** lavas (Tanaka et al., 1992). However, in a DEM produced using MOLA (see Figure 4.35) the floor can be seen to stand above the surrounding plains. MOC analysis of the floor of the depression carried out in Chapter 3 (Figure 3.43a) shows that it is composed of many erosional features such as yardangs, and depositional features such as dunes. Channels on the flanks of Hecates Tholus travel down into the depression and

may have deposited soft, easily erodible material on the floor of this feature. Subsequent erosion of this material would explain the formation of the yardang features visible in MOC images. This 'collapse feature' can be ascribed to the occurrence of at least one large impact event, as evidence for impact ejecta can be observed in the walls of the collapse feature as shown in Figure 3.46a in Chapter 3. A series of landslides may have been responsible for further increasing the size of the depression, and for depositing loose, easily erodible material onto the floor of the depression.

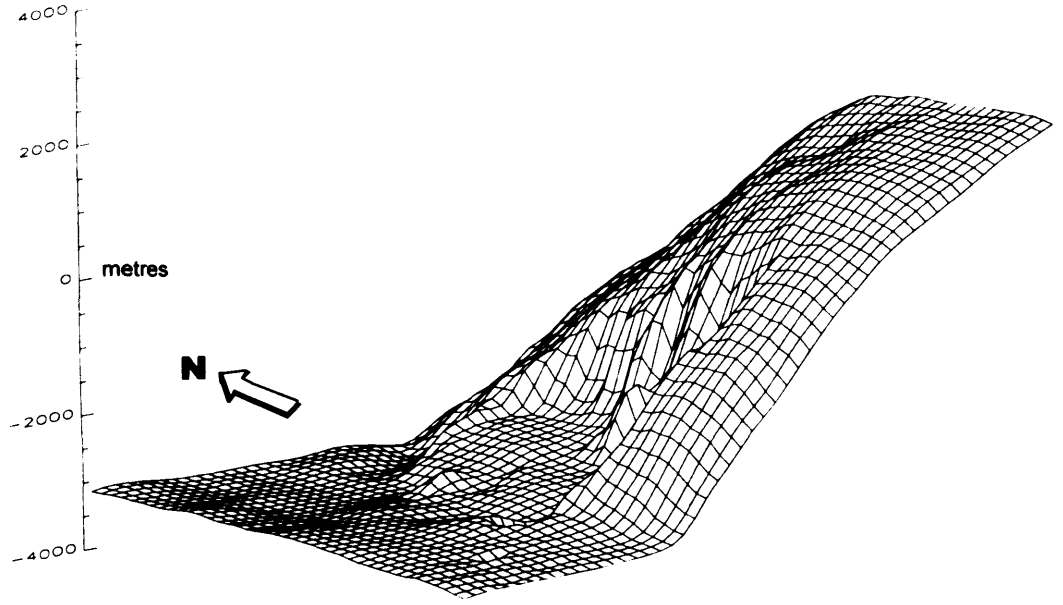

Figure 4.35: Digital Elevation Model of the western flank of Hecates Tholus, where the edge of the volcano meets the surrounding plains. The section of the flank that is missing can easily be seen in this image, where elevations have been exaggerated ~40 times. It shows that the base of the depression in the flank of the volcano is raised above the surrounding surface, and thus is unlikely to have been embayed by lavas from Elysium Mons. The depression is thought to have been formed by an impact event (see text).

4.45 Volcanic Ridge Features

One of the most intriguing features in the mapping area are the volcanic ridges, indicated by unit **Vr** on Figure 4.4 and labelled on Figure 4.29. The largest of these is an elongated mound or rise which displays a central ridge that runs longitudinally down the length of the mound. Extending laterally from the ridge are several other round-topped ridges that give the mound a 'ribbed' appearance (see Figure 4.22). The ridge

extends off the mound at either end onto the surrounding plains (**Txp** unit). Analysis of this feature in high-resolution MOC images reveals that the slopes of the mound have a pitted appearance (see Figure 4.36), which in some places resembles pits observed in MOC images of the Martian polar terrain. In many places the ridge has a pronounced, sharp apex, and there are several ridges with rounded apexes that are perpendicular to this central ridge and comprise the 'ribs' of the feature. Further down the slopes of the 'volcanic ridge feature', the surface is covered in small, interweaving cracks. The contact with the plains on the west side is abrupt in some places, where a wrinkle-ridge feature separates the two units, but to the eastern side of the feature the slopes of the volcanic ridge terminate in a lobate, almost flow-like edge.

There is a large amount of evidence for the presence of ice in the area surrounding this feature as already discussed elsewhere in this chapter and in Chapter 3, so it seems likely that ice was involved in the formation of this feature. There is another, smaller example of this feature directly to the southwest, and its ridge trends in the same direction as that of the larger one. Moore (1982) suggested that these Martian ridged-hills look similar to Icelandic moberg hills and ridges (see Thorarinsson et al., 1973) which form by subglacial fissure eruption. Moore (1982) therefore attributed a volcanic origin to these Martian hill/ridge features. The new evidence from the MOC images regarding the presence of ice, both in the surrounding area and in the images of the largest volcanic ridge (see Chapter 3 sections 3.4 and 3.7) supports this suggestion. Therefore unit **Vr** is taken be volcanic in origin and to have formed by the extrusion of fluid lava from the ridge under a layer of ice that was subsequently removed.

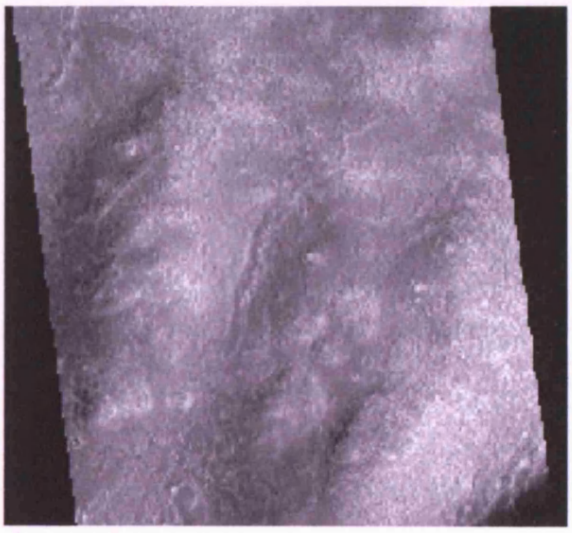

Figure 4.36: Part of MOC image M2200153, showing the textured pits and undulating ridges found on the slopes of the volcanic ridge feature.

4.5 Stratigraphic Observations

The following diagram (Figure 4.37) is a summary of the relative ages of the units reviewed, and aims to show the order in which they were formed and some of the relationships between them as determined by mapping. The geologic history of the area describing the formation of the units is given in section 4.7. As can be seen from Figure 4.2, ejecta from impacts has accumulated throughout the history of the region. Previous mapping studies have categorised the impact craters according to whether the ejecta were rayed or fluidised in appearance, which potentially indicates how much ground-ice was present at the time of impact (Carr et al., 1977a; Mouginis-Mark, 1979; Wood et al., 1978; Hale, 1983; Cintala and Mouginis-Mark, 1980). They have also been mapped according to the amount of weathering they have undergone, using this as an indication of the age of the impact (eg. Tanaka et al., 1991). In this study, the extent of the impact ejecta has been mapped, and in each case the area within the mapped boundary represents the pulverised material of the unit in which the impact occurs.

Figure 4.37: Correlation of Mapping Units

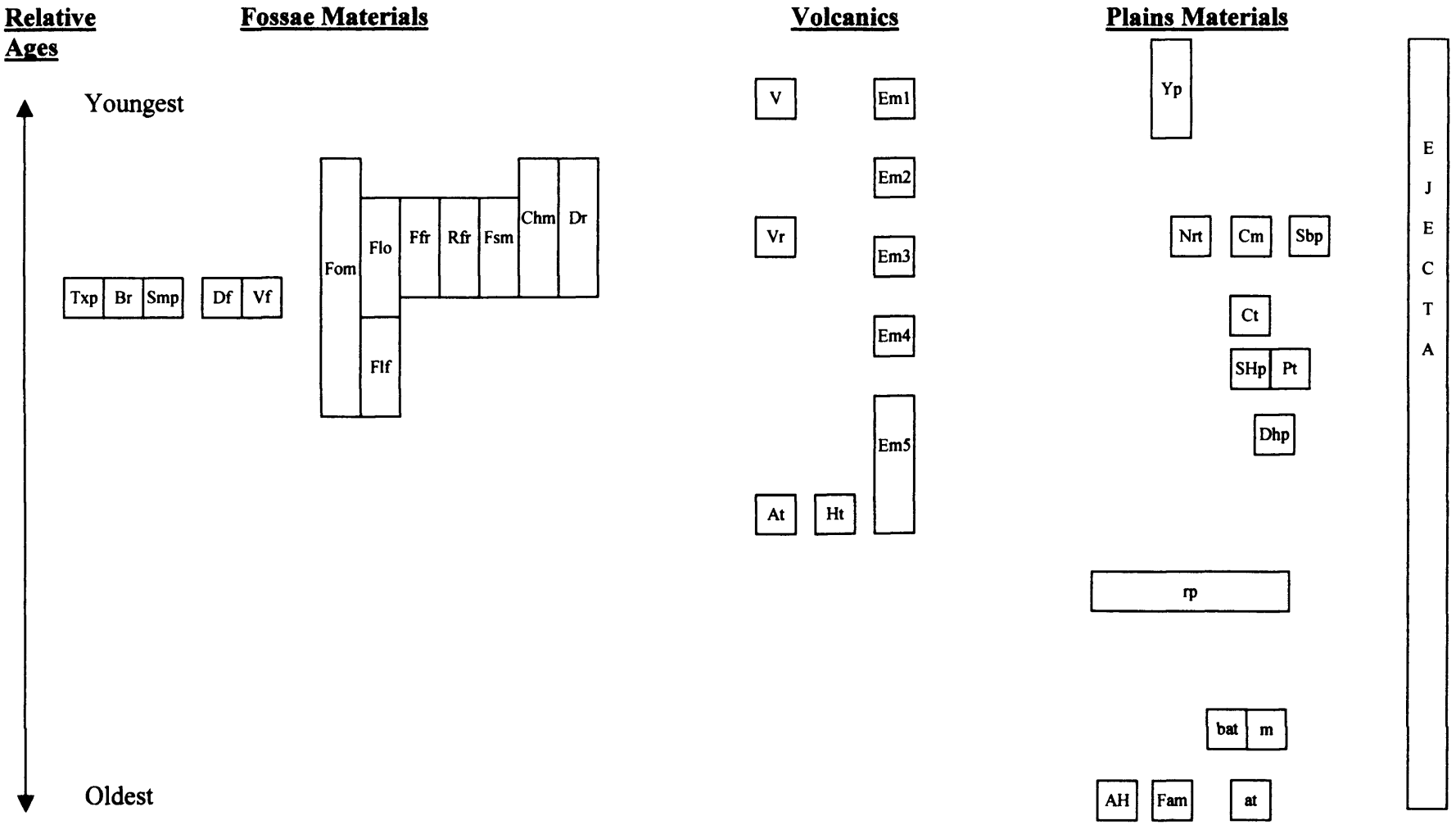

4.6 Models

It has already been stated that Elysium Mons appears to be offset on top of a larger, older volcanic edifice. The presence of many graben and some Fossae that appear to be concentric to Elysium Mons (Figure 4.38) provide scope for determining whether this is the case. Lines were drawn perpendicular to all of the arcuate graben surrounding Elysium Mons to see if any of them would cross each other and thus indicate the centre of a stress field caused by the active volcano. Although, as expected, some of them did appear to be concentric to the main Elysium Mons caldera, many of the arcuate fossae and graben were oriented around an area ~100 kilometres to the west of the Elysium Mons caldera. This would place the centre of the major local stress field in the area that is now covered by the young flood lavas of unit Em2 (see Figures 4.2 and 4.38). It is therefore proposed that this may represent the centre of the Ancient Volcano (AVE) underlying Elysium Mons and this later re-activated to produce the **Em2** lavas. The geometric tests carried out showed that the orientations of the graben were somewhat variable between the Elysium Mons caldera and the centre of the older volcano. This implies that the stress regime under which the graben were formed was gradually changing, and that there could have been a shift in vent activity to accompany this.

It is interesting at this point to make a comparison between the appearance of the Elysium volcanic complex and the terrestrial volcanic complex at Ardnamurchan in the Northern Highlands of Scotland, because there are major similarities between these two areas. The western part of the peninsular at Ardnamurchan is composed mainly of volcanic vents, ring-dykes and cone-sheets (see Figure 4.39). Ring-dykes are arcuate, inclined sheets of igneous rock that have a vertical axis and near-vertical or outward-dipping contacts (Kearey, 1996). They are thought to have been produced when part of the summit of the volcano collapses downwards into the magma reservoir, thus allowing magma to well up around the edges. Cone-sheets are a type of small ring intrusion with margins which dip inwards, supposedly towards the top of the magma reservoir (Kearey, 1996). They are possibly emplaced during the uplift of a central, conical block associated with a pressured magma reservoir, and are therefore formed in an opposite way to ring-dykes. These two different types of features are formed in close relation to

the calderas and vent systems of volcanoes. The geological map in Figure 4.39 shows that the ring dykes and cone sheets are arranged in a concentric series but that the orientation of these sets of features has varied slightly. The positioning of these features has enabled geologists to determine that there have been three volcanic centres over time here, each in a different position to the last (Richey et al., 1930). The first shift resulted in the location of the second centre being approximately 5 kilometres from the first. The second shift moved the volcanic centre approximately 3 kilometres. Ring dykes occur within 1 or 2 kilometres of each of the three vents, and the cone sheets occur further out at around 2 to 7 kilometres from the volcanic centres.

Given the similarity in appearance between Ardnamurchan and the Elysium Mons/AVE summit area, it is easy to suggest that some of the arcuate graben around the summit of the AVE and Elysium Mons are the surface expressions of ring-dykes and cone sheets. Also that the change in orientation of the graben shows a similar pattern to the shifting of volcanic centres at Ardnamurchan. Unfortunately, since the concentric graben are more than 20 kilometres from the caldera of Elysium Mons it seems unlikely that these can be ring dykes or cone sheets related to this volcano. However, volcanoes, and thus also calderas, on Mars can be much larger than those on Earth (Mouginis-Mark et al., 1992), so these concentric graben could be the surface expressions of ring dykes and cone sheets related to the caldera of the AVE. Any graben that appear to be concentric to Elysium Mons must be owing to other effects such as loading of the volcanic pile. It is possible that the unit **EM2** (young flow) may have been emplaced inside a depression that was left once the vent area of the AVE had collapsed during the formation of the ring-dykes, as is seen to have happened on the Scottish island of Mull (Ager, 1975).

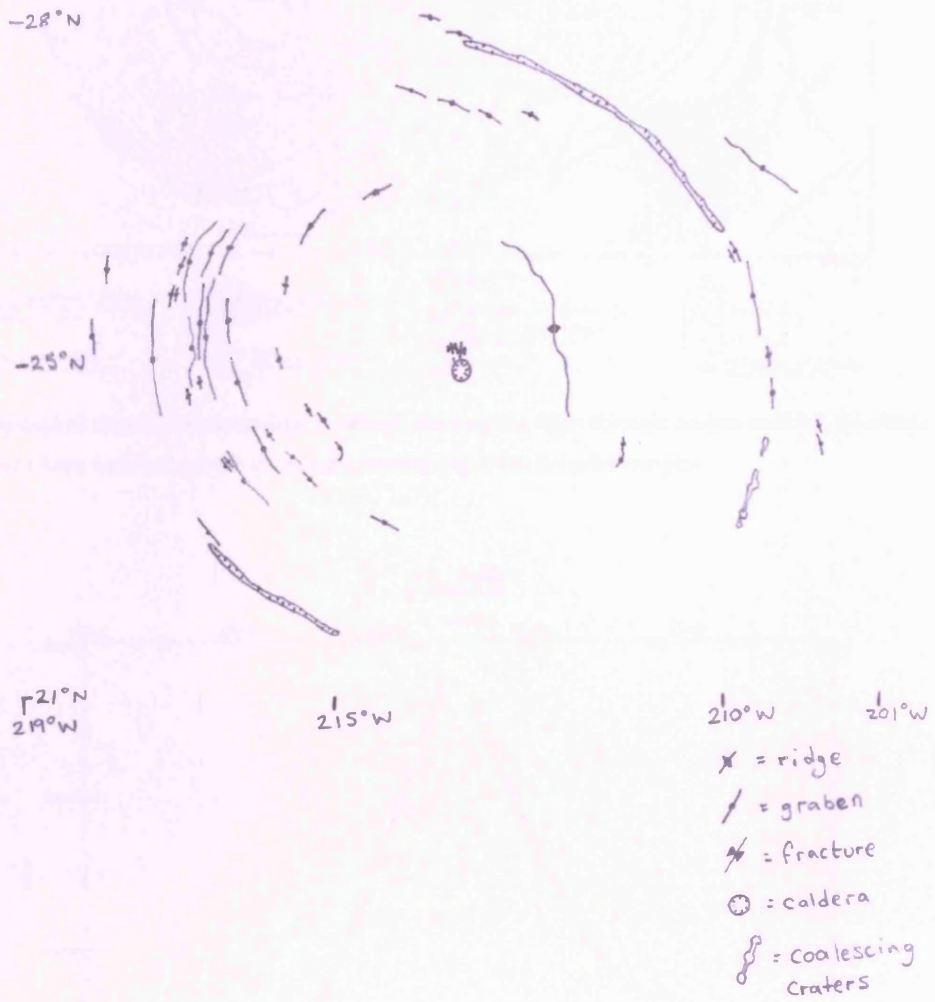

Figure 4.38: Map of graben, ridges and fractures around Elysium Mons. The graben surrounding Elysium Mons could be the surface expression of ring dykes and cone sheets related to the older volcano, the AVE. These features look similar in appearance to the terrestrial features found at Ardnamurchan (see Figure 4.39).

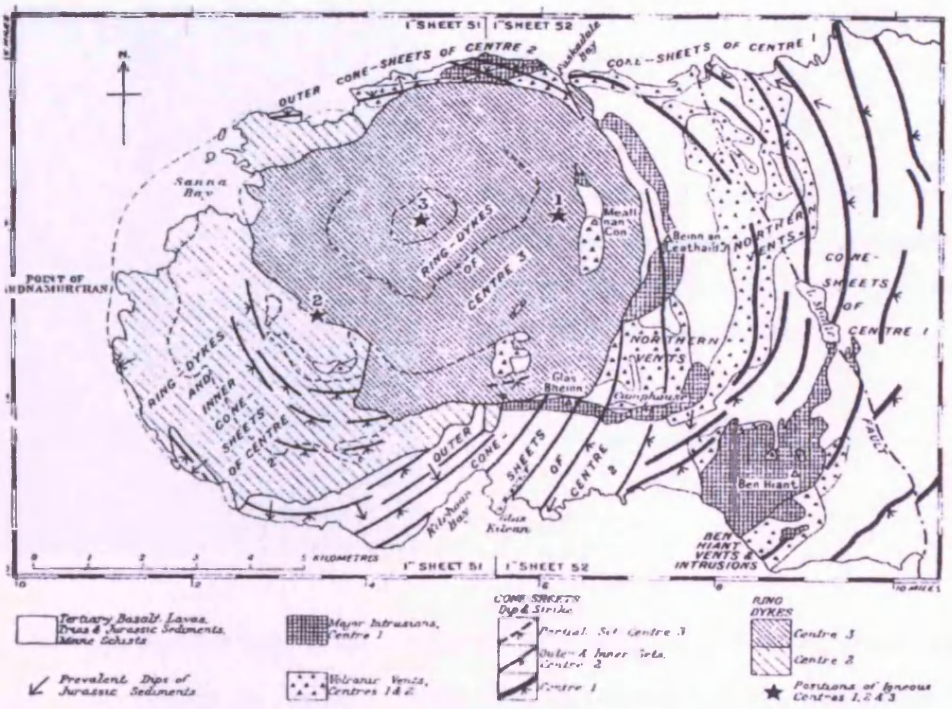

Figure 4.39: Geological map of Ardnamurchan, Scotland, showing the three volcanic centres and ring dyke/cone sheet complexes. Broken lines within ring dyke complexes indicate important intrusive margins.

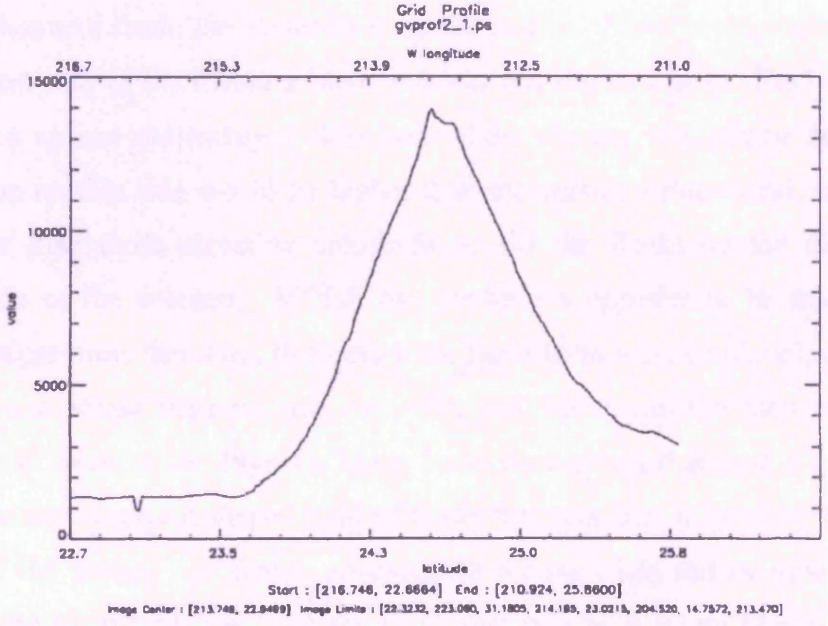

Figure 4.40(a): A profile across the Elysium Mons volcano produced in IDL using the programme Gridview. A context image is provided in Figure 4.40(b) to show where this profile was taken. The caldera of the volcano can be seen in the middle of the profile, and the depression to the left is caused by an impact crater. The elevation difference between the left and right-hand flanks where they meet the surrounding plains is obvious in this profile.

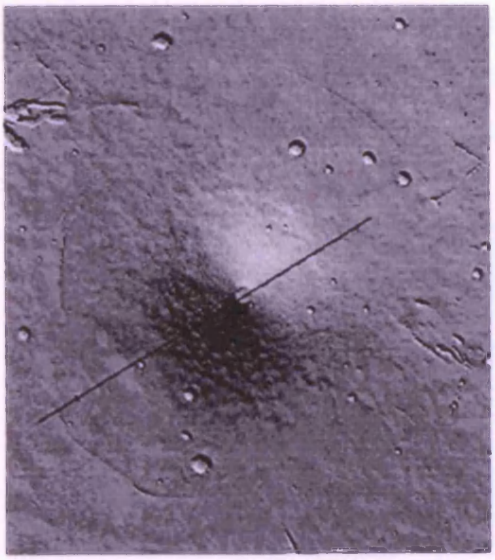

Figure 4.40(b): A shaded topography image of the summit and surrounding of Elysium Mons, produced un IDL. The straight black line indicates the position of the profile in Figure 4.40(a).

MOLA profiles across the suspected vent area for the AVE, show something unusual. The profile in Figures 4.40(a) and (b) shows that the southwest flank of Elysium Mons has a lower elevation than that of the opposite side of the volcano. On the southwest flank, where Elysium Mons Main edifice lavas (**Em4**) meet the younger flood lavas (**Em2**), the elevation of the surface is ~1350 metres. At a similar distance on the northeastern flank, the elevation is ~3500 metres. Since geological mapping of the southwest area of the Elysium Mons volcano has shown that the **Em2** flood lavas have built up against and embayed older parts of the volcano, it would be expected that the elevation on this side would be higher than the current value found, and perhaps even higher than those elevation values found for the flanks on the diametrically opposite side of the volcano. MOLA has shown the opposite to be true. It seems reasonable to assume, therefore, that before the flood lavas were emplaced, either some of the existing shield material was removed, and the depression later replaced by younger flood lavas, or the Elysium Mons lavas were diverted around a point on the surface to leave a crescent-shaped field of flows that was later infilled by flood lavas. Analysis of the images has shown no evidence for materials further downslope that might account for a landslide from the southwest side of Elysium Mons. However, more detailed MOLA contour maps (Figure 4.41) show patches of higher ground surrounding the **Em2** lavas, which may represent tongues of **Em4** lavas which formed by curving around topographic highs that existed before the flood lavas were emplaced. The sequence of events favoured by the author is that this previously existing topographic high was actually the vent of the older volcano, and it caused **Em4** lavas to

be diverted, and to be emplaced more easily on the northern flanks of the volcano. Collapse of the summit of the AVE, as previously discussed, may have occurred and the depression formed was later filled by lava (**Em2**).

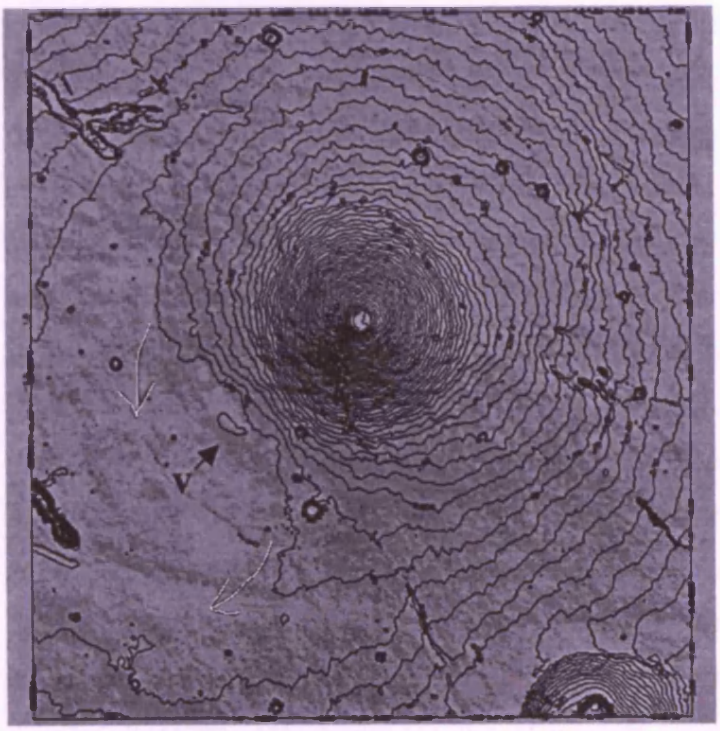

Figure 4.41: Contour map of the Elysium Mons summit and surrounding area. The contours are spaced 50 metres apart and clearly show how, to the south of the volcano, there is an area where the lavas from Elysium Mons wrapped around the summit area of the ancient volcano (in the direction of the arrows) and were then embayed by younger flood lavas. The potential vent for the Em2 lavas is also highlighted (v).

Mechanisms of formation of the Fossae have already been discussed, and analyses carried out in this study show that there is further evidence to support the previous assumptions that both water and lava have been intermittently discharged from the distal ends of the Fossae. It is easy to suggest a source for the lava, since the Fossae could have acted as large flank fissures to erupt Elysium Mons lavas. However, it is more difficult to suggest a source for the water that was also discharged. Although there is much evidence in the region for ground-ice (see Chapter 1 and Chapter 3), it cannot account for all the water that must have been present to form the features observed. This is because much volcanism occurred and any ground-ice present near the surface would have been melted and would have interacted with the lava long before the Fossae were established. Unless the ground-ice was replenished by localised precipitation (perhaps related to the gaseous volcanic emissions), there must have once been a hydrothermal system present in Elysium Planitia.

The evidence for a former lake further to the south of Albor Tholus (Scott and Chapman, 1995) in the Elysium Basin suggests that liquid water may have been present

in this area on the surface for substantial periods of time, at around the time that volcanism was still occurring at Elysium Mons. Scott and Chapman (1995) suggest that a paleolake started to form in the Elysium Basin (southeast of the mapping area) during the Middle Amazonian era. The source for the lake would have been the large outflow channels and runoff from the highlands. The paleolake is thought to have drained and evaporated in the Late Amazonian era and widespread volcanism on the Elysium Rise ceased. Therefore it is possible that large volumes of water were present when volcanism was occurring at the larger volcanic edifices in Elysium. The heat from the magma chambers in Hecates Tholus, Albor Tholus, and later Elysium Mons could have kept water warm and liquid at depth. This water could then have flowed to the surface either intermittently or as springs, to react with lava flows, modify existing features, and produce the channels of Granicus Valles, Apsus Valles, Tinjar Valles and Hrad Valles which extend from the Fossae into Utopia Planitia, northwest of the mapping area. MOLA contour maps show that the Fossae nearly all terminate at the base of the Ancient Volcanic Edifice (**Em5**), and that it is from the point where the base of the AVE meets the surrounding plains that the fluids are discharged. The Fossae do not all terminate at the same elevation, so it is proposed that, rather than the base of the Ancient Volcano representing the top of a water table, the hydrothermal system was contained at pressure under the weight of the volcanic materials of the AVE and Elysium Mons, and the water could only escape where the Fossae created a conduit to the surface.

4.7 Geologic Summary

This section gives a more general history for the area, incorporating the models that have been presented for the formation of landforms into the sequence of events that have been determined by mapping.

1. Early flood volcanism and uplift creates the ancient highlands units of **AH**, **Fam** and **at**. These units undergo subsequent impact cratering and faulting, and erosional modification. Mass wasting of the **at** unit occurs to produce unit **m**.
2. Later in the history of the region the formation of a plains unit by plains volcanism occurs from large fissures. The lavas cool and contract, and the weight of the lava sheets creates compressional tectonic forces that form the

wrinkle ridges of the Ridged Plains unit (**rp**). This unit embays and buries much of the **AH**, **Fam** and **at** units, and extensively buries areas of **at** to form **bat**.

3. As the rate of plains volcanism declines, central vent volcanism takes over and the growth of the Hecates Tholus volcanic edifice (**Ht**) and the Albor Tholus volcanic edifice (**At**) commences. Another volcano, the AVE or Ancient Volcanic Edifice (**Em5**), also starts to form between Albor Tholus and Hecates Tholus.
4. Erosional processes, by the action of wind and/or water (ice), break up the Ridged Plains (**rp**) in the north of the mapping area to form unit **DHp**. Further erosion of the western edge of **DHp** forms units **SHp** and **Pt**.
5. Towards the end of the formation of Hecates Tholus, the structure becomes almost totally surrounded by material (**Em5**) from the AVE to the south. Activity from Albor Tholus also ceases and the volcano is completely surrounded by the **Em5** lavas. Growth of the AVE continues until the lavas from this volcano form a broad shield ~1500 kilometres in diameter. The Elysium Fossae start to form on the flanks of the AVE and lava starts to erupt from them, forming part of the Fossae Lava Flows (**Flf**) unit. Explosive activity occurs in the later stages at the summit of Hecates Tholus (Mouginis-Mark et al., 1982).
6. Later, the onset of renewed tectonic activity leads to a shift in vent activity. Lavas start to flow to form the main Elysium Mons construct (**Em4**). Activity is more concentrated on the north side of the volcano as flows are diverted around the summit of the AVE. More graben and ridges form, which become further sources for the **Flf** (Fossae Lava Flows) unit.
7. Substantial volumes of water become present in the region at this time, possibly linked to the development of crater lakes and fluvial channels to the southeast of the mapping area. A hydrothermal system under the extensive volume of material of the AVE is the source for water that is erupted from some of the Fossae. It is also a possible source of water and ground-ice in the surrounding plains, and modifies many areas of the Ridged Plains to form the Smoothed Plains (**Smp**) and the Textured Plains (**Txp**) north of the AVE and Elysium Mons.
8. More lava erupted from the Fossae reacts with water on or near the surface to create the characteristic pitted nature of the Lobate Fossae Material (**Flo**).

Subsequent to this, the release of more water from the Fossae scours wide channels in the **Flo** material forming the **Fsm** unit. As the water/mud flows it erodes the (**Flo**) material forming the fractured unit **Ffr**. Where there are underlying tectonic influences, erosion of **Flo** forms patches of aligned ridged material and this is termed Ridged Fractured Material (**Rfr**). Deposition of the material eroded by the water/mudflows occurs, and further erosion of the plains forms the Disrupted Materials (**Dr**) unit. Lava and water are alternately erupted several times, to form layers of Fossae Materials that are highlighted by the MOLA data.

9. Flow of material from the Fossae breaks up some of the surrounding plains to the west of the mapping area, forming the Broken Terrain (**Br**), and modifying flank fissure flows from Elysium Mons and Fossae Lava Flows (**Flf**) to form the Disrupted Flow (**Df**) and Vent flow (**Vf**) units.
10. The melting of ground-ice by **Em4** lavas leads to the collapse of the overlying ground, and the formation of the Chaotic Terrain. Water from this collapse, as well as from the Fossae, causes modification of the surrounding units, forming the **Ctm** (modified Chaotic terrain), **Nrt** (Narrow Ridged Terrain) and, further north, the Subdued Plains (**Sbp**).
11. Lava flows with centralised channels (**Em3**) are erupted from Elysium Mons, many from flank fissures, and overlie the flanks of the AVE. Graben are still forming at this time, and the increasing presence of water in this area is forming small channels within the **Em5**, **Em4** and **Em3** flow fields. Activity at many of the Fossae decreases from this stage onwards.
12. The youngest field of flows (**Em2**) is erupted from vents southwest of the main Elysium Mons edifice. They embay some of the Fossae, and smaller graben, and cover the summit of the AVE.
13. Late stage volcanic activity in the ice-rich plains produces the Volcanic Ridges (**Vr**).
14. In the late stages of Fossae activity, substantial volumes of water are continuously released from one of the Fossae and form a narrow, well-defined channel that can be traced for hundreds of kilometres down the regional slope into the Utopia Planitia region. Water is also released along a large fracture trending in the direction of the regional slope and produces a channel that may also be traced for a long distance. The floors of these channels are covered with

deposited sediments that have been termed Channel Materials (**Chm**). Layered materials that have been emplaced on the floors of the Fossae through all stages of activity are termed Fossae Material (**Fom**).

15. Some of the most recent activity in the mapping region has been around the summit of Elysium Mons, where this study has shown evidence for a localised explosive event. There was extensive volcanic activity in the southeast of the mapping region where there has been extensive volcanic activity (Plescia, 1990) as well as the release of water from narrow fissures (Burr and McEwen, 2002) to form the Young Plains (**Yp**) unit. The small volcano (**v**) is inferred in this study to be relatively recent. Volcanic activity in this region shifted to the southeast in the later stages of its history.

The major differences between this work and previous studies are highlighted below:

- It has never before been stated that Elysium Mons was emplaced on top of a larger, older volcanic edifice (the AVE)
- It has formed off-centre on top of the AVE as a summit cone
- It has not been stated before that several different eruptive episodes have occurred at the Fossae
- The Fossae material was erupted at points where the Fossae crossed the edge of the AVE
- A hydrothermal system has been inferred to have formed underneath the Elysium volcanic complex
- A pyroclastic fall deposit has been found on the summit of Elysium Mons

Parts of the general history of the area concerning these new findings will therefore differ from previous studies. A comparison between the stratigraphic correlation of mapping units has not been directly carried out here between this study and previous mapping of this area. This is because only relative timescales have been used between the units in this study, not timescales relating to the Amazonian, Hesperian and Noachian ages as in previous mapping of this area.

4.8 Additional Data

Although much of the analysis in this study has been carried out using MOC and MOLA data, there are other sources of data that can provide useful information. Two useful sources are also from MGS: the TES (Thermal Emission Spectrometer) data, and the gravity modelling (produced using the Spherical Harmonics Data). During the lifetime of the MGS mission, and during the course of this study, the Mars Odyssey Mission also reached Mars and sent back some useful information that is incorporated in this study. More recently the Mars Exploration Rovers have provided some surface results from Gusev Crater and from Meridiani Planum (see Chapter 1).

4.81 TES Data

The TES instrument measures the thermal inertia of the surface of Mars, which means that it measures how well the top few centimetres of surface materials on Mars retain and emit the heat absorbed during the day from the Sun. Regional and global maps have been produced showing the thermal inertia of the surface at a spatial resolution of 3 kilometres. Since the properties of the surface affect the way it absorbs and emits heat, TES can provide information regarding the particle size, rock abundance, exposures of bedrock and degree of erosion of the surface of interest. Dusty materials and sediments do not retain heat as well as exposed bedrock, so exposed rocks will have a higher thermal inertia than fine-grained material. TES can also determine surface compositions, since surface minerals radiate heat obtained from the Sun back to space in characteristic ways that can be identified and mapped by the instrument.

Initial results show that the plains north of the dichotomy are more silicic in nature, with an andesitic composition dominated by plagioclase feldspar and volcanic glass (Bandfield et al., 2000), whereas those to the south of the dichotomy are more basaltic (dominated by plagioclase feldspar and clinopyroxene). Further analysis shows that Tharsis, Arabia and Elysium exhibit low thermal inertia values. An interpretation of this suggests that Elysium (and the other two areas) are composed of deposits of loose fine-grained material, several centimetres deep, and that few rocks or coarse surface materials are exposed (see Bandfield et al., 2000, and references therein). Since the Elysium region is relatively ancient compared to other areas on Mars, substantial dust cover may be expected. Also, with the evidence gained in the mapping analysis

carried out in this study, it may be that much of the fine-grained material is derived from explosive eruptions in the later stages of activity from Elysium Mons and particularly from Hecates Tholus, as well as sediments from the fluvial activity that occurred around the Fossae. A more silica-rich composition requires magma to have undergone further differentiation than with more basaltic compositions, and may be the result of higher water contents, cumulate formation, and /or repeated partial melting (BVSP, 1981; Gill, 1981; McSween, 1999).

One of the major problems with determining surface compositions using TES, is that there is a large amount of dust cover on Mars, so the surface materials analysed may not be representative of the actual rock units present, particularly since the global dust storms may distribute materials over great distances. There is an error of ~6 kilometres in the TES data, due to factors inherent in the positioning of all MGS data (as discussed in Chapter 2). The resolution of TES is not as high as that of the THEMIS instrument of Mars Odyssey, and little high-resolution data for the mapping area was readily available for this study.

4.82 Gravity Data

The gravity modelling carried out using MGS Spherical Harmonics has already been briefly discussed in Chapter 2. The latest gravity model GMM-2 is still at a low resolution (several square kilometres), and has yielded contour maps with contour spacings of 50 mGals. These contour maps show a good correlation between gravity data and Elysium Mons, with a high gravity anomaly of over 700 Mgals corresponding exactly to the summit of Elysium Mons. Albor Tholus and Hecates Tholus show poorer correlation, and the gravity anomalies are offset, presumably because the edifices are older than Elysium Mons (so that there has been more compensation in their vicinity) and have undergone significant burial. In general the AVE has a corresponding positive gravity anomaly, but the area to the north and west of the volcanoes has a negative anomaly, perhaps corresponding to the area where the surface has been significantly eroded by materials flowing from the Fossae. To the northwest of this, in Utopia Planitia, there is a small positive gravity anomaly, which may be due to loading of the sediments from the Fossae onto the plains.

4.83 Mars Odyssey

Mars Odyssey has a Thermal Emission Imaging System (THEMIS) which can measure the visible and infrared parts of the spectrum. It works in a similar way to the MGS TES, and can determine the distribution of several different minerals on the surface of Mars, but has a higher spatial resolution than TES, being able to produce images with a resolution of 100 metres per pixel. The mineral mapping of Mars Odyssey has not been useful in this current study because so far only selected areas of the surface have been studied by Mars Odyssey scientists, and the use of the raw data was deemed too time-consuming to make a study of these data worthwhile during this project.

The visible THEMIS images clearly show boundaries between different rock-types. However, they were not directly used for the mapping, because they only became available once the mapping part of this study was completed. Since the scale of the images in many cases bridged the gap between the high-resolution MOC images and the lower-resolution Viking images, the Odyssey images were sometimes used to check whether unit boundaries had been placed correctly, and also to try to observe surface textures, particularly of the lava flows. Unfortunately, few of the lava flows that were of interest in the mapping area were imaged by Odyssey.

The data that were of the most interest and use to this study were those produced by the Gamma Ray Spectrometer (GRS), which can detect the different minerals present in the surface materials, and also has two neutron detectors which calculate the abundance of hydrogen present in the upper metre of the surface, and hence can be used to infer the presence of water, presumably as ground-ice. Global maps of the neutron density of the Martian surface during different seasons of the Martian year have been produced by Odyssey mission scientists, and they show dusty, water-ice-rich mantling deposits that are layered, metres thick and latitude dependent, occurring in both hemispheres from mid-latitudes around ~30° to the poles (Head et al., 2003). The ice deposits found at present are thought to have been emplaced about 2.1 to 0.4 Myr ago and are undergoing reworking, degradation and retreat in response to the current instability of the near-surface ice. These data show that water-ice is present at the latitude covered by much of the northern section of the mapping area, and that presence and emplacement of ice under the ground surface in the mapping region was likely in the past when the area was more geologically active than it is today.

4.9 Conclusions

Geological mapping of this region using not only the Viking images but also MOC and MOLA, has revealed several new aspects of the geology of this region. It has shown that Elysium Mons formed on top of an older, larger volcanic edifice, and that it formed off-centre due to a shift in vent activity which must be linked to changes in the magma reservoir and magma supply routes under the volcano. Shaded MOLA topography has revealed that several eruptive episodes occurred from the Fossae, and that the Fossae material was erupted at points where the Fossae crossed the edge of the Ancient Volcanic Edifice.

There is much evidence from images, as well as from Mars Odyssey, that much of this area was underlain by ground-ice at some point in the history of the region, and that this ground-ice has had a marked effect on the formation and emplacement of rock units and features. Some of the rock materials are pitted or patterned due to the involvement of water and/or ice, and there are many channels in the region that appear to have been carved by the long-term flow of water on the surface. It is proposed in this study that the heat of the magma reservoirs within and beneath the volcanic edifices allowed a hydrothermal system to form underneath the volcanoes, and was the source of much of the water that flowed out of the Fossae and formed the channels to be seen today. MOLA data have highlighted evidence that discharge of water and lava from the Fossae were erupted during separate episodes on several different occasions.

Although the most recent volcanic activity appears to have occurred in the southeastern part of the mapping area (around the Cerberus Fossae), a relatively recent pyroclastic-fall deposit has been discovered by the author on the summit of Elysium Mons that had not been easily visible before in the Viking images. This deposit appears to have been erupted from a series of small pits near the caldera, and probably occurred in the later stages of the life of the volcano. Hecates Tholus has also been found in previous studies (Mouginis-Mark et al., 1982) to have had a late-stage pyoclastic-fall deposit erupted from the summit.

5.0 Lava flow studies – theory and methods

One of the most intriguing things about Martian lava flows, as mentioned in Chapter 1, is the fact that many have travelled great distances, often over shallow slopes, yet the lower gravity on Mars will make the lava act as though it is flowing over an even shallower equivalent slope. One of the aims of this study is to work out how these long flows can occur. The most obvious reasons for this are:

1. Martian lavas are less viscous than terrestrial lavas and may also have been erupted at higher temperatures and, hence, at lower viscosities, therefore allowing them to travel further before cooling makes them come to rest;
2. the lava was erupted at a high effusion rate and was emplaced so quickly that it managed to flow long distances before either the supply of magma ran out or the flow front cooled sufficiently to halt the progress of the flows;
3. the lava was slow moving with a lower effusion rate but was able to flow long distances under an insulating crust that kept the lava hotter and fluid for longer than flows where the lava is flowing in an open channel.

Points 1 and 2 can be referred to as 'rapid' emplacement, and point 3 as 'insulated' emplacement (Keszthelyi and Self, 1998). On Earth there are also many areas where long lava flows have occurred, and flood volcanism has produced thick sheets of lava covering vast areas of land. For example, the Columbia River Basalts Group (CRBG) in the USA is built up of ~300 different flows, each ranging in volume between several hundred and 3,000 kilometres^3, and having lengths of up to 600 kilometres (Tolan et al., 1989). Many studies have been carried out in the past to determine how these flows could have been emplaced (Shaw and Swanson, 1970; Danes, 1972; Walker, 1973; Hulme, 1974; Malin, 1980; Head and Wilson, 1986; Pieri and Baloga, 1986; Pinkerton and Wilson, 1994; Wilson and Head, 1994). Observations on Earth show that most of the well-preserved long terrestrial lava flows appear to consist of inflated pahoehoe that has been emplaced in the 'insulated' mode (Self et al., 1997; Keszthelyi and Self, 1998), and has led Self et al. (1998) to develop the hypothesis that the "Standard Way of Emplacing Long Lavas" (SWELL) was as inflated pahoehoe sheet flows. However, there is still considerable debate regarding whether slow-moving inflated flows could have been responsible for all such large lava

flows, since brecciated flow tops that do not fit in with a pahoehoe style of advance have also been found at some flood basalt sites (MacDonald, 1953; Self et al., 1998; Frey et al., 2000). Also, the study carried out by Anderson et al. (1999) of the flow of lava in tubes at Hawaii shows that pulsed inflation through a network of tubes was responsible for inflation of flows. They found it to be unlikely that the efficient transfer of large enough quantities of lava required for the larger volcanic flow events, such as flood basalts, could have occurred in this way and propose that rapid emplacement is more likely. A more recent study of Martian flood lavas undertaken by Keszthelyi et al. (2000) has shown that the lavas analysed were probably emplaced as a mixture of insulated sheet flow, and flood-like break-outs. The Martian flows were likened to two examples in Iceland that appeared to exhibit a mixture of aa and pahoehoe characteristics. Clearly, in order to find out more about lava flows on Mars, what is needed is a way of determining emplacement mechanisms, and a model developed using terrestrial lava data, but which can be applied to extra-terrestrial lavas and which will give some estimates of flow emplacement times from which estimates of rheological properties can be made.

Previous attempts to model Martian lava flows were discussed in Chapter 1. One model that is suited to the study of extra-terrestrial lavas is the 'flow growth model' of Kilburn and Lopes (1991), which will be discussed later in this chapter and which relates measurable parameters of the flow (maximum length, maximum width, average thickness and average angle of underlying slope) to the time taken to emplace the flow. This model has previously been applied to lava flows on Mars, but was limited by a poor knowledge of thickness and underlying slope for the flows. Since the success of the MGS mission, the thicknesses and slopes can be calculated more accurately, so that better results can be obtained and the techniques used for measuring the lava flows will be discussed in section 5.3. The measurements will be used in the following chapter to obtain emplacement times for flows from two volcanoes on different parts of Mars, and to infer some of the rheological properties of the lavas.

The flow growth model will be discussed in detail in section 5.3, but it is important to note that there are two factors that must be established about a lava flow before this model can be used. Firstly, the flow must be of a 'simple' kind, meaning that it must have been emplaced all as one unit during the same eruption episode. This information must be

gained by analysing images of the flows. Secondly, the flow must be an aa flow, as this model is specific to the way in which aa flows are emplaced. Not all lava flows form as aa, therefore a description of the way that different types of lava flows form and how it is possible to identify the different kinds in the field is given in the following section. Section 5.2 will explain how the lava flows analysed in the present study were selected.

5.1 Types of lava flows

Knowledge of how flows form and continue to grow is important when trying to establish the mode of emplacement of a flow using only mathematical models and observations of morphology from images. This section will deal with the formation and growth of different types of lava flows. It is assumed that the lava flows in this study have compositions similar to terrestrial and lunar basalts (see Chapter 1). Assuming a basalt or basaltic-andesite composition of less than 50wt% silica (less than 55wt% for basaltic-andesite) means they can therefore be classified on surface appearance and mode of advance in the same way as terrestrial sub-aerial lava flows.

As soon as lava is erupted from a vent it starts to cool and crystallise owing to loss of heat via radiation. Eventually the flow may form either a channel or a tube and thus make the transport of lava from the vent to the front of the flow more efficient. Flow of lava in channels is generally favoured by short-lived eruptions with higher effusion rates and the lava tends to have a higher velocity (Rowland and Walker, 1990; Keszthelyi and Self, 1998). Tube-fed flows tend to result from longer-lived, uninterrupted eruptions with lower effusion rates and lava velocities (Rowland and Walker, 1990; Keszthelyi and Self, 1998). Whether the flow forms a tube or a channel is dependent on whether the lava surface can develop a continuous crust, which, in turn, is dependent on eruption conditions. After eruption, lava can develop a strong, solid crust within a few minutes (Kilburn and Lopes, 1991). The actual rate of crust production depends on the cooling conditions (Danes, 1972; Pinkerton and Sparks, 1976; Park and Iversen, 1984; Head and Wilson, 1986; Dragoni, 1989; Crisp and Baloga, 1990b). As the crust solidifies it is being pulled downslope by the more mobile lava interior. If the 'pull' of the more mobile lava is strong enough to break up the crust, the lava will start to flow in an open channel; but if the pull is

too weak to continuously break the newly forming crust then a continuous surface crust will develop that is anchored to the flow margins, and the fluid lava will travel underneath in a tube. Flows that break up the crust during advance will have fronts that move forward as a single unit (Kilburn and Lopes, 1988). Flows with continuous crusts have flow fronts that advance by small amounts of lava escaping through holes or weak spots in the crust (MacDonald, 1953; Swanson, 1973).

There are three major categories for sub-aerial lava flows: aa (see Figure 5.1), pahoehoe (see Figure 5.2) and blocky, the significance of which was first highlighted by MacDonald (1953). The major difference is the appearance of the crust of each type of flow, which is caused by its method of emplacement. Aa flows are generally emplaced as simple sheets that advance as single units. The flow advances in a rolling motion, similar to the way caterpillar tracks move forward. Open channels, bounded by marginal levées of cooled solid rock, often evolve to transport lava to the front. Owing to the constant breaking up of the crust, the surfaces of these flows are irregular, frequently fractured and usually covered in a layer of rough, irregular shaped fragments that are between several centimetres and tens of centimetres in diameter (Kilburn, 1990). It is flows of this type that will be analysed using the flow growth model.

Blocky lavas advance as sheets and look similar to aa, with irregular, fractured surfaces and a covering layer of rocky fragments. However, the fragments tend to be smooth and angular, and are larger in size than those of aa flows, having dimensions of tens of centimetres up to metres across. Since blocky flows are more common for lavas with higher silica contents (greater than 55 wt%) than basalts, basaltic aa and pahoehoe flows will be of more importance during this study.

Pahoehoe flows tend to have smooth surfaces that are normally continuous. The surfaces may form a typical ropy texture, caused when the flexible lava crust is deformed by the motion of the lava (Fink & Fletcher, 1978). The fronts of these flows are fed by lava flowing in tubes and they often grow by a process of inflation. Inflation is a mechanism where the upper surface of the lava flow is lifted by the injection of liquid lava into the core of the flow. It was first applied to pahoehoe lavas by Macdonald (1953), and the formation of typical inflation features were described by Theilig (1984) and Walker (1991). The

process was described in detail by Hon et al. (1994) after their observations of actively inflating flows on Kilauea Volcano, Hawaii.

The surface textures of aa and pahoehoe are therefore an obvious way to identify each in the field. Other ways to distinguish between aa and pahoehoe besides surface texture include: a difference in (1) cross-sectional appearance (Kilburn and Guest, 1993; Aubele et al., 1988; Thordarson, 1995; Thordarson and Self, 1996; Spry and Stephenson, 1996; Self et al., 1996,a&b, 1997, 1998; Cashman & Kauahikaua, 1997), and (2) internal small-scale features, such as the shapes and distribution of vesicles, crystallinity and joints (Thordarson, 1995; Self et al., 1996, 1997; Cashman & Kauahika, 1997). It is therefore quite easy to distinguish between fresh aa and pahoehoe flows in the field. However, it is not possible to use many of these methods for the flows under consideration in this study owing to their remote nature. The presence of channels and collapsed tubes as well as analysis of small-scale surface features visible in the MOC images will be used to determine the different types of flows being studied in this thesis. Comparisons of the usual morphology and sizes of terrestrial flows will also be made to results of the measurements carried out using the MOLA data in this study.

Figure 5.1: Photograph of the 1983 aa flow of Mount Etna, Sicily. Note the characteristic rubbly flow surface texture. The paler flow is overlain by a darker, younger flow.

Figure 5.2: Photograph of the 1651 lava flow of Mount Etna, Sicily. In the foreground there is a good example of a pahoehoe flow (approximately 9 metres long in this image), showing the characteristic ropy surface texture typical of these flows. The flows around this are rather broken and blocky, and have been emplaced in this way owing to a sudden change of slope at this point.

Aa flows often start as fluid sheets. The flow front soon starts to solidify and towards the end of the eruption may be nearly solidified; it thus normally advances by a mixture of fracturing and flow (Kilburn and Lopes, 1988). Once the fluid sheet has stopped widening, flow is concentrated downhill and the flow forms a channel. The fronts thicken as the flow advances because they cool and slow down relative to the more fluid lava up-slope (Kilburn and Guest, 1993). They can grow by as much as ten times their original thickness and end up with a typical thickness (on Earth) of around 20 metres (Guest, 1982; Lopes and Guest, 1982). The front of an aa flow can come to rest in one of two ways. The supply of lava feeding the flow may stop, and the flow comes to a halt. These can be called "supply controlled" flow fields (Guest et al., 1987; Kilburn and Lopes, 1988). Alternatively, the flow front might solidify so much that it comes to rest even though there is still a constant supply of lava, thus having reached the maximum cooling-limited distance from the vent (Wadge, 1978). In this case the lava will fill up inside the channel, working its way backwards towards the start of the flow. This puts pressure on the margins of the flow until eventually a weak spot is found that can be breached and the lava can escape (Kilburn and Lopes, 1988). This breach can often be used to supply a new flow. A cycle of breaching of flow margins can lead to the formation of many interconnected flows. This is known as a flow field (Nichols, 1936; Walker, 1971; Wadge, 1978; Kilburn and Lopes, 1988).

Pahoehoe flows generally have slower effusion rates than aa flows, and therefore advance more slowly. They are thin when first erupted, with flow fronts and margins

typically having a thickness of only tens of centimetres (Walker, 1996; Keszthelyi & Denlinger, 1996). Advance is by lava escaping through small breaks in the crust, forming small tongues of material, and also by inflation (the "lava rise" mechanism described by Walker, 1991). Inflation is where new lava from upstream enters the tongues and lobes of the flow downstream and gently lifts the crust, thus thickening the flow. This can be an efficient process, increasing the thickness of flows by several metres within a few weeks (Hon et al., 1994). The growth of the flow continues in this way and many of the pathways for new lava entering into older flow material downstream stay connected under the crust, forming a network of tubes through which the lava can travel to the flow front (Anderson et al., 1999; Hon et al., 1994). In this way, the lava can maintain a high temperature and fluidity. This is particularly true where the tubes become partly drained so that there is a gap above the fluid lava where hot gases that have escaped from the lava can accumulate, as these can keep the lava close to eruption temperatures. Although pahoehoe flows advance more slowly than aa flows, they can remain hotter and more fluid for longer and so achieve lengths greater than those of aa flows of a similar volume.

This discussion of how aa and pahoehoe lava flows form and advance can be used to determine the kinds of features that may be used to distinguish aa and pahoehoe flows in the present study. Aa flows might have central channels, have rough surfaces and should thicken towards the flow front; they might also reveal breakouts (breaches of the flow margins) from which flow fields have developed. Single pahoehoe flows are expected to be thinner, smoother in appearance in the images, with flow boundaries composed of small tongues of material and to exhibit advance via breakouts from the flow front; they might also show distinctive inflation features, such as flat-topped sheet flows, inflation ridges, tumuli (see Figure 5.3) and inflation pits (Theilig and Greeley, 1986; Walker, 1991; Keszthelyi & Pieri, 1993; Hon et al., 1994; Self et al., 1996; Stephenson and Whitehead, 1996; Whitehead and Stephenson, 1996).

However, there can be complications in these general guidelines. For example, flow of lava in tubes is not just a feature of pahoehoe flows. Tubes can develop in aa flows if the tops of the levées bounding an open channel start to curve in and eventually meet up, thus enclosing the channel and forming a tube (Sparks et al., 1976; Guest et al., 1980; Guest et al., 1987; Peterson and Swanson, 1974; Greeley, 1987; Calvari and Pinkerton, 1998).

This generally only happens after the flow has been active for several weeks, and the tube will serve as a feeder for the flow further downstream. There are also transitional lava types, such as slab pahoehoe, which, although labelled as pahoehoe flows, are actually more similar in their mode of advance to aa flows (Keszthelyi and Self, 1998). It is also possible to find small patches (formed by breakouts or spill-overs) of pahoehoe in an aa flow (Macdonald, 1972; Jurado-Chichay and Rowland, 1995; Kilburn, 1990,1996), and similarly to find patches of slab pahoehoe or aa in inflated pahoehoe flows (Macdonald, 1953; Keszthelyi & Pieri, 1993; Kilburn, 1990,1996). The reasons for transitions and apparent transitions between flow types will be discussed in the next section. These observations show that it can sometimes be difficult to determine the dominant style of emplacement, particularly for flows as inaccessible as those on Mars, and that it is not possible to use just one morphological feature to determine the emplacement style of a flow.

Figure 5.3: Photograph of a tumulus formed during the emplacement of the Balze Soprane pahoehoe flow of Mount Etna, Sicily. A tumulus is created when the upward pressure of slow-moving molten lava within a pahoehoe flow swells or pushes the overlying crust upward. Since the solid crust is brittle, it usually breaks to accommodate the "inflating" core of the flow, forming characteristic cracks, as can be seen down the centre of this tumulus. The tumulus in this picture is ~20 metres in diameter.

5.2 Selection of lava flows for this study

When selecting the lava flows for the modelling it was important that flows should be:

- easy to define in the images and will therefore provide easily measurable distances
- traversed by enough MOLA profiles to provide accurate thickness and slope measurements
- located in an area of geological interest
- ones for which some emplacement characteristics had already been inferred in previous studies because this would enable a comparison to be made with the new results obtained from the more accurate MOLA data
- simple (emplaced as one unit as the result of one eruptive episode), since this type of flow can be studied using the flow growth model. Complex flows (the result of more than one eruptive episode) were not used because it was found to be difficult to determine the flow thickness of a multiple flow field.
- aa and **not** pahoehoe, because the flow growth model can only be used for aa flows

It has already been discussed that it can be difficult to determine whether Martian lava flows were aa or pahoehoe just from observation and analysis of the images. Analysis of lava flow surface textures both in the Viking and MOC images did not allow for the determination of type of flow using the sorts of features discussed in section 5.1. Therefore two techniques have been used in this study in order to determine which of the flows found in the areas finally chosen for study were aa and which were pahoehoe. The techniques used and numbers of aa and pahoehoe flows found in each area studied are discussed here. Obviously the emplacement times of pahoehoe flows cannot be modelled using the flow growth model, but inferences about their emplacement, as well as the significance of finding evidence for their existence on the flanks of Martian volcanoes will be discussed later in Chapter 6.

5.21 Selection of lava flows

It was decided that lava flows from two different areas on Mars would be studied in this thesis so that the results could be compared. The two volcanoes chosen were Elysium Mons and Alba Patera, the major characteristics for which have been discussed in Chapter 1. These volcanoes are different in several ways and it was hoped that the results of this study would reflect this. Elysium Mons is a shield volcano, and Alba Patera is one of the more unusual patera volcanoes (flattened saucer-shaped volcanic constructs that appear to be unique to Mars). The difference in overall shape may reflect differences in either the type of lava found in each area, or in the emplacement regimes of the flows. Also, Alba Patera has a longer and more diverse history than Elysium Mons, having spanned the time period when volcanic activity on Mars shifted from being explosive to effusive, as well as showing evidence for major tectonic activity (Plescia and Saunders, 1979; Scott and Tanaka (1980, 1986), Cattermole, 1990). Both areas have evidence for fluvial activity (Baker, 1982; Mouginis-Mark et al.,1988; Gulick and Baker, 1990; Berman & Hartmann, 2002; Burr et al., 2002) and, particularly in Elysium, the presence of ground-ice (Carr and Schaber, 1977; Christiansen and Greeley, 1981; Hale, 1983; Mouginis-Mark et al., 1984; Mouginis-Mark, 1985, Cave, 1993) which may also have influenced volcanic activity (Mouginis-Mark et al., 1982; Wilson and Head, 1983; Squyres et al., 1984; Mouginis-Mark, 1985). The reasons behind the choice of particular flows are detailed in the following two sections.

5.21(a) Elysium Mons

Since many of the lava flows in this region have already been mapped and characterised without the aid of MOLA data, it was the aim of this thesis to study some of these same flows to try to enhance the present knowledge of flow emplacement mechanisms in this area. In a previous study, Mouginis-Mark and Yoshioka (1998) chose 59 long lava flows to the north and west of the caldera of Elysium Mons, and took estimates of their widths, lengths, area and the distance from the summit of Elysium Mons to the 'vent end' (proximal end) of each flow. They also gave co-ordinates of the proximal

end of each flow so that they could easily be identified in the Viking photomosaics. In their study, the flows were categorised by their morphology into several groups: lobate; long linear; ponded; and simple flows, but they did not differentiate between aa and pahoehoe lava flows.

Using photoclinometry (a technique that allows the user to determine shape from shading), Mouginis-Mark and Yoshioka (1998) obtained topographic profiles across several of the flows in their study area, and came to the conclusion that at least some of the flows were segmented. They inferred this to mean that the flows grew by a series of pulses so that the lava had enough hydrostatic pressure to break through the crust at the snout to form the segments, and that the segments had not formed by the overlap of consecutive flows. Using their measurements, Mouginis-Mark and Yoshioka (1998) estimated that the flows in Elysium were long-lived, taking years or even decades to form. They did not find any evidence for post-emplacement inflation, and inferred that the emplacement of the segmented flows must be due to unusual conditions such as exceptionally shallow local slopes or the influence of an underlying permafrost layer.

It was decided that some of these same flows would be studied as part of this thesis, and that the results obtained could be compared with the previous study. Obviously with MOLA there was no need for photoclinometry to be used and much better measurements of flow thickness could be obtained. Also, longitudinal profiles along each flow could be produced, as well as profiles of the underlying slope, which help greatly in determining emplacement characteristics for both aa and pahoehoe flows.

For the purposes of the present study, all of the flows in the study by Mouginis-Mark and Yoshioka (1998) were categorised into simple and complex flows. This was based on their appearance in the images, with complex flows appearing to have been emplaced as a number of overlapping flows, each of which had a width that was narrower than the total planimetric flow width. Simple flows were relatively smooth in the images, appearing to have been emplaced as the result of one event. Those flows that were complex were not used, since these were found to be difficult to measure with MOLA. The segmented flow fields were observed to be complex flows and thus were not directly studied, although the use of MOLA did allow something about their emplacement to be inferred.

23 well-preserved simple flows were chosen in Elysium and each labelled with a number corresponding to those used in the Mouginis-Mark study. One other well-defined flow was chosen (Flow B) which had not been previously studied but was found to lie within the chosen area. Most of the flows chosen were of the sheet or tabular kind (Carr et al., 1977), except flows 17, 21, 28 and 50 which show a central channel bounded by levées (see Figure 5.4 for the positions of these flows). None of the sources of the flows were visible, presumably because they had been covered up either by lava from the flow or from later eruptions, or by aeolian processes, so the length values will be underestimated. In fact, some of the flows could not even be traced as far as Mouginis-Mark and Yoshioka (1998) traced them, so that length values given in this thesis will differ from those in their study. A map of the locations of the lava flows studied around Elysium Mons is shown in Figure 5.4. Once the simple flows were chosen they were separated into aa and pahoehoe using the techniques that will be described in section 5.22.

Figure 5.4: Map to show the positions of the Elysium lava flows studied using the flow growth model. **F** denotes one of the Elysium Fossae, **C** denotes the caldera of Elysium Mons, and **R** indicates the positions of two of the ridges surrounding Elysium Mons. All other features indicated on this map are graben, many of which are concentric to the Elysium Mons caldera. Area shown is ~ 680 kilometres across.

5.21(b) Alba Patera

Alba Patera has been the focus of much study (see Carr et al., 1977; Scott et al., 1981a,b; Cattermole, 1987 & 1990; Mouginis-Mark et al., 1988; and Kilburn and Lopes,

1990) over the past several decades, and the important aspects of this previous work were summarised in Chapter 1.

Several different types of lava flows have been observed on the flanks of Alba Patera (Carr et al., 1977), but those of interest to this study are the well-defined flows found on the summit area and flanks of Alba Patera studied by Kilburn and Lopes (1990). They studied 18 flows where the vents could be reasonably inferred back to a graben or the summit caldera, measured their maximum widths and lengths, and estimated their thickness and underlying slopes in order to use the flow growth model to obtain values for flow duration. These values were then used to produce values for effusion rates, given the volume of each flow. Since MOLA was not available at that time to produce a more accurate measure of the flow thickness and underlying slope, it seems useful to repeat the study using the new data to see whether there are differences between the two sets of results. Only 11 of the flows studied by Kilburn and Lopes were used in this present lava flow study because one of their flows was a complex flow, another was not covered by enough MOLA profiles, and the ones further down the flanks of the volcano were so modified by graben that it would have been difficult to obtain meaningful thickness and slope values. The 11 flows studied are shown in Figure 5.5. All of the flows are simple, and all are tabular or sheet flows except for flows 4 and 7, which have central channels. Although Kilburn and Lopes (1991) believed all the flows in their study to be aa, the techniques applied in the present study show that some were actually pahoehoe and cannot therefore be modelled using the flow growth model.

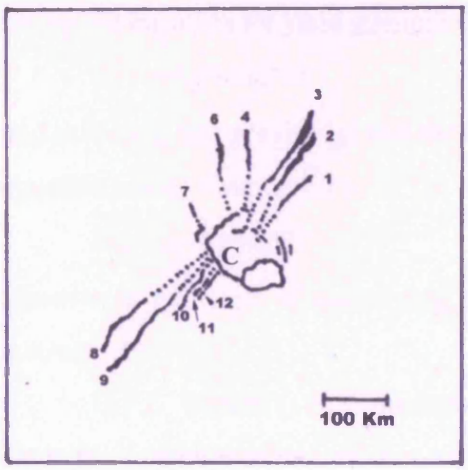

Figure 5.5: Map of all the Alba Patera lava flows studied in this thesis. This diagram has been modified from one given in Lopes and Kilburn 1990. Dotted lines denote the inferred length of the flow as traced back to the apparent source. **C** represents the main central caldera of Alba Patera.

5.22 Determination of type of flow

The appearances of the flows in the images were used in this study to infer whether the flow is likely to be a product of a single eruptive episode or not. However, the appearance could not be used to determine whether the flows were aa or pahoehoe. Two techniques were applied here to help to classify the flows in both volcanic areas into aa or pahoehoe flows. Those flows that were aa could then be studied using the flow growth model. The two methods used were downstream resistance and fractal analysis and both are outlined in the following sections.

5.22(a) Downstream resistance

The term 'yield strength' was discussed in Chapter 1. It is a measure of how much force needs to be exerted on the lava before it will move. The balance of the forces promoting and resisting movement of the lava determine whether it will move forward, and by how much, and depends on those forces making the lava spread laterally as well as making it flow down slope. Flows in this study have an 'apparent yield strength' (Sy_a), which can be thought of simply as a measure of the force preventing a flow from moving downhill. The main resisting forces are probably those imposed by a thickening crust as the flow cools, as well as frictional forces against the ground as the flow moves forward. Sy_a can therefore also be thought of as the 'downstream resistance of the flow' (r_d). By taking the equation for yield strength (Sy) that was given in Chapter 1:

$$Sy = \rho * g * \sin\alpha * H \quad (5.1)$$

and assuming that gravity (g) and the density (ρ) of the lava are constant, then the resulting equation can be used to represent the downstream resistance of the flow:

$$Sy_a = r_d = \sin\alpha * H \quad (5.2)$$

where α is the angle of underlying slope and H is the average thickness of the flow (in metres).

G.P.L Walker (1967) produced a plot showing the variation of thickness against slope for a number of lava flows on Mount Etna. This plot is reproduced in Figure 5.6 and

shows that the lavas were found to plot between two boundaries. The shape of the curve of the top boundary can be said to suggest that hsinα is a constant, and thus that the lavas have a maximum effective bulk lava yield strength (Chester et al., 1985). Since hsinα has been used as a measure of apparent yield strength for the Martian lavas in this study, it would be expected that the Martian lavas would show a similar pattern. Figures 5.7 and 5.8 show plots of flow thickness against the angle of slope, and the maximum hsinα values do appear to produce curves similar to that shown in Figure 5.6. This therefore provides evidence that the lavas appear to be behaving like those on Earth in terms of the way they have flowed, and that this method of using hsinα values to categorise the flows is valid.

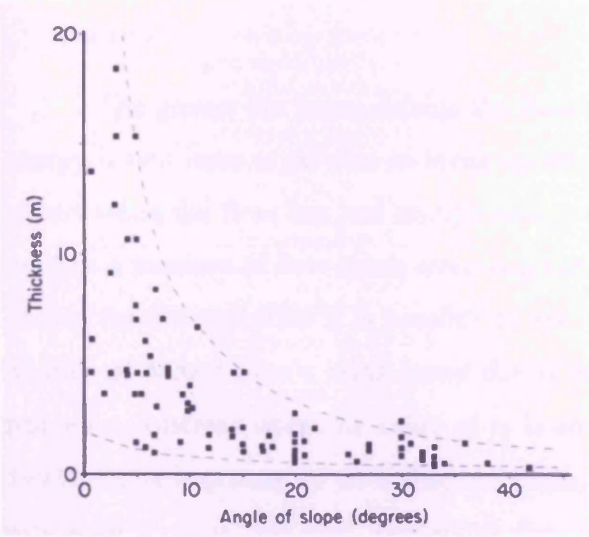

Figure 5.6: Plot taken from Chester et al., 1985, which was modified from one produced by G.P.L Walker (1967), showing thickness against slope for a variety of young lava flows on Mount Etna. The lower and upper boundaries (indicated by a dashed line) suggest minimum and maximum bulk lava yield strengths of 10^3 and 10^5 Pa respectively. However, the limits are due to conditions for breaking the surface crust and are therefore not reliable for determining yield strengths (Kilburn, 2004).

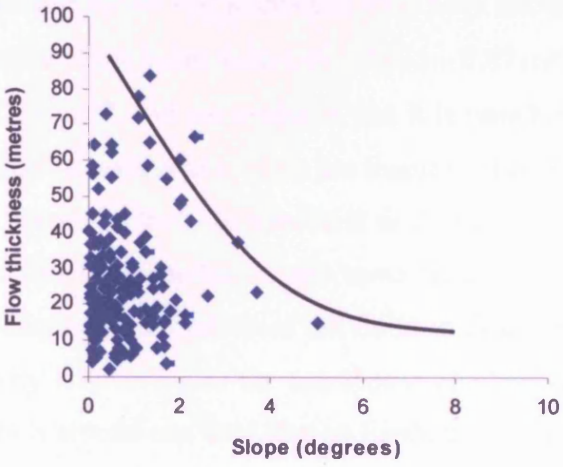

Figure 5.7: Plot of thickness against slope for all measured points along all of the Alba Patera lava flows. Note the curve formed along the upper boundary of the points on the plot. This is similar to that of the plot shown in Figure 5.6, indicating that these lavas have an apparent yield strength. This upper boundary represents the maximum limiting conditions for the Alba Patera aa flows (see text). The flow thicknesses are greater and the slopes shallower for the Martian lavas when compared to the terrestrial ones.

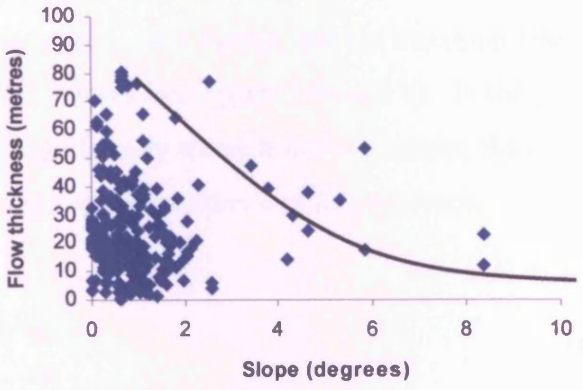

Figure 5.8: Plot of thickness against slope for all measured points along all of the Elysium Mons lava flows. A similar curve is observed for the upper boundary of the points in this plot as for those shown in Figures 5.6 and 5.7, also indicating that the Elysium lavas have an apparent yield strength. This upper boundary represents the maximum limiting conditions for the Elysium Mons aa flows (see text).

The greater the forces driving the flow forward, the faster it will flow and the more energy it will have to be able to break up the crust. The transition from pahoehoe to aa occurs when the flow has just enough energy to persistently break the crust. If r_d can be used as a measure of how much force is driving the flow forwards, then if a value of r_d is known for this transition it is possible to use it to categorise flows into aa and pahoehoe. Studies of Mount Etna's lavas found that if the r_d falls below 0.1 metre then the flow is pahoehoe, whereas when the value of r_d is above 0.1 metre then the flow is aa (Kilburn, 1993). It is important to note that, on Earth, flows with $h\sin\alpha < 0.1$ metres tend to be pahoehoe tongues and toes, not entire flow fields (especially for flow data plotted by Walker (1967) and shown in Figure 5.6). However, on Lanzarote for example, single pahoehoe sheets >10 kilometres long have thicknesses of 1-2 metres on slopes of ~2°, and therefore have $h\sin\alpha$ values of ~ 0.035 – 0.07 metres. These flows will be discussed further in Chapter 7, and are evidence that it is possible to categorise flows by their $h\sin\alpha$ value. Terrestrial values of r_d were not found to rise above 1 metre, and this therefore represents the maximum limit for terrestrial aa flows. If we assume that the way in which lava flows on Mars is controlled by the same factors as those on Earth, it is possible to use this technique to infer which of the flows in this study are aa, and which are pahoehoe. Since gravity is involved in the calculation of yield strength (see equation 5.1), and gravity on Mars is around one third that on Earth, the r_d for Martian lavas will be different. The slope and the thickness of the lava on Mars will have to have higher values in order to exceed the

yield strength of the lava and make it flow down hill. Therefore r_d will have to be three times larger on Mars than on Earth. In this study, the maximum r_d value for aa flows has been taken to be 3 metres, and the transition from aa to pahoehoe has been taken to occur at r_d=0.3 metres (see Figure 5.9a and b). In the two plots shown in Figure 5.9 only one point lies significantly above hsinα = 3 metres, thus showing that this is a realistic upper limit, so giving further confidence in this approach.

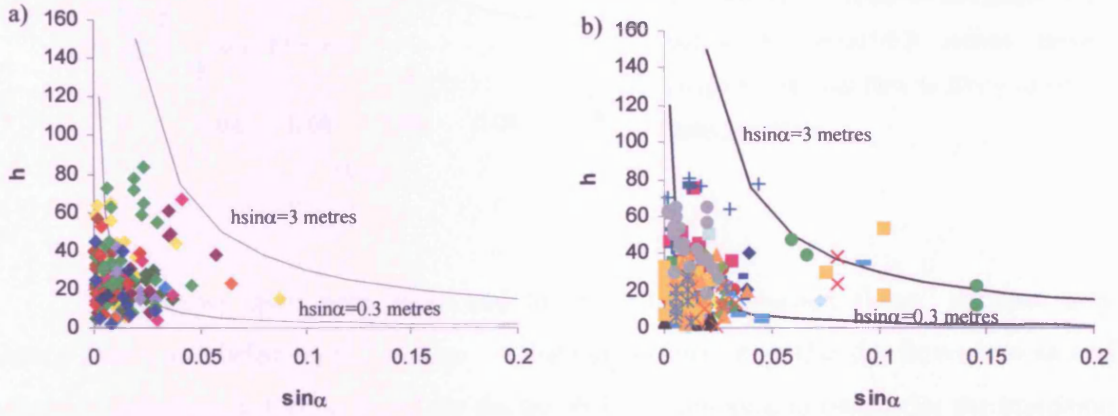

Figure 5.9: Plots showing h against sinα for **(a)** all the Alba Patera lava flows and **(b)** all the Elysium Mons lava flows studied. In each case the top curve represents hsinα=3 metres and the lower curve represents hsinα=0.3 metres. Different symbols represent points on different lava flows. It is possible to see that in almost all cases the points plot below the maximum of hsinα=3 metres, with only 1 major anomalous value found for the Elysium Mons lavas. The lower curve represents the transition between aa and pahoehoe lava flows. It is this line that was used to try to identify whether the flows were aa or pahoehoe. If all the points of an individual flow plot above hsina=0.3 metres, then the flow is likely to be aa, and below it the flow is likely to be pahoehoe. Flows that plotted in both areas of the graph were said to be 'transition' flows (see text).

For each flow, the thickness and sine of slope values for each point where a MOLA profile crossed the flow were plotted (see Figure 5.10). Also on the graph would be two lines, one representing r_d=3 metres, and one representing r_d=0.3 metres. If all the points fell under the r_d=0.3 metres line, then the flow was said to be pahoehoe. The flows for which points all plotted above r_d=0.3 metres were categorised as aa. For Elysium Mons, flows 50, 48, 45, 31, 23 and flow B, were found to have points that all fell under the r_d=0.3 metres line and so are inferred to be pahoehoe flows. Flows 35, 44, 43 and 24 were inferred to be

aa. At Alba Patera only flow 6 was inferred as aa, with flows 3, 10 and 12 inferred as pahoehoe.

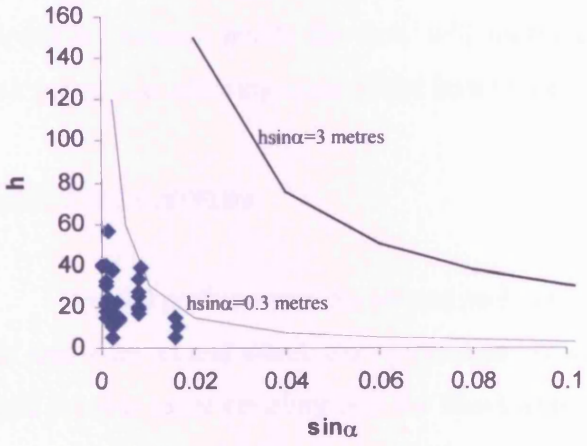

Figure 5.10: Plot of h (thickness) against sinα (sine of the angle of slope) for all thickness measurements made along flow 3 on Alba Patera. The upper and lower curves in this graph represent different values of hsinα in metres. The fact that all the points on this graph plot below the hsinα=0.3 metres curve suggests that this flow is likely to be a pahoehoe flow.

Many flows from both areas had to be termed "transition flows" because they plotted above and below r_d=0.3 metres. A further way to categorise the flows into aa and pahoehoe therefore had to be found, so fractal analysis was used to categorise the transition flows into aa or pahoehoe. The fact that so many flows were transition flows highlights the point that was made in section 5.1, that it is possible for a pahoehoe flow to transform into an aa flow further downstream. It is also possible to find patches in a flow where it is briefly transformed into another type of flow. For example, the transformation from pahoehoe to aa can be explained by the fact that as the flow progresses the crust will be thickening, and it may reach the stage where, in order for the flow to progress down hill, the surface must be persistently broken. It will thus continue to flow as an aa flow.

Since highly fragmented lava surfaces cannot recombine to form a continuous surface once more, aa flows can never transform into pahoehoe ones. When it may appear as though this has happened (apparent transitions), it is generally due to two processes. The slower moving lava that is erupted towards the end of an eruption (as the eruption slows) may form pahoehoe flows where the previously erupted faster lava was aa. Also, breaching or overtopping of aa channel levées may lead to the formation of a slow moving, thin layer of lava that may form a pahoehoe flow. These transitions may be accompanied by a change in slope because, if the angle of slope alters, the amount of energy available to drive the

flow forward is altered and the rate of movement of the flow forward will change. For example, if the slope decreases, the flow will slow down or even briefly come to a halt until the flow thickens enough to start moving forward again. During the time it is stationary the hydrostatic pressure inside the flow will increase and may cause the crust to break at a weak point, thus allowing some of the lava to escape and possibly flow as a pahoehoe flow.

5.22(b) Fractal analysis

Fractal analysis was the second technique used to determine which of the flows in each area were aa and which were pahoehoe. A second technique was necessary because it would provide more certainty that the flows used in the modelling were aa since this is an important assumption of the model used.

As explained in section 5.1, aa and pahoehoe flows advance differently, thus it happens that their flow margins will have a different plan-view (see Figure 5.11). Pahoehoe flows, advancing as a series of tongues and lobes, produce flow margins that are 'self-similar'. This means that the shapes of embayments and protrusions at the edge of the flow would appear similar if they were observed at the metre-scale on the ground and then observed again at a scale of tens or even hundreds of metres (in an aerial photograph for example). This is called scale-independent or 'fractal' behaviour. Fractals are objects, either real or mathematical, that look the same at all scales (Mandelbrot, 1967). The fact that pahoehoe flows show this behaviour is probably due to the fact that the mode of flow advance is by budding, where lava punctures the crust to form a new flow lobe. This is highly dependent on crustal restraint, and is thus controlled by forces that are of the same type at all scales.

Figure 5.11: This diagram compares the typical boundaries of an aa flow and a pahoehoe flow. The aa flow does not have so many embayments and branches as the pahoehoe flow, and thus can be said to be more similar to a straight line than the boundary of the pahoehoe flow. Thus the aa flow boundary will have a lower 'D' value (see text).

The driving forces behind aa flows are usually far greater than the crustal resistance. The shape of the margins of these flows is therefore more dependent on the rheological resistance of the internal lava. Thus, although from the ground the margins of an aa flow would be irregular due to crustal debris, at the hundreds of metres scale the flow would only show small variations in the shape of the margins. This means that the shape of the margins becomes less irregular as a larger area of the flow is viewed, due to the fact that the major control on the shape of the margins changes from being the irregular crustal debris, to the rheology of the flow. In theory then, aa flow margins will show less fractal behaviour than those of pahoehoe flows.

The fact that lava flow margins are fractal was recognised by Bruno et al. (1992,1994), who developed a technique to determine the fractal dimension (D) of lava flows, which is a measure of how far the flow margin deviates from being a straight line. They used the 'structured walk' method to determine D, which involves measuring a lava flow boundary using a progressively smaller measuring tool, then plotting the resulting estimate of boundary length against the size of the measuring tool (rod length). When plotted on a log-log scale this produces a straight line, the gradient of which can be used to derive D as shown in equation 5.3:

$$D = 1 - m \qquad (5.3)$$

where m is the gradient of the line on the graph. The straighter the line then the smaller the D value, thus showing how much fractal behaviour is being exhibited by the flow. A lava flow that shows highly fractal behaviour will have a higher D value. A more in depth discussion of this method can be found in the work by Bruno et al. (1992, 1994). Their work showed that aa and pahoehoe flows do indeed show differences in their values of D, with pahoehoe flows having higher values of D than aa ones. According to Bruno et al., D for aa flows ranges between 1.05 and 1.09, whereas pahoehoe flows showed a range for D of between 1.14 and 1.23).

Since some of the fractal analyses carried out by Bruno et al. (1992, 1994) had involved obtaining D from aerial photographs of the Earth, as well as orbital images of Venus, the Moon and Mars, it seemed a good method to choose for the present study in order to further determine the types of flows present in the study areas. The downstream resistance analysis carried out in this study had already shown which flows were more likely to be aa, and which were more likely to be pahoehoe. It was therefore decided that if the values of D could be worked out for these two groups of flows, then a range of values could be obtained for each. These could then be used to determine whether a flow that was 'intermediate' in the downstream resistance analysis had a value of D that corresponded to being aa or pahoehoe. Using rod lengths of 1, 2, 4, 8 and 16 millimetres (corresponding to actual lengths of 0.490, 0.981, 1.963, 3.927 and 7.855 kilometres on the ground), estimates of part of each of the boundaries of all the lava flows in this study were obtained. Every time, the left-hand side of the flow was used for consistency, and the length of the boundary measured was determined by the length covered by three of the 16 millimetre rod lengths. Where the flow was too short to fit in three of the 16 millimetre rods, only two of them were used. Instead of using real 'rods' as would be done in the field, the lengths were measured with a ruler on tracings from the Viking photomosaics. See Table 5.1 for the results of the fractal analysis for the Elysium and Alba lava flows that had already been categorised into aa or pahoehoe using the downstream resistance graphs.

Volcano	Aa		Pahoehoe	
Elysium Mons	*Flow number*	*D*	*Flow number*	*D*
	35	1.3031	31	1.4052
	44	1.3260	23	1.3575
	43	1.1774	B	1.2957
	24	1.2386	45	1.3723
			48	1.3105
			50	1.4079
Alba Patera	*Flow number*	*D*	*Flow number*	*D*
	6	1.2487	3	1.3595
			10	1.3649
			12	1.1015

Table 5.1 showing the results of fractal analysis carried out on flows from both the Elysium and Alba regions. All these flows showed downstream resistance plots that were indicative of either aa or pahoehoe flows. The anomalous value for flow 12 is discussed in the text.

The range of D for aa flows was found to be 1.1774 to 1.326, and that for pahoehoe flows between 1.2957 and 1.4079. Clearly this leaves an intermediate range of 1.2957 to 1.326. This means that, if any of the intermediate flows from the downstream resistance analysis fall into this range, all the evidence (downstream resistance graphs, images and flow profiles) have to be studied to decide what sort of flow they are most likely to be. The values of D obtained in this study are higher than those obtained by Bruno et al. (1992, 1994), but this could be because slightly different methods of measuring the distances on the flow boundaries were used in the two studies. Bruno et al. (1992, 1994) digitised their flow boundaries and then used a computer algorithm to determine length estimates using different 'rod' lengths. Since that computer algorithm was not available for the present study, a manual method of measuring rod lengths was used, thus opening the door to human error. However, measurements made with the ruler were accurate to 0.5 of a millimetre, and the same error applies throughout the analysis, so that the values obtained can still be used to categorise the flows relative to each other.

Flow number 12 was the only anomalous value found. The downstream resistance graph for flow 12, as well as the shape of the longitudinal profile, both indicate that it is a pahoehoe flow. However, it has a value of D = 1.1015 which is indicative of an aa flow (according to the work of Bruno et al. (1992, 1994), and all other values obtained in the present study). Observations of the image of this flow show it to be relatively straight and to have smooth margins. It is possible that some of the small variations that were present in

the margins were missed when the flow was traced, or that this particular flow was not as clear as some of the others in the images. However, in this study, the value of D obtained for flow 12 was just treated as an anomaly, since the rest of the flows had D values that fitted the theory well.

Volcano	Flow number	D	Type of flow
Elysium Mons	17	1.2876	Aa
	19	1.2319	Aa
	21	1.1015	Aa
	22	1.5296	Pahoehoe
	26	1.5255	Pahohoe
	28	1.0853	Aa
	30	1.3831	Pahoehoe
	32	1.4153	Pahoehoe
	36	1.1344	Aa
	39	1.1371	Aa
	40	1.0316	Aa
	41	1.3071	Aa
	46	1.1895	Aa
	47	1.3259	Pahoehoe
Alba Patera	1	1.2796	Aa
	2	1.358	Pahoehoe
	4	1.1707	Aa
	7	1.0363	Aa
	8	1.1505	Aa
	9	1.588	Pahoehoe
	11	1.0887	Aa

Table 5.2 Results of fractal analysis on all flows that were judged to be 'intermediate' by downstream resistance analysis alone. Those flows that had a value of D of less than 1.2957 were judged to be aa flows, and those with D > 1.326 were pahoehoe flows. Only flow 41 was found to lie in the intermediate range, but was judged to be aa because more of the points on the downstream resistance plot were above $h\sin\alpha=0.1$, and also because of its appearance and the fact that the flow thickens towards the end, as is typical of aa flows.

The values of D and the type of flow determined for each 'intermediate' lava flow are shown in Table 5.2. It was found that, of all the flows being studied in Elysium, 13 were inferred to be of the aa type and 11 were inferred pahoehoe. On Alba Patera, 6 of the flows were inferred aa, and 5 were inferred pahoehoe. Once it was clear which of the flows in each area were aa, it was possible to proceed with the modelling.

5.3 Modelling

This section will summarise the work of Kilburn and Lopes (1988, 1991) in developing the Flow Growth Model that is applied to aa flows from Elysium Mons and Alba Patera in this thesis. The model was chosen because it is particularly suited to the study of extra-terrestrial lava flows in a number of ways. Firstly, since the model relates flow field dimensions and underlying slope to eruption duration, no explicit knowledge of lava rheology or gravitational acceleration is needed because the effects of both of these occur indirectly through their influence on flow field thickness. Values of flow thicknesses and underlying slopes can be obtained for Martian lava flows using MOLA data, so this model can be applied. Kilburn and Lopes (1988) studied the growth of terrestrial lava flow fields and developed their model to be specific to the cooling and flow regimes they observed, assuming that control on flow-field growth was scale-independent. Therefore, as long as the Martian lavas were emplaced in similar cooling and flow regimes as the terrestrial ones used for the construction of the model, the difference in gravity between Earth and Mars should not affect the way in which the model is applied to the Martian flows. The planimetric similarity of lavas on Alba Patera, Elysium Mons and the Earth (despite contrasting environments and differences in volume by two to three orders of magnitude) is consistent with a scale-independent control on flow field growth so the model is an appropriate one. Lastly, Kilburn and Lopes (1988) argue that the results of their model can be further improved by the reduction of measurement uncertainties, most importantly topography, to obtain better values of ground slope and flow thickness. The data from MOLA is precise to 37.5 cm on the types of slopes found in the two volcanic areas chosen, so the measurements of slope and thickness used in the present study should produce improved results with this model.

5.31 The flow growth model

From their field observations of aa lava flows on Mount Etna, Sicily, Kilburn and Lopes (1988) determined a way to categorise flows based on their width/length ratios and the location of their maximum width. Their observations into the factors affecting flow

field growth led to a method for categorising flows based on whether they thickened, widened or lengthened after the emplacement of an initial flow and were used to form a model that described the growth of flows on Mount Etna. Later this model was refined, and data from Mount Etna were combined with those from other terrestrial volcanoes to produce a quantitative model that related final flow field dimensions, underlying slope, and eruption duration to each other (Kilburn and Lopes, 1991). It is this model that will be used to find the eruption durations for flows on Alba Patera and Elysium Mons. The following is a summary of the work of Kilburn and Lopes (1988,1991) and Lopes and Kilburn (1990) and is intended to aid understanding of how the eruption durations of the Martian lavas in this study were calculated.

As discussed in Chapter 1, several pairs of characteristics of lava flows can be related to one another, such as the positive relationship that was found between flow field length and effusion rate by Walker (1973). The fact that these relationships exist means that there is an element of systematic behaviour in the emplacement of flow fields. Flow fields grow by the repeated formation of new flows from existing ones; either a flow splits into branches (bifurcates) upon reaching a topographic obstacle, or it breaches or overflows its cooled margins. Since breaching and overflow require the formation of a cooled crust in order to occur, they must be cooling-dependent processes and therefore will show systematic behaviour over time. Bifurcation around topographic obstacles is more of a random process and therefore will not show systematic behaviour. Cooling is therefore an important part of the flow growth model. In order to see how cooling affects the growth of lava flows it is necessary to look at the different types of flow field growth. To do this, it is necessary to first consider the smallest unit of a flow field: the single flow unit.

A single flow is a body of lava that maintains fluid continuity along its whole length during emplacement and is fed by a single eruption. If no further effusion occurs from the source of the flow once the flow has come to rest, then this will be classed as a single or 'S-type' flow. From their observations on Mount Etna, Kilburn and Lopes (1988) found that 'S-type' flows have a low (~0.7) maximum width to maximum length (Wm/Lm) ratio and that the location of the maximum width is usually within the last 50% of their lengths (see Figure 5.12). If however, effusion continues after the first flow has been emplaced, the lava will continue to be erupted as a new flow by thickening, widening or lengthening of

this initial flow. The successive emplacement of flows in this way forms a flow field, the end product of which is a multiple flow field ('M-type' flow). M-type flows have larger values (~2.5) of Wm/Lm and usually reach their maximum thickness within the first 50% of the total flow length (see Figure 5.12). If the initial flow is emplaced in a time t_i (which represents all the time that lava was being supplied to the initial flow, even during simple thickening by inflation), then a maturity index T* can be derived in order to tell whether the flow is of S-type or M-type. The maturity index can be defined as $T^*=T/t_i$ where T is total eruption duration for the entire flow field and is measured in days. S-type flows will have a maturity index of $T^*=1$, and M-type flows will have $T^*>1$.

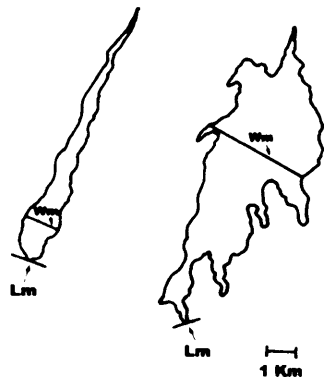

Figure 5.12: This diagram shows two plan views of lava flows; the one on the left is an example of an s-type flow, the one on the right an example of an m-type flow. Lm is the point to which the maximum length is measured. Wm denotes the point along the flow where maximum width is measured. Note that Wm occurs in the distal 50% of the S-type flow, but the proximal 50% for the m-type flow. (Diagram modified from that given in Lopes and Kilburn, 1990).

M-type flows can be further categorised by the way in which they form. Those flows that grow by thickening owing to the superposition of flows on top of the initial flow can be termed MT flows. Flows that grow by the breaching of the upstream part of the initial flow and then lava flowing laterally from the initial flow can be termed MW flows, since they widen the flow field. Finally, those flow fields that grow by the breaching and formation of flows from the distal part of the initial flow, and therefore lengthen it, can be classified as ML flows. It is possible to normalise the Wm/Lm ratio by dividing by the width/length ratio of the initial flow. The normalised width of a flow field can be defined as W*/L*:

$$W^*/L^* = (Wm/Lm)/(w_i/l_i) = (Wm/w_i)/(Lm/l_i) \quad (5.4)$$

where w_i and l_i refer to the equilibrium width and the final length of the initial flow. It is then possible to work out which M-type flow is being observed simply by calculating the normalised relative width. MW flows will have a $W^*/L^* > 1$, MT flows will show a ratio that is equal to 1, and ML flows will have $W^*/L^* < 1$. Field data and observations of eruptions from several different volcanoes (Etna, Vesuvius, Hekla, Arenal, Mauna Loa and Kilauea; the original references for these are quoted in Kilburn and Lopes (1991)) showed that aa flows tended to be of either the S or MW type. Kilburn and Lopes (1991) therefore developed the flow growth model for these flow types.

Assuming that the dimensions of the flow field correspond to the state of the flow at time T, the following general expression relates final flow field dimensions to eruption conditions:

$$W^*/L^* = f(T^*) \quad (5.5)$$

or $$(Wm/Lm) = (w_i/l_i)f(T/t_i) \quad (5.6)$$

where f(variable) denotes "a function of" the variable in brackets, and varies according to which type of flow field is being modelled. For example, S type flows have $(W/L)^* = T^* = 1$. It is normally only possible to obtain measurements of Wm, Lm and T for flow fields, so that in order to model flow field growth, expressions must be found for the initial flow characteristics in equation 5.6 (w_i, l_i and t_i), and the way in which the flow field of interest has been emplaced must be determined so that $f(T/t_i)$ can be derived.

Since flow growth depends strongly on conditions at the flow front, Kilburn and Lopes concentrated on this area to study the ways in which the length and width of the initial flow are controlled. They made an assumption that flow advance is controlled by conditions in the Rear Frontal Zone (RFZ) of the flow (see Figure 5.13) which is thought to have uniform laminar flow in a one-dimensional wide sheet and flows as an approximately Newtonian fluid. With these assumptions, the velocity of the flow can be determined using the Jeffreys equation (Jeffreys, 1925):

$$U = (\rho g h^2 \sin\alpha)/(b\mu_a) \quad (5.7)$$

where ρ and μ are bulk density and apparent viscosity of the RFZ, which has mean depth h, α is the slope angle of the underlying surface, g is gravitational acceleration, and b is a constant that has a value of 3 for flows that are much wider than they are deep. Knowing the velocity of the flow enables the distance (l_i) travelled by the flow in time t_i to be calculated. An additional correction factor has to be added into the equation because there will be some unsteady flow advance expected at the very beginning of the eruption and towards the end.

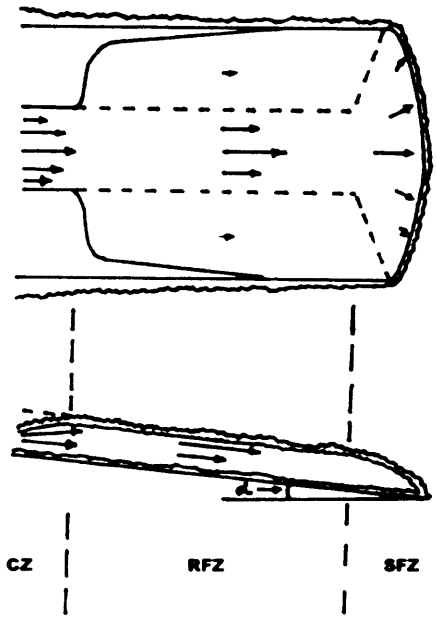

Figure 5.13: Simplified diagram of a typical aa lava flow front, modified from a diagram given in Kilburn and Lopes, 1991. The labels along the bottom of the diagram refer to the different parts of the flow front, CZ representing the Channel Zone, RFZ representing the Rear Frontal Zone, and SFZ representing the Snout Frontal Zone. The vertical dashed lines represent the transitions between the different zones. The arrows on both the plan-view and the cross-section represent the relative velocities of the lava within the flow.

In order to calculate the width of the initial flow Kilburn and Lopes (1991) assumed that most of the spreading of the flow occurs in the Snout Frontal Zone (SFZ), and that widening stops in the transition between the SFZ and the RFZ (see Figure 5.13). Since Kilburn and Lopes considered the flow front to be moving as an approximately Newtonian fluid, it was thought that spreading would be halted by the crust. Therefore steady-state widening can occur when the rate at which the flow spreads is around the same rate as both crustal deformation and the healing of cracks in the crust by chilling. Once the rates are no

longer equal, widening begins to slow as lateral flow is resisted by a thickening crust. Field observations of crustal deformation as well as rates of advance for the SFZ (where most spreading is assumed to occur) were used to obtain values for these factors (see Kilburn and Lopes, 1991) and were included as a correction factor for chilling of the crust in the calculation. The way the flow spreads laterally was accounted for using an equation that describes the relationship between the outward driving hydrostatic force of the lava and the resisting shear force across the ground as it flows. A second correction factor was included for the small amount of spreading that occurs in parts of the flow front other than the SFZ. All of these were combined in order to allow the calculation of w_i.

In this model, the initial flow is assumed to come to rest when the flow front has cooled and solidified so much that further movement cannot occur. The flow emplacement time, t_i, is similar to the timescale of heat loss from the flow through incandescent surfaces, t_R, such as cracks or lava overflows (Crisp and Baloga, 1991), and so t_i is best modelled as being limited by radiative cooling. However, Crisp and Baloga (1990b) and Kilburn and Lopes (1991) recognised that this radiative cooling model only approximately matches cooling time scales in the field. The differences between values of modelled time scales and those time scales observed for active flows in the field were then used as a correction factor in the calculation of t_i.

Now that l_i, w_i and t_i can be calculated, the last part of the equation that needed to be defined was the part concerning the emplacement regime of the flow field. Kilburn and Lopes (1990) observed many aa and blocky lava flow fields and determined that most were of the S or MW type. Therefore, in formulating the flow growth model, they assumed that the flow fields in question were of these two types. They also assumed that: the individual flows making up the flow field had similar dimensions and emplacement times; that the flows were active one at a time, and that they propagated from the proximal part of the flow near the vent area; and also that the flow field dimensions were not determined by the size and shape of the vent. L_m could therefore be approximated to l_i, since the flows all started near the vent. The number of flows in a flow field could be ascertained by calculating Wm/w_i or by dividing the time taken to emplace the total planimetric area of the flow field (t_p) by t_i. However, the value of t_p/T may not always equal one, as the planimetric area of the flow field may be fixed yet flows may still be being emplaced on top of older flows

(even in an MW-type environment). This was solved with a final correction factor that could be ignored for S type flows.

Kilburn and Lopes (1991) found that, when values were given for all the correction factors, they tended to counterbalance each other. When equation 5.5 was rearranged in dimensional form using the expressions determined for w_i, l_i and t_i, the final equation obtained was:

$$(Wm/Lm)*H^2*\sin\alpha = (b/m)\ k\ T \qquad (5.8)$$

where b the frictional constant that was given in equation 5.7 and has a value of 3 for flows that are much wider than they are deep; m is a correction factor for unsteady advance (with a nominal value of 1.2); and k is the lava thermal diffusivity, which was taken to have a value of 4.2×10^{-7} $m^2.s^{-1}$ and is typical of basaltic and andesitic lavas. In this case, since T is measured in days, then the value of k used in equation 5.8 must also be measured in days and thus has a value of 0.036288 $m^2.d^{-1}$. If values for b, m and k are inserted, the equation can be rearranged to find T:

$$\frac{(Wm/Lm)*H^2*\sin\alpha}{0.0922} = \frac{(Wm/Lm)*H^2*\sin\alpha}{\sim 0.1} = T \qquad (5.9)$$

The denominator in equation 5.9 can be rounded up to 0.1 for ease of use since the estimates of some of the terms used in the model (particularly the constants that usually counter-balance each other) are subject to some uncertainty. Thus, to estimate the emplacement time for S-type or MW-type aa flow fields, it is only necessary to know the final flow dimensions of width, length and thickness, and to have a value for the slope of the ground underlying the flow. Physical characteristics of the lava, such as viscosity and density as well as a value for gravity do not appear as they are incorporated indirectly through their control on the length, width and thickness of the flow.

As with all studies of this kind there are some limitations to consider when applying the model. Some of the limitations of this model concern the accuracy of measurements and input factors. For example, there are limitations to measurements of distance that are

made from the images of the lava flows. This is because camera artifacts tend to broaden features at the limiting resolution of the camera (Carr et al., 1977) and image enhancement tends to accentuate contrasts and thus any measurements made are subject to errors. Since the Martian lavas are ancient they can be eroded or buried significantly in places, which can make it difficult to measure the dimensions of the flows accurately. The same is true for the determination of vent position, which means that effusion rates may be under or over-estimated depending upon the measurements made by the author. Other input factors that present limitations to the model are the fact that methods of determining those flows that are simple and those that are complex will differ between studies and therefore interpretations will differ amongst authors. When considering Martian lava flows it is also prudent to mention that effusion rates on Mars may be influenced by larger fissure sizes than those found on Earth, thus they cannot be used to directly infer lava composition by comparison with terrestrial conditions.

Limitations that are inherent in the model concern the fact that the assumption is made that flow of the lava was steady, uniform and laminar as the flow was emplaced. Therefore the model does not address potential modifying factors. These include: changes in lava properties with time; conditions where flows are narrow with respect to their depth; the modification of channel margins by local overflow and accretion of crustal debris; and the development of tubes and variations in the shape and position of the feeding vent. However, Kilburn and Lopes (1991) consider that these modifying processes are unlikely to alter the basic mechanisms by which a flow field can evolve, and that the general pattern expected among the lavas they studied will remain unchanged and thus representative of a systematic mode of growth. Further development and improvements of the model could be achieved by: conducting detailed observations of flow front motion and crustal behaviour; studying the temporal variations in discharge rate and the effect of local variations in ground slope and topography; considering the application of non-Newtonian rheological models to the frontal zone; and also by carrying out further analysis of lava cooling and associated rheological changes of the lava.

It is important to mention the amount of error inherent in the flow growth model and the reasons for it. When the relation between final flow field dimensions, underlying slope and eruption duration were plotted for the terrestrial flows used by Kilburn and Lopes

(1991), there was scatter of +/- 82% about the main trend. This blurring of the trend was mainly caused by measurement errors inherent in the lava flow data, particularly for values of thickness and emplacement time. A smaller percentage of the error was caused by the uncertainty of values for the correction factors used and also by the constants in equation 5.9, for which no direct measurements could be made.

5.32 Flow measurements

Measurements of the size and shape of the lava flows were necessary in order to use the flow growth model to calculate the duration of the eruptions. However, other measurements were also necessary in order to produce longitudinal flow profiles and underlying slope profiles, which gave more clues to the style of emplacement for both aa and pahoehoe flows. Therefore, the same measurements were made on all flows, regardless of whether they were aa or pahoehoe. The values of all measurements taken for all flows are given in the Appendix at the back of this thesis. The way these measurements were taken is outlined below.

5.32(a) Flow dimensions

The following measurements were taken so that the values could be inserted into the flow growth model (equation 5.9). For details of how measurements of the flows were made for the Elysium flows and the Alba flows in the previous two studies mentioned see Mouginis-Mark and Yoshioka (1991) and Kilburn and Lopes (1990), respectively. The values given for the maximum length, maximum width, and area for flows on Alba Patera have been taken from the study by Kilburn and Lopes.

Maximum Length

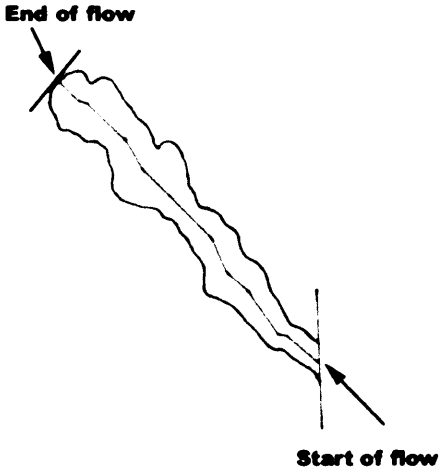

Figure 5.14: This image shows an outline of flow 39, and highlights where the flow was thought to start and finish, thus indicating direction of flow. The line drawn centrally down the flow, always following the direction of flow, was used to measure the length of the flow. By measuring along the line from the beginning to the end of the flow, the total flow length could be calculated. For every flow in this study, 1mm was equal to 490.975metres. The total length for flow 39 was calculated to be just over 25 kilometres.

For the Elysium flows, the flow was traced as far as it was visible on the high-resolution photomosaics. The end nearest the vent (the proximal end) was then treated as the start of the flow and the length of the flow was measured from this point. A line was drawn longitudinally through the centre of the flow, always following the direction of flow (see Figure 5.14). The scale of the image was calculated, the central line could be measured in millimetres and the value converted to kilometres accordingly to give a maximum length value. Obviously this value will be an underestimate because the vents were not visible for most of the Elysium flows.

For the Alba Patera flows, the measurement of length was made in a similar manner, but two length measurements were made. The length of the flow for as far as it could be observed in the image was called the 'maximum traced length'. Kilburn and Lopes (1990) also inferred vent positions for all the Alba Patera flows, and the total distance from the inferred vent to the end of the traced flow is given as the 'inferred maximum length'. For flows 1 – 12 the vents were taken as fissures in or around the largest of the two summit calderas, as shown in Figure 5.5. It is due to this that there will be two values for the duration of each Alba Patera flow. The maximum traced length is likely to be an underestimate. However, the inferred maximum length may be an overestimate, as it is not

100% certain that the flow was erupted from the inferred area and may have had a source closer to the start of the traced flow (see Kilburn and Lopes, 1990).

Maximum Width

The maximum width was found by observation of the images and measured perpendicular to the length line (Figure 5.14), so that it was at right angles to the direction of flow. The location of the maximum width was measured by finding the distance from the proximal end of the flow to the position of the maximum width. Once the maximum width and the maximum length were found, Wm/Lm could be calculated. As mentioned previously, if this ratio is low and Wm is located in the distal 50% of the flow then there is a greater likelihood that the flow is similar to terrestrial S-type flows, and is thus composed of a single flow unit. This is true for the Alba Patera flows where Wm/Lm was found to have a value of between 0.056 and 0.112, and where for most flows Wm was in the distal 50% of the flow (see Table 6.5 in Chapter 6). For the Elysium flows the range for Wm/Lm was higher (mostly between 0.120 and 0.268, with one flow having a Wm/Lm of 0.370). However, with the exception of this one flow, the values were not as high as those given for the M-type flow field in the study by Lopes and Kilburn (1990), which had values of between 0.275 and 0.302, so they are all likely to be S-type flows. Also, the location of maximum width for most of the flows is very close to or within the distal 50% of the flow (see Table 6.3 in Chapter 6).

Thickness

The locations of MOLA ground tracks across each lava flow are traced onto an overlay that can be used in conjunction with the tracing of the lava flow (see Figure 5.15). Since the ground tracks in this study are always oblique to the direction of flow, one side of the flow in the MOLA profile will be further downhill than the other (see Figure 5.16). The thickness at each point along the flow is worked out by taking the elevation of a laser spot in the centre of the flow profile (C in Figure 5.16) and subtracting a value for the underlying surface at this point. The underlying surface is calculated by finding the

average elevation between points just next to the lava flow profile on either side (left-hand side and right-hand side values in Figure 5.16). For the flow growth model, the thickness of the centre of each MOLA profile that crosses the flow is calculated, and then an average of all the thickness values for that flow is obtained and inserted into equation 5.9.

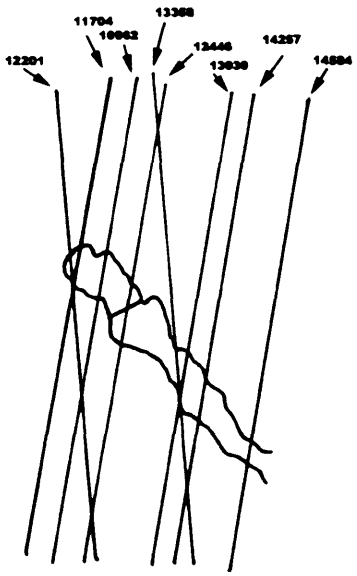

Figure 5.15: The positions of the MOLA ground tracks that were found to cross flow 39 have been superimposed on the outline of the flow in this image. Ground tracks from individual MOLA orbits have been labelled according to orbit number. The line drawn across the lava flow that crosses orbit number 12446 has been drawn perpendicular to the length line shown in Figure 5.14. Since the thickness measurements used in this study were taken at the centre of the flow, the line in this image has been drawn to cross the MOLA ground track at the point where this central thickness value was measured.

Since the centre of the section across the lava flow in the MOLA profile (Figure 5.16) will actually be between points A and B, the actual position of the thickness value is located halfway along the MOLA ground track between points A and B. Therefore, although it would be ideal to have all thickness values for central points along the flow, it is important to note that sometimes the thickness measurement point does not lie in the middle of the flow. This means that if the flow is not flat-topped like the one in Figure 5.16 it can provide a misleading value. It is always difficult trying to measure the cross-flow profiles of lavas, as was highlighted by the work of Fink and Zimbelman (1985). They showed that it was possible to make incorrect assumptions about pre-flow topography when sections through the flow were not available.

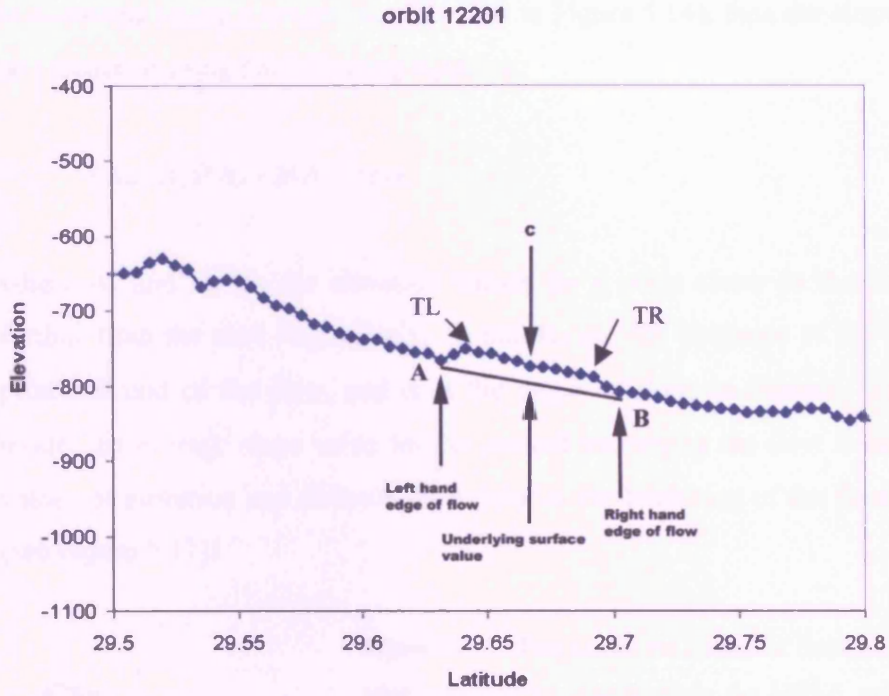

Figure 5.16: This figure shows part of orbit 12201 (the position of which is shown in the previous figure). Each point on the graph represents the elevation of a single MOLA laser 'footprint'. In the centre of the graph it is possible to see a section through lava flow 39, the left-hand (A) and right-hand (B) edges of which are highlighted on the graph. The elevation value of the ground underlying the centre of this section through the flow was calculated by subtracting the value of the elevation at the right-hand side of the flow (B) from the elevation of the left-hand side (A). A line has been drawn between these points to represent the inferred underlying surface. Since the direction of flow is pointing into the page and the orbit ground-track is oblique over the flow (see Figure 5.15), one side of the lava flow will be at a higher elevation than the other side, thus making the flow appear to slope from left to right in the graph. The central point of the flow (C), from which flow thickness was calculated, was worked out as the point equidistant from the top left (TL) and top right (TR) MOLA points on the profile.

Slope

As Figure 5.17 shows, when several MOLA ground tracks cross a lava flow, there are several points along the flow where a value of the elevation of the ground next to the flow can be obtained (like points A and B in Figure 5.17). This means that if the distance along the flow of these two points, A and B for example, from the proximal end of the flow

is measured (using a length line like that in Figure 5.14), then the slope between them can be calculated using the following equation:

$$(A_e - B_e)/(A_d - B_d) = \tan\alpha \qquad (5.10)$$

where A_e and B_e are the elevation values for a point closer to the start of the flow and further from the start respectively, A_d and B_d are the distances of the two points from the proximal end of the flow, and α is the angle of slope in degrees. For the flow growth model, an average slope value for the ground underlying the flow is obtained by using the values of elevation and distance for a point at the beginning of the flow, and one at the end (see Figure 5.17).

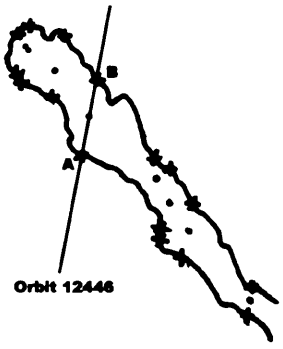

Figure 5.17: This shows the outline of flow 39. The crosses along the edge represent the places where the MOLA ground-tracks crossed the edges of the flow. Points A and B are where the ground-track from orbit 12446 crosses the edges of flow 39. Since these two points occur at different distances from the proximal end of the flow, it is possible to use them to determine the slope of the underlying ground surface between these two points. The black dots positioned down the centre of the flow represent the positions where the flow thickness measurements were made. Since the elevations and distances of the points marked by the crosses along the side of the flow are known, it is possible to determine the slope of the ground where each flow thickness measurement was made.

Area and Volume

Once flow duration was calculated, the volume of the flow was needed so that effusion rate could be calculated. Volume was calculated by multiplying the area of the flow by the average thickness of the flow. For Elysium, the area was found by overlaying a sheet of transparent graph paper over the tracing of the lava flow and counting the number of squares and parts of squares that covered the flow. Since the scale for the tracing of the flow could be obtained from the image, it was possible to work out the area covered by one

square and then multiply this value by the number of squares that fell within the outline of the lava flow.

5.32(b) Other measurements

Since morphological parameters have been used in the flow growth model to infer the mode of flow emplacement, and these values can be said to show some degree of control by cooling, it seems likely that other morphological parameters of a flow may be related to one another. Therefore, further measurements were made in order to find out if there were any links between various characteristics of each flow. At each thickness measurement point (the middle of each MOLA profile across the flow) the distance along the flow using the length line, and the width perpendicular to the length line were determined. Also, the thickness of the left and right edges of the flow was calculated, and the elevations of the ground immediately either side of the flow (see Figure 5.18) and the distances to these points from the proximal end of the flow were noted. The slope and elevation values of the surface underlying the central elevation point were also recorded. Many of these values were plotted against one another in Microsoft Excel to see if a pattern emerged (see Chapter 6), and some were used to determine the mode of emplacement of the flow (as discussed in section 5.22). The relative velocities of the flows as compared to one another were also determined. The effusion rate was assumed to be constant and therefore set to a value of 1. It was then divided by the cross-sectional area of each section of the flow that was traversed by a MOLA profile to give a relative velocity value for that point. The way the cross-sectional area was calculated is shown in Figure 5.18. This would show how the velocity changed over distance along the flow and enabled comparisons to be made between flows.

Two important graphs that were produced were the flow surface profiles and the underlying surface profiles, as these could give a good insight into how the flow was emplaced, even for pahoehoe flows that could not be modelled. The underlying surface graph is a plot of the inferred elevation of the ground underneath the central point on the MOLA profile of the lava flow, against the distance of this point from the start of the flow. When this plot is combined with the flow surface profile (a plot of the surface elevation

values of the lava flow at the same central points along the flow) the resulting graph provides information on the emplacement of the flow. For example, it was possible to see where the flow had been ponded in a depression or changed in thickness in response to a change in the slope of the underlying surface. A discussion of these graphs and all other plots of morphological parameters is given in the next chapter, Chapter 6.

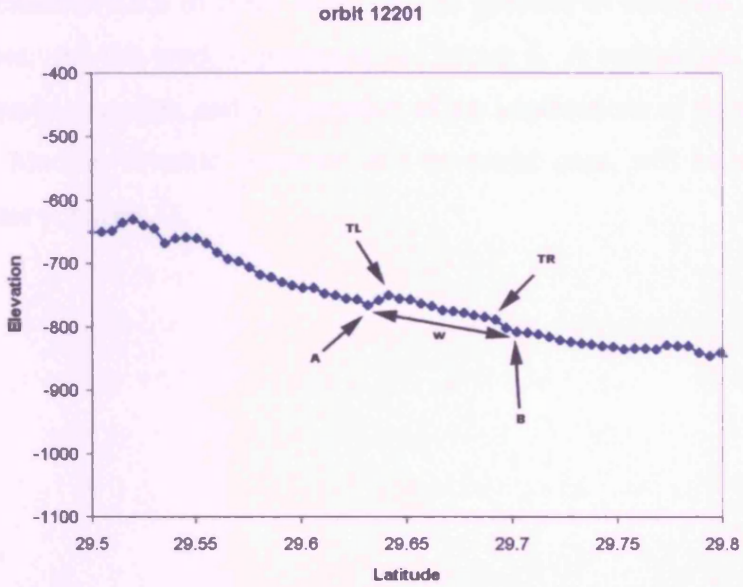

Figure 5.18: The left and right-hand side underlying surface elevation values (A and B) are labelled on this MOLA profile across a section of flow 39. Also labelled are the top left-hand edge and top right-hand edge elevation values for the flow. These are the points where the transition between the edge of the flow and the top of the flow is thought to occur. The thickness values for the left hand side of the flow would be calculated in this case by subtracting A from TL, and the right-hand side thickness would be calculated by subtracting B from TR. Whichever side of the flow had the greatest value was multiplied by the flow width at this point (as measured perpendicular to the length line on a tracing of the flow), to obtain an estimated value for the cross-sectional area of the flow, at each point along the flow where a MOLA profile was obtained. Thus the cross-section was simplified to the area of a rectangle, but this gave a good enough estimate for the purposes of this study.

5.4 Conclusion

The knowledge gained in this chapter about the types of flows in each area of study, combined with all the measurements made using MOLA and the observations made from the images, meant that the individual lava flows could now be studied. All flows were

analysed for their mode of emplacement using observational images, the shape of various plots produced using the MOLA measurements, as well as the measurements made from the images. Measurements made on the aa flows (but not the pahoehoe flows) were also used to produce estimates of emplacement times for each flow using the flow growth model. Given these estimates for the flow duration, and having measured the morphological characteristics of these flows, it was possible to calculate flow velocities, and effusion rates. All this work is presented in Chapter 6. A comparison of these results with those of previous studies, and a discussion of the implications of these findings, with respect to both Martian volcanic processes and terrestrial ones, will be presented in the discussion chapter (Chapter 7).

6.0 Lava flow studies – results and analysis

In this chapter the results of the lava flow measurements made in this study are presented, along with results of the calculations carried out using the flow growth model. Modes of emplacement for all the flows are discussed, and any differences between lava flows from the two different volcanoes will be analysed. Further discussion and implications of the results presented in this chapter can be found in Chapter 7.

6.1 Results of aa flows

For ease of comparison later in this chapter, the results of the measurements and initial analysis of the aa flows from both Elysium Mons and Alba Patera are presented first. Since the flow growth model cannot be used for pahoehoe flows, (Chapter 4), the aa and pahoehoe flows will be discussed separately, with particular reference to the appearance of the pahoehoe flows and evidence to show how they were emplaced. The reader is reminded that the way in which the lava flows were categorised into aa and pahoehoe has been described in Chapter 5.

6.11 Elysium Mons aa flows

Thirteen of the flows studied around Elysium Mons have been inferred to be aa flows. These are flows 17, 19, 21, 24, 28, 35, 36, 39, 40, 41, 43, 44 and 46. The positions of these flows can be seen in Figure 6.1. The flows do not all occur in one particular area, and they do not appear to occur as close to the summit as some of the pahoehoe flows. Four of the Elysium flows in this study have visible central channels. Three of these channelised flows have been classified as aa, which is to be expected since central channels are typical of aa flows. The fourth channelised flow in Elysium has been classified as pahoehoe and the central channel observed is thought to be the surface expression of a collapsed lava tube (section 6.31).

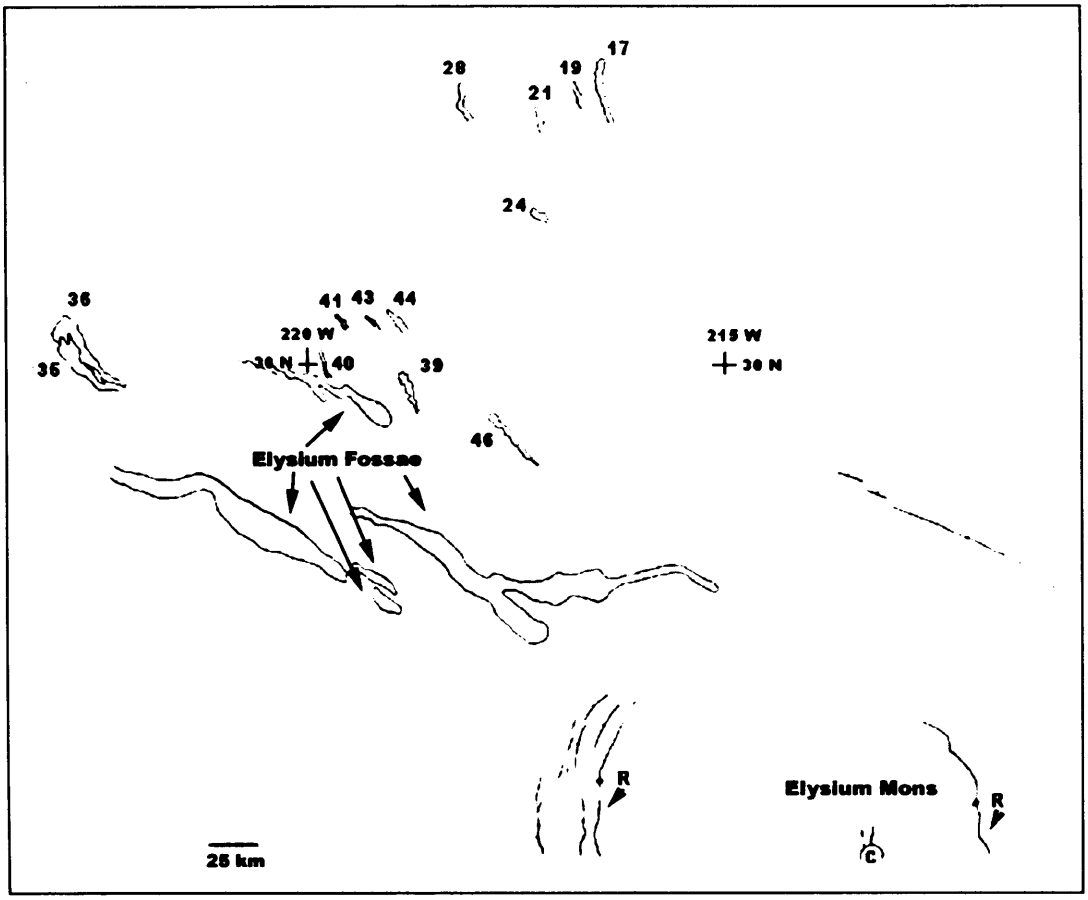

Figure 6.1: sketch map of the northwestern flank of Elysium Mons and surrounding plains. The positions of the aa lava flows analysed in this study are shown. The areas labelled C and R indicate the position of the Elysium Mons caldera (**C**) and various prominent ridges (**R**) around the Elysium Mons volcanic edifice.

6.11(a) Appearance

Only 38% of the flows show a marked increase in width towards the end of the flow. The widths of the rest of the flows remain generally constant at all stages along each flow, and these tend to be the narrower flows. The average of all the maximum widths of the flows is 5.4 kilometres, although several of the flows have maximum widths of over 10 kilometres. At the resolution of the Viking photomosaics, the surfaces of most of the flows appear smooth, and it is not possible to see any of the characteristic surface rubble that is usually found at the surface of aa flows (Macdonald, 1953, 1972; Kilburn, 1990). Several of the flows show surfaces that have many depressions and/or small features that resemble sinuous rilles at this scale (see Figures 6.2 and 6.3). Some of the depressions are probably

small impact craters, but others may be explosive pits, perhaps where lava and ground-ice have interacted. On Earth sometimes the levées on either side of an aa lava channel can meet to form a tube (Guest et al., 1980; Calvari and Pinkerton, 1998), so that the depressions may be the skylights formed between areas of lava flow that have roofed over. The rille-like features may be areas where small lava channels have developed on the surface of a sheet flow.

Figure 6.2: part of a Viking photomosaic showing flow 39. The arrows point to specific surface features on the flow, **c** indicates features that may be small impact craters, and **d** indicates a linear depression which may have been formed through collapse of the overlying lava flow surface. This image is 22 kilometres in width and north is towards the top.

Figure 6.3: part of a Viking photomosaic showing several depressions on the surface of flow 44. The areas indicated by the arrows labelled **c** are the sites of circular depressions that may be impact craters, but could also have been formed by phreatomagmatic activity. The arrow labelled **d** points to a narrow, linear depression that resembles the volcanic rilles seen elsewhere in this area, and may have been formed by erosion by lava flowing across the surface of the flow. Alternatively it could be a small tube or channel within the flow, or may have formed tectonically. The image is 40 kilometres across and north is towards the top.

Since they cast relatively large shadows at their edges in the Viking photomosaics, these flows appear to be thick, compared to some of the other flows in the region. When measured with MOLA, the average thickness is ~20.5 metres, with the minimum value being 11.4 metres, and the maximum being 45.8 metres (see Table 6.1). Analysis of the thickness profiles of these flows shows that in some cases anomalous thickness values occur, so that one of the points on the plot has a much higher or lower value than expected

when compared to adjacent points on the plot. In some cases this can be explained by looking at the location of the MOLA footprint in the image. Usually such anomalies are caused by the presence of small depressions or impact craters that were measured instead of the flow surface by MOLA.

The central channels visible on three of the flows are well defined and all have marginal levées. Figure 6.4 is an image of flow 17, which shows the best example of a central channel. The channel extends from the start of the flow to almost two thirds of the way downstream along the flow, and this is typical for all three channelled flows studied in Elysium. The process of back-filling of channels has been described in Chapter 5, and these three lava flows may be examples of where this process has occurred. On Earth this often occurs because the flow comes to rest before eruption from the vent has stopped (Pinkerton and Wilson, 1994), as observations of the 1983 eruption of Mount Etna by Guest et al. (1987) showed, and may indicate that this is also the case for the channelled flows analysed in this study.

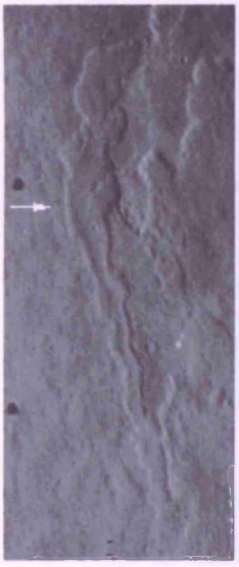

Figure 6.4: part of a Viking photomosaic showing flow 17. Direction of flow was from the bottom of the image towards the top and a clearly defined central channel occurs from the start of the flow until approximately two thirds of the way along the flow (up to the white arrow). This is the best example of a flow with a central channel among the Elysium aa flows analysed in this study. The image is ~14 kilometres across and north is towards the top.

Where a flow suddenly narrows, and often at the same time changes direction slightly, it is impossible to say, just using an image, whether this has occurred due to the breaching of the crust to form a breakout from the flow front, or whether it is just an example of an older flow being overlapped by a younger one. MOLA can be used to

produce longitudinal flow thickness profiles to highlight whether there are any changes in thickness at these abrupt changes in flow direction, and also can show whether there is a marked change in slope at this point that may have affected the flow. Such sudden changes in width and direction only occur twice in this set of lava flows, and the reasons for these changes are examined in the next section using the MOLA data.

6.11(b) Emplacement

Slope

There are several examples where the aa flows in Elysium have been affected by slope. In particular, the formation and modification of the central channels exhibited by flows 17, 21 and 28 appear to have been largely affected by slope. In Figure 6.5(a), it can be seen that the channel in flow 28 does not extend along the whole length of the flow, but is only visible from the start of the flow to a point approximately halfway along it. The point where the channel ceases to be visible in this image corresponds to a change of direction and widening of the flow, along with a change in slope from ~1.5° to 0.29°, which can be seen in Figure 6.5(b). Thus, if the disappearance of the channel halfway down the length of the flow is due to lava filling up the channel from the distal end of the flow back towards the flow front, it could be that at this point the lava could not back-up over the steeper slope, and further thickened the distal end of the flow. Both of the other two flows that exhibited central channels, flows 17 and 21, showed a similar pattern of flow thickening and a change in slope where the channel disappears, although it was not so distinct for flow 21. An alternative explanation for the disappearance of the channels could be that the channels formed owing to the drainage of the flow onto lower dipping slopes. This is shown not to be the case because the flows thicken up on the steeper slopes and if the flows drained it would be expected that the flow would spread out and thin at this point.

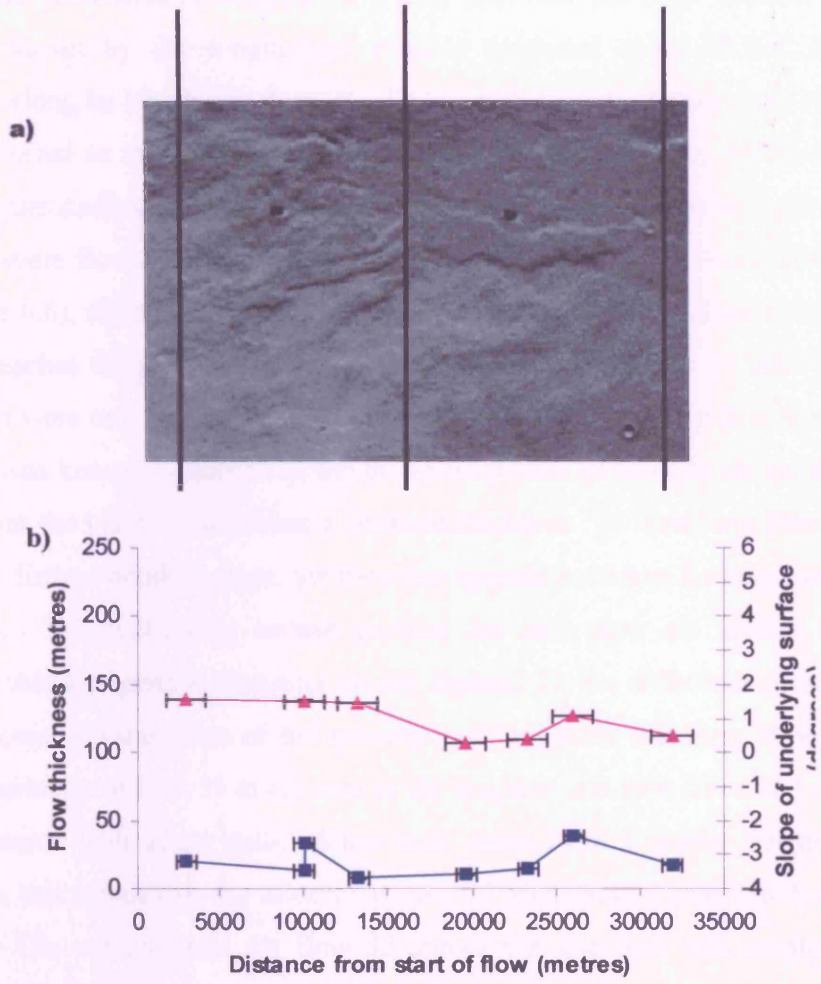

Figure 6.5: (a) part of a Viking photomosaic showing flow 28. Direction of flow is from right to left in the image, and north is towards the right. The left-hand black line indicates the start of the flow and the black line on the far right shows where the flow terminates. The middle black line indicates a clearly defined central channel that ends about 15 kilometres along the flow. This coincides with a change in underlying slope and flow thickness that can be seen in Figure **6.5(b)**. In Figure **6.5(b)** the blue line represents the flow thickness profile of flow 28, and the pink line represents the underlying slope values for this flow. Both the x and y error bars are plotted in this diagram for both plot lines. The error on the distance for the blue plot is +/- 600 metres, and for the pink one it is +/- 1200 metres. The error in thickness for the blue plot is +/- 0.375 metres, and the error on the slope value (pink plot) is +/- 0.000625°. These errors are consistent for all flow thickness and slope plots in this thesis and will be the same for all subsequent graphs where the error bars will not be included.

Flow 35 is another example of a lava flow that has been affected by changes in slope, as shown by the longitudinal profiles produced using MOLA data. At ~12 kilometres along its length, the flow travelled over the margin between the steeper volcanic edifice (referred to in Chapter 4 as the Ancient Volcanic Edifice, AVE), and the flatter, shallower surrounding volcanic plains (see Chapter 4). This change in slope coincides with the point where flow 35 thickens, and the flow remains at this thickness until it terminates (see Figure 6.6), although it widens a little. Flow 36, which lies close to flow 35, spreads out as it reaches the plains. Although flow 36 is covered in part by flow 35, the MOLA thicknesses were only taken over the places where both sides of the flow are visible so that the shape was known. Analysis of the thickness profile of flow 36 shows that as the flow spreads over the plains it maintains a constant thickness. In short, one flow thickens upon reaching a distinct break in slope, yet the other spreads out when flowing over similar slope conditions. The underlying surface profiles for each flow are similar in appearance, indicating that topographic obstacles do not account for the difference in the behaviour of the two flows. Examination of the velocity profiles shows that flow 36 was travelling at twice the velocity of flow 35 at the start of the eruption, but both flows had similar velocity values towards their distal ends. Since both flows have a similar length of around 60 kilometres, this means that the velocity of flow 36 declined at a more rapid rate than that of flow 35. The velocity plot for flow 35 shows that the flow was emplaced at a more constant but lower velocity.

Since flow 35 can be seen to overlie flow 36 in the Viking images, flow 35 must be younger that flow 36, but it seems likely, given the proximity of the two flows, that they had the same magma source. The apparent difference in the reaction of the two flows to a change in slope may have resulted from the mode of emplacement, perhaps because different modes of emplacement meant that the flows reacted differently to changes in slope and topography. A channelised flow will not widen much even on reaching a shallower slope (Swanson et al., 1975), whereas sheet and tube-fed flows spread out to fill wide areas, even on shallow slopes (Mattox et al., 1993). Thus flow 36 may have been emplaced as a sheet or developed a system of tubes that enabled the flow to spread out on reaching the shallow slope. Flow 35 however does not show any evidence for channelised flow that would have caused the flow to be confined and thicken up instead on reaching the

shallow slope. Different rates of cooling may also have had an effect by causing the front of one flow to develop a thicker crust before the other flow and so thicken more (as explained in Chapter 5). Different modes of emplacement or even differences in effusion rate would have caused this to happen.

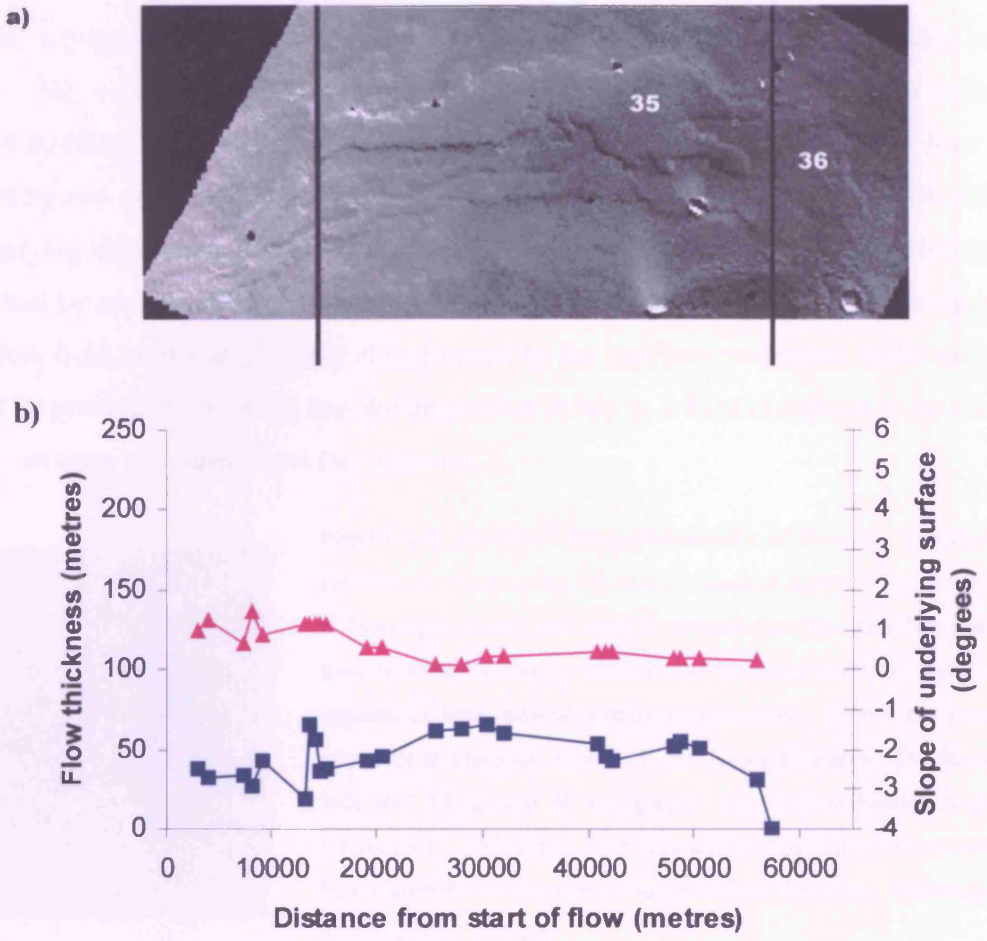

Figure 6.6: **(a)** part of Viking image 541A22 showing flows 35 and 36 (labelled), which is ~80 kilometres across. Flow 35 shows a gradual increase in width from the beginning of the flow to the end, and branches into two at the distal end. Flow 36 is narrow towards the start of the flow but widens dramatically towards the end. The difference between the two flows may have been due to differences in effusion rate, or to topographical control. The left-hand black line indicates the edge of the AVE and corresponds to change in flow thickness as shown in Figure 6.6(b). The right-hand black line denotes the edge of the flow. **Figure 6.6 (b):** The blue line represents the flow thickness profile of flow 35, and the pink line represents the underlying slope values for this flow. Although flow 36 maintains a relatively steady thickness all along its length, flow 35 seems to have been affected by the change in slope where the AVE grades into the surrounding plains, and thicken at this point without significant widening.

Topography

There are several good examples within this set of flows where topography has influenced the way the flows were emplaced. In some cases obstacles are visible in the images that influenced either the direction or the morphological parameters of a flow. For example, topographic obstacles influence the whole of Flow 28, as it is possible to see (Figure 6.5a) where the flow was channelled between two ridges. In a different example, flow 24 exhibits an abrupt change in direction where it is possible that the flow was diverted by one of the many small graben visible in the surrounding area. MOLA profiles of underlying slope show that the flow also appears to have flowed within a depression and was halted by an area of higher standing ground. Flow 24 has been emplaced on top of an older flow field, so it was probably also diverted by the smaller topographic highs and lows formed by previous flow fields, and the depression in which it flowed appears to be a valley formed between two older flows (see Figure 6.7).

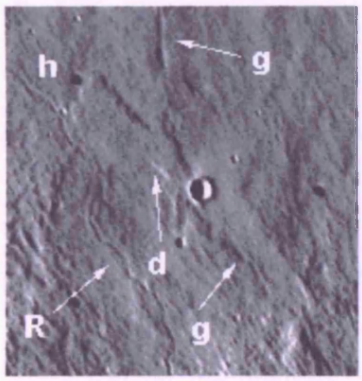

Figure 6.7: part of a Viking photomosaic of flow 24. The start of the flow is obscured by a prominent impact crater. Flow direction is from right to left, and north is towards the top. The flow can be seen to abruptly change direction at the point indicated by **d** and appears to have flowed within a depression. Where the ground increases in elevation at point **h**, the flow terminates. The features indicated by **g** and **R** are graben and a rille/channel feature, respectively. These may have diverted the flow direction and could be responsible for the abrupt change in flow direction. The image is 34 kilometres in width.

In other cases it appears, just from analysis of the images, that some of the flows have advanced by breakouts, as some of the flows narrow and change direction abruptly. Flow 46 is an example of one of these flows: there are at least two points where the flow abruptly narrows, although it does not change direction (see Figure 6.8a). The flow thickness profile (Figure 6.8b), shows that the thickness of the flow is relatively constant. A constant thickness must have been preserved by changes in the speed of the flow, so that where the flow was channelled through a narrow area, the velocity increased. The boundaries of the flow are irregular, probably due to topographic control. Flow 46 appears

to spread out after the second narrowed section, perhaps due to a reduction in slope (see Figure 6.8b).

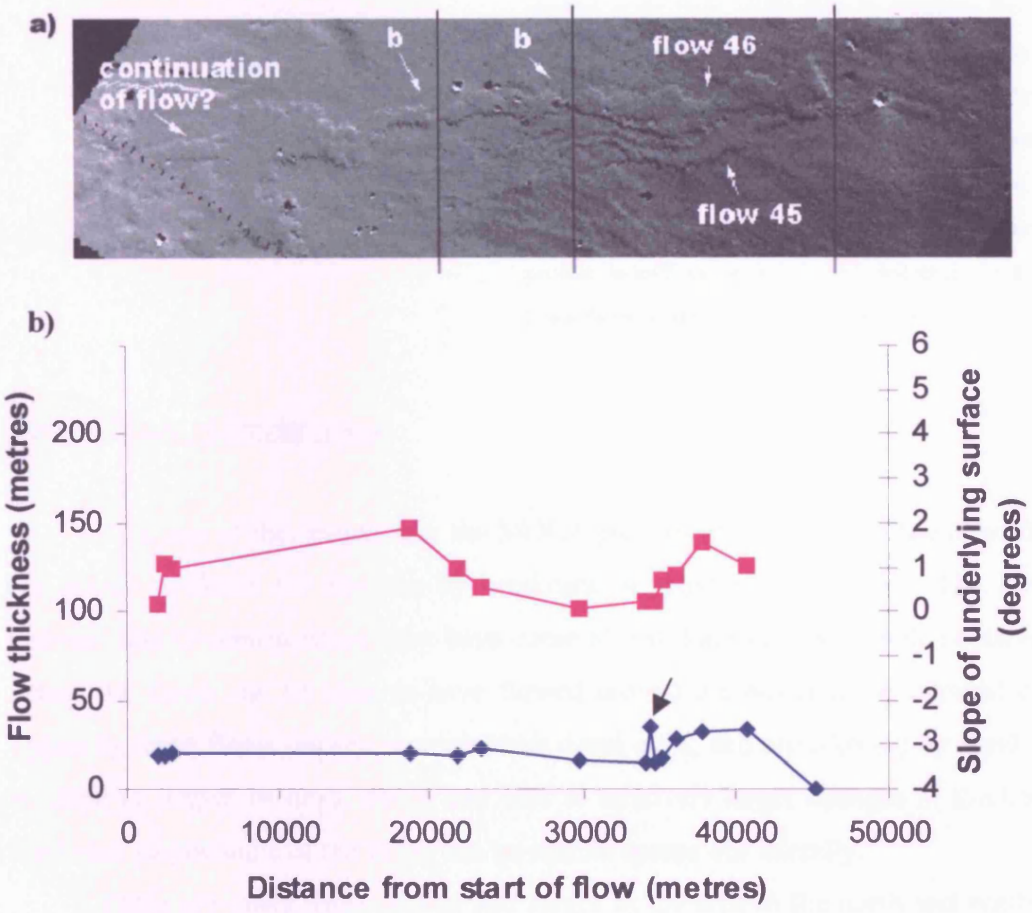

Figure 6.8: **(a)** Part of Viking image 541A26 showing lava flows 45 and 46. At two points along flow 46 the flow narrows suddenly, which could indicate the position of a breakout (indicated by **b** on the image). Analysis of the flow thickness profile for flow 46 (Figure 6.8b) shows that a constant thickness is maintained at these points, and the underlying slope profile for the same flow shows that they appear not to be related to specific changes in slope. The direction of flow is from left to right in this image, and a section of flow that might be a proximal part of flow 46 is indicated on the image. It may have been covered by later flows, but alternatively flow 46 may have erupted from the edge of the flow field at the left-hand side of the image. The image is ~90 kilometres in width and north is towards the right. The left-hand and middle black lines are highlighting breakouts, the right-hand black line indicates the end of flow 46; **(b)** graphs showing the underlying slope (pink line) and flow thickness (blue line) profiles for flow 46. The arrow indicates an anomalous thickness value thought to indicate a place where flow 46 overlies flow 45.

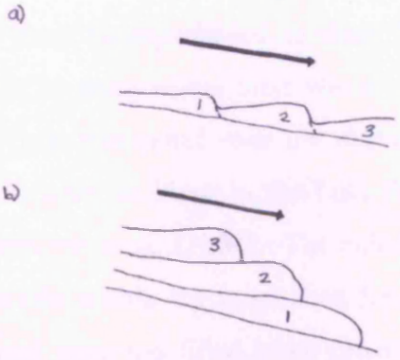

Figure 6.9: Diagram to show two different modes of advance for lava flows. The flow in **(a)** has advanced as a series of breakouts, with the younger lava (3) being erupted at the front of the flow by breaking through the crust of an older flow. A longitudinal thickness profile of this flow would not show an overall change in thickness. In **(b)**, a series of flows have been emplaced on top of one another, so that the youngest flow (3) lies on top of the older flows and the longitudinal flow profile would show a gradual decrease in thickness towards the distal end of the flow.

General Mode of Emplacement

Analysis of the images and the MOLA profiles of the Elysium Mons aa flows has not shown evidence for advance by breakouts or growth by inflation. The flows have widened and thickened where they have come to rest due to a topographic obstacle, and in places the flows can be seen to have flowed around the obstacle, or changed direction. Typically these flows thicken towards their distal ends, and are affected by small changes in slope (1 degree or less), which can lead to relatively larger changes in thickness. On shallower slopes some of the flows can be seen to spread out laterally.

There are many small graben and ridges in the area to the north and north-west of the Elysium Mons construct (such as those visible in Figures 6.2, 6.3 and 6.7), which could be examples of the types of vents that were the source of the flows in this section. The original vents of the flows being studied have probably been covered up by the eruption itself, or later eruptions, and also by fine-grained deposits. In Figure 6.8(a) it is possible to see that the proximal end of flow 46 was covered by younger flows that formed a large flow field, and also to see that there is an area within the large flow field that looks as though it might be a continuation of flow 46. The start of flow 46 was not measured from this point and, in this event, the flow lengths given in this study may thus be underestimates.

Three of the flows in this section have developed and subsequently advanced via channels. Some of the other flows may have done the same but they may have been roofed

over later, or have been completely filled in by back-fill of lava. It would therefore appear that most flows behaved as sheet flows. Where there are small rilles in the crust these might be areas where there was a topographic obstacle that cut a line through the crust as the crust was rafted over the obstacles. This has been observed in some terrestrial flow fields, such as those in the Laki flow field in Iceland (see Figure 6.10) as described by Keszthelyi et al. (2000). The rilles observed in the present study may also be small lava channels within the large flow field. Depressions in the crust mark where the flow has flowed over and filled small pre-existing depressions, or they could be small impacts, or even explosive pits like those next to the Elysium Mons caldera (see Chapter 4), but on a smaller scale. The amount of water/volatiles in this area in the past makes interactions between these and the lava likely (Mouginis-Mark, 1985).

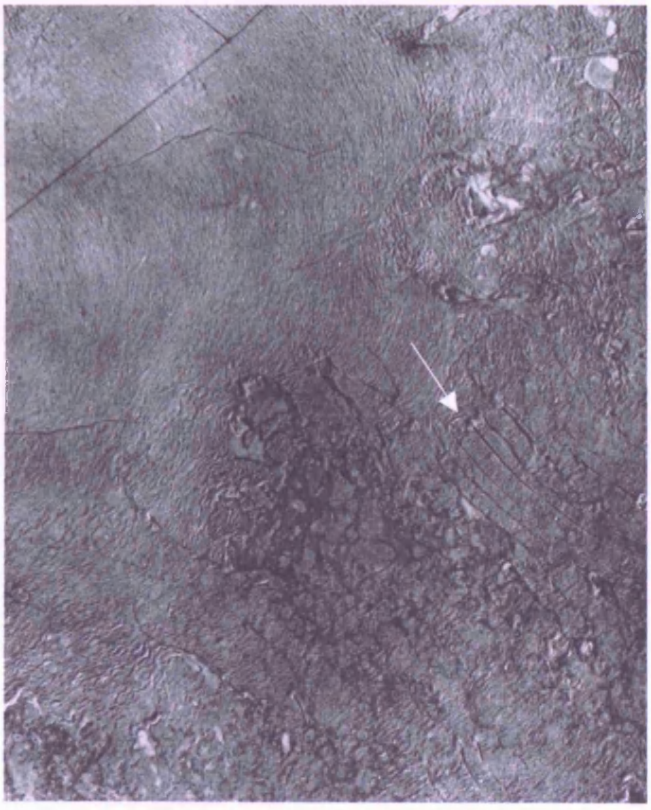

Figure 6.10: showing an aerial photograph of part of the Laki lava flow field in Iceland. The arrow indicates an area where high-standing topographic obstacles have punctured the lava crust and cut depressions in the crust of the lava as it moved from top left to bottom right in this photograph. Lineations seen on the surface of some of the lava flows in this study may have formed in a similar manner. A road in the top left of this image provides scale.

Rheological Controls

Plotting some of the measurements made on the lava flows against each other can sometimes highlight relationships that provide important insights into the way the lava flows were emplaced, and often help to link the information gained by analysis of the images and that of thickness and topography/slope profiles. Often, the plots reflect the rheological properties of the lava itself, rather than just the effects of slope and topography. The graphs of the Elysium Mons aa lavas show some clear trends, as well as some less obvious trends.

A plot of the downstream resistance for individual points along the flow, against the distance of each point from the start of the flow, shows that generally the downstream resistance for each of the aa flows increases towards the end of the flow. As the flow progresses, factors such as cooling, crystallisation and degassing of volatiles will all mean that the crust of the flow will thicken and the lava will become more viscous, thus making it more difficult for it to move. Since the downstream resistance of the flow is a measure of the forces preventing forward motion of the flow, it is expected that this value would increase along the length of a lava flow. Flow 21 provides a good example of one of the Elysium aa flow downstream resistance graphs (see Figure 6.11). This flow can also be seen to thicken towards the end, as might be expected when the flow has developed a thick crust at the flow front and thus increased the downstream resistance. Although the last point plotted in Figure 6.11 appears anomalous, it must be remembered that the general positive trend of the graph is the important feature of this graph and similar plots for the other flows.

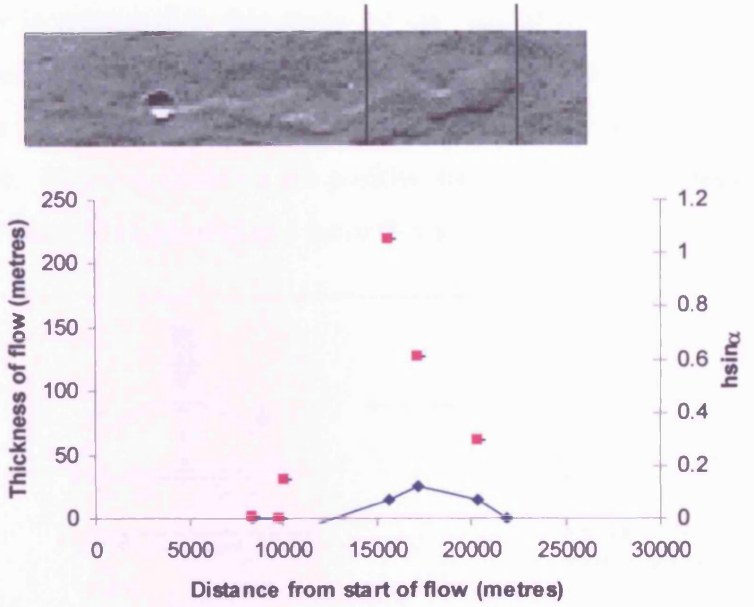

Figure 6.11: The image of flow 21 at the top of this diagram was taken from Viking image 541A27 and is ~25 kilometres across. Beneath this is a flow thickness profile (blue) for the same flow, which shows that the flow thickens towards the distal end. The left-hand vertical black line on the image shows where the thickening starts and it seems to coincide with the point where the central channel ceases. The scatter plot (pink) shows the values for downstream resistance at different points along the flow. These values increase towards the distal end of the flow as might be expected of a cooling, crystallising and degassing lava flow. Error bars are given for the downstream resistance values.

Another graph used for analysis of the flows is flow thickness against width for each of the measured points along the lava flow. In the case of the Elysium aa flows, there is a positive trend to this graph, which shows that as the thickness of the flow increases, so does the width. This might seem surprising at first, since when a lava flow widens it should thin to conserve mass. However, this could in fact be related to the hydrostatic pressure of the lava. Lava spreads laterally because the thickness of lava at the centre of the flow is greater than the thickness at the edges of the flow. The extra weight of the lava causes hydrostatic pressure, which pushes the lava outwards from the middle of the flow towards the edges and causes spreading (see Figure 6.12). This continues until the thickness of the lava at the centre of the flow decreases and the hydrostatic pressure is no longer strong enough to cause lateral flow. The pressure being exerted on the flow to cause it to spread

laterally is measured in this study by the 'lateral resistance', the plot of which will be discussed later in this section. Thicker flows may be wider because a wider 'base' of lava may be needed to support a thicker flow, and thus maintain a balance of hydrostatic pressure. Figure 6.13 shows the positive trend between thickness and width exhibited by flow 24, which is typical of this set of flows.

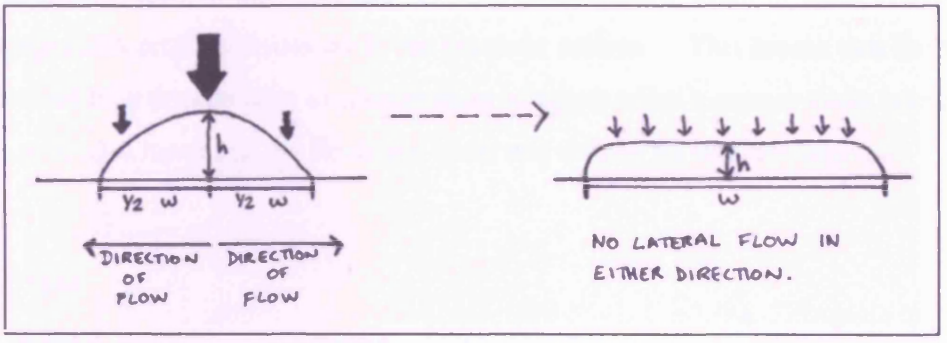

Figure 6.12: Diagram to explain measurement of lateral resistance in this study. The diagram on the left represents a newly emplaced lava flow that is thicker in the middle than at the edges. The weight of the flow in the middle is greater than at the edges (as shown by the vertical arrows) so the flow spreads out in the directions shown until the pressure exerted by the weight of the lava is equal across the flow as shown in the diagram on the right-hand side. Since h (flow thickness) is reduced by the lateral movement of the lava in both directions across the width (w) of the flow, the equation for lateral resistance is: (h/(0.5w)) * (h/(0.5w)). The equation for lateral resistance can then be re-written as $h^2/(0.5w)^2$ or h^2/w.

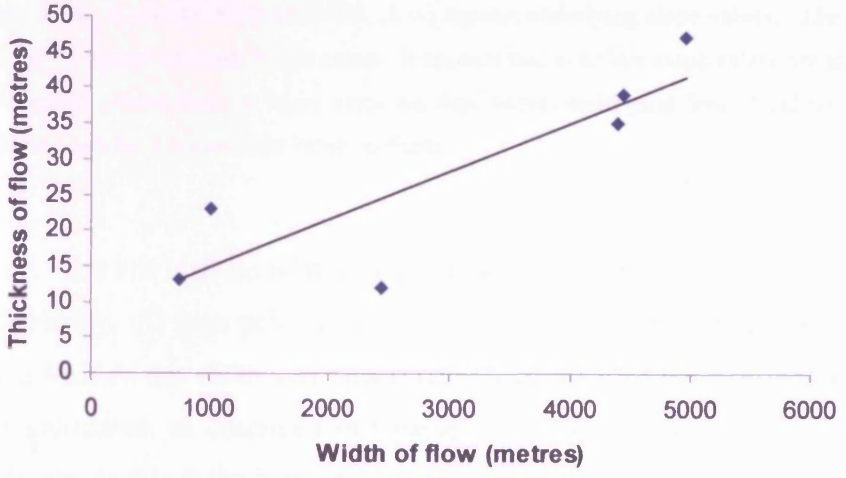

Figure 6.13: A plot of thickness of flow against flow width for flow 24. The plot shows a positive trend that is typical of flows in this group.

The value for thickness divided by width for each point along the flow has been plotted against the slope value at each point to try to discover how much of an effect slope had on each flow. Generally for this set of flows there is a positive trend (see Figure 6.14 of flow 21). A positive trend means that, as the slope increases, the thickness may increase, the width decreases, or both of these occur to some extent. Both of these effects occur in the images and profiles discussed in the previous section. This means that the flow must narrow and thus thicken (due to conservation of mass) when a steeper slope is encountered, and it must also mean that the flows get wider and thinner on shallow slopes.

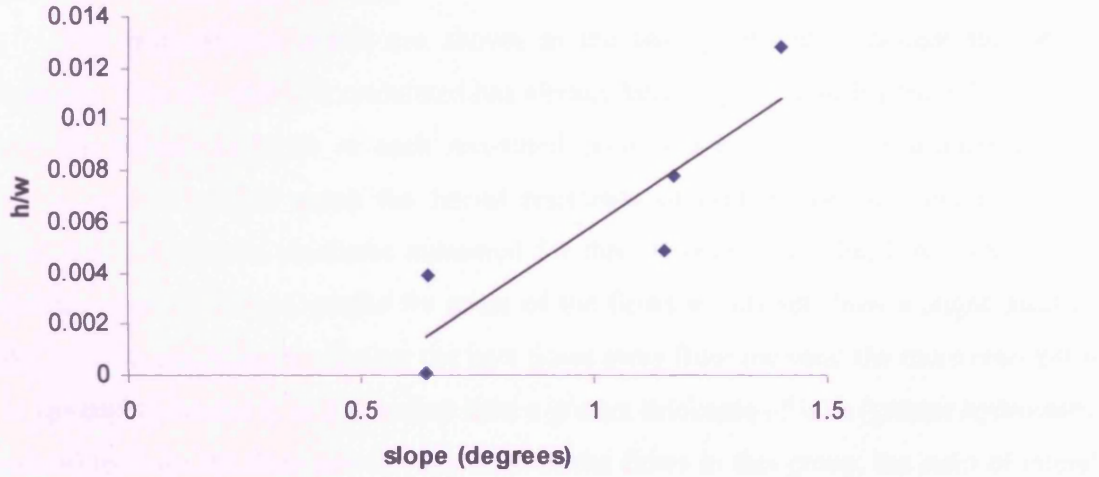

Figure 6.14: A plot of thickness/width (h/w) against underlying slope values. The graph shows a positive trend that is typical of flows in this group. It appears that even low slope values are an important factor in the emplacement of lava flows on Mars, since the slope values underlying flow 21 did not exceed 2 degrees. This would be considered a low slope value on Earth.

The last obvious relationship that was found between the flow measurements is that for velocity. At each point along the flow where thickness measurements have been made using MOLA, the width was measured on the image of the flow and a cross-sectional area was calculated, as described in Chapter 5. Since the cross-sectional area is based on a rectangle, as this is the best way to approximate the shape of the flow, it is therefore only a

very basic estimate, but the figures obtained have been inserted into equation 6.1 to determine a crude estimate for the velocity of the flow:

$$1 / (\text{flow edge thickness} * \text{width}) \qquad (6.1)$$

where 1 represents a constant effusion rate (as discussed in Chapter 5). Obviously this only gives a relative velocity value, since the estimate of the cross-sectional area is a general one, and effusion rate cannot be constant throughout an eruption. However, the plots obtained in this study show some interesting results. For the Elysium aa flows, the velocity generally decreases with distance from the start of the flow, and this is probably due to degassing, cooling and crystallising as mentioned above, so would be expected.

The less obvious trends are shown in the two graphs that concern the lateral resistance. The way that it is calculated has already been explained in Figure 6.12. In one graph the lateral resistance at each measured point along the flow is plotted against distance, and in another graph the lateral resistance of each measured point is plotted against the downstream resistance measured for that same point on the flow. The lateral resistance against distance graphs for some of the flows in this set show a slight positive trend. This suggests that the further the lava flows away from the vent, the more resistant it is to spreading out and it will therefore take a greater thickness of lava (greater hydrostatic pressure) to make the flow spread. For most of the flows in this group, the ratio of lateral resistance to downstream resistance shows a slight negative correlation, which may mean that flows thicken rather than widen towards the distal end.

To sum up, flows generally thicken towards the distal end; their downstream resistance increases in the same direction; they thicken more than they widen downstream, and their velocity decreases towards the flow front. This suggests that the flows have been emplaced in a cooling regime similar to that of terrestrial aa flows. Thus, the use of the flow growth model to determine emplacement times of the flows is justified. The results of the flow growth model calculations are given in section 6.2.

6.12 Alba Patera aa flows

Six of the flows on Alba Patera have been found to be aa flows, these are flows 1, 4, 6, 7, 8 and 11. The positions of the flows are given in Figure 6.15. There does not appear to be any kind of pattern to the way they were emplaced. Flows 4, 6 and 7 on the north and north-west part of the summit are relatively close together compared to the positioning of the other flows and, as discussed previously, are likely to have been emplaced in the same way because they probably had the same or similar magma supplies and similar regional slopes during emplacement. Out of all 11 flows studied in the Alba Patera region, only two have central channels, and both of these appear in the aa group which will be discussed in this section. Since channels are a common feature of aa flows then this provides further evidence that these flows are likely to be aa flows.

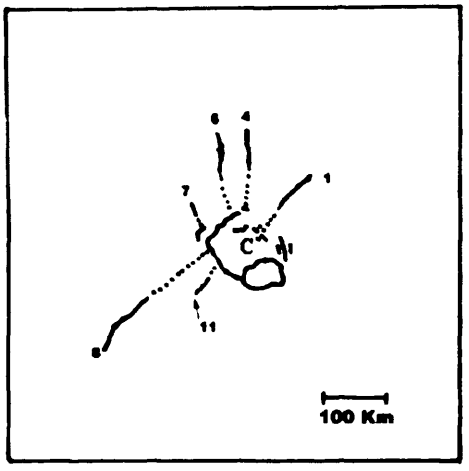

Figure 6.15: Sketch map showing the positions of the 6 aa flows analysed in this study. The flows have been numbered according to the work of Kilburn and Lopes (1991) and the map has been modified from the same paper. The feature labelled C is the caldera complex of Alba Patera. The positions of some of the graben are indicated and the inferred length of each flow back to the source is indicated by the dotted line.

6.12(a) Appearance

These flows are all relatively narrow when compared to those in other groups in this study. The average 'maximum width' of all these flows is 4.7 kilometres, and ranges between 2.3 and 8.5 kilometres. Most of the flows do not widen towards the end and maintain a steady width along the whole length of the flow. Those flows that do widen towards the end only do so by around 2 kilometres, and narrow again before terminating. Flow 6 is the only flow that bifurcates.

The images of these flows tend to be much clearer than those of the Elysium flows. This is probably due, in part, to the fact that parts of Alba Patera are younger than Elysium Mons, so the flows being studied at Alba Patera have been less modified and eroded, and are not so obscured by fine-grained deposits. In places some of these flows appear to have rough surfaces, and they do not possess the flat, 'tabular' surface texture that is shown both by some of the flows in Elysium, as well as by some of the pahoehoe flows at Alba Patera. The boundaries of the flows generally show little branching. As in Elysium, though, despite the fact that the images are clearer, they are not at a high enough resolution to see any of the characteristic surface rubble expected of aa flows, and none of the MOC images cover any part of these flows. Although the flows do have several impact craters superimposed on them, and there are areas of the flows that appear uneven rather than smooth, there are no obvious pits, ridges, rilles or other smaller-scale features visible in the Viking images.

Flow 8 is cut by a large system of graben (see Figure 6.16), and the flow can be traced across the floor of several of the graben. This shows that these graben must have been formed after the emplacement of flow 8. The pahoehoe flow, flow 9, can also be seen to be cut by graben in this way, as have other flows in the area that have not been included in this study. This means that potentially all the flows in this study had been emplaced before the major tectonic activity that formed the graben occurred, perhaps providing important clues as to the development of Alba Patera in the later stages of activity.

The flows all appear to be relatively thick in the images compared to the Alba Patera pahoehoe flows described in the next section, since they cast long shadows and are easily visible in the images. Measurements by MOLA show the average thickness of all these to be 21.7 metres thick, but the averages of each of the flows ranges between 18 and 24 metres (see Table 6.2). Analysis of the images shows, that on appearance alone, none of the flows appear to have advanced by breakouts. None of the flows studied in this set exhibit points where the direction of the flow abruptly narrows and/or changes direction.

The channelled flows are different in appearance from those in the aa group of Elysium. The channels in both the flows where they occur, extend the complete length of the flows (see flow 7 in Figure 6.17). They do not appear to have undergone back-filling such as the Elysium Mons flow discussed in Figure 6.5.

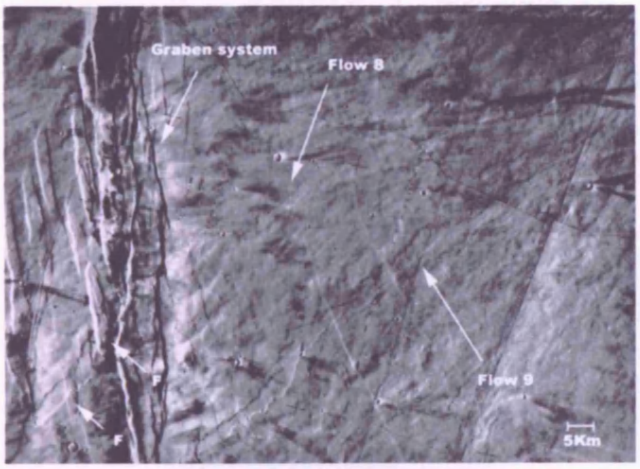

Figure 6.16: Part of a Viking high-resolution photomosaic of part of the summit area of Alba Patera. The position of the aa flow, flow 8, is indicated and it can clearly be seen to cross the region that is now covered by a wide graben. The points indicated by the arrows labelled **F** are places where flow 8 can be seen on the floor of the graben, thus indicating that the process that formed the graben occurred after flow 8 was laid down. Direction of flow was from top right to bottom left.

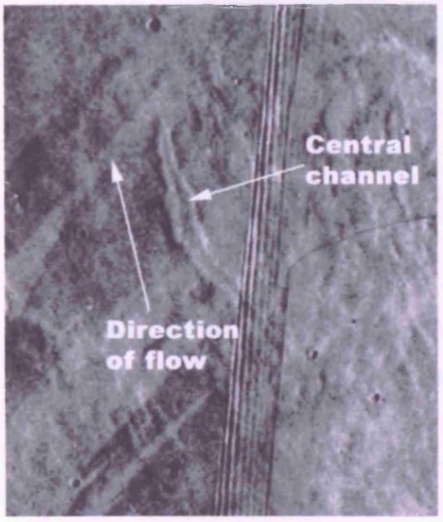

Figure 6.17: Part of a Viking high-resolution photomosaic of part of the summit region of Alba Patera. The flow visible in the image is flow 7 and is an example of one of the channel-fed flows studied at Alba. The channel is in evidence right to the end of the flow, and in this way it differs from the channelised flows in Elysium that ceased around halfway along the flow. For scale, The obvious impact crater at the top of the image is 1 kilometre across.

Other flows in this area may have originally advanced via channels, as they appear to have some levée-like features along their margins (see Figure 6.18). Flow 4 appears to have a raised feature in the middle of the central channel, creating a braided appearance to the channel (see Figure 6.19). Possibly this was part of a levée that broke off during the emplacement of the flow and blocked the channel, as has been observed for terrestrial flows (Frazzata and Romano, 1984; Guest et al., 1987; Lipman and Banks, 1987), causing it to have a braided appearance. However, if the flow was still active once this had occurred it would be likely that lava would have accumulated inside the channel behind the blockage and eventually flowed over the levées, and no evidence of this can be seen in the image.

Similar features are found in the MOC images of the flows on the flanks of Olympus Mons (see Chapter 3). Therefore, on appearances, it would seem that the aa flows at Alba Patera advanced with central channels, rather than by sheet flow as in Elysium, which may be reflected in contrasting emplacement times and flow velocities between the two flows.

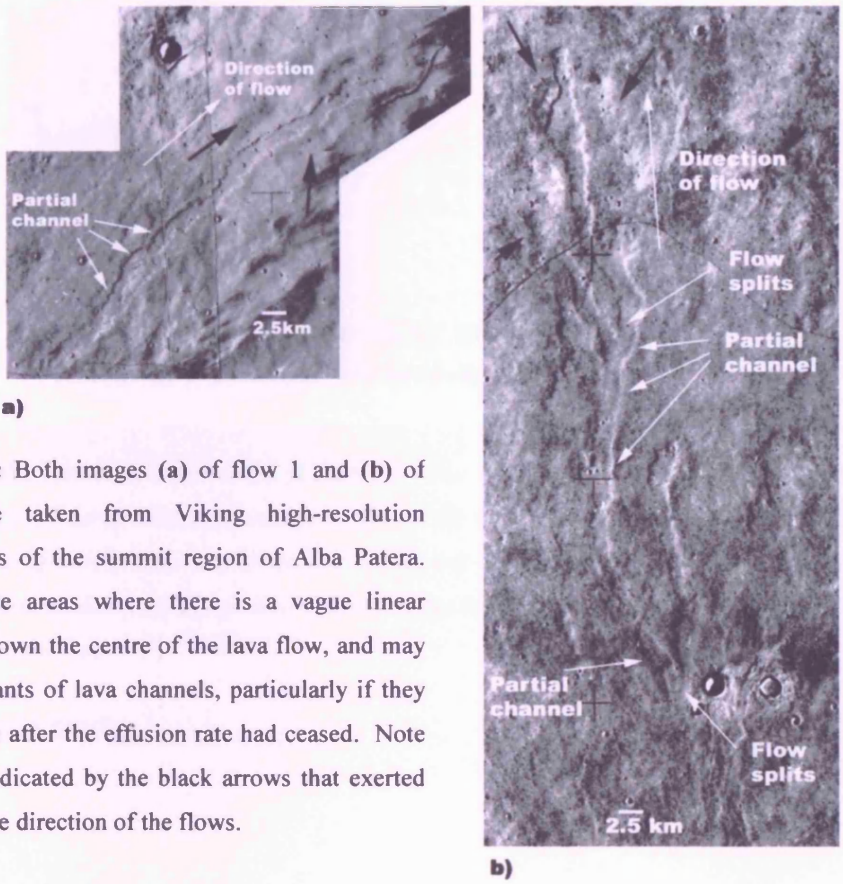

Figure 6.18: Both images **(a)** of flow 1 and **(b)** of flow 6 are taken from Viking high-resolution photomosaics of the summit region of Alba Patera. Both indicate areas where there is a vague linear depression down the centre of the lava flow, and may be the remnants of lava channels, particularly if they did not drain after the effusion rate had ceased. Note the ridges indicated by the black arrows that exerted control on the direction of the flows.

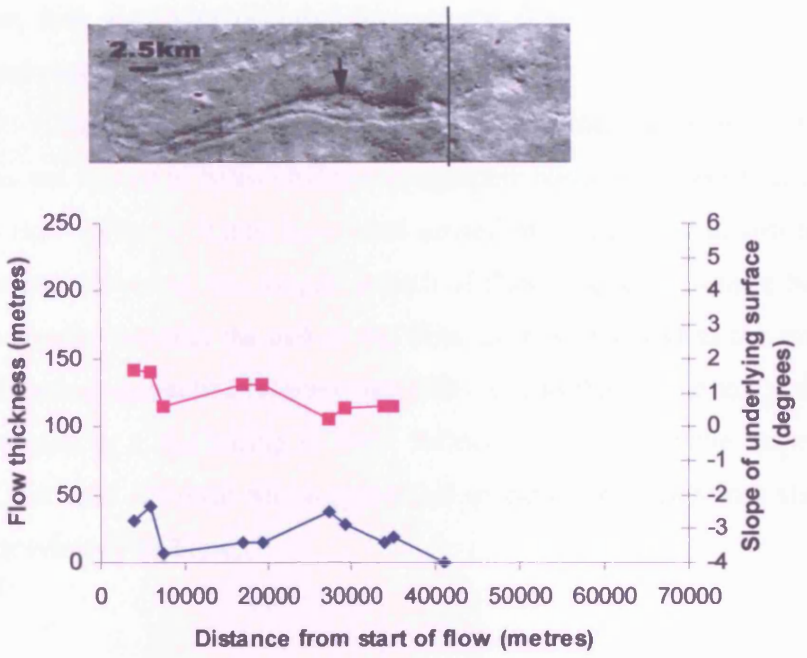

Figure 6.19: The lava flow in the image at the top is flow 4, and the arrow indicates an area where a small topographic high is located within the central channel of the flow, and may be the remnant of part of a channel wall that became detached. This flow seems to exhibit a well-developed relationship between underlying slope and flow thickness as shown by the plots of flow thickness (blue) and underlying slope (pink). The black line shows the end of the flow.

6.12(b) Emplacement

Topography

Most of the flows in this group do not appear to have met many topographic obstacles that have diverted them and noticeably changed the original direction of flow. The most common way these flows are diverted is by flowing along ridges or the edges of older flows. There are two flows that have been most affected by topography, and these are flows 1 and 6. Several ridges (see Figure 6.20) control the direction of flow 1, two of which are probably the surface expression of older tube-fed lava flows. Apart from being diverted along the edges of the ridges, there is a hill at the distal end of flow 1 that may have been the reason the flow came to rest. The thickness profile produced by MOLA shows that the flow does thicken slightly towards the end, which though typical of an aa

flow, may also have occurred because the flow slowed and thickened once it could not travel past the hill.

Flow 6 is the only flow that exhibits branching amongst this set of flows. There does not appear to be an obvious topographic obstacle present in the images to explain why the flow splits, so it may have been caused by slope and that will be discussed in the next section. However, the longest branch of flow 6 appears to have been directly affected by topography towards the end of the flow as it is observed in the images to have narrowed after being channelled between two hills. It also thickens at this point, which appears to be unrelated to a shallowing in slope following analysis of the slope graph produced using MOLA, and although this is typical of aa flows, may therefore also be due to the forced narrowing of the flow.

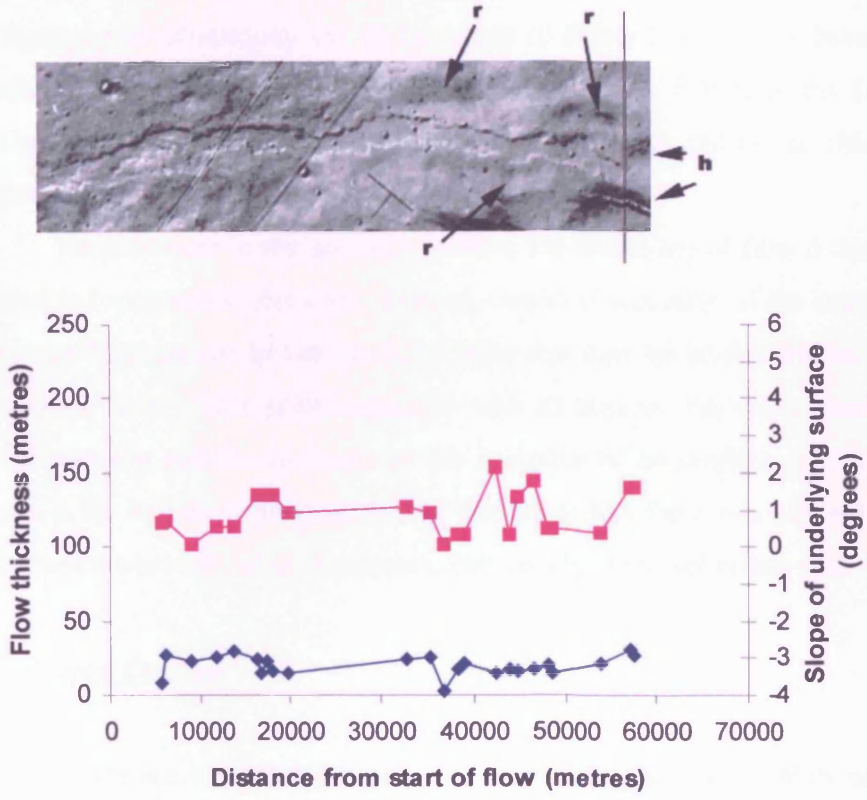

Figure 6.20: The flow in the image at the top is flow 1 which appears to have been channelled through a valley formed by several ridges. The ridges (r) are probably the surface expression of older tube-fed lava flows. The plots beneath the image show that the flow thickness (blue) is related to even small changes in slope (pink), and that although the flow is relatively thin (~20 metres) it thickens by several metres at the distal end. The flow appears to thicken on shallow slopes and thin on steeper slopes. The flow terminates before several hills (h) and the end of the flow is indicated by the black line.

Slope

Most of the flows do not show a marked correlation between thickness and slope, but there are a few examples that do. Analysis of the slope graphs produced using MOLA show that changes of around 1° have a small effect on the thickness of flow 1 (see Figure 6.20). It may be that in this case, since the flow is confined between two ridges, changes in slope have to be accommodated by changes in thickness rather than width, and are more obvious than for those 'unconfined' flows.

Of the six flows in this group, four (flows 1, 4, 6 and 8) show a thickening towards the distal end of the flow in the thickness profiles, but not all this thickening corresponds to a change in slope. Those that do not thicken as a result of slope could be doing so because of topographic obstruction (as in the cases of flows 1 and 6), or because of the natural cooling and thickening process that occurs for aa flows. However, the thickening observed in flow 4 does appear, from analysis of the data, to be related to changes in slope (see Figure 6.19).

As discussed in the previous section, the branching of flow 6 does not appear to be related to topographic obstacles. Instead, careful observation of the image shows that there are some features just before the bifurcation that may be levées that are partially obscured from view now. This point coincides with an area on the slope graph where the slope remains steady, and the thickness profile is similar to the profiles of breakouts (as shown in Figure 6.9). It is therefore proposed by the author that there was a breach in the levée walls at the point where the slope becomes steady and the flow splits into two.

Rheological Controls

There are several major points to discuss concerning the plots of the different lava flow measurements. Firstly, two-thirds of the flows show a positive relationship between h/w and slope. However, there is no obvious relationship in the graphs between thickness and width when they are plotted against each other, nor did a relationship seem obvious when profiles of flow thickness were compared with plots of changes in slope. The

positive relationship between h/w and slope must mean that the dimensions of the flow are changing to conserve the mass of the flow as the angle of slope of the underlying surface changes. Slope must be more important in the emplacement of these flows than first appears from analysis of thickness profiles and plots of changes in slope. This relationship may have been obscured by a scarcity of measurements at points along the flows where changes in slope would have been more obvious. It may also be that changes in thickness accommodated for the change in slope, as the widths of the flows appear to stay similar along each flow. The fact that thickness and width measurements do not appear to be related must mean that other factors were involved that had more influence than the effect of internal hydrostatic pressure. These other factors may have been slope, as well as topographic features (such as ridges) that confined the width of the flow.

The plots of downstream resistance against distance show that the resistance increases towards the distal end of each flow, and thus shows that the flows were cooling, crystallising and degassing as they flowed. The values of $h\sin\alpha$ remain under 0.1 metre, as is the case for all the other sets of flows in this study. There is also a slight positive trend in the relationship between lateral resistance and distance from the start of each flow. These trends mean that the lava cooling process on Mars is likely to be similar to that which occurs on Earth, and that emplacement mechanisms must be similar too. In some cases the lateral resistance stays at a similar value all along the flow, which could perhaps be one of the reasons that the flows maintained steady widths as they flowed. There is no obvious relationship between the ratios of downstream resistance and lateral resistance.

As has been the case for all the flows studied so far, the velocity of this set of flows generally decreases with distance from the vent. Cooling effects, as well as a slowing effusion rate, are the likely factors for this. Again, as with the aa flows in Elysium, these Alba Patera aa flows show a steep decline in velocity at the start of each flow, which levels off into a slower, steadier decline as each flow progresses. Figure 6.21 clearly highlights the steep decline in velocity for one of the Alba Patera aa flows. The graph is typical of these flows, and is similar to the typical velocity graphs of the Elysium aa flows. Comparison between this graph and the plot of velocity for an Alba pahoehoe flow (Figure 6.40) highlights the steeper decline for the aa flow. This difference is to be expected because in an aa flow the lava is generally progressing in open channels and cools a lot

faster than for pahoehoe flows where the lava is insulated from the atmosphere by travelling in tubes.

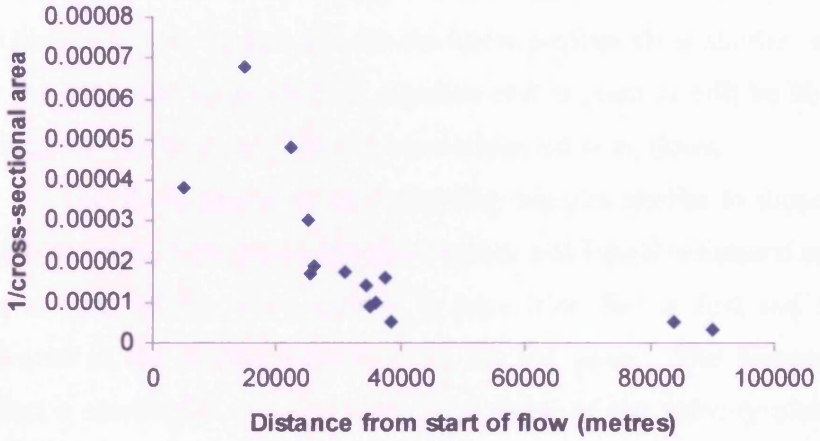

Figure 6.21: Plot of velocity (1/cross-sectional area) against distance from start of flow for flow 8. The graph has a steeper curve towards the start of the flow, which then levels out to become much shallower. This plot is typical of the pattern exhibited by the Alba Patera aa flows.

General Mode of Emplacement

Analysis of the data has shown that many of these flows probably advanced as channel-fed flows, with at least two of the flows showing definite channels, while others exhibit features that may be the remnants of levées/channels. The two obviously channelled flows do not show any signs of back-filling as they did in Elysium. One of the channelled flows, flow 4, shows a 'braided' effect, possibly caused by a piece of broken levée wall being carried downstream. Another flow, flow 6, appears to be the only example among this set of lavas that underwent a breakout. This may have occurred by the breaching of a levée wall that caused the flow to split into two branches, and slope measurements using MOLA show that this appears to have been aided by a change in slope conditions.

The topographic control for these flows was primarily confinement by ridges (probably the surface expression of large tube-fed flows) and the edges of older lava flow fields. Slope appears to have been an important factor in the emplacement of these flows, as indicated by the relationship between h/w and slope. The flows do not maintain a

similar thickness all the way along and many thicken towards the distal end, sometimes due to shallowing slope, sometimes due to topographic control. There is no evidence for inflation in this set of flows using the data obtained in this study. The thickening towards the distal end and the fact that the thickness profiles show shorter, steeper flow fronts than for the pahoehoe flows (both in Elysium and in Alba as will be discussed later), are both indications that these are likely to have advanced as aa flows.

The flows appear to show cooling regimes similar to those that characterise lava flows on Earth, with increasing downstream and lateral resistance as each flow progresses. The cooling of the flows appears to have been fast at first and then levelled off as is reflected in the relative velocity plots for the flows. The decreasing velocity may also reflect a slowing in effusion rate. The shape of the velocity plots for the aa flows are different from the pahoehoe ones, since the aa flows have a sharper decline in velocity rates than the pahoehoe. This strengthens the idea that this set of flows advanced as aa with central channels where the surface of the flow is less insulated than when lava forms pahoehoe flows.

6.2 Modelling

6.21 Elysium Mons

Table 6.1 on the following page gives the maximum lengths and widths of each of the Elysium Mons aa lava flows and the average thickness (h) of each flow. The table also gives the area and volume of each flow, as well as the slope of the ground on which the flow was emplaced. Values for maximum width / maximum length (Wm) / (Lm), and also the distance to the maximum width / maximum length (DWm) / (Lm) are also given in the table. These are used to help to indicate whether the flow is of an S-type, as discussed the previous chapter. Inserting several of these values into the flow growth model (equation 6.2) gave the values for emplacement time, T, which are shown in Table 6.2.

$$\frac{(Wm/Lm)*H^2*\sin\alpha}{0.1} = T \qquad (6.2)$$

Flow Field	(Lm)	Wm	(Wm)/(Lm)	(DWm)/(Lm)	Area	h	Volume	slope
	Km	Km	%	%	km2	m	km3	degrees
17	35.6	4.9	0.138	64	79.7	18.0	1.4	0.978
19	17.4	2.5	0.141	72	35.6	13.4	0.5	1.142
21	21.8	3.4	0.157	46	48.8	11.4	0.6	1.114
24	13.3	4.9	0.370	89	48.0	28.1	1.3	0.612
28	31.7	4.4	0.140	60	101.2	19.6	2.0	0.708
35	57.4	11.5	0.201	20	341.6	45.8	15.6	0.412
36	61.6	14.7	0.239	24	274.0	18.1	5.0	0.393
39	25.3	4.9	0.194	68	76.2	17.6	1.3	0.973
40	20.1	2.5	0.122	16	33.0	28.1	0.9	0.614
41	17.4	4.7	0.268	6	40.3	15.2	0.6	0.930
43	10.1	2.0	0.195	93	15.4	13.9	0.2	1.039
44	22.8	4.4	0.194	48	60.3	15.9	1.0	1.061
46	45.2	5.4	0.120	96	120.8	22.2	2.7	0.706

Table 6.1: Table showing values of measurements made on all the Elysium aa flows. Lm is the maximum length, Wm is the maximum width and h is average thickness. Wm/Lm and distance toWm (DWm) as a percentage of the flow are used as one way to determine whether the flow is of the S-type (as described in Chapter 5).

Flow Field	T	Q	U	t_R
	days	x 10^3 $m^3.s^{-1}$	m.s-1	days
17	7.6	2.18	0.054	5
19	5.1	1.10	0.040	3
21	4.0	1.62	0.064	3
24	31.3	0.50	0.005	7
28	6.6	3.47	0.055	5
35	30.3	5.97	0.022	11
36	5.4	10.67	0.132	5
39	10.2	1.52	0.029	4
40	10.3	1.04	0.023	7
41	10.1	0.70	0.020	4
43	6.8	0.36	0.017	3
44	9.0	1.23	0.029	4
46	7.3	4.27	0.072	6

Table 6.2: showing values calculated by inserting the measurements in Table 6.1 into the flow growth model of Kilburn and Lopes (1991). T is the time taken to emplace the flow, Q is the effusion rate, u is the velocity and t_R is the time taken to emplace the flow calculated using a method derived by Crisp and Baloga (1990b) for comparative purposes.

From the emplacement time, T, other estimates can be made about the way each flow was emplaced. The effusion rate for each of the flows is calculated by dividing the volume of the flow (in metres^3) by the emplacement time (in seconds), to obtain a value of $m^3.s^{-1}$. The value has a magnitude of $x10^3$ due to the effects caused by gravity on Mars being about one third of the gravity on Earth. The calculation gives an average effusion rate, the actual value being greater at the beginning of the eruption and much less towards the end. Table 6.2 also gives the calculated average velocities for the flow. This is calculated by dividing the length of the flow (in metres) by the time taken to emplace the whole flow (in seconds). Lastly, t_R has been calculated for each flow. Since the flow growth model assumes that $ti=t_R$, then calculating t_R using the cooling model of Crisp and Baloga (1990b) should give similar values for emplacement times as those produced using the flow growth model. For basaltic and andesitic eruptions on Earth, t_R is approximately equal to h/4 (see Crisp and Baloga, 1990b, for a detailed discussion of their model), and this is how values of t_R in Table 6.2 have been calculated.

Using the flow growth model it can be seen that the Elysium Mons flows in this study were emplaced in times ranging between several days to around 1 month. Considering the magnitude of some of these flows, this would appear to be a relatively short amount of time. The calculated range of average effusion rates for these flows is 0.36 x 10^3 $m^3.s^{-1}$ to 10.67 x 10^3 $m^3.s^{-1}$. It is likely that the highest effusion rates for these eruptive events occurred at the beginning of the eruption when magma pressures were high, as this is typical of terrestrial volcanic eruptions (Walker, 1973; Thorarinsson and Sigvaldason, 1962). Also, the lowest effusion rates probably occurred towards the end of the eruption (Lipman and Banks, 1987), and may be due to lower pressure in the magma chamber, and also because of an intermittent supply of lava. Therefore, the actual range of effusion rates could be much greater than given here. The range of velocities calculated for this group of flows is between 0.005 $m.s^{-1}$ and 0.132 $m.s^{-1}$, which is between 18 metres per hour and just over 475 metres and hour. Of course, the range for this is probably greater too, as it is related to the effusion rate.

The values of t_R given in Table 6.2 are found to generally match the calculated values for T if the value of T is only several days, but where the emplacement time calculated is ≥ week then the values do not fit so well. The longer emplacement times relate to those flows that are relatively thicker than the rest of the flows in this group. This can be related to cooling, since the further a thinner flow has to travel, the faster it will need to travel in order to reach that point before cooling brings it to a halt. Thicker flows cool more slowly, owing to the ratio of surface area to volume, so can take longer to reach the same distance before cooling. As t_R is a measurement of cooling from radiative cracks in the crust of lava flows, it might not model these thicker flows so well because the cracks will cool and crust over eventually, reducing the rate at which heat can be lost.

6.22 Alba Patera

The way in which the measurements shown in Table 6.3 (below) were made has already been discussed in the previous chapter. Due to the fact that vent positions could be inferred for the Alba Patera flows, two values are present for many of the flows giving a maximum and minimum value according to the inferred (i) and traced (t) lengths of the lava flows.

Flow Field	(Lm)t	(Lm)i	Wm	(Wm)/(Lm)t	(Wm)/(Lm)i	(DWm)t/(Lm)t	(DWm)i/(Lm)i	$Area_{min}$	$Area_{max}$	h	V_{min}	V_{max}	Slope
	Km	Km	Km	%	%	%	%	km^2	km^2	m	km^3	km^3	degrees
1	66.8	127	3.8	0.056	0.03	40	68	165	314	20.47	3.38	6.43	0.780
4	51.7	125.5	4.5	0.087	0.036	72	88	134	324	23.11	3.10	7.49	0.545
6	91.4	145.6	6	0.066	0.041	70	81	306	487	23.88	7.31	11.63	0.659
7	20.1	42.7	2.3	0.112	0.053	58	80	33	67	18.07	0.60	1.21	1.881
8	90.4	224.9	8.5	0.094	0.038	49	80	342	644	24.40	8.35	15.71	0.576
11	50.2	58.7	3.3	0.065	0.055	96	97	129	150	20.54	2.65	3.08	0.186

Table 6.3: Table showing values of measurements made on all the Alba Patera aa flows. In this case measurements were made for both the inferred and the actual traced lengths, following the work of Lopes and Kilburn (1990)

The values in Table 6.4 have been calculated in the same way as for the aa flows of Elysium (Table 6.2). A range of values can be given for the aa flows according to the maximum and minimum lengths found for the flows.

Flow Field	T(min)	T (max)	Q(min)	Q(max)	u(min)	u(max)	tR
	Days	days	X 10^3 $m^3.s^{-1}$	x 10^3 $m^3.s^{-1}$	m.s-1	m.s-1	days
1	1.71	3.25	12.04	43.57	0.24	0.86	5.12
4	1.82	4.42	8.11	47.58	0.14	0.80	5.78
6	2.70	4.31	19.63	49.78	0.25	0.62	5.97
7	5.77	12.27	0.56	2.43	0.02	0.09	4.52
8	2.26	5.63	17.15	80.35	0.19	1.15	6.10
11	0.77	0.90	34.15	46.44	0.65	0.88	5.13

Table 6.4: Showing values calculated by inserting the measurements in Table 6.3 into the flow growth model of Kilburn and Lopes (1991). T is the time taken to emplace the flow, Q is the effusion rate, u is the velocity and tR is the time taken to emplace the flow calculated using a method derived by Crisp and Baloga (1990b) for comparative purposes. The table has more results than Table 6.2 for the Elysium aa flows because two length values were given for each of the Alba Patera flows as mentioned previously.

The emplacement times calculated ranged between less than a day and just over 12 days. Given that the traced lengths of the flows were all tens of kilometres long, and some of the inferred lengths were over one or two hundred kilometres in length, the short emplacement times seem surprising and point to high effusion rates and velocities. Values of t_R generally fit well with the values for T (max) that have been calculated from the inferred flow lengths. However, the values do not fit well with those of flow 11 that had a short emplacement time of between 0.77 and 0.9 of a day. In this study therefore, the t_R calculation is not the best way to model the duration of flows that are emplaced in a short period of time time (less than a day).

The range of effusion rates calculated for these flows was 0.56 x 10^3 $m^3.s^{-1}$ to 34.15 x 10^3 $m^3.s^{-1}$ when using the traced flow values, and 2.43 x 10^3 $m^3.s^{-1}$ to 80.35 x $10^3.s^{-1}$ using the inferred flow lengths. Although, as mentioned for the Elysium lavas, the actual range may have been far greater due to varying effusion rates throughout each eruptive event. Using these values of effusion rate the velocities calculated ranges between 0.02 and 0.65

$m.s^{-1}$ for the traced flow lengths and 0.09 to 1.15 $m.s^{-1}$ using the inferred flow lengths. This corresponds to a range of 72 metres to 2.34 kilometres per hour for the traced flows or 324 metres to 4.14 kilometres per hour for the inferred flows.

6.23 Analysis

In general the Elysium and Alba Patera lavas differ in several ways. The Elysium lavas appear to have been emplaced more often as sheet flows, whereas those in Alba almost all seem to have advanced via channels at some point in their emplacement. Both sets of flows were affected by small changes in slope, but the Elysium flows appear to have been more affected by topographic obstacles and also by the sub-surface volatiles that were present at the time of emplacement (see Chapters 3 and 4). Both sets of flows generally show a typical thickening towards their distal ends and have been subject to similar cooling and rheological controls as terrestrial lavas, making the use of the flow growth model relevant.

Flow thickness values in Elysium range between 11 and 46 metres, and at Alba the range of flow thickness values is smaller, between 18 and 24.5 metres. Flow lengths at Elysium Mons are generally shorter than at Alba Patera, the traced extent of the flows at Elysium ranging between 10 and 62 kilometres, but at Alba this range for traced flow length being 20 to 91 kilometres. Since the Alba flows are generally longer and thinner it may be expected that the flows would travel faster, due to the reasons explained in the previous section. Maximum widths for the Elysium flows seem variable, having a range of between 2 to ~15 kilometres, and at Alba the flow widths appear to have been more steady at 2.3 to 8.5 kilometres. This may provide further evidence for the way both sets of flows are thought to have advanced. The channelised aa flows might be expected to all have similar widths since the bounding of the flow by levées will have inhibited spreading. The Elysium flows, emplaced as sheets of aa, might have been expected to spread out more and attain greater widths than flows bounded by levées. Slope values for both areas appear to have been similar, Elysium slope values ranging between 0.4 and 1.15° and Alba ground slopes being between ~0.2 and 2°.

The emplacement times calculated using the flow growth model are different for both of the areas. The emplacement times of the Elysium flows are generally longer than those for the Alba flows. Therefore, the resulting effusion rates and velocities calculated are higher for Alba Patera than they are for Elysium Mons. Comparisons between the two are not equally based, since some of the values calculated for Alba Patera have used values from the inferred flow lengths. However, even comparing results produced using the traced flow values from each area (rather than the inferred lengths at Alba), there is clearly a difference between the two areas. Some of the traced Alba flows have been emplaced in a few days, sometimes in less than a day, and the longest emplacement time was just under 6 days. In contrast, the fastest Elysium flow was emplaced in 4 days and most flows took ~ 2 weeks or longer to be emplaced. Maximum effusion rates at Alba Patera calculated for the traced flows are larger by 20 x 10^3 $m^3.s^{-1}$ (20,000 $m^3.s^{-1}$). Where flows in Elysium can travel up to ~1/2 kilometres in an hour, the flows in Alba Patera have been calculated to travel over four times this distance in the same amount of time.

There could be many reasons for the differences found between these two lavas. Aa flows that are emplaced as sheets rather than via channels tend to take longer to be emplaced (Kestheyli & Self, 1998), as a channel provides the most effective way to transport the lava quickly. Since the Elysium flows are thought to have been emplaced more often as sheet flows and the Alba ones more often as channel flows, this could be one factor in the marked difference in velocities and emplacement times. Secondly, the two volcanoes studied in this thesis are of two different types, and thus may have completely different lava compositions and eruptive mechanisms. The fact that Alba Patera is longer-lived than Elysium Mons (Plescia and Saunders, 1979; Scott and Tanaka (1980, 1986), Cattermole, 1990) may mean that the magma reservoirs of Alba Patera had longer to develop and magma had longer to differentiate before eruption, thus it could very likely have erupted lava of a different composition from Elysium Mons. The summit of Alba Patera exhibits evidence for several caldera collapse events (Cattermole, 1990) and shows that these did not all occur in one place on the summit, as in the case of Elysium Mons (see Chapter 6). It is likely that Alba Patera had a well-developed magma reservoir system. Elysium Mons is thought to have been the product of a vent-shift event (see Chapter 3), and Mouginis-Mark & Rowland (2001) determined that the caldera formed from a single

collapse event. Therefore the magma reservoir system may not have been so well developed or long-lived as at Alba Patera, and thus the magma may not have had much time to differentiate. Therefore lavas at Alba Patera may be more evolved and be more like basaltic andesite in composition, as suggested in the work by Schneeberger and Pieri (1988). Effusion rates may also be different because magma chamber sizes could have varied between the two volcanoes, and they may also have depended on how easily magma could travel to the surface.

Lastly the probable presence of sub-surface volatiles in the Elysium region, as evidenced by many different features that were discussed in the mapping chapter (Chapter 4) as well as by Carr and Schaber (1977), Christiansen and Greeley (1981), Baker (1982), Hale (1983), Mouginis-Mark et al. (1982), Mouginis-Mark et al. (1984), Mouginis-Mark (1985), and Cave (1993) may have affected the way the flows were emplaced. The interaction of the lava flows with sub-surface water may have caused phreatomagmatic explosions to occur that disrupted the flows as they were emplaced. Potential craters formed in this way were observed in the Viking images of at least one of the flows in Elysium (see Chapter 4). Although there are many channels on the flanks of Alba Patera which could potentially be fluvial (Gulick and Baker, 1990), it is unclear whether the Alba flows studied in this thesis ever did interact with water or other volatiles during emplacement. Therefore the disruption of the Elysium flows as they were being emplaced may be another factor which made the flows at Elysium flow differently from those at Alba Patera.

6.3 Results of pahoehoe flows

6.31 Elysium Mons pahoehoe flows

Eleven of the Elysium flows studied are thought to be pahoehoe flows. These are flows 22, 23, 26, 30, 31, 32, 45, 47, 48, 50 and B and their positions are shown in Figure 6.22. Many of these flows occur closer to the central vent of Elysium Mons than the aa flows, and are not scattered amongst the aa flows, but occur in groups. This is probably to be expected because the same source of lava and similar conditions of emplacement, such

as regional slope, would be expected to lead to similar types of flow emplacement. Only one of these flows has a central channel, which is more likely to have been a collapsed lava tube than an open channel when the flow was emplaced, since tubes are more common in pahoehoe flows than aa ones.

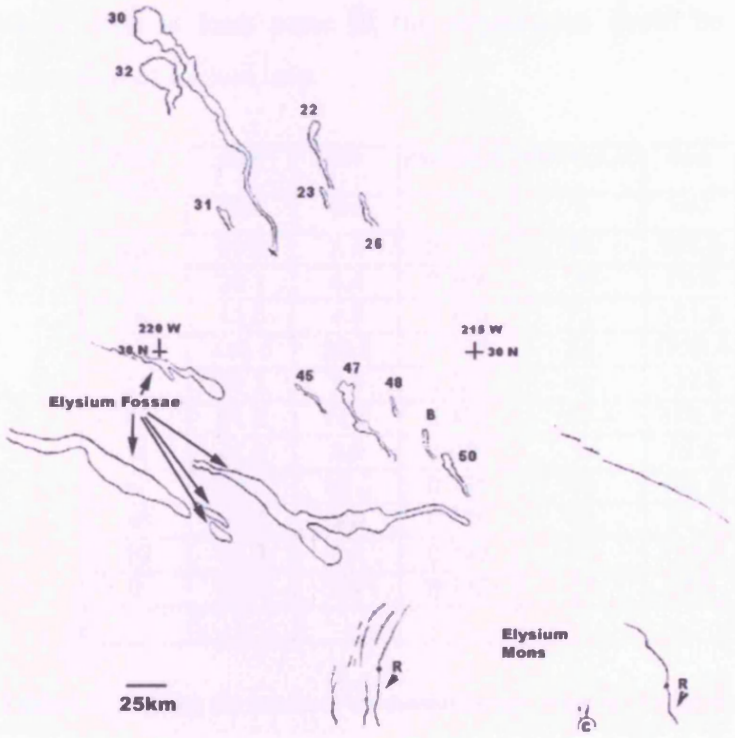

Figure 6.22: Sketch map of the northwestern flank of Elysium Mons and surrounding plains. The positions of the pahoehoe lava flows analysed in this study are shown. The areas labelled C and R indicate the positions of the Elysium Mons caldera (**C**) and various prominent ridges (**R**) around the Elysium Mons volcanic edifice.

6.31(a) Appearance

Table 6.5 shows the results of the measurements made on the Elysium Mons pahoehoe flows. Just over half of the flows increase in width towards the end of the flow, with the rest of the flows maintaining a generally constant width along the whole of their lengths. The average maximum width is 9.4 kilometres, although flows 30 and 32 have maximum widths of over 20 kilometres. Several of the flows exhibit 'ridge-like' features,

and many have depressions on their surfaces (see Figures 6.23 and 6.24). Since none of the flows have been imaged by MOC, it is difficult to assess whether these features are evidence of inflation. They are rather larger than typical terrestrial inflation features (tumuli and inflation pits etc.), being at a scale of hundreds rather than tens of metres in size. Many of the depressions may be impact craters that are just beyond the limit of the resolution of the images. Since it has been proposed by many researchers, as well as in the present study (see Chapter 4), that there is much ground-ice present to the north of Elysium Mons, then at least some of the depressions could be explosive pits formed by the interaction of ice and lava.

Flow Field	(Lm)	Wm	(Wm)/(Lm)	(DWm)/(Lm)	Area	h	Volume	slope
	Km	Km	%	%	km2	m	Km3	degrees
22	61.9	7.4	0.119	94	155.5	22.2	3.4	0.938
23	24.1	4.4	0.184	35	75.6	9.9	0.8	1.066
26	43.5	4.9	0.113	71	161.0	14.2	2.3	1.425
30	185.3	25.5	0.138	94	1723.4	21.0	36.2	0.450
31	32.2	7.4	0.229	10	137.8	13.6	1.9	1.298
32	51.8	22.6	0.436	67	674.1	63.0	42.5	0.303
45	41.0	3.9	0.096	7	76.6	10.1	0.8	0.641
47	82.2	10.3	0.125	85	430.2	33.9	14.6	0.709
48	22.3	3.9	0.176	22	58.1	17.5	1.0	0.569
50	32.9	8.1	0.246	75	138.2	16.2	2.2	0.673
B	29.9	5.2	0.172	21	36.6	19.2	0.7	0.688

Table 6.4: showing the results of the measurements made on the Elysium pahoehoe flows. These measurements are similar to those shown in Table 5.1 for the Elysium aa flows.

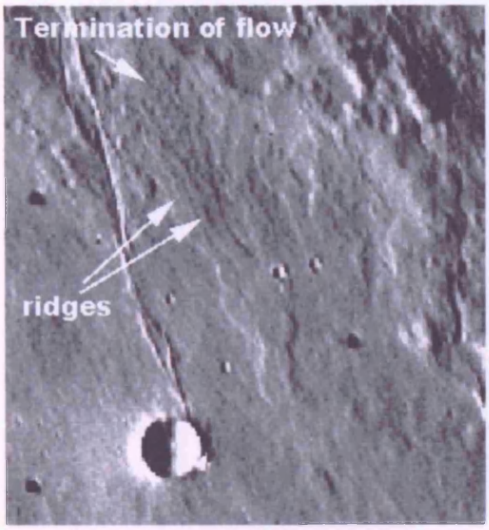

Figure 6.23: part of Viking image 541A25, showing lava flow 31. The flow surface exhibits several ridges unlike any seen on the aa flows in this study. For scale, the largest impact crater in the image is 4 kilometres in diameter and north is towards the top.

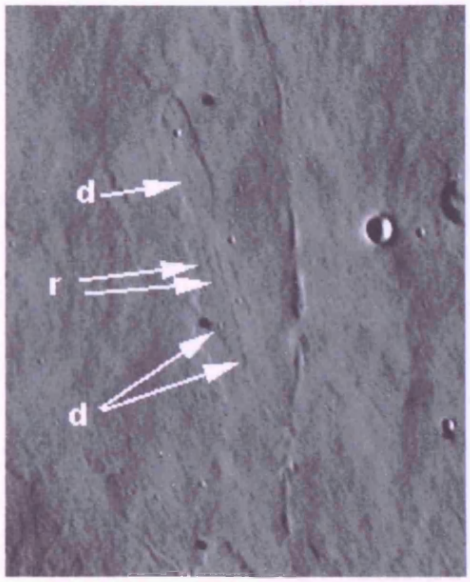

Figure 6.24: part of Viking image 541A27 showing lava flow 23. Depressions (**d**) and ridges (**r**) can be seen on the flow surface and the flow appears to be thin because it casts little shadow in places. The image is 36 kilometres across and north is towards the top.

Obviously, the resolution of the images does not allow reveal the detailed surface texture of the flows, however, they do not have the sheet-like appearance of the aa flows. The flows appear to have changed direction as they flowed, more often than the aa flows, which is consistent with the mode of advance of pahoehoe flows by the production of small tongues and lobes of lava breaking through a thin crust.

Flows 30 and 32 are the two most unusual flows of this set, flow 32 being wider and thicker than the rest of the flows in this section, and flow 30 being longer and wider than the rest. These flows do have a sheet-like, almost tabular appearance, and have an unusual pitted surface texture (see Figure 6.25). As will be explained in the next section, they have both been highly controlled by topography during emplacement, and it is proposed in this study that the flows travelled over ice-rich ground as they were emplaced, thus creating explosions that formed pseudocraters, the source of their pitted appearance.

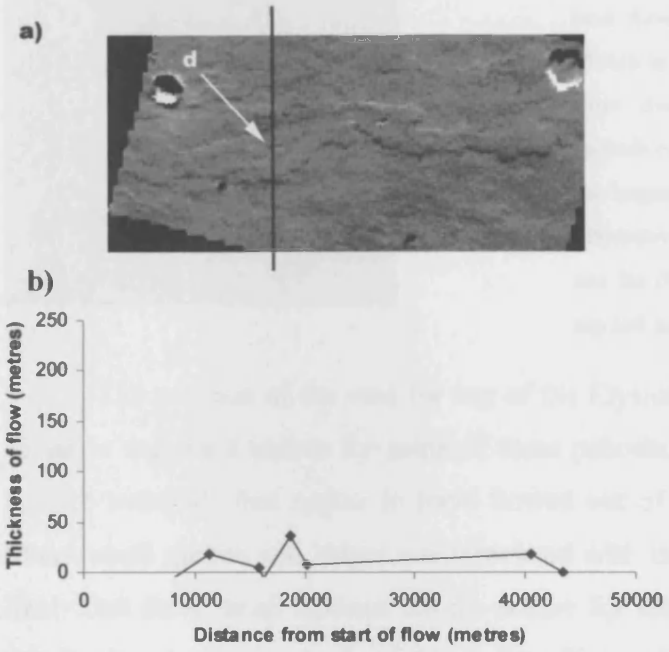

Figure 6.26: (a) Part of Viking image 541A27 showing lava flow 26. The depression indicated at **d**/black line appears to have been measured by MOLA instead of the surrounding surface and has produced an anomalously low thickness value in the longitudinal flow thickness profile shown in part **(b)**. North is towards the bottom right of the image in **(a)**. This flow has a thickness profile that is typical of pahoehoe flows, having a long front/snout that does not thicken as much as the aa flow fronts do.

The one flow that exhibits an obvious 'channel' is flow 50. The channel is not as well defined as those for the aa flows, where the transition from channel base to levée is well defined in the images. Therefore, it seems more likely that this channel was formed by the subsequent collapse of a lava tube roof once the lava had stopped flowing through it. It is possible to see an area where the channel appears to have formed by the coalescence of several pits (see Figure 6.27).

again implies that the crust has thickened somewhat, due to cooling, and will have been an important control on how far the flow could spread. These two results show that, although the flows may have advanced under an insulating crust, substantial cooling still occurred. However, once the flow had halted due to cooling, inflation may have subsequently occurred, giving the lava enough strength to puncture the crust and continue to move forwards, forming a breakout, as apparently happened in the cases of flows 22 and 45. The plot of the ratio of lateral resistance against downstream resistance does not show any trend. This is interpreted to mean that both factors are equally important in controlling the extent of the flow at the start of each flow as they are towards the distal ends.

The plots of thickness against width show a positive trend, as they do for the aa flows. This is probably due to the increased hydrostatic pressure exerted at the centre of thicker flows as explained in section 6.11(b). The h/w against slope graphs do not show a trend for the pahoehoe flows. This was expected because, as found when examining the thickness and slope profiles, the flows generally do not seem to have changed thickness or width in response to a change in slope.

The most interesting graphs, however, are the plots of velocity against distance. These show a general decrease, as would be expected, and show that velocity appears to have been constant most of the way along the flow before gradually decreasing towards the end (see Figure 6.35). The relative velocities of these flows are lower than those of the aa flows, particularly at the start of each flow. The plots do not exhibit the pattern shown by the aa flows where the velocity at the start of the flows decreases sharply before levelling off. It is proposed then that this is further evidence that these flows advanced as pahoehoe, since the insulating crust would mean that heat would not be lost so quickly as with the open aa channels, so the decline in velocity would be more gradual (Pinkerton & Wilson, 1994; Keszthelyi, 1995; Dragoni et al., 1995; Sakimoto et al., 1997; Keszthelyi & Self, 1998).

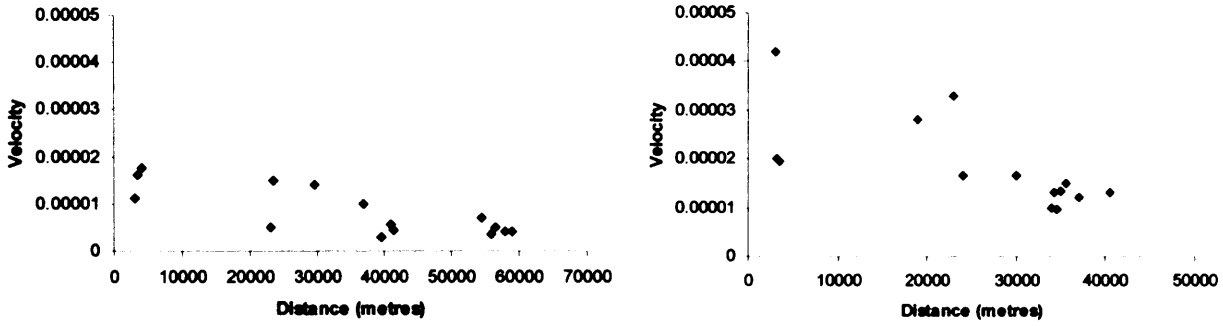

Figure 6.35: Two velocity plots, one for an Elysium pahoehoe flow (flow 22, left) and one for an Elysium aa flow (flow 46, right). The aa flow exhibits a steeper curve at the beginning, whose slope decreases halfway along the flow. The pahoehoe flow shows a shallower curve and a steadier decline in velocity. This is thought to be highlighting differences in the mode of advance for each type of flow. The plots are typical for the flows in each group, and velocity was determined using the value 1/cross-sectional area at each measured point along the lava flow.

General Mode of Emplacement

The thickness profiles produced are typical of pahoehoe flows, showing either that the flows had a similar thickness all along the flow, or that the flow front has a less steeply sloping front than the profiles of the aa flow fronts. The general lack of correlation between flow thickness or width with changes in slope may be taken as evidence for inflation, since any changes that did occur due to changes in slope may have been obscured by the subsequent thickening of the flow by inflation. This may help to explain why many of the flows appear to have a similar thickness all along their lengths. Other evidence for inflation includes the pits and ridges that have been observed in some of the images of the flows.

At least two of the flows advanced by breakouts, and more may have done so but have later been obscured by inflation. The velocity of the flows is relatively slower than that of the aa flows in the previous section, and overall shows a slow but steady decline possibly indicating that the flows were insulated during their advance. This may explain why the longest of all the Elysium flows in this study is found in this set of lava flows, since the lava can travel further because it stays hotter longer than lava travelling in an open

channel. Cooling has still been found to be an important control on the flows though, and probably produced thicker crusts that meant that any further growth of the flow would have to follow a period of inflation. The flows are generally thinner than the aa ones, which is typical of pahoehoe flows, but the thickest of all the flows studied in Elysium also occurs here. This thicker flow has been inferred to have formed by the infilling of a topographic depression, which may have been aided by inflation of the flow. Indeed, topographic features seem to have been an important control on the emplacement of these flows, and slope does not appear to have had such a great effect.

The source of lava can be inferred for more of these flows than for the aa flows, since these flows are surrounded by more small vents and ridges. The sources of some of the flows are apparently related to the Elysium Fossae. In fact, some of the flows may have been emplaced upon some of the muddy/watery deposits erupted from the Fossae, since features that may be explosion pits have been observed on at least two of the flows, thus indicating the occurrence of phreatomagmatic activity.

6.32 Alba Patera pahoehoe flows

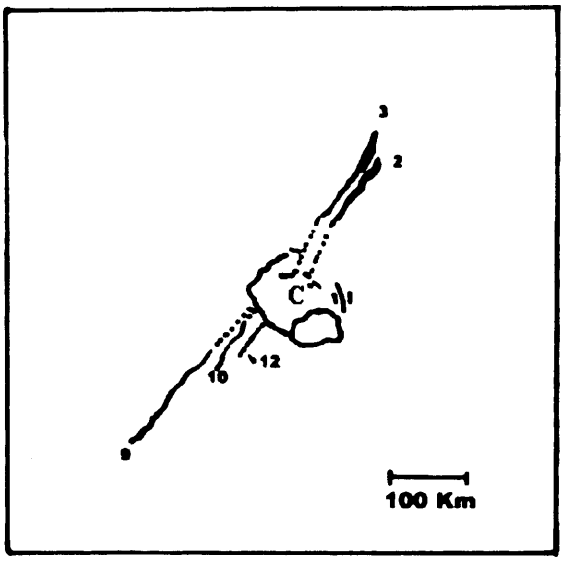

Figure 6.36: Sketch map showing the positions of the 5 pahoehoe flows analysed in this study. The flows have been numbered according to the work of Kilburn and Lopes (1991) and the map has been modified from the same paper. The feature labelled C is the caldera complex of Alba Patera. The positions of some of the graben are indicated and the inferred length of each flow back to the source is indicated by the dotted line. The flows appear to occur in groups at two particular points on the edge of the caldera.

Of the five flows that were found to be pahoehoe at Alba Patera, three of them (flows 2, 9 and 10) show significant widening towards the distal ends. The flows appear to occur in groups as is shown in Figure 6.36. Flows 2 and 3 occur close together on the north-east side of the summit, and flow 9, 10 and 12 occur close together to the south-west of the caldera. It is therefore possible to assume that each group formed from similar magma supplies and were emplaced on similar regional slopes. No central channels would be expected if these were pahoehoe flows, and indeed no central channels are visible in any of the images of the flows.

6.32(a) Appearance

Table 5.6 shows the results of the measurements made on the Alba Patera pahoehoe flows. Two sets of values are given for some of the measurements since vents for the flows in Alba Patera could be inferred, and thus an inferred and a traced value are given (see previous chapter). Some of the flows have been found to increase in width towards their distal ends, with the average (maximum) widths of the flows ranging between 2.8 and 11.3 kilometres, and an average (maximum) width for all the flows being 6.94 kilometres. The widths of the flows are generally variable along the lengths of the flows, with the maximum width generally being located in the distal 50% of the length of each flow (see Table 5.6). The average (maximum) width for this set of flows is smaller than that of the Elysium pahoehoe, but larger than the average (maximum) width for either of the two sets of aa flows in this study.

Shadow lengths in the Viking images show that the flows appear to be relatively thick compared to the pahoehoe flows studied at Alba Patera for this thesis. Indeed, the average thicknesses of these flows as measured by MOLA range between 17.77 metres and 36.87 metres, with an overall average thickness value of 27.98 metres. This average thickness value is larger than that for any of the other sets of flows in this study. The range of thicknesses is however similar to that of the Elysium pahoehoe flows (except for flow 32, see section 6.31(a).

Rheological Controls

Of all the plots of the various measurements made on these flows, there are only two that show obvious relationships. The plots of velocity show that these flows moved slowly relative to similar plots for the aa flows and that the values for velocity remained similar all along the lengths of the flows. The flows did not experience a sudden decrease in velocity at the beginning of the flow as the aa flows did, but the velocity did decrease towards the distal ends of the flows (see Figure 6.40). This would fit with the idea that these flows were emplaced under an insulating crust so that the heat loss from the lava occurred more slowly than for the aa flows.

The plots of thickness values against width values show a positive trend and clearly show that these two factors are related. The trend means that the thickness value increases as the width increases, and that if one decreases so will the other. Since some of the flows have been observed to thin as they widen this result might seem surprising. However, it is a general result and could be an indication that many of the flows underwent inflation during or after they were initially emplaced, thus eventually making flows thicker at points where they initially thinned due to other factors such as widening.

The fact that no relationship has been found between h/w and slope highlights the finding in the previous section that changes in thickness are not necessarily related to slope for this set of flows. Also, no relationships have been found between downstream resistance and distance from the start of each flow, lateral resistance and distance from the start of each flow, or for the ratio of downstream resistance to lateral resistance. The downstream resistance plots either display similar values all along a flow, or have many different values at around the same distance along a flow. If the flow is travelling in an insulated tube and the lava loses heat slowly then it might be expected that the downstream resistance would not increase significantly along most of the flow because it will not be cooling or crystallising very much, which are major factors in increasing downstream resistance. This is also true for lateral resistance and so therefore the ratio between these two factors is not likely to show a pattern either.

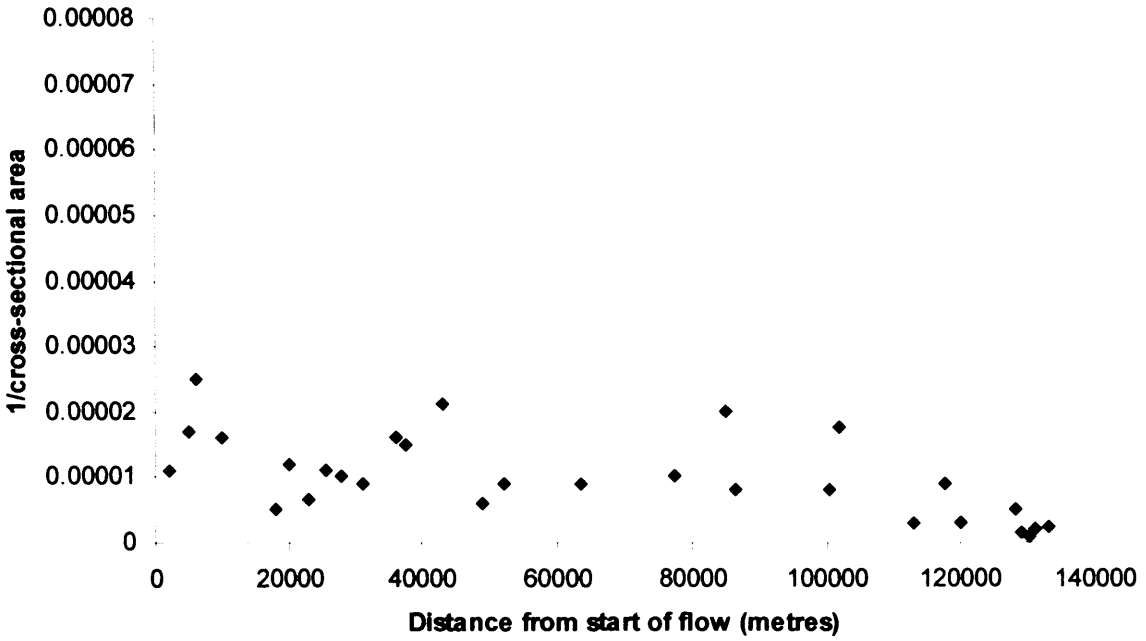

Figure 6.40: Plot of velocity (1/cross-sectional area) against distance for flow 9 at Alba Patera. The values for velocity stay relatively constant along the flow, only decreasing markedly in the last 20 kilometres of the flow. This could indicate insulated flow of lava in tubes which reduces the rate at which lava loses heat. This plot can be compared to the plot in Figure 6.21 to show the difference between a typical pahoehoe velocity plot and an aa one.

General Mode of Emplacement

These flows appear to have been emplaced in two areas on the summit of Alba Patera and thus each group of flows is assumed to have similar source magmas and to have flowed over similar regional slopes. The average thickness of these flows is greater than for any of the other sets of flows in this study, and changes in thickness do not appear to be related to changes in the angle of slope. Relationships found between thickness and width suggest that the flows may have grown in thickness by inflation, thus explaining the large average thickness and the fact that it often appears that emplacement of the flow was not affected much by changes in slope. The segmented appearance of the thickness profiles might therefore have been caused by the inflation of the flow after initial emplacement, but may also be due to the lack of enough measurements from MOLA.

Two of the flows have advanced by breakouts. Generally the surfaces of the flows are smooth and tabular and the boundaries are irregular, with many protrusions that may have been the start of failed breakouts. It is proposed that these flows advanced by the creation of small lobes and tongues of material from the front of the flow, which sometimes produced large breakouts that altered the direction of advance. There has been little obvious topographic influence on these flows.

6.33 Analysis

It is difficult to compare the Elysium lava pahoehoe flows with those at Alba Patera, because no duration times for the emplacement of the flows were calculated. However, of the analyses made of the emplacement of both sets of flows it is clear that they show similar styles. Both sets of flows show two or three examples of advance by breakouts, and also possible evidence for inflation. It is also thought that the lobate nature of the flow boundaries is evidence for the advance of these flows by the repeated puncturing of the crust and the production of lobes and tongues of material. Changes in slope do not appear to have had such a great effect on the pahoehoe flows as it did on the aa flows. However, this is probably misleading, as any changes in thickness due to slope may have been obscured by post-emplacement inflation.

This study shows that slopes at Alba Patera are shallower than at Elysium. The range of average slope values for Alba Patera is between 0.234 and 0.476 degrees, whereas the range in Elysium is between 0.303 and 1.425 degrees. The average thicknesses of flows at Alba Patera are generally greater than for the flows at Elysium Mons, although the range of thickness is similar when flow 32 is omitted, as it is an unusual case. The generally greater thicknesses at Alba Patera may be related to the lower slope values observed, and may also have been caused by a greater proportion of inflation at Alba Patera, than at Elysium Mons. Half of each of the sets of flows are found to widen towards the distal ends of the flows, but at Elysium they reached greater widths. It would therefore seem that the Elysium Mons flows tended to widen more as they advanced, and the Alba Patera flows preferentially thickened. This may have been related to differences in the rates of cooling and production of crust, since faster rates of cooling will produce thicker crusts that inhibit

lateral flow thus forcing the flow to thicken by inflation. The thickness profiles of the flows are different in some ways. Both sets of flows show examples of 'typical' long, thin pahoehoe flow fronts. Of those that do not show this pattern, the Elysium flows have thicknesses that are constant along the whole length of each flow, whereas those at Alba Patera show much variation in thickness where they repeatedly thicken and thin. The Alba Patera flows may show this pattern because the flows had to inflate before advancing further via breakouts.

In appearance, the two sets of flows were noticeably different. The Alba Patera flows have smooth and tabular, almost featureless surfaces except for the many small impact craters visible, with no obvious pits or ridges. In comparison, the Elysium flows exhibit several examples of ridges and depressions, and one flow displays a set of coalescing depressions, which may be the surface expression of a collapsed lava tube as is often observed on Earth (Oberbeck et al., 1969; Carr et al., 1977; Mouginis-Mark et al., 1988; Sakimoto et al., 1997). Two of the Elysium flows appear to have flowed over ice-rich ground producing an unusual pitted appearance. There are several examples in the set of Elysium flows, where the flows had been diverted or affected by topography, but the Alba Patera flows do not appear to have been so influenced by topographic obstacles.

It is possible in some cases in both areas to infer vents that are likely to have been the source of lava flows. It is generally difficult to see vents for most of the flows (aa or pahoehoe) at Elysium. However, it is easier to infer vents for the pahoehoe flows since many of them originate in the 'vent flow' unit (see Chapter 4), where there are many small chains of hills, ridges and sinuous rilles (see Chapter 4) which are probably similar in appearance to those features that acted as vents for some of the Elysium flows. Interestingly, flow 30 appears to have issued from one of these ridges. The vent flow area is associated with the Elysium Fossae, so the flows erupted from the Fossae (unit **Elf**, see Chapter 4) may have been similar to the pahoehoe flows in this study. The vents for the Alba flows were inferred by Kilburn and Lopes (1991) as discussed previously. It is interesting to note that the pahoehoe flows in both areas appear to have been erupted in groups, and also generally occur closer to the summits of the volcano than the aa flows. They may be closer to the summit because they were late-stage eruptions that were emplaced when effusion rates were lower.

Comparisons of some of the pahoehoe plots with those of the aa flows show that there appear to be significant differences between the aa and pahoehoe flows. The most obvious are the shapes of the longitudinal thickness profiles, and also the change in velocity graphs. The thickness profiles for the pahoehoe flows are generally thinner than the aa ones, and have longer, less steeply sloping flow fronts. The velocity profiles clearly show that in a number of places the pahoehoe flows did not have a rapid decrease in velocity towards the start of the flow, but maintained a steady speed along most of their lengths. This would be expected of a flow where the lava is insulated as it flows within a tube, because cooling would be more gradual. The insulated nature of the pahoehoe flows may therefore explain the great lengths reached by some of the flows. Several of the pahoehoe flows from both areas reached traced lengths of 100 kilometres or more. Although many of the Alba Patera aa flows reached similar lengths, that was probably achieved by the faster flow of the lava. The pahoehoe flows may have been able to travel these great distances at a slower pace, simply because they were insulated.

6.4 Initial conclusions of lava flow study results

It is clear from this study that there are two main sets of flows in addition to the two types of flows (S-type and M-type) found by Lopes and Kilburn (1990). The flows can be divided into aa or pahoehoe by the values obtained for $h\sin\alpha$ (as a measure of apparent yield strength/downstream resistance), and also by carrying out fractal analysis of the margins of each flow. The aa flows appear to have flowed as channels or sheets, and appear to have undergone similar emplacement and cooling regimes as lava flows on Earth. They were therefore ideally suited to the use of the flow growth model.

Estimates of duration times, and therefore effusion rates and velocities as well, could not be calculated for the pahoehoe flows given the lack of visible or measurable fissure lengths. However, it is clear from the generalised velocity profiles that these flows did have steadier velocities during most of the eruptive episode than the aa flows. Where changes in slope do not appear to have caused a change in flow thickness or width in the pahoehoe flows, post-emplacement inflation has been invoked as a mode of growth for the flow, which will obscure changes in thickness due to slope. Although few features that

may be caused by inflation are visible, this does not necessarily exclude this process and may infer that the inflation process on Mars either occurs differently from that on Earth, or may just produce different features.

The aa and pahoehoe flows appear to have advanced differently at each volcano. The Elysium aa flows are thought in this study to have advanced as sheet flows rather than via channels, whereas many of the Alba Patera aa flows probably advanced via channels. This may at least partly explain the differences observed in the emplacement times of the two sets of flows. The pahoehoe flows also appear to have advanced differently, with the ones at Elysium tending to widen as they advanced, whereas the ones at Alba Patera appear to have thickened more than widened. Analysis shows that the flows in Elysium appear to have been more affected by topographic obstacles than the aa flows at Alba Patera, but this is probably due to differences in terrain at each volcano, rather than differences in the flow characteristics. In both areas the aa flows seemed to be more affected by changes in slope than the pahoehoe lavas, although as mentioned previously this is thought to be the result of post-emplacement inflation in the case of the pahoehoe flows.

Although the thickness and slope measurements made using MOLA data are a great improvement on those values used in previous studies, the results in this chapter are still subject to measurement errors, and errors inherent in the flow growth model that were discussed in Chapter 5. It has been estimated that the errors on measurements made result in a total error of +/- ~25%. The errors on the terrestrial data and Alba Patera data used in the studies by Kilburn and Lopes (1991) and Lopes and Kilburn (1990) were around +/- 80%. It seems unlikely that errors on measurements of thickness and slope in the current study are as high as those for terrestrial lavas owing to the fact that there are fewer topographic variations on Mars than on Earth. Also the MOLA data are more accurate than the estimates of thickness and slope used by Lopes and Kilburn (1990), thus the results presented here are an improvement on the previous study of Alba Patera. Comparisons between the results found in this study, and results found in previous studies of lava flows at Elysium and Alba will be given in the discussion chapter (Chapter 7). Implications for general Martian volcanism, as well as those for terrestrial volcanism will also be presented in Chapter 7.

7.0 Discussion and conclusions

The MGS mission has provided a wealth of data concerning the geology of Mars, and it continues to do so. Combining the MOC and MOLA data with previously existing data and research has enabled useful results to be produced in the current study. These results have important implications for Martian and terrestrial geology, which will be discussed in this chapter. A review of the uses of the MOLA data set as a geological tool will also be given.

7.1 The geology of the area surrounding the Elysium Montes

7.11 Evolution of volcanic centres

The results from the mapping chapter (Chapter 4) helped to establish the relative ages of each of the volcanic constructs in the mapping area, and highlighted some surprising features of Elysium Mons. It has become clear from the contour maps and topographic profiles drawn across the volcano that Elysium Mons is offset from the centre of the topographic high often referred to as the "Elysium Bulge". It is inferred in this study that Elysium Mons has been emplaced as a separate volcano on the upper flanks of a larger, older volcano (termed the AVE) that is responsible for much of the volcanic material observed around the Elysium Montes at the current time (see Figure 4.2 in Chapter 4). The material from the AVE is thought to have embayed and surrounded the volcanic constructs of Hecates Tholus and Albor Tholus before growth of Elysium Mons commenced.

The fact that Elysium Mons has been emplaced as a 'summit cone' on the flanks of the AVE, implies that there has been a shift in vent activity in this area at some point in the past. Elysium Mons was emplaced ~100kilometres to the northeast of the vent for the AVE, which is thought in this study to have be infilled by younger flood lavas after the emplacement of the main edifice of Elysium Mons. As suggested in Chapter 4, these younger lavas may have resulted from the formation of ring dykes around the older volcanic complex. A similarity between the Elysium Mons volcanic complex and the terrestrial volcanic complex at Ardnamurchan has already been discussed in Chapter 4.

Although this led to the suggestion that the arcuate graben around Elysium Mons may be the surface expression of ring-dykes and cone sheets that occurred during the formation of the AVE caldera, it did not indicate a reason for the shifting of vent positions. It is possible in the case of the Elysium volcanic complex that a change in the magma source occurred and that this new magma supply created different lava conduits to the surface. Alternatively, the lava conduits that supplied the AVE may have become blocked, perhaps owing to pauses in magma supply, and the lava exploited new pathways to the surface and began to erupt from a different location ~100 kilometres from the original vent. Shifting positions of magma reservoirs have been implied in the formation of the caldera complex of the Martian volcano Ascraeus Mons (Scott and Wilson, 2000). In this case Scott and Wilson (2000) proposed that there has been cyclical oscillation between one large central magma reservoir and several, smaller peripheral reservoirs. They state that this implies substantial variations in both position and rate for the magma supply from the Martian mantle, as well as for the distribution of stresses within the volcanic edifice. Variations in the distribution of stresses within the AVE, perhaps owing to tectonic activity or changes in magma pressure, may have been a further contributing factor in the vent shift at the AVE/Elysium Mons volcanic complex.

The terrestrial volcano Mount Etna that is located in Sicily, Italy, should be mentioned at this point, because it is an active volcano which exhibits an element of vent shift and probable changes in the position of magma reservoir, and may thus provide an insight into the plumbing of the AVE/Elysium Mons volcanic complex. At present the volcano has a central summit cone in which several volcanic craters exhibit almost constant activity. This is apparently fed by a central conduit supplying magma from a reservoir that is approximately 20 kilometres below sea level (Chester et al., 1985). However, in the late-sixteenth and seventeenth centuries, the output rate of lava was considerably higher than it is now, and the texture of the lava erupted was different. This implies that conditions within the magma supplied to the surface were different, and also that there were probably differences in the magma ascent rate and plumbing of the volcano, compared to present day conditions (Guest and Duncan, 1981; Duncan and Guest, 1982). Further back in time than this, volcanic activity at Mount Etna comprised of several episodes of caldera collapse, combined with pyroclastic flows and the emplacement of lava domes. The compositions of

material erupted suggests that there were high-level magma storage systems, perhaps existing as a plexus of dykes beneath the volcano down to depths of ~3kilometres below sea level (Guest and Duncan, 1981). Chester et al. (1985) state that conditions such as these may only have been temporary and that for much of the life span of the volcano the larger, deeper magma reservoir fed activity at the surface. Field evidence shows that shifts in position of the central conduit have occurred over time at Mount Etna (Chester et al., 1985 and references therein). Although the cause of this is unknown, it has been suggested by Maguire (1983) that magma rising from depth enters a 'clearing house' from which the magma is distributed via an intersection of dykes and fissures to other parts of the volcano including the summit.

Clearly it is impossible to decide, simply from photogeological analysis, the major reason for the vent shift observed at Elysium Mons. However, the author proposes that the vent shift was a major event that occurred over a relatively short period of time. This is because, although no major unconformity was observed in the images, no evidence for other major summit vents was found. The mechanism favoured for this shift in vent position is that a change in the rate of magma supply under the AVE caused some of the conduits feeding the main vent of the volcano to become blocked. In this case the magma exploited new paths towards the surface and may have collected in a complex of dykes and fissures to form a high-level magma reservoir under the location now occupied by the younger volcano, Elysium Mons. Magma would then be preferentially distributed to this volcano and activity at the vent of the AVE would cease until the final event that formed the younger lavas of **EM2** (Elysium Mons unit 2 – young flow).

Topographic profiles across Elysium Mons show that the north-eastern flank of the volcano appears to be the site of concentrated lava flow activity, since this side of the volcano is over 2000 metres higher than the opposite flank at similar distances from the caldera. It is possible that lava flows may have preferentially flowed down this northeastern side of the volcano at the start of the formation of Elysium Mons, since this direction was also down slope from the centre of the AVE. As Elysium Mons developed and grew larger, lava flows would have eventually started to flow in all directions from the vent and ultimately formed the shield that is observed now. The way in which the flows from Elysium Mons appear to have formed a crescent around the area now occupied by the

7.12 Explosive activity

The mapping and MOC image analysis part of this study also highlighted the fact that dark, unconsolidated, fine-grained material was found at the summit of Elysium Mons and appeared to have been erupted explosively from several pits/volcanic craters to the west of the Elysium Mons caldera. This deposit was not visible in high-resolution images of the summit area and thus it is proposed that it must be relatively thin when compared, for example, with the ash-fall deposit on the western flank of Hecates Tholus, which Mouginis-Mark et al. (1984) thought to be ~100 metres thick. It is proposed by the author that the pyroclastic deposits at the summit of Elysium Mons are relatively recent, since they have not been obscured by superposed materials, nor been removed by the wind. If both Hecates Tholus and Elysium Mons have undergone late-stage explosive activity, it raises the question of whether this is unique to the evolution of these two Elysium Montes, or whether late-stage explosive activity is common in the growth of many of the Martian volcanoes. MOC image analysis of both Olympus Mons and Alba Patera shows that much unconsolidated and easily erodible material is present at the summits of these two volcanoes. This was not expected since the summit areas of both volcanoes should have been resurfaced more recently than those of Hecates Tholus and Elysium Mons. It has been proposed in Chapter 3 that explosive activity had occurred at both Olympus Mons and Alba Patera in order to account for the levels of unconsolidated material observed. Thus the present study shows that, at least for the four volcanoes studied in this thesis, late-stage explosive activity is likely to have occurred during the evolution of each. It is possible that at the summits of the volcanoes the high elevations there have meant that a 'frost' of water ice has formed, which may have interacted with any lava erupted at a late-stage. This could cause phreatomagmatic explosions that may be the source of much of the unconsolidated material observed in the MOC images. No ground-ice was observed in the MOC images in the study, but it would be useful to bear this in mind for future studies.

7.13 Eruptions from the Fossae

Mapping using the MOLA data has also indicated high levels of activity at the Elysium Fossae. Although it had been previously found that material (probably water or lahars) was erupted from the Elysium Fossae (Christiansen and Greeley, 1981; Mouginis-Mark, 1985), the true extent of activity at the Fossae has been highlighted here using MOLA. This study has shown that several episodes of activity occurred, and both water (or mud) and lava flows were erupted from them. This leads to the questions regarding the source of the water that was erupted from the Fossae, how the water remained liquid for a long enough period of time to carve the channels observed, and why the eruptions from the Fossae were periodic.

Most of the Elysium Fossae occur in the material that has been attributed to the AVE. Of those Fossae that appear to have been the source of effusion of material, all of them release material at or near the point where the AVE grades into the surrounding plains. This suggests that eruption of material can only occur on the outer fringes of the AVE and that the material of the AVE (in this area at least) is porous, since water has presumably been stored in it and can travel through it. It is inferred that the Elysium Fossae have a magma source, since some of them have also erupted lava. One model for the way in which eruption from the Fossae occurred is given in Figure 7.2.

It is possible that, in the initial stages of growth, activity at the AVE was mainly dominated by pyroclastic activity, in much the same way as has been suggested at Alba Patera (Mouginis-Mark et al., 1988). Then activity became more effusive and the porous pyroclastic materials were buried by volcanic material that would later act as a 'cap rock', impeding the flow of any ground-water from the pyroclastic rocks up to the surface. It is proposed in this study that the Elysium Fossae initially formed as graben (potentially the surface expression of dykes), which penetrated the pyroclastic layer below at the outer reaches of the AVE where the layer of 'cap rock' was thinnest. Melt-water stored in the pyroclastic rock could then be released which enlarged the Fossae, started to carve the channels observed today, and deposited the sediments indicated during the mapping, and observed in the MOC images. The Fossae that formed where fractures in the rock could act as a conduit for magma, released lava to form the Fossae Lava Flows (**Flf**) unit. The

Gulick (1998) showed that hydrothermal systems on Mars are able to focus water flow, and transport and re-circulate large volumes of ground water to the surface for periods of time in excess of 10^5 years. The length of some of the channels may be surprising, particularly if it is supposed that water becomes replenished and is re-circulated underneath the volcano. However, Gulick and Baker (1987), showed that if the ground surface is composed of permeable materials such as basalt lava flows, then the water will infiltrate and recharge near-surface aquifers. If these aquifers eventually intersect with the surface further down slope they may initiate sapping and therefore perhaps further water flow at distal locations. This may be the mechanism that explains how the water from the Fossae travelled such great distances.

7.14 Overall implications

One of the major aims of this study is to further characterise the geology of the area surrounding the Elysium Montes and to improve knowledge of the overall geological history of the area. This has been achieved and the results of the mapping part of this study have also presented many opportunities for further study. The idea that Elysium Mons formed as the result of shifting vents inevitably leads to the question of whether this has occurred in other areas of Mars. As yet, no evidence for substantial vent shifts on the scale of that inferred at the AVE/Elysium Mons volcanic complex has been presented for any of the other Martian volcanoes. There are, however, several cases where multiple collapse events at the summits of volcanoes have produced caldera complexes, such as has been discussed for Ascraeus Mons, and which implies small-scale shifts in magma supply routes. Future studies using the MOLA data may highlight potential vent shifts at volcanic complexes elsewhere on Mars, in the same way as for the AVE/Elysium Mons complex.

Evidence to show the ways in which the volcanoes evolved has been interesting, since in most cases it is thought that explosive activity ceases at the onset of effusive activity from the Martian volcanoes. If further study were to show that most of the Martian volcanoes underwent late-stage explosive activity then this would mean that Martian

volcanism is more varied than first thought, since it would imply not only varying volatile concentrations in the magma supply, but that magmas may differentiate over time on Mars as they do on Earth, and thus a greater variety of rock types may be present on the surface of Mars.

It is clear from the evidence found not only in the mapping carried out in this thesis, but also in previous studies, that water has been present both on the surface and underground (mainly as ground-ice) within the area surrounding the Elysium Montes. Although this study has not identified a source for this ice/water, it has shown that the volcanic activity in this area has been responsible for mobilising much of the water. The model presented in Figure 7.2, if correct, could have important implications, since a hydrothermal system related to the Elysium Montes could have provided a habitat for life to evolve and thrive.

7.2 Lava flow studies

7.21 Comparisons with results from similar studies

It was clear from the results presented in Chapter 6 (lava flow studies - results and analysis) that there have been at least two different emplacement styles for the lava flows studied at both Alba Patera and Elysium Mons. Also, there were clear differences between the two volcanoes in terms of the results obtained for emplacement times and effusion rates for the inferred aa flows studied at each location. These differences have been discussed in Chapter 6. It was one of the aims of this study to determine whether similar results would be obtained when values for thickness and slope calculated using MOLA were used to replace the estimates used in previous studies of lava flows from both Alba Patera and Elysium Mons. A discussion of this therefore follows.

Elysium

In their study, Mouginis-Mark and Yoshioka (1998) measured the lengths, widths and distance from the caldera of 59 lava flows in Elysium. They analysed both S-type and M-type flows, although they did not distinguish between the two in their study. In particular they studied those flows to the north of the volcano in greater detail, since the resolution of the images there was higher (40m/pixel compared to 150metres/pixel) compared to the images of the rest of the lava flows. These flows were M-type flows and were compared in appearance to the M-type Alba Patera flows of Lopes and Kilburn (1990) by Mouginis-Mark and Yoshioka. Using fractal analysis methods similar to those employed by Bruno et al., 1992, they determined that the flows were aa, and they were able to produce profiles across the flows using photoclinometry (Davis and Soderblom, 1984). In this way they found an average flow thickness of between 40 and 60 metres, and estimated underlying slope values to be around 0.5 degrees over distances of several hundreds of kilometres (US Geological Survey, 1991). Mouginis-Mark and Yoshioka took these values to be typical for all the flows (M- and S-type) in their study, and thus estimated flow volumes of between 0.8 and 164 kilometres^3 (for flow thicknesses of 40 metres), and 1.2 to 246 kilometres^3 (for flows that were 60 metres thick). Deciding upon an effusion rate of between 10^2 and 10^4 $m^3.s^{-1}$, which was an intermediate value derived from the results of many previous Martian studies, they estimated that emplacement times for each of the flows must have ranged between ~1 year and several decades.

An important part of their findings was that five of the flows for which the thicknesses had been derived showed a 'segmented' form. They inferred this to mean that the flows ceased flowing for a period of time before flow re-activation and advance from the front of the leading edge. They put forward the idea that this mode of advance must have been due to unusual emplacement conditions. These could have been unusually flat pre-existing terrain, unusual basal conditions such as abundant permafrost (Mouginis-Mark, 1985), or rare upstream conditions that promoted the pulsing of the flow (such as the periodic breaching of a perched lava lake).

The use of MOLA in the present study enabled more accurate values of slope and flow thickness to be determined. Slopes for the Elysium lavas were found to range between

0.4° and 1.3°. It would therefore appear that the estimates of slope in the previous study were minimum values. The thickness values measured using MOLA were generally around 20 metres, clearly much thinner than the estimates used before. One of the major reasons for this difference (apart from the inaccuracy of the photoclinometric measurements) is because previous measurements were made from M-type flows. As the M-type flows are composed of several overlapping individual flow events, the overall thickness measured is likely to be greater than that for a single flow. Emplacement times calculated for the aa flows in this present study are much shorter than those in the previous study, although the effusion rates calculated (0.36×10^3 to 10.67×10^3 $m.s^{-1}$) fit in well with those chosen by Mouginis-Mark and Yoshioka.

In terms of emplacement and flow advance there are both similarities and differences between the two studies. Many of the individual MOLA profiles showed that the photoclinometric profiles of the flows had been correct. In places the flows appeared to be flat-topped and tabular, while in other places there was evidence for central channels, and also small-scale undulations of several metres. Most of the aa flows studied did thicken towards the distal end of the flow, as found by Mouginis-Mark and Yoshioka, but the pahoehoe flows tended to have longer, thinner flow fronts. Although the aa flows were not found to have undergone any post-emplacement inflation, in the present study some evidence was found to point towards the occurrence of this for the pahoehoe flows.

None of the flows in the present study were thought to have advanced in 'segments'. Although none of the 'segmented' flows analysed by Mouginis-Mark and Yoshioka (1998) were studied in depth in the present study, the fortuitous placement of a single MOLA track enabled a longitudinal profile to be obtained (Figure 7.3) along one of these 'segmented flows'. This clearly showed that it was an 'M-type' flow, which had been emplaced by the successive overlapping of consecutive flows. Thus the segments observed are found to be sections of overlapping flows, as demonstrated by the stylised sketch in Figure 7.4(b). In contrast, a typical flow profile for the Elysium flows that are inferred by the author to have advanced via breakouts is shown in Figure 7.4(a). The MOLA data show that the long flows in this region therefore do not have to have been emplaced under the unusual conditions invoked by Mouginis-Mark and Yoshioka (1998).

Mouginis-Mark and Yoshioka (1998) stated that flows over 100 kilometres long must infer that the volcano producing the flows must be capable of generating and erupting large volumes of melt at one time. Many of the flows in the present study were shorter than those of Mouginis-Mark and Yoshioka (1998), but there was one that had a length of over 100 kilometres. Interestingly, the average length for the pahoehoe flows in Elysium was 55kilometres and for the aa flows it was only 29 kilometres. Observations of terrestrial pahoehoe flows show that they generally travel more slowly than aa ones (Self et al., 1998; Keszthelyi and Self, 1998). It is therefore suggested in this study that Elysium Mons may have produced sustained levels of a moderate volume of lava over a longer period of time to produce these long pahoehoe flows, rather than a larger volume of melt in a shorter time. Since the aa flows are generally shorter in this study it follows that when smaller volumes of lava were erupted quickly, then aa flows would have been produced.

The flows in the previous study were estimated to have volumes of between ~0.8 and 164 kilometres^3. In the present study, volumes of the Elysium flows are thought to have ranged between 0.2 and 42.5 kilometres^3. Since Mouginis-Mark states that a flow volume of >10 kilometres^3 is large by terrestrial standards, then those flows on Mars may have had a great impact on their environment (Plescia, 1993; Robinson et al., 1993). Mouginis-Mark and Yoshioka took the composition of these lava flows to be basaltic (McSween, 1985; Banin et al., 1992; Soderblom, 1992) and assumed that they had 1%wt for the released water content of the parent magma (Greeley, 1987; McSween and Harvey, 1993). They also assumed that the lava had a mean density of $2.5x10^3$ kg.m^3. If the total flow volume they calculated was 817-1226 kilometres^3, this would have injected 2.04 to 3.01 x 10^{13} kg of water vapour into the atmosphere. As stated in their study, this is only around 0.2% of the amount of water vapour calculated by Plescia (1993) to have been released by the Cerberus Fossae. Since it was also thought that the flows may have been emplaced in timescales spanning several decades, Mouginis-Mark and Yoshioka (1998) decided that this would not have released the vapour at a volume significant enough to have had much effect on the environment.

Flow volumes, and therefore volumes of water vapour produced, for the flows calculated in this study are smaller that those in the previous study. Since the present study

shows that many of the flows were emplaced in short time scales of a few days to several weeks, the immediate impact of the eruption on the environment may still have been significant. The results from the present study therefore show that Mouginis-Mark and Yoshioka (1998) may have underestimated the impact on the environment from the emplacement of the flows in their study. If the flows analysed in Chapter 6 are typical of simple 'S-type' flows in the Elysium region, then many more flows erupted from Elysium Mons were emplaced over a few days or weeks, thus injecting a sudden, large volume of water vapour into the atmosphere. This would clearly have an effect, if only temporarily, on the immediate environment.

Lastly, although Mouginis-Mark and Yoshioka did not find evidence for inflation in the Elysium lavas, they did not discount it completely. They stated that the lower gravity on Mars may have allowed the entire surface of the flow to rise, rather than just in small, localised areas of the flow as seen on Earth (Walker, 1991). This may explain why there were few potential 'inflation features' observed in this present study, even where increases in flow thickness did not correspond to slope or topography and may therefore indicate inflation.

Alba Patera

Using the flow growth model which they developed using data from terrestrial lava flow fields, as discussed in Chapter 5, Lopes and Kilburn (1990) calculated eruption durations, average discharge rates and average velocities for 18 flows on the summit area and upper flanks of Alba Patera. It was inferred that all of the flows in the study were sheet or tabular flows (Carr et al., 1977; Cattermole, 1990; Schneeberger and Pieri, 1991), except for flows 4 and 7 which display obvious channels and were classified by Schneeberger and Pieri (1991) as "levéed". They also inferred that all flows in the study were aa, and most of them were simple 'S-type' flows, although they did study one M-type flow as well. Slope values and flow thicknesses had to be estimated, but flow width and length could be measured from the medium and high-resolution images which had a resolution of under 95 metres per pixel. In each case the source vent for each flow could be determined or

inferred, and two values for flow length were given. One value was the traced length of the flow for as far as it could be seen on the image, and one was the inferred length (which was the traced length plus the distance from the proximal end of the traced flow to the inferred source vent).

Of the 18 flows studied by Lopes and Kilburn (1990), only 11 were analysed in the present study, and they were all S-type flows. The measurements of flow width and length were taken to be the same as those given in the previous study, but measurements for flow thickness and underlying slope were obtained using MOLA. For the flows analysed in the present study Lopes and Kilburn used estimates for the underlying slope of between 0.4 and 0.6°. Slope values obtained using MOLA showed a more variable range of slope values for the same flows, with values of between 0.2 and 1.9°. Average thicknesses, estimated using shadow length measurements, were found to be between 34 and 78 metres. Average values measured using MOLA were found to be ~18 to ~24 metres thick. Therefore, flow thicknesses were smaller in reality than they had been estimated to be prior to MOLA. However, Lopes and Kilburn (1990) do mention that photoclinometry gave lower values than those obtained by shadow width measurements, and that if values were found to be even 30% lower than their estimates then this would still not affect their final conclusions. Thus, the lower end of the thickness range determined by Lopes and Kilburn is an acceptable estimate, but the higher end of the range (~78 metres), is greater than any of the values measured using MOLA.

Of the 11 flows analysed in the present study, only 6 were inferred to be aa. Lopes and Kilburn (1990) observed during their study that few of the lava flows on Alba Patera can be identified as having levées. However, analysis of those flows that were identified as being aa flows in the present study, showed that several of them may have been emplaced via channels which subsequently became buried (by back-fill of lava) or roofed over (Carr et al., 1977; Cattermole 1987) thus giving them a tabular or sheet-like appearance. Examples of the appearance of these flows have already been given in section 6.12(a). When Lopes and Kilburn determined emplacement times for the S-type flows analysed in the present study they found the times to range from 4.4 to 19 days, using the traced flow lengths (Lm_t), and 5.2 to 46 days using the inferred flow lengths (Lm_i). When the MOLA values were used instead of the previous estimates, the range of values for the same set of

flows was calculated to be 0.77 to 5.77 days using Lm_t values and 0.9 and 12.27 days using Lm_i values. The timescales calculated using the values obtained from the MOLA measurements are obviously shorter than those produced when using the estimates for slope and thickness. It would appear that, using the new values and assuming there were no pauses during emplacement, none of the flows analysed took longer than 2 weeks to be emplaced. This therefore means that the effusion rates calculated in the present study would also have been higher than those of the previous study. Effusion rate values in the present study range between 0.56 to 34.15 $x10^3$ $m.s^{-1}$ (Lm_t) and 2.43 to 80.35 $x10^3$ $m.s^{-1}$. Values for effusion rate in the previous study were 0.7 to 11 $x10^3$ $m.s^{-1}$ (Lm_t) and 2.7 to 52 $x10^3$ $m.s^{-1}$ (using Lm_i values).

As mentioned previously, lava that flows in channels tends to be emplaced more quickly than lava that is emplaced as a sheet (Keszthelyi and Self, 1998). If, as it is proposed in this study, the flows were mainly emplaced via channels, then a shorter emplacement time and average flow velocity should be expected for these types of flows than the sheet-type. Velocities for the previous study ranged between 0.01 and 0.1 $m.s^{-1}$ (Lm_t) and 0.08 to 0.4 $m.s^{-1}$ (Lm_i). The range of velocities for both the traced lengths and maximum length of the flows analysed in this study are between 0.02 and 0.65 $m.s^{-1}$ (Lm_t) and 0.09 and 1.15 $m.s^{-1}$ (Lm_i). The lower ends of all of these ranges are similar, but it is the upper end where the difference is obvious. Thus, the insertion of the more precise measurements made using MOLA data have reduced the emplacement times of the flows by over a month in some cases, as well as indicating that many of the flows travelled more quickly than was previously thought.

The compositions proposed for the Alba Patera lavas range from ultramafic (Cattermole, 1987), to andesitic (Baloga et al., 1987; Schneeberger and Pieri, 1988). A value of k (4.2 $x10^{-7}$ m^2s^{-1}) for basaltic/andesitic lavas at typical eruption temperatures has been used during this study and during the previous study (see Chapter 5). However, Lopes and Kilburn also worked out a value of k for ultramafic lavas by combining thermal data for compositionally similar komatiites and peridotites (Lopes and Kilburn, 1990). This gives a value of k= 1.6 x10-6 m^2s^{-1}, which is about 4 times larger than the value of k for basaltic/andesitic lavas. This means that ultramafic lavas would yield eruption durations 4 times shorter than those in this study, and average effusion rates and velocities 4 times

larger. This means that some of the flows in this study would have been emplaced in only two or three hours, which seems unlikely, given the dimensions of the flows. Therefore a basaltic/andesitic composition is favoured in the present study.

Lopes and Kilburn (1990) found that although the duration times of the Alba Patera flows were similar to those observed in present day terrestrial eruptions, the effusion rates calculated were much larger than those for typical present day eruptions. They stated that if the eruptions are assumed to have been driven by buoyancy forces, the higher effusion rates on Alba Patera may reflect a combination of larger source pressures, lower magma viscosities (and yield strengths if applicable), and larger fissure dimensions compared with terrestrial examples (Wilson and Head, 1983). Since the effusion rate values obtained in the present study are even higher than the ones calculated by Lopes and Kilburn (1990) then the same combination of factors is thought to be responsible.

7.22 Comparisons with results for other lava flow studies on Mars

As discussed in Chapter 1, there have been many attempts in previous studies to relate the final flow morphology of Martian lavas to conditions of emplacement or lava chemistry (Hulme, 1976; Carr et al., 1977b; Moore et al., 1978; Zimbelman 1985; Pieri and Baloga, 1986; Fink and Fletcher, 1978; Fink, 1980; Theilig and Greeley, 1986; Crisp and Baloga, 1990a; and Lopes and Kilburn, 1990). Many studies enabled the calculation of yield stress or viscosity, and others gave values for average effusion rates and flow durations. The models used in these previous studies have all been discussed in Chapter 1 (except for the flow growth model of Kilburn and Lopes (1991), which was discussed in Chapter 5). The results of those studies for which effusion rates and/or durations were calculated are presented in this section. The comparison between these values produced in previous studies, for several different Martian volcanoes, and those calculated in the present study will be discussed.

Discussion and conclusions

Volcano	Model Type Used	Effusion Rate $m^3.s^{-1}$	Duration (days)	Velocity ($m.s^{-1}$)
Olympus Mons (1 flow)	Relating levée width and underlying slope to yield stress and thus lava composition.	380 – 470		
Arsia Mons (4 flows)	After Hulme (1976)	10^3 - 10^4		
Ascraeus Mons	After Hulme (1976)	18 – 60		
Ascraeus Mons (same flows as in study by Zimbelman, 1985)	Radiation cooling model using a finite thickness and partial exposure of flow core.	10 – $2x10^4$		
Alba Patera	Radiative cooling model where flows were either thermally mixed (Q_m) or thermally unmixed (Q_u, see text).	Q_m = 42 – 233 $x10^3$ Q_u = 27 – 151 $x10^3$		
Alba Patera	After Pieri and Baloga (1986)			
Levéed flows:		155 – 5846 $x10^3$		
Sheet flows:		Q_u = 8 – 877 $x10^3$ Q_m = 13 – 1348 $x10^3$		
Tube flows:		Q_u = 134 – 1047 $x10^3$ Q_m = 206 – 1610 $x10^3$		
Alba Patera	Thermally unmixed radiative heat loss model (after Pieri and Baloga, 1986)			
Group 1 sheet flows (most summit sheet flows)		5 – 112	0.98 – 5.9	0.129 – 2.455
Group 2 sheet flows (flank sheet flows)		1.3 – 783	1 – 13.9	0.0964 – 0.594
Group 3 (tube and channel-fed lavas)		37 – 975	5.6 – 20.8	0.061 – 0.278

Tharsis Montes (Ascraeus/Pavonis Mons)	Various	Overall: ~5 x10^4 - ~10^5		
	After Pieri and Baloga (1986)	9 x10^2 - 10^6		
	After Kilburn and Lopes (1991)	10^5 to 4 x10^6		
	After Pinkerton and Wilson (1994) (using the Gratz number to determine when flow of lava in a central channel will stop due to conductive cooling.	600 – 2000		
	After Pinkerton and Wilson (1988) (using an equation that calculates the effusion rates of volume limited flows).	4 x10^4 – 2 x10^8		
	Channel geometry and the Jeffreys Equation (Jeffreys, 1925)	5 – 11 x10^4		
Elysium Mons	After Kilburn and Lopes (1991)	0.36 x10^3 – 10.67 x10^3	~4 to ~31	0.005 – 0.132
Alba Patera	After Kilburn and Lopes (1991)	0.56 x10^3 – 80.35 x10^3	~1 to ~12	0.02 – 1.15

Table 7.1: Estimates of effusion rates and other eruption conditions for several Martian volcanoes. In the studies car
& 1990) the flows were categorised into different types, and thus several ranges of values are given for effusion rates
Zimbelman (1998), various different methods for calculating effusion rate were employed for the same set of flows
brief outline of each model used has been given but greater detail can be found in Chapter 1.

When compared directly to other values obtained for effusion rates on Alba Patera, the values calculated in the present study for the Alba Patera aa flows generally fit into the lower end of the ranges calculated in previous studies. The only exception is for the results produced by Cattermole (1990), where the results calculated using the flow growth model have generally higher values. In terms of the other volcanoes listed in Table 7.1, the values for the flows on Alba Patera produced in the present study seem to be average and therefore appear to be sensible figures. The Alba Patera flows in the present study appear to have been emplaced with higher effusion rates than those for which estimates have been given at Olympus Mons (Hulme, 1976). This is also true for values found at Ascraeus Mons (Zimbelman, 1985), although other estimates for this volcano are around the same or higher than values obtained in this study. It must be noted here that the results produced by Zimbelman (1985) have inherent errors and thus may be anomalous. This is because, when using Hulme's method for determining flow emplacement by measuring levée width, Zimbelman (1985) used final flow dimensions in an equation that used the width of the levées after they have initially formed. Thus inevitably the results calculated are not a true representation of flow emplacement.

It is interesting to note that where several different methods have been used for the same set of flows (Zimbelman, 1998) the values obtained are variable, and an estimated intermediate value must be chosen. Thus all values obtained from these methods should be treated as a general estimate of actual eruption conditions, which may be different by at least one degree of magnitude in reality. They can however, be used to compare the volcanoes to each other to try to infer differences in eruption style.

The effusion rate values obtained for Elysium Mons in the present study seem to be at the lower ends of the ranges given for many of the volcanoes in Table 7.1. They seem to be more consistent with values obtained for Olympus Mons (Hulme, 1976), and the other Tharsis Montes, rather than those of Alba Patera. This is perhaps not surprising when the morphology of the different volcanoes is examined, since the Tharsis Montes and Elysium Mons are more similar in appearance to each other and to the Hawaiian shield volcanoes, and Alba Patera is not similar to any other volcano, Martian or otherwise.

7.23 Comparisons of the aa flows to terrestrial flow values

Using the flow growth model it can be seen that the range of effusion rates for the Elysium aa flows is 0.36 x 10^3 $m^3.s^{-1}$ to 10.67 x 10^3 $m^3.s^{-1}$. The lower end of this range is comparable with effusion rates from terrestrial volcanoes in modern times. For example, the overall effusion rate of flows from Mauna Loa (Hawaii) is 10 – 1000 $m^3.s^{-1}$ (Malin, 1980). Also, the average effusion rate for the Laki flow in Iceland was found to be 6.0 x 10^2 $m^3.s^{-1}$ (Walker, 1973). However, the higher end of the range is only comparable to the large flood-lava events. Examples of these are the flows found in North Queensland (Australia), where an average effusion rate of 12 x 10^3 $m^3.s^{-1}$ was calculated (Stephenson and Griffin, 1976). Also the Roza flow of the Columbia River Flood Basalts, which had an average effusion rate of 11.6 x 10^3 $m^3.s^{-1}$ per kilometre of vent (Swanson et al., 1975).

The range of effusion rates calculated for the Alba Patera flows using the flow growth model, was 0.56 x 10^3 $m^3.s^{-1}$ and 80.35 x $10^3.s^{-1}$. Values in this range are higher than those for the Elysium aa lavas, however, the lower end of the range is still comparable with the overall effusion rate of the Hawaiian volcanoes on Earth (Malin, 1980) as well as the Laki flow in Iceland. The higher end of the range is much larger than even those values given for the terrestrial flood lavas. As mentioned in section 6.2 in Chapter 6, the larger effusion rates at Alba Patera, when compared to those flows on Elysium Mons or the terrestrial flows mentioned in this section, may be owing to the larger fissure widths, rather than any difference in source pressure, magma viscosities or yield strengths. The flows studied by Lopes and Kilburn (1990), and also analysed in the present study are thought to have been the result of the most recent effusive activity on Alba Patera (Lopes and Kilburn, 1990; Cattermole, 1987, 1990; Scott and Tanaka, 1980, 1986). Alba Patera has undergone much tectonic stress in the past to create the numerous large graben observed today (Carr, 1984; Plescia and Saunders, 1979; Wise, 1976). It therefore seems likely that these, or crustal weaknesses related to them, could have been exploited by the magma to produce flows with large effusion rates.

The velocity of the Elysium aa flows was found to be in a range of between 0.005 and 0.132 $m.s^{-1}$. This appears to match values for the average rates of advance for terrestrial basalts (0.01 to 0.1 $m.s^{-1}$) (Lopes and Kilburn, 1990). For example, mean

velocities for the 1983 Mt Etna flow have been calculated as ~0.005 $m.s^{-1}$ (Frazzetta and Romano, 1984), and for the 1989 Etna flow it was calculated to be ~0.01 $m.s^{-1}$ (Lopes and Lopes, 1990). The 1982 andesite flow at Arenal (Costa Rica) was found to have a mean velocity of 0.001$m.s^{-1}$ (Borgia and Linneman, 1990). The velocities of the Alba Patera aa flows were found to be within a range of between 0.02 and 1.15 $m.s^{-1}$. The mean velocity of these flows is generally higher than that of the Elysium aa flows, but the lower end of the range is still comparable with the range of terrestrial lava flow velocities given above. The higher end of the velocity range for the Alba Patera lavas may be the result of the different ways that the flows from the two areas have been emplaced, with the Elysium lavas being emplaced as sheets, while the Alba Patera lavas were emplaced via channels and may thus have been faster (see Chapter 6). Greater effusion rates at Alba Patera would also have caused velocities to be higher.

Durations for emplacement of the Elysium Mons aa lavas ranged between 4 and just over 31 days. Since the 27 kilometre long 1984 aa flow at Mauna Loa was emplaced in just three weeks (Lipman and Banks, 1987), the duration values obtained for these aa flows seem realistic. The values for t_R are similar to the durations calculated by the flow growth model in most cases, although the pattern seems to fit less well for the flows with longer emplacement times. Flow durations for the Alba Patera aa flows range between just under 1 day and just over 12 days. These durations are generally shorter than those found for the Elysium flows, and also appear to be shorter than the emplacement of similar length flows on Earth. Again, the calculated values of t_R do seem to correspond quite well to the duration values calculated using the flow growth model. Exceptions to this pattern are the flows that were found, with the flow growth model, to have exceptionally short or exceptionally long duration times compared to the rest of the flows in this set of lavas. Flows with longer emplacement times than predicted by t_R may have grown by simple thickening (not overlap of younger flows) after initial emplacement of the planimetric area of the flow.

7.24 Overall Implications

7.24(a) Aa flow studies

Where results obtained in the present study were compared with results for the previous studies of the same lava flows at Elysium Mons and Alba Patera, several new and important finding were made. Firstly, Mouginis-Mark and Yoshioka (1998) and Lopes and Kilburn (1990) only inferred the presence of aa flows at Elysium Mons and Alba Patera respectively. However, the hsinα analysis using MOLA data, as well as the fractal analysis showed that the presence of both aa and pahoehoe is likely at both volcanoes. At Elysium, measurements using MOLA show that the value for slope can be higher than estimated by Mouginis-Mark and Yoshioka (1998), and that their estimates of flow thickness were up to three times higher than found using MOLA. MOLA measurements resulted in the finding that aa lava flows at Elysium Mons were emplaced more quickly than suggested by Mouginis-Mark and Yoshioka (1998). This led to the suggestion that these flows may have injected a substantial volume of water vapour and other gases into the atmosphere over a relatively short period of time and this may have had a temporary effect on the local environment. The presence of 'segmented' flows that were emplaced under unusal conditions has been discounted using the MOLA data, which show that the 'segmented flows' of Mouginis-Mark and Yoshioka (1998) are the result of separate overlapping lava flows, and not breakouts from the front of a single flow.

At Alba Patera the new values of underlying slope and flow thickness resulted in faster emplacement times, and thus greater effusion rates and velocities for the inferred aa flows that were previously studied by Lopes and Kilburn (1990). Image analysis of the flows highlighted the possibility that more of the flows were emplaced via channels than was suggested in the previous study. This may help to explain the difference between the higher values for emplacement time calculated for Alba Patera flows than those calculated for flows at Elysium Mons, which are implied to have been emplaced as slower moving sheets. Calculations of effusion rate, flow emplacement time and velocity compare well with results produced from other previous studies of Martian volcanoes using different flow modelling techniques. Results from the flow growth model generally fit into the ranges

produced in previous studies, and show that Elysium Mons effusion rates are more closely matched to those for other Martian shield volcanoes than to the Alba Patera effusion rates.

It has been established in this study that the flows in both areas appear to have been emplaced in similar cooling conditions to Earth, mainly because most plots of downstream resistance showed an increase towards the end of the flow. This suggests that Martian lava flows are subject to controls similar to those on Earth, and thus the use of the flow growth model to calculate the emplacement times for the inferred aa flows in this study was justified. Emplacement times and velocities for flows from both volcanoes were apparently similar to those on Earth even though they were emplaced on shallower slopes than are generally found on Earth. This may be owing to the fact that effusion rates for flows from both Martian volcanoes were higher than terrestrial lava flows. Some effusion rates calculated are even greater than effusion rates calculated for the terrestrial Flood Basalt Provinces. Larger fissure sizes are thought to be responsible for this difference, particularly at Alba Patera. Further contributing factors may include differences in the rate of magma production and the volume of magma stored in the reservoir beneath each volcano before eruptions commence.

7.24(b) Pahoehoe flow studies

High-resolution MOC image analysis has provided further evidence for the inferred presence of both aa and pahoehoe flows at Alba Patera and at Elysium Mons. Since both types of flow are found to have formed in the terrestrial Flood Basalt Provinces (Keszthelyi, 2003), as well as from terrestrial volcanoes such as Mount Etna in Sicily (Chester et al., 1985), it seems reasonable to expect that both types of flow have been erupted at both Elysium Mons and Alba Patera. However, the finding of both types has important implications for the development of lava flows on Mars, since it is generally thought that pahoehoe flows form more slowly and that aa are emplaced quickly. The fast emplacement of the aa flows found in this study fits in well with the general view that long lava flows on Mars must have been emplaced quickly to have travelled long distances and often over shallow slopes. It is suggested that these flows travelled quickly owing to high effusion rates, which are the result of large fissure widths, the generation of large volumes

of magma, and the storage of this magma in larger reservoirs than on Earth for long periods of time before eruption.

Emplacement times have not been calculated for the pahoehoe flows, so the speed at which the pahoehoe flows was emplaced is still unknown. As discussed in Chapter 5, there is still considerable debate over whether ancient terrestrial long lava flows (such as those found in the Flood Basalt Provinces) were emplaced quickly as proposed by Swanson et al. (1975) or slowly as more recently proposed by Self et al. (1998). The implications of pahoehoe being present on the Martian volcanoes in this study are important since the 'Standard Way of Emplacing Long Lavas' suggested by Self et al.(1998) infers that emplacement by sheets of inflated pahoehoe is the usual way in which long terrestrial lavas are emplaced. Some evidence has been found that post-emplacement inflation has occurred in the pahoehoe flows, both from the lava flow studies section and the MOC image analysis section of this thesis. Therefore it is possible that the pahoehoe flows inferred at Alba Patera and Elysium Mons were emplaced relatively slowly under an insulating crust, and the flows grew by both the puncturing of the crust at the toe of the flow, and also by inflation of the flow. Indeed, flow velocity profiles for many of the pahoehoe flows show that the flows appear to have advanced at a steady rate that fits this emplacement mechanism. As mentioned during the discussion, the slow emplacement of long flows infers that the volcano can produce and erupt moderate volumes of lava over longer time-scales than the erupting aa flows. This would seem to contradict magma supply rates for the aa flows, and may infer that rates of magma supply varied over the life-spans of both Alba Patera and Elysium Mons. However, there is an alternative mechanism for the fast emplacement of pahoehoe flows may exist, as discovered in field studies on Earth.

One place on Earth where fast emplacement of a pahoehoe flow has occurred is in Lanzarote, in the Canary Islands. Solana et al. (2004) studied the Montana de las Nueces flow-field, which was emplaced during the final stages of the 1730-1736 Timanfaya eruption, details of which had been recorded by observers at the time of its emplacement. This flow consists of sheets of pahoehoe lava that covered 32 kilometres^2 and reached almost 21 kilometres in length within just 4 weeks. Solana et al. (2001) found that the lavas have pahoehoe surface features but internal structures that are normally associated with massive aa flows (such as distorted vesicles; fingers of denser material pushed up into

the crust; and entrained pieces of crust in the dense core). They calculated that the flows had effusion rates of ~50 m^3s^{-1} and advanced over slopes of ~1° at a speed of around 0.002-0.33 $m.s^{-1}$, clearly similar to values found for some of the inferred Martian aa flows in this study. They concluded that these flows were emplaced at a rate of advance that suggested they were at the transition between pahoehoe and aa. Importantly, they also concluded that surface appearance and morphology of pahoehoe flows does not provide sufficient grounds for constraining the rate and style of emplacement of the flow. If similar processes occur on Mars this has important implications for the present study, since it means that many if not all of the pahoehoe flows in the current study may have also been emplaced at this transition, but the lack of information concerning the internal structure of the flows does not allow for rigorous modelling of the emplacement of these flows. The question of whether some of the long lava flows on Mars can have been emplaced slowly still cannot therefore be answered. Field data for Martian lava flows must be returned before it is possible to determine the balance between flows that were emplaced quickly and those that were emplaced more slowly.

7.3 Martian surface processes

The MOC high-resolution image analysis highlighted several major facts about the surface of the areas studied in this thesis. Firstly, it was apparent that much unconsolidated, fine-grained material was visible in many of the images analysed, even in areas that were thought to be relatively young. This is particularly true in the case of the summits of both Alba Patera and Olympus Mons and has lead to the conclusion that pyroclastic activity has occurred during the growth of these two volcanoes, perhaps even in the late stages of activity at the summit. Much of the image analysis was carried out on the area around and to the north of Elysium Mons. Here it has been shown that there is much evidence for the deposition of fine-grained materials, as well as the removal and dispersal of these by the action of the wind. Evidence has also been found to indicate the presence of ground-ice both now and in the past, since potential periglacial and thermokarst features have been observed. The presence of ground-ice may also be responsible for the unusual appearance of some of the impact craters observed in the MOC imagery. The flow of water across the

surface in this area has also been studied, since high-resolution images of fluvial channels are available. These have shown that although high levels of unconsolidated fine-grained materials have obscured much of the evidence for flow, deposits from the flow in these channels have still been observed on the banks of the channels.

The fine-grained, unconsolidated material ('dust') observed in the high-resolution MOC images has been one of the surprising results from this study, because although observation of this material was anticipated, it has been present in greater amounts than expected, and covers more of the surface than predicted, even on some of the relatively young surfaces. The origin of much of this material may be the result of the high levels of wind erosion that has been inferred from the observations of yardangs and other features in the MOC images. Dispersal of this material occurred over a wide area probably owing to the global dust storms that take place on Mars. The high levels of wind erosion occurring in the MOC images must be due to the fact that many of the surface materials in the areas analysed in this study are relatively soft and easily erodible. As suggested in Chapter 3, many of these materials are probably volcanic in origin, being either ash-rich or composed of mudflows. Although it was originally thought that, prior to the Viking mission to Mars, levels of wind erosion on Mars would be higher than on Earth due to faster wind speeds and entrainment of larger particles (Sagan, 1973; Greeley et al., 1982) this was found not to be the case since neither wind speed nor particle size were larger than on Earth (Arvidson et al., 1979; Greeley et al., 1982). It is therefore proposed in this study that the levels of wind erosion observed are not high enough to produce the vast quantities of 'dust'observed in the MOC images and that much of the fine-grained material has been produced from explosive volcanic activity.

Studies of the differences between environmental conditions acting on magmas as they reach the surface (Wilson and Head, 1983; Wilson, 1984) have shown that the lower gravity on Mars relative with the Earth will cause Martian volcanoes to have larger magma chambers and wider feeder dykes to the surface, forming the larger fissures discussed earlier in this chapter. Another consequence of the lower gravity is that gases can come out of solution at greater depths in the Martian lithosphere and that gases are released more quickly and efficiently from lavas once they are erupted on the surface. Therefore Mouginis-Mark et al. (1992) suggest that given similar volatile contents to terrestrial

magmas, a larger fraction of volcanic eruptions are likely to be explosive on Mars than on Earth. Therefore, the fact that explosive volcanism is likely on Mars, coupled with the evidence found in the image analysis that pyroclastic activity has been more prevalent than first thought at the four volcanoes studied, has lead to the proposal in this study that much of the fine-grained 'dust' observed has a pyroclastic origin. This may also explain the high numbers of small (100 metres in diameter or less) craters that have been observed in the MOC images, particularly on the upper flanks of Elysium Mons. Although many of these are impact related it is possible that many have been caused by volcanic explosions, perhaps due to the reaction of hot lava with ground-ice.

Analysis of the high-resolution MOC images has shown that although some of the surface features observed are unusual and do not appear to have any terrestrial analogues, other features are similar. This is particularly true for the periglacial features observed since they appear to occur on a similar scale to Earth, and also for the aeolian processes, since features appear to form in a similar way to those on Earth. MOC image analysis as well as analysis carried out in other sections of this thesis therefore appears to show that many Martian surface processes occur in a similar way to terrestrial ones regardless of differences such as surface pressure and temperature and differences in gravity between the two planets.

7.4 MOLA as a geological tool

As discussed in Chapter 1, a major aim of the MGS mission was to use the MOLA instrument to collect data that could be used to determine the topography of the surface of Mars at a scale of several metres. It was hoped that this would allow planetary scientists to characterise the regional geology of Mars and also study the geomorphology of both large and small-scale surface features. During the current study an in-depth understanding has been gained regarding how the MOLA instrument works and also regarding the ways in which MOLA data can be used.

MOLA can be used in a number of ways that makes it a useful geological tool. For example, for the first time scientists are able to produce accurate slope data for areas several hundreds of metres across, as well as for larger, regional areas. This is clearly

useful for studies in which a value of slope is necessary (such as for the modelling of lava flows as in the present study). It is also useful in determining the direction of flow for materials that have flowed following the regional slope, thus highlighting for example, where large deposits of fluvial sediment may occur. Slope can also indicate why surface units may have a characteristic appearance, since some features or processes may occur preferentially on a slope (such as gullies, slumping and other erosional features). The measurement of the slope of geological features, such as volcanoes, can also give clues to the particular formation processes that produced them, such as indicating the difference between the shallow slopes of a shield volcano and the steeper slopes of a composite volcano.

The real strength of MOLA as a geological tool is the fact that the data can be manipulated in many ways. Topographic profiles of individual features just a few kilometres across can be constructed, to provide knowledge regarding the shape and height or depth of the feature in question, such as lava flows and graben. Contour maps with contour spacing of only several metres apart over any area of the Martian surface can be created, and the same data can also be used to construct DEMs that are more detailed than previously available prior to MGS. The contour maps and DEMs help planetary scientists to visualise the Martian surface and identify geological features and also relationships between features and surface units. In the ways discussed here MOLA can show whether individual units are overlapping each other, can allow scientists to determine the thicknesses of individual units, and to determine the dimensions of features. All this can be used for geological analysis.

One of the most important uses of the MOLA data has been to use the data to produce a global topographic map. This has put the whole of Martian geology into perspective. The elevation difference between the northern lowlands and the southern highlands has been quantified. Areas of the northern lowlands have been found to show depressions that were probably formed during large impact events millions of years ago, and were previously not discovered prior to MGS. The paths used by flash flood events as well as smaller streams of water are visible, and potential coastlines have been determined using MOLA. These data can also be used as a base upon which to build all future knowledge. Information regarding surface elevation and roughness can be used when

determining future landing site locations, and the gravity modelling carried out using MOLA data will enable better calculations for orbiting spacecraft as well as for the studies of the interior of Mars.

Although it has proved to be a useful tool, there are some aspects of the data that currently make some geological analyses difficult. For example, each MOLA laser footprint has a diameter of 168 metres on the Martian surface (when MGS orbits at a height of 400 kilometres). This means that topographic profiles cannot be produced for features that are in the size-range of only a few hundreds of metres. It also means that the elevation value for each laser footprint is really an average of the whole area covered by the footprint, so where the elevation does not vary a great deal then the elevation value will be representative of the surface. However, it also means that where the ground slopes more steeply, the average elevation value obtained will not be so representative, thus introducing a larger uncertainty in elevation measurement. The spacing between two MOLA laser footprints (centre-to-centre) on the surface is ~300 metres, therefore there is no overlap between data points in the same orbit. The problem with this is in the fact that smaller geological features (less than a kilometres across) may only have been covered by three or four laser footprints, and this can provide misleading topographic profiles.

The rotation of the planet as MGS travels in orbit results in the fact that the MOLA ground tracks cover the Martian surface diagonally (as shown in Figure 2.4 in Chapter 2). In order to obtain individual MOLA profiles across features it is necessary to choose features that trend perpendicular to the MOLA groundtrack. If a longitudinal profile along a feature is desirable then this can be obtained most easily by choosing features that trend in the same direction as a MOLA ground track. This therefore precludes the study of many Martian features using individual profiles. However, computer programmes such as Gridview do allow the user to produce profiles across any feature using the gridded data. There are some data gaps in the MOLA data set. This means that when shaded DEMs are produced using the gridded data, some interpolation between data points occurs in some computer programmes. This can be misleading when interpreting the data.

Given the differences in co-ordinate systems and reference spheroids used between MGS and previous missions, it is difficult to match up MOLA profiles to images of the surface of Mars. There is also a difference between the reference frames used for MOLA

and MOC so that these are also difficult to match. Clearly, this is a major difficulty when using the MOLA data to analyse Martian geology. Since all future missions will now use the same co-ordinate system as MGS MOLA, this problem should not occur in the future. Image data from the mission that followed MGS, the Mars Odyssey spacecraft, can already easily be matched with MOLA.

With a vertical accuracy of ~1 metre, and a precision of around 37.5cm (on low slopes), the MOLA instrument makes an ideal tool for the study of small-scale geological features. However, the errors in horizontal accuracy, plus the sizing of the MOLA footprints and the distance between each footprint mean that the analysis of the geomorphology of small-scale features (around 100 metres across or less), is not possible. However, as it has been demonstrated in this study, the MOLA instrument is an important and useful tool for geological analysis of planetary surfaces, both for mapping studies, and for the geomorphological analysis of features that are several kilometres across or more.

7.5 Conclusions

7.51 Summary of major conclusions

- Elysium Mons was emplaced as a summit cone on the flanks of an older, larger volcanic edifice, here termed the 'AVE'. This is thought to have occurred as a result of a vent shift.
- A late-stage explosive event occurred at the summit of Elysium Mons.
- Eruptions from the Elysium Fossae were periodic as a result of a pulsed supply of both water and magma.
- Both aa and pahoehoe lava flows were interpreted to occur at Alba Patera and Elysium Mons.
- The inferred Alba Patera aa flows were emplaced more quickly and had larger effusion rates than the inferred aa flows erupted from Elysium Mons, perhaps because lavas at Alba Patera were erupted from larger fissures and may have had differences in composition from the Elysium lavas.

- Durations and velocities of both the Elysium and Alba aa lavas were similar to many lava flows on Earth.
- The lower end of the range of effusion rates were similar to the larger Hawaiian flow events, but the upper end of the range exceeded effusion rate values for flows even at the terrestrial Flood Basalt Provinces.
- The large volume of unconsolidated, fine-grained material observed in the high-resolution MOC images is inferred to be volcanic in origin and points to the occurrence of much explosive activity on Mars in the past.
- Pyroclastic activity is thought to have occurred at some point during the growth of Olympus Mons.
- Wind activity on the flanks of the volcanoes is responsible for much burial and erosion of lava flows.
- Small-scale aeolian and periglacial processes on Mars appear to occur in a similar way as they do on Earth regardless of environmental differences between the two planets.
- The MOLA data and MOC images are important and useful tools in the study of the geology of Mars.

7.52 Further Work

As with all studies of this kind, there are always new ways to extend the work. Although further data such as that outlined above would enable a deeper understanding of the area studied in this thesis, there are still many ideas for further work just using the data currently available. MOLA is a valuable mapping tool, and since all the current published geological maps of Mars available have been produced using data that was available prior to the MGS mission, detailed mapping could be carried out of any area of interest on Mars. In particular it would be interesting to know whether other volcanic provinces on Mars have developed in a similar way to the Elysium Montes, with a vent shift being an important part of the evolution of the volcanoes. The MOC images would also be important to the mapping since they can provide details about small-scale surface processes and features.

The study of volcanic processes on Mars could be extended by analysing MOC images of the summit areas of other volcanoes on Mars to ascertain whether these also appear to have undergone late-stage summit activity like that postulated at the volcanoes in the current study. The images from the Mars Odyssey mission could be used in conjunction with the MOC images because the Odyssey images cover a larger area of Mars at a lower resolution and thus provide some context for the high-resolution MOC images. Also, MOLA could be used to study lava flows at other volcanoes on Mars. It would be necessary to find large flows several kilometres in width and tens of kilometres in length in order to use MOLA to produce profiles of the flows similar to those profiles produced in this study. Similar methods to those used in this study could be applied to determine whether the lava flows at these other volcanoes were aa or pahoehoe, and to calculate the eruption durations, effusion rates and velocities of the aa flows. These could therefore be compared to the results obtained in the present study to see if there are any major differences between the volcanoes.

There are at least three ways in which volcanic studies can be extended at the AVE/Elysium Mons volcanic complex. Firstly, if the annular graben surrounding Elysium Mons are taken to be the surface expressions of cone-sheets formed in relation to the caldera of the AVE then it would be possible to obtain estimates of the depth to the surface of the underlying magma reservoir for the AVE. This is because cone-sheets are inclined inwards and downward towards a common focus that is located within or upon the surface of the underlying magma reservoir. The depth to the focus is obtained by plotting the underground continuation of the cone-sheets, assuming that the inclination of the individual sheets is constant. Of course, it is not possible to ascertain the angle of inclination for the cone-sheets from the images. However, a range of angles (based on terrestrial field data) could be used to determine a range of estimates for the depth. As it has been proposed that the vent shift at the AVE/Elysium Mons complex led to the formation of a higher-level magma reservoir underneath Elysium Mons, this would provide a maximum depth for the position of the magma reservoir that supplied Elysium Mons.

A second way to extend the study of volcanism at the AVE/Elysium Mons complex is by finding a means to test the emplacement times and other values calculated for the aa flows. An ideal method would be one that uses only measurable parameters in a similar

way to the flow growth model of Kilburn and Lopes (1991). Kilburn (2004) has developed a study that may be applicable as it shows how the conditions for flow fracturing can be used to quantify limits on the ways in which lava flows are emplaced. The study states that aa lava flows are emplaced via persistent crustal failure and constant rates of advance. Fracturing of the crust is by the crust breaking persistently under its own weight, but also by a pulling force exerted on the crust by the core of the flow. The model developed by Kilburn (2004) enables: (1) the calculation of minimum and maximum thicknesses, rates of advance and maximum flow length for aa flows; and (2) the maximum thicknesses and rates of advance for individual pahoehoe tongues. The expressions for flow length and advance rate rely mainly on estimates of mean underlying slope, thus making them useful for the modelling of Martian lava flows, and enabling testing of results produced using the flow growth model. In order to calculate flow emplacement time, the model requires a value for acceleration due to gravity. Initial calculations show that this produces significantly different values for the Martian lava flows in this study compared to results obtained using the flow growth model of Lopes and Kilburn (1990) and Kilburn and Lopes (1991). Further work using the model of Kilburn (2004) would be worth pursuing and can be applied to the flows from Alba Patera as well as Elysium Mons.

Lastly, the knowledge of emplacement times and volumes of lava flows for Elysium Mons and Alba Patera, may enable the calculation of a minimum construction time for the formation of each volcano if the volume of each volcano was estimated. Clearly it would involve assuming that all flows erupted were aa because no emplacement times are available for the pahoehoe flows. It would also mean that the growth of the volcano by the successive deposition of pyroclastic materials would have to be ignored. However, it would be interesting to see how these calculations compared with ages estimated from crater counts, and in the case of Elysium Mons, would provide a constraint on the timing of the AVE vent shift event.

The Mars Odyssey THEMIS instrument has been returning data regarding mineral distribution on the surface of Mars for nearly two years. As discussed in the mapping chapter of this thesis, these data have better resolution than the data returned by the MGS TES instrument. A mineral map of the Elysium mapping area produced using these data from THEMIS could then be used to test boundaries of units in the geological map

produced in this thesis. It would also be useful to combine these compositional data with the MOLA data when mapping further areas of the Martian surface.

Further work in Elysium using MOLA could focus on the channels emanating from the Elysium Fossae. It could involve obtaining profiles across the larger channels and determining how they were formed, as well as how much fluid they had transported. MOLA could also be used to determine volumes of sediments deposited around the channels and even perhaps the volume of lava that was erupted from each of the Fossae. This may allow the calculation of how much lava was erupted in each episode of eruption from the Fossae and thus could provide a starting point for modelling of the supply of magma within the volcanic complex.

There is much scope for using the high-resolution MOC images in extended studies of the work presented in this thesis. For example, the high-resolution MOC images can be used to study the surface textures of other ice-rich areas of Mars. Areas that are potentially water ice rich have been highlighted by the gamma ray spectroscopy data returned from the Mars Odyssey mission. It could therefore be interesting to study small-scale surface features in these potentially ice-rich areas and determine whether features similar to those observed in the current study are found.

Other MOC image studies could focus on the importance of aeolian erosional processes on Mars by studying aeolian features observed in other areas of Mars, since this was found to be an important process in Elysium. It may also be useful to use the MOC images to study the texture of 'petal' impact crater ejecta elsewhere on Mars, in order to determine whether all ejecta of this type exhibits the 'jumbled' appearance observed in the current study. The appearance of this ejecta and the distribution of craters that exhibit it may be important in refining models of the formation of these craters. If the 'jumbled' ejecta appears to be unique to the Elysium region then it would suggest that unique sub-surface conditions are present in this region. Other studies on impacts might focus on the presence of the small (less than 100 metres in diameter) craters that are present on the flanks of Elysium Mons. Since it has been proposed in this study that they may be volcanic in origin it might be useful to analyse the flanks of other volcanoes and other volcanic areas for similar numbers of small craters. This may be particularly important in relatively young

volcanic areas such as around the Cerberus region of the Elysium Basin, since high numbers of impact craters would not be expected here.

Lastly, the high-resolution MOC images could be used in studies of channels on Mars. Although some evidence for fluid flow was found in the current study, the high levels of unconsolidated, fine-grained materials meant that much of this evidence, if it did exist, is now not present. However, deposits of material thought to be fluvial sediments were found. Another extension of the current study could therefore be to analyse channels in other areas of Mars, perhaps areas that are less mantled with loose material, to see if further evidence for fluid flow, as well as fluvial deposits can be found.

In conclusion, the MGS MOC and MOLA instruments have provided a wealth of information about the geology of Mars. Much new information and some new findings have been presented in this thesis that have shown just some of the ways in which the new data can be used, and further studies using this data, as well as new data from future missions to Mars, will undoubtedly continue to improve our understanding of the Red Planet.

References

Abshire J. B., Sun X. and Afzal R. S. (2000) Mars Orbiter Laser Altimeter: Receiver Model and Performance Analysis. *Applied Optics,* **39**, No. 15, 2449 – 2460.

Acua, M. H., Connerney J. E. P, Wasilewski P., Lin R. P, Anderson K. A, Carlson C. W., McFadden J., Curtis D. W, Reme H., Cros A., Medale J. L., Sauvaud J. A., d'Uston C., Bauer S. J., Cloutier P., Mayhew M. and Ness N. F. (1992) Mars Observer magnetic fields investigation. *J. Geophys. Res.* **97,** No.E5, 7799-7814.

Acua, M. H., Connerney J. E. P, Wasilewski P., Lin R. P, Anderson K. A, Carlson C. W., McFadden J., Curtis D. W, Mitchell D., Reme H., Mazelle C., Sauvaud J. A., d'Uston C., Cros A., Medale J. L., Bauer S. J., Cloutier P., Mayhew M., Winterhalter D. and Ness N. F. (1998) Magnetic field and plasma observations at Mars: Initial results of the Mars Global Surveyor Mission. *Science* **279**, 1676-1680.

Afzal R. S. (1994) Mars Observer Laser Altimeter: Laser transmitter. *App. Optics* **33**, 3184 – 3188.

Afzal, R. S., Yu A. W., Zayhowski J. J., and Fan T. Y. (1997) Single-mode high-peak-power passively Q-switched diode pumped ND:YAG laser. *Optics letters* **22**, 1314.

Ager D. V. (1975) *Introducing geology* (2nd ed.), Faber and Faber Ltd.

Allen C. C. (1978) Areal distribution of Martian rampart craters. *Icarus* **39**, 111-123.

Allen C. C. (1979) Volcano-ice interactions on Mars. *J. Geophys. Res.* **84**, 8048-8059.

Anderson R. S. (1988) The pattern of grainfall deposition in the lee of aeolian dunes. *Sedimentology* **34**, 175-188.

Anderson S. W., Stofan E. R., Smrekar, S. E., Guest J. E. and Wood B. (1999) Pulsed inflation of pahoehoe lava flows: implications for flood basalt emplacement. *Earth Planet. Sci. Lett.* **168**, 7 – 18.

Arvidson R., Guinness, E. and Lee, S. (1979) Differential Aeolian redistribution rates on Mars. *Nature* **278**, 533-535.

Aubele J. C., Crumpler L. S. and Elston W. E. (1988) Vesicle zonation and vertical structure of basalt flows. *J. Volcanol. Geotherm. Res.* **35**, 349 - 374.

Bagnold R. A. (1941) *The physics of blown sand and desert dunes.* Methuen & Co. Ltd., London.

Baird A. K., Toulmin III P., Clark B. C., Rose Jr, H. J., Keil K., Christian R. P. and Gooding J. L. (1976) Mineralogic and petrologic implications of Viking geochemical results from Mars: Interim report. *Science* **194**, No. 4271, 1288-1293.

Baker V. R. (1982) *The channels of Mars.* Austin: Univ. of Texas Press.

Baker V. R., Strom R. G., Croft S. K., Gulick V. C., Kargel J. S. and Komatsu G. (1991) Ancient oceans, ice sheets and the hydrological cycle on Mars. *Nature* **352**, 589 – 594.

Baloga S., Pieri D. C, Plescia J. and Davis P. (1987) "Profiles of lava flows at Alba Patera, Mars" (abstract), *LPSC XVIII*, 42 – 43.

Bandfield J. L., Hamilton V. E. and Christensen P. R. (2000) A global view of Martian surface compositions from MGS-TES. *Science* 287, 1626 – 1630.

Banin A, Clark B. C. and Wanke H. (1992) "Surface chemistry and mineralogy". In, *Mars* (eds., Kieffer H. H., Jakosky B. M., Snyder C. W., and Mathews M. S.), Univ. of Arizona Press, Tuscon, 594 – 625.

Barlow N. G. (1988) Crater size-frequency distributions and a revised Martian relative chronology. *Icarus* **75**, 285 – 305.

Barlow N. G. and Bradley T. L. (1990) Martian impact craters: Correlations of ejecta and interior morphologies with diameter, latitude and terrain. *Icarus* **87**, 156-179.

Basaltic Volcanism Study Project (BVSP) (1981) *Basaltic Volcanism on the Terrestrial Planets*, New York, Pergamon Press.

Berman D. C. and Hartmann W. K. (2002) Recent Fluvial, Volcanic, and Tectonic Activity on the Cerberus Plains of Mars. *Icarus* **159**, 1-17.

Blasius K. R. and Cutts J. A. (1976) Shield volcanism and lithospheric structure beneath the Tharsis plateau, Mars. *Proc. LPSC* VII, 3561 – 3573.

Borgia, A. and Linneman, S.R. (1990) "On the evolution of lava flows and the growth of volcanoes." In *Lava Flows and Domes: emplacement mechanisms and hazard implications,* (ed., Fink, J.H), Springer-Verlag, Berlin, 208 – 243.

Breed C. S. and Grow T. (1979) "Morphology and distribution of dunes in sand seas observed by remote sensing". In, McKee (1979), 253 – 303.

Breed C. S, McCauley J. F and Whitney M. I (1989) "Wind erosion forms". In, *Arid zone geomorphology* (ed., Thomas D. S. G), Belhaven, London, 284 307.

Bridges N. T. and Barlow N. (1989) Variation of Martian rampart crater ejecta lobateness in comparison to latitude, longitude, terrain and crater diameter. *Lunar Planet. Sci.* XX, 105-106.

Brookfield M. E. and Ahlbrandt T. S (eds.) (1983) *Eolian sediments and processes*, Developments in Sedimentology, **38**, Elsevier, Amsterdam.

Bruno B. C., Taylor G. J., Rowland S. K., Lucey P. G. and Self S. (1992) Lava Flows Are Fractals. *Geophys. Res. Lett.* **19**, No. 3, 305 – 308.

Bruno B. C., Taylor G. J., Rowland S. K. and Baloga S. M. (1994) Quantifying the effect of rheology on lava-flow margins using fractal geometry. *Bull. Volcanol.* **56**, 193 – 206.

Burr, D.M, Grier, J.A, McEwen, A.S., Keszthelyi, L.P. (2002a) Repeated aqueous flooding from the Cerberus Fossae: Evidence for very recently extant, deep groundwater on Mars. *Icarus*, **159**, 53-73.

Burr D. M., McEwen A. S. and Sakimoto S. E. H. (2002b) Recent aqueous floods from the Cerberus Fossae, Mars. *Geophys. Res. Lett.* **29**, No.1, 13-1 – 13-4.

Calvari S. and Pinkerton H. (1998) Formation of lava tubes and extensive flow field during the 1991 – 1993 eruption of Mount Etna. *J. Geophys. Res.* **103**, 27291-27301.

Capen C. F. and Martin L. J. (1971) The developing stages of the Martian yellow storm of 1971. *Lowell Obs. Bull.* **7**, No.157, 211-216.

Capen C. F. and Martin L. J. (1972) Mars' great storm of 1971. *Sky and teles.* **43**, 276-279.

Carr M. H. (1973) Volcanism on Mars. *J. Geophys. Res.* **78**, 4049-4062.

Carr M. H. (1974) The role of lava erosion in the formation of lunar rilles and Martian channels. *Icarus* **22**, 1 – 23.

Carr M. H. (1981) *The surface of Mars*. New Haven, Conn., Yale Univ. Press.

Carr M. H. (1984) "Mars". In, *The geology of the terrestrial planets* (ed. Carr M. H), *NASA Special Publication* **469**, 206 – 263.

Carr M. H., Crumpler L. S., Cutts J. A., Greeley R., Guest J. E. and Masursky H. (1977a) Martian impact craters and emplacement of ejecta by surface flow. *J. Geophys. Res.* **82**, 4055-4065.

Carr M. H., Greeley R., Blasius K. R., Guest J. E. and Murray J. B. (1977b) Some Martian Volcanic Features as Viewed From the Viking Orbiters. *J. Geophys. Res.* **82**, No. 28, 3985 – 4015.

Carr M. H. and Schaber G.G. (1977) Martian permafrost features. *J. Geophys. Res.* **82**, No. 28, 4039 – 4054.

Cas R. A. F. and Wright J. V. (1987) *Volcanic Successions Modern and Ancient*, Allen and Unwin, London.

Cashman K. V. and Kauahikaua J. P. (1997) Re-evaluation of vesicle distributions in basaltic lava flows. *Geology* **25**, 419 – 422.

Cattermole P. (1987) Sequence, Rheological Properties, and Effusion Rates of Volcanic Flows at Alba Patera, Mars. *Proc. Lun. Planet. Sci. Conf. XVII, Part 2, J. Geophys. Res.*, **92**, No. B4, E553 – E560.

Cattermole P. (1990) Volcanic Flow Development at Alba Patera, Mars. *Icarus* **83**, 453 – 493.

Cattermole P. (1996) *Planetary volcanism: A study of volcanic activity in the solar system* (2nd ed.), John Wiley & Sons/Praxis Publishing Ltd.

Cave J. A. (1993) Ice in the Northern Lowlands and Southern Highlands of Mars and Its Enrichment Beneath the Elysium Lavas. *J. Geophys. Res.* **98**, No. E6, 11079 – 11097.

Chapman C. R. (1974) Cratering on Mars I. Cratering and obliteration history. *Icarus* **22**, 272 – 291.

Chapman C. R. and Jones K. L. (1977) Cratering and obliteration history of Mars. *Ann. Rev. Earth Planet. Sci.* **5**, 515 – 540.

Chester D. K., Duncan A. M., Guest J. E. and Kilburn C. R. J. (1985) *Mount Etna: The anatomy of a volcano*, Chapman and Hall Ltd., London.

Christensen P. R. (1988) Global albedo variations of Mars: Implications for active aeolian transport, deposition and erosion. *J. Geophys. Res.* **93**, 7611 – 7624.

Christensen P. R., Anderson D. L., Chase S. C., Clark R. N., Kieffer H. H., Malin M. C., Pearl J. C., Carpenter J., Bandiera N. and Brown F. G. (1992) Thermal emission spectrometer experiment - Mars Observer mission. *J. Geophys. Res.* **97**, no. E5, 7719-7734.

Christensen, P. R., Anderson D. L., Chase J. S. C., Clancy R. T., Clark R. N., Conrath B. J., Kieffer H. H., Kuzmin R. O., Malin M. C., Pearl J. C., Roush T. L. and Smith M. D. (1998) Results from the Mars Global Surveyor Thermal Emission Spectrometer. *Science* **279**, 1692-1698.

Christiansen E. H. (1989) Lahars in the Elysium region of Mars. *Geology* **17**, 203 – 206.

Christiansen E. H. and Greeley R. (1981) "Mega-lahars(?) in the Elysium region, Mars" (abstract) *LPSC XII*, 138 – 140.

Christiansen E. H. and Ryan M. P. (1985) "Volcanic debris flows in the Elysium region of Mars" (abstract) *LPSC XVI*, 239 – 241.

Cintala M. J. and Mouginis-Mark P. J. (1980) " Martian fresh crater depths: More evidence for substrate volatiles?" (abstract), *LPSC XI*, 143 – 145.

Colgate S.A. and Sigurgeirsson T. (1973) Dynamic mixing of water and lava. *Nature* (Lond) **244**, 552-555.

Condit C. D. (1978) Distribution and relations of 4- to 10-km diameter craters to global geologic units of Mars. *Icarus* **34**, 465 – 478.

Cooke R. S. J., McKee C. O., Dent V. F. and Wallace D. A. (1976) "Striking sequence of volcanic eruptions in the Bismarck volcanic arc, Papua New Guinea in 1972-74". In: *Volcanism in Australasia* (ed. Johnson R. W.) Elsevier.

Crisp, J. and Baloga S. (1990a) A method for estimating eruption rates of planetary lava flows. *Icarus* **85**, 512-515.

Crisp J. and Baloga S. (1990b) A model for lava flows with two thermal components. *J. Geophys. Res.* **95**, No. B2, 1255-1270.

Crumpler L. S. and Aubele J. C. (1978) Structural evolution of Arsia Mons, Pavonis Mons and Ascraeus Mons: Tharsis region of Mars. *Icarus* **34**, 496 – 511.

Cutts, J.A and Smith, R.S.U (1973) Eolian deposits and dunes on Mars. *J. Geophys. Res.* **78**, No.20, 4139-4154.

Dalu G., Salusti G. and Zirilli, F. (1988) Time evolution of magmatic tongues. *Phys. Earth Planet. Inter.* **50**, 88 – 91.

Danes Z. (1972) Dynamics of lava flows. *J. Geophys. Res.* **77**, 41430 – 41432.

Davies, M. E., Abalakin V. K., Brahic A., Bursa M., Chovitz B. H., Lieske J. H., Seidelmann P. K., Sinclair A. T. and Tjuflin Y. S. (1992) Report of the IAU/IAG/COSPAR, Working Group on Cartographic Coordinates and Rotational Elements of the Planets and Satellites: 1991. *Celest. Mech. Dyn. Astron.* **53**, 377-397.

Davies, M. E., Abalakin V. K., Bursa M., Lieske J. H., Morando B., Morrison D., Seidelmann P. K., Sinclair A. T., Yallop B., Tjuflin Y. S. (1995), Report of the IAU/IAG/COSPAR Working Group on Cartographic Coordinates and Rotational Elements of the Planets and Satellites: 1994, *Cel. Mech. Dyn. Astron.* **63**, 127.

Davis P. D and Soderblom L. A. (1984) Modeling crater topography and albedo from monoscopic Viking Orbiter images, I, Methodology. *J. Geophys. Res.* **89**, 9449 – 9457.

De Hon, R.A. "Classification of Martian lacustrine basins" (abstract), *LPSC XXII*, 293 – 294 (1991)

De Gans W. (1988) Pingo scars and their identification. In *Advances in periglacial geomorphology* (ed. Clark M. J.), Chichester: John Wiley and Sons Ltd., 299-322.

De Vaucouleurs G. (1954) *Physics of the planet Mars*, Faber and Faber, London.

De Vaucouleurs G., Davies M. E. and Sturms Jr., F. M. (1973) Mariner 9 areographic coordinate system. *J. Geophys. Res.* **78**, no. 20, 4395 – 4404.

Dietrich, W.E and Smith, J.D (1984) Bedload transport in a river meander. *Water Resour. Res.* **20**, (10), 1355-1380.

Dragoni M. (1989) A dynamical model of lava flows cooling by radiation. *Bull. Volcanol.* **51**, 88-95

Dragoni M., Piombo A. and Tallarico A. (1995) A model for the formation of lava tubes by roofing over a channel. *J. Geophys. Res.* **100**, 8435 – 8447.

Duncan A. M. and Guest J. E. (1982) Mount Etna: variations in its internal plumbing. *Geophys. Surveys* **5**, 213 – 227.

Duxbury T. C., Kirk R. L., Archinal B. A. and Neumann G. A. (2001) "Mars geodesy/cartography working group recommendations on Mars cartographic constants and coordinate systems" (abstract) ISPRS WG IV/9: Extraterrestrial Mapping Workshop "Planetary Mapping 2001", USGS, Flagstaff, Arizona, USA.

Duxbury T. C., Kirk R. L., Archinal B. A. and Neumann G. A. (2002) Mars geodesy/cartography working group recommendations on Mars cartographic constants and coordinate systems. *International archives of the phoogrammetry, remote sensing and spatial information sciences* **34**, No. 4, 743 – 746.

El-Baz F. and Maxwell T. A. (1982) *Desert landforms of Southwest Egypt: A basis for comparison with Mars.* NASA CR-3611, Washington, DC, USA.

Fagents S. A., Pace K. and Greeley R., "Origins of small volcanic cones on Mars" (abstract) *LPSC XXXIII* (2002).

Fink, J. H. (1980) Surface folding and viscosity of rhyolite flows. *Geology* **8**, 250-254.

Fink, J.H. and Fletcher, R.C. (1978) Ropy pahoehoe: Surface folding of a viscous fluid. *J. Volcanol. Geotherm. Res.* **4**, 151-170.

Fink J. H. and Zimbelman J. R. (1985) "Field measurements of the 1983-4 lava flows at Kilauea and Mauna Loa volcanoes (abstract), *LPSC XVI*, 238 - 239.

Fisher R. V. and Schminke H. (1984) *Pyroclastic rocks*, Springer-Verlag, Berlin.

Fiske, R.S, and Jackson, E.D. (1972) Orientation and growth of Hawaiian volcanic rifts: the effect of regional structure and gravitational stresses. *Proc. Roy. Soc. Lond.*, Series A, **329**, 299-326.

Fiske, R.S, Simkin T. and Nielsen (Eds.) (1987) *The volcano letter*, Smithsonian Institution Press, Washington D. C.

Flemal R. C. (1976) Pingos and pingo scars: Their characteristics, distribution, and utility in reconstructing former permafrost environments. *Quaternary Research* **6**, 37-53.

Francis P.W. and Wood C.A. (1982) Absence of silicic volcanism on Mars: Implications for crustal composition and volatiles abundance. *J. Geophys. Res.* **87**, 9881-9889.

Francis P.W. and Wadge G. (1983) The Olympus Mons aureole: Formation by gravitational spreading. *J. Geophys. Res.* **88**, 8333 – 8344.

Frazzetta G. and Romano R. (1984) The 1983 Etna eruption event chronology and morphological development of the lava flow. *Bull. Volcanol.* **47**, 1079 – 1096.

French H. M. (1996) *The Periglacial Environment* (2nd ed.) Addison Wesley Longman Limited. 249 – 253.

Frey H. (1986) "Pseudocraters as indicators of ground ice on Mars" (abstract), *LPSC XVII.*

Frey H., Lowry B. L. and Chase S. A. (1979) Pseudocraters on Mars. *J. Geophys. Res.* **84**, 8075-8086.

Frey H. and Jarosewich M. (1982) Subkilometer martian volcanoes: Properties and possible terrestrial analogs. *J. Geophys. Res.* **87**, 9867 - 9879.

Frey. H., and Schultz R.A.. (1988) Large Impact Basins and the Mega-Impact Origin for the Crustal Dichotomy on Mars. *Geophys. Res. Lett.* **15**. 229-232.

Frey H. V., Sakimoto S. E. H. and Roark J. H. (1998) "A tale of two craters: MOLA constraints on timing of the formation of the crustal dichotomy boundary zone and its associated topography on Mars" (abstract) *LPSC XXVIIII*, no. 1507.

Frey F. A., Coffin M. F., Wallace P. J., Weis D., Zhao X., Wise S. E., Wähnert V., Teagle D. A. H., Saccocia P. J., Reusch D. N., Pringle M. S., Nicolaysen K. E., Neal C. R., Müller R. D., Moore C. L., Mahoney J. J., Keszthelyi L., Inokuchi H., Duncan R. A., Delius H., Damuth J. E., Damasceno D., Coxall H. K., Borre M. K., Boehm F., Barling J., Arndt N. and Antretter M.. (2000). Origin and evolution of a submarine large igneous province: the Kerguelen Plateau and Broken Ridge, southern Indian Ocean. *Earth and Planet. Sci. Lett.* **176**, 73–89.

Fryberger S.G. (1979) "Dune forms and wind regime". In, McKee E. D. (1979), 305 – 397.

Fryberger S.G. and Ahlbrandt T.S. (1979) Mechanisms for the formation of Aeolian sand seas. *Z. Geomorphol.*, **23**, 440-460.

Fryberger S.G. and Dean G. (1979) Dune forms and wind regimes. In *A Study of Global Sand Seas* (ed. Mckee E. D.),137-169, Geological Survey Professional Paper 1052.

Gardner, C. S. (1992) Ranging performance of satellite laser altimeters, *IEEE Trans. Geosci. Remote Sens.*, **30**, 1061 – 1072.

Garvin, J. B., Frawley J. J. and Abshire J. B. (1999) Vertical roughness of Mars from the Mars Orbiter Laser Altimeter. *Geophys. Res. Lett.*, **26**, 381 – 384.

Gatto,L.W. and Anderson,D.M. (1975) Alaskan Thermokarst Terrain and Possible Martian Analogs. *Science* **188** ,255 –257.

Gill J. (1981) *Orogenic andesites and plate tectonics*, Springer-Verlag, New York.

Greeley R. (1987) The role of lava tubes in Hawaiian volcanoes. *U. S. G. S. Prof. Paper* **1350**, 1584 – 1602.

Greeley R. and King J. S. (1977) *Volcanism of the Eastern Snake River Plain, Idaho: A comparative planetary geology guidebook.* NASA, Washington, DC, USA.

Greeley R., Fink J. H., Gault D. E., Snyder D. B., Guest J. E. and Schultz P. H. (1980) Impact cratering in viscous targets: Laboratory experiments. *Proc. Lunar Planet. Sci. Conf.* **XI**, 2075-2097.

Greeley R.and Spudis P. (1981) Volcanism on Mars. *Rev. Geophys. Space Phys.* **19**, 13 – 41.

Greeley R., Leach R. N., Williams S. H., White B. R., Pollack J. B., Krinsley D. H. and Marshall J. R. (1982) Rate of wind abrasion on Mars. *J. Geophys. Res.* **87**, No. B12, 10009 – 10024.

Greeley R. and Iversen J. D. (1985) *Wind as a geological process on Earth, Mars, Venus and Titan.* Cambridge University Press, Cambridge.

Greeley R. and Guest J. E. (1987) Geologic map of the eastern equatorial region of Mars. *U.S. Geol. Surv. Misc. Invest. Ser. Map I-1802-B.*

Greeley, R., and Crown, D.A. (1990) Volcanic geology of Tyrrhena Patera, Mars. *J. Geophys. Res.* **95**, 7133-7149.

Greeley R., Lancaster N., S. W. Lee S. W. and Thomas P. (1992) "Martian aeolian processes, sediments, and features". In, *Mars* (eds. Kieffer H. H., Jakosky B. M., Snyder C. W., and Mathews M. S.), 730-766, Univ. of Arizona Press, Tuscon.

Greeley R., Fagents S. A., Harris R. S., Kadel S. D. and Williams D. A. (1998) Erosion by flowing lava: Field evidence. *J. Geophys. Res.* **103**, No. B11, 27325 – 27345.

Greeley R. and Fagents S. A. (2001) Icelandic pseudocraters as analogs to some volcanic cones on Mars. *J. Geophys. Res.* **106**, No. E9, 20527 – 20546.

Grizzaffi P. and Shultz P. H. (1989) Isidis basin: Site of ancient volatile-rich debris layer. *Icarus*, **77**, 358 – 381.

Guest J. E. (1982) Styles of eruption and flow morphology on Mount Etna Volcano: A review of recent Earth Science studies (ed. Romano, R), *Mem. Soc. Geol. Ital.* **23**, 49 – 73.

Guest J. E., Underwood J. R. and Greeley R. (1980) Role of lava tubes in flows from the Observatory Vent, 1971 eruption on Mount Etna. *Geol. Mag.* **117**, 601 – 606.

Guest J. E. and Duncan A. M. (1981) Internal plumbing of Mount Etna. *Nature* **290**, 584 – 586.

Guest J. E., Kilburn C. R. J., Pinkerton H. and Duncan A. M. (1987) The evolution of lava flow fields: observations of the 1981 and 1983 eruptions of Mount Etna, Sicily. *Bull. Volcanol.* **49**, 527 – 540.

Gulick V. C. (1998) Magmatic intrusions and a hydrothermal origin for fluvial valleys on Mars. *J. Geophys. Res.* **103**, 19365-19387.

Gulick V. C. and Baker V. R. (1987) "Origin and evolution of valleys on Martian volcanoes: The Hawaiian analog" (abstract). LPSC XVIII, 376 – 377.

Gulick V. C. and Baker V. R. (1990) Origin and evolution of valleys on Martian volcanoes. *J. Geophys. Res.* **95**, 14325 – 14344.

Hale W. S. (1983) "Central structures in Martian impact craters: Morphology, morphometry, and implications for substrate volatile distributions" (abstract), *LPSC XIV*, 273 – 274.

Hall J. L., Soloman S. C. and Head J. W. (1986) Elysium region, Mars: Tests of lithospheric loading models for the formation of tectonic features *J. Geophys. Res.* **91**, 11377-11392

Harris S. A. (1977) The aureole of Olympus Mons, Mars. *J. Geophys. Res.* **82**, 3099 – 3107.

HartmannW.K. (1973) Martian Cratering 4:Mariner 9 Initial Analysis of Cratering Chronology. *J. Geophys. Res.* **78** ,4096 – 4116.

Hartmann W. K. (1978) Martian Cratering V: Toward an Empirical Martian Chronology,and its Implications. *Geophys. Res. Lett.* **5**, 450 –452.

Hartmann, W.K (1999) Evidence for recent volcanism on Mars from crater counts. *Nature*, **397**, 586-589.

Hartmann W. K. and Berman D. C. (2000) Elysium Planitia lava flows: Crater count chronology and geological implications. *J. Geophys. Res.* **105**, No.E6, 15011 – 15025.

Head J. W. and Wilson L. (1980) "The formation of eroded depressions around the sources of lunar sinuous rilles: Observations" (abstract) *LPSC XI*, 426 – 428.

Head J. W. and Wilson L. (1981) "Lunar sinuous rille formation by thermal erosion: Eruption conditions, rates and durations" (abstract), *LPSC XII,* 427 – 429.

Head J. W. and Wilson L. (1986) Volcanic processes and landforms on Venus: theory, predictions and observations. *J. Geophys. Res.* **91**, 9407-9446.

Head, J. W. and Wilson L. (1989) Basaltic pyroclastic eruptions: Influence of gas - release patterns and volume fluxes on fountain structure, and the formation of cinder cones, spatter cones, rootless flows, lava ponds and lava flows. *J. Volcanol. Geotherm Res.* **37** , 261- 271.

Head, J.W. III, Kreslavsky M., Hiesinger H., Ivanov M., Pratt S., Seibert N., Smith D. E. and Zuber M. T. (1998) Oceans in the past history of Mars: Tests for their presence using Mars Orbiter Laser Altimeter (MOLA) data. *Geophys. Res. Lett. 25,* 4401-4404.

Head J. W., Kreslavsky M., Hiesinger H. and Pratt S. (1999a) "Northern seas and oceans in the past history of Mars: New evidence from Mars Orbiter Laser Altimeter (MOLA) data" (abstract no. 1352), LPSC XXX.

Head J. W., Hiesinger H., Ivanov M. A., Kreslavsky M. A., Pratt S. and Thomson B. J. (1999b) Possible ancient oceans on Mars: evidence from Mars Orbiter Laser Altimeter data. *Science*, **286**, 2134 – 2137.

Head J. W., Mustard J. F., Kreslavsky M. A., Milliken R. E. and Marchant D. R (2003) Recent ice ages on Mars. *Nature* **426**, 797 – 802.

Heisinger H. and Head J. W. (1999) "Shorelines on Mars: Testing for their presence using Mars Orbiter Laser Altimeter (MOLA) data" (abstract) *LPSC XXX,* 1370.

Hess S. L. (1973) Martian winds and dust clouds. *Planet. Space. Sci.* **21**, 1549 – 1557.

Hodges C. A. and Moore H. J. (1979) The sub-glacial birth of Olympus Mons and its aureoles. *J. Geophys. Res.* **84**, 8061 – 8074.

Hodges C. A. and Moore H. J (1994) *Atlas of volcanic landforms on Mars.* U.S.G.S Prof. Paper No. 1534.

Hon K., Kauahikaua J., Denlinger R. and Mackay K. (1994) Emplacement and inflation of pahoehoe sheet flows: observations and measurements of active lava flows on Kilauea Volcano, Hawaii. *Geol. Soc. Am. Bull.* **106**, 351 – 370.

Hoyt, J. H. (1966) Air and sand movement to the lee of dunes. *Sedimentology* **7**, 137-143.

Hulme G. (1973) Turbulent lava flow and the formation of lunar sinuous rilles. *Modern Geol.* **4**, 107 – 117.

Hulme G. (1974) The interpretation of lava flow morphology. *Geophys. J. R. Astr. Soc.* **39**, 361 – 383.

Hulme G. (1976) The determination of the rheological properties and effusion rate of an Olympus Mons lava. *Icarus* **27**, 207 – 213.

Hulme G. (1982) A review of lava flow processes related to the formation of lunar sinuous rilles. *Geophys. Surv.* **5**, 245 – 279.

Hulme G. and Fielder G. 1977 Effusion rates and rheology of lunar lavas. *Phil. Trans. R. Soc. London* **A285**, 227-234.

Hunter R. E and Richmond B. M. (1988) Daily cycles in coastal dunes. *Sed. Geol.* **55**, 43 – 67.

Jeffreys H. (1925) Flow of water in an inclined channel of rectangular section. *London, Edinburgh, Dublin Philos. Mag. And J. Sci.* **49**, 793 – 807.

Johnson, A. M. (1970) *Physical processes in geology*. San Francisco, Freeman, Cooper, and Co.

Jurado-Chichay Z. and Rowland S. K. (1995) Channel overflows of the Pohue Bay flow, Mauna Loa, Hawaii. *Bull. Volcanol.* **57**, 117 – 126.

Kallianpur K. and Mouginis-Mark P. J. (2001) "Slopes of Martian volcanoes" (abstract), *LPSC XXXII.*

Kargel J.S.and Strom R.G. "Ancient Glaciation on Mars" (abstract) *LPSC XXI*, 597 – 598 (1990).

Kearey P. (1996) *The New Penguin Dictionary of Geology*, Penguin Books Ltd.

Keszthelyi L. (1995) A preliminary thermal budget for lava tubes on the Earth and planets. *J. Geophys. Res.* **100**, 20411 – 204120.

Keszthelyi L. and Pieri D. C. (1993) Emplacement of the 75km long Carrizozo lava flow field, south-central New Mexico. *J. Volcanol. Geotherm. Res.* **59**, 59 – 75.

Keszthelyi L. and Denlinger R. (1996) The initial cooling of pahoehoe flow lobes. *Bull. Volcanol.* **58**, 5 – 18.

Keszthelyi L. and Self, S. (1998) Some physical requirements for the emplacement of long basaltic lava flows. *J. Geophys. Res.* **103**, No. B11, 27447 – 27464.

Keszthelyi L., McEwen A. S. and Thordarson T. (2000) Terrestrial analogs and thermal models for Martian flood lavas. J. Geophys. Res. 105, No. E6, 15027 – 15049.

Keszthelyi L. (2003) Flood lavas on Earth, Io, and Mars (abstract). In *"Planetary Volcanism" RAS 'G'/VMSG Meeting,* London.

Kilburn C. R. J. (1990) "Surfaces of aa flow-fields on Mount Etna, Sicily: Morphology, rheology, crystallization and scaling phenomena". In (Ed. Fink J. H.) *Lava flows and domes. IAVCEI Proc. Volcanol.* **2**, 129 – 156.

Kilburn C. R. J. (1993) Lava crusts, aa flow lengthening and the pahoehoe-aa transition. In *Active lavas* (eds. Kilburn C. R. J. and Luongo G.), 263 – 280. UCL Press, London.

Kilburn C. R. J. (1996) ".Patterns and predictability in the emplacement of subaerial lava flows and flow fields". In (eds. Scarpa R. and Tilling R. I) *Monitoring and mitigation of volcano hazards*. Springer, Berlin, 491 – 537.

Kilburn C. R. J. (2004) Fracturing as a quantitative indicator of lava flow dynamics. *J. Volcanol. Geotherm. Res.* **132**, 209 – 224.

Kilburn C. R. J. and Lopes R. M. C. (1988) The growth of aa lava flow fields on Mount Etna, Sicily. *J. Geophys. Res.* **93**, No. B12, 14759 – 14772.

Kilburn C. R. J. and Lopes R. M. C. (1991) General patterns of flow field growth: aa and blocky lavas. *J. Geophys. Res.* **96**, No. B12, 19721 – 19732.

Kilburn C. R. J. and Guest J. E (1993) "Aa lavas of Mount Etna, Sicily". In *Active lavas* (eds. Kilburn C. R. J. and Luongo G.), 73– 106. UCL Press, London.

King J. S and Riehle J. R. (1974) A proposed origin of the Olympus Mons escarpment. *Icarus* **23**, 300 –317.

Knight M.D. and Walker G.P.L. (1988) Magma flow directions in dikes of the Koolau Complex, Oahu, determined from magnetic fabric studies. *J. Geophys. Res.* **93**, 4301-4319.

Knott P. (1979) The structure and pattern of dune forming winds. Unpublished Ph.D. dissertation, University of London.

Kocurek G., Townsley M., Yeh, E., Sweet M. and Havholm K. (1992) Dune and dune-field development stages on Padre Island, Texas: effects of lee airflow and sand saturation levels and implications for interdune deposition. *J. Sed. Petrol.* **62**, 622 – 635.

Lancaster N. (1989) Star dunes. *Progress in Physical Geography* **13**, 67-91.

Lee, S.W. (1984) Mars: Wind streak production as related to obstacle type and size. *Icarus* **58**, 339-357.

Lemoine F. G., Rowlands D.D, Smith D. E. Chinn D. S., Pavlis D. E., Luthcke S. B., Neumann G. A. and Zuber M. T. (1999) Orbit determination for Mars Global Surveyor during mapping. AAS Paper 99 – 328, AAS/AIAA Astrodynamics Specialist Conference, Girdwood, Alaska.

Lemoine F. G., Smith D. E., Rowlands D. D., Zuber M. T., Neumann G. A and Chinn D. S. (2001) An improved solution of the gravity field of Mars (GMM-2B) from Mars Global Surveyor. *J. Geophys. Res.* **106**, No. E10, 23359 – 23376.

Lipman P. W and Banks N. G. (1987) Aa flow dynamics, Mauna Loa, 1984. *U. S. G. S. Prof. Paper* **1350**, 1527 – 1567.

Livingstone I. And Warren A. (1996) *Aeolian Geomorphology: an introduction.* Addison Wesley Longman Limited.

Lopes R. M. C., Guest J. E. and Wilson C. J (1980) Origin of the Olympus Mons aureole and perimeter scarp. *Moon and Planets* **22**, 221 – 234.

Lopes R. M. C. and Guest J. E. (1982) Lava flows on Etna, a morphometric study. In: (eds. Coradini A, Fulchignoni M) *The comparative study of the planets.* Reidel, Dordrecht.

Lopes R. M. C. and Kilburn C. R. J. (1990) Emplacement of lava flow fields: Application of terrestrial studies to Alba Patera, Mars. *J. Geophys. Res.* **95**, No. B9, 14383 – 14397.

Lucchitta B. K. (1984) Ice and debris in the fretted terrain, Mars. *Proc. LPSC XIV, J. Geophys. Res. Suppl.* **89**, B409 – B418.

Lucchitta B. K. (2001) Antarctic ice streams and outflow channels on Mars. *Geophys. Res. Lett.* **28**, No. 3, 403 – 406.

Lucchitta B. K., Ferguson H. M. and Summers C. (1986) Sedimentary deposits in the northern lowland plains, Mars. *Proc. LPSC XVII , J. Geophys. Res. Suppl.* **91**, E166 – E174.

Macdonald G. A. (1953) Pahoehoe, aa and block lava. *Am. J. Sci.*, **251**, 169 – 191.

Macdonald G. A. (1972) *Volcanoes*, Prentice-Hall, Englewood Cliffs, NJ.

Mackay J. R. (1986) "Frost mounds". In, *Focus: Permafrost geomorphology, The Canadian Geographer*, **30**, 363 – 364.

MacKinnon D. J. and Tanaka K. L. (1989) The impacted Martian crust: Structure, hydrology, and some geologic implications. *J. Geophys. Res.* **94**, No. B12, 17,359 – 17,370.

Malin M. C. (1977) Comparison of volcanic features of Elysium (Mars) and Tibesti (Earth). *Geol. Soc. Am. Bull.* 88, 908 – 919.

Malin M. C. (1980) Lengths of Hawaiian lava flows. *Geology* **8**, 306 – 308.

Malin, M. C., Danielson, G. E., Ingersoll, A. P., Masursky, H., Veverka, J., Ravine, M. A., and Soulanille, T. A., 1992, The Mars Observer Camera, *J. Geophys. Res.* **97,** No. E5, 7699-7718.

Malin, M. C., Carr M. H., Danielson G. E., Davies M. E., Hartmann W. K., Ingersoll A. P., James P. B., Masursky H., McEwen A. S., Soderblom L. A., Thomas P., Veverka J., Caplinger M. A., Ravine M. A., Soulanille T. A. and Warren J. L. (1998) Early Views of the Martian surface from the Mars Orbiter Camera of Mars Global Surveyor. *Science* **279,** 1681-1685.

Mandelbrot B. B. (1967) How long is the coast of Britain? Statistical self-similarity and fractional dimension. *Science* **156**, 636 – 638.

Masursky H., Dial A. L., Jr., and Strobell M. E. (1978) Geologic map of the Phoenicis Lacus Quadrangle of Mars. *U.S. Geol. Surv. Misc. Invest. Ser. Map I-896.*

Mattox T. N., Heliker C., Kauahikaua J. and Hon K. (1993) Development of the 1990 Kalapana Flow Field, Kilauea Volcano, Hawaii. *Bull. Volcanol.* **55**, 407 – 413.

McBride K. (1992) "Geologic mapping of the Elysium region of Mars" (abstract) *LPSC XXIII*, 865 – 866.

McCarthy J. J., Rowton S., Moore D., Luthcke S., Pavlis D. E., Tsaoussi L. S., Rowlands D. D. and Marshall J. A. (1994) Geodyn systems descriptions and operations manuals. *NASA/GSFC and Hughes-STX Contractor Report.*

McCauley, J. F. (1973) Mariner 9 evidence for wind erosion in the Equatorial and mid-latitude regions of Mars. J. *Geophys. Res.* **78**, 4123-4137.

McGill G. E. and Dimitriou A. M. (1990) Origin of the Martian global dichotomy by crustal thinning in the late Noachian or early Hesperian. *J. Geophys. Res.* **95**, 12595 – 12605.

McKee E. D. (ed.) (1979) *A study of global sand seas, USGS Prof. Paper* **1052.**

McKenzie D. and Nimmo F. (1999) The generation of Martian floods by the melting of ground-ice above dykes. *Nature* **397**, 231 – 233.

McSween H. Y. (1985) SNC meteorites: Clues to Martian petrologic evolution. *Rev. Geophys.* **23**, 391 – 416.

McSween H. Y. and Harvey R. P. (1993) Outgassed water on Mars: constraints from melt inclusions in SNC meteorites. *Science* **259**, 1890 – 1892.

Melosh H. J. (1989) *Impact cratering: A geologic process.* Oxford Monographs on geology and geophysics, No. 11, Oxford Univ. Press, Inc., New York, USA.

Moore H. J. (1980) Geologic map of the Sinus Sabaeus Quadrangle of Mars. *U.S. Geol. Surv. Misc. Invest. Ser. Map I-1196.*

Moore H. J. (1982) "Mapping volcanic features on Mars" (abstract), in (ed. Holt H. E.) *Reports of Planetary Geology Program – 1981, NASA Tech. Mem. 85127*, 132 – 133.

Moore H. J., Arthur D. W. G. and Schaber G. G. (1978) Yield strengths of flows on the Earth, Mars and Moon. *Proc. LPSC IX,* 3351 – 78.

Morris E. C. (1982) Aureole deposits of the Martian volcano Olympus Mons. *J. Geophys. Res.* **87**, 1164 – 1178.

Mouginis-Mark P.J. (1979) Martian fluidised crater morphology: Variations with crater size, latitude, altitude, and target material. *J. Geophys. Res.* **84**, 8011-8022.

Mouginis-Mark P. J. (1981a) Ejecta emplacement and modes of formation of Martian fluidised ejecta craters. *Icarus* **45**, 60-76.

Mouginis-Mark P. J. (1981b) Late-stage summit activity of Martian shield volcanoes. *Proc. LPSC XII*, 1431-1447.

Mouginis-Mark P. J. (1985) Volcano/ground ice interactions in Elysium Planitia, Mars. *Icarus* **64**, 265 – 284.

Mouginis-Mark P. J. and Brown S. H. (1981) "Regional volcanic studies in Elysium Planitia, Mars", *Rpts. Plan. Geol. Prog. 1980-1981, NASA Tech. Mem.* **82385**, 258 – 260.

Mouginis-Mark P. J., Wilson L. and Head J. W. (1982) Explosive volcanism on Hecates Tholus, Mars: Investigation of eruption conditions. *J. Geophys. Res.* **87**, No. B12, 9890 – 9904.

Mouginis-Mark P. J., Wilson L., Head J. W., Brown S. H., Hall J. L. and Sullivan K.D. (1984) Elysium Planitia, Mars: Regional geology, volcanology, and evidence for volcano-ground-ice interactions. *Earth, Moon and Planets* **30**, 149 – 173.

Mouginis-Mark P. J. and Mathews A. (1987) Geology of the Olympus Mons caldera, Mars. *Eos: Trans. AGU* **68**, 1342.

Mouginis-Mark P.J.,Wilson L. and Zimbelman R.J. (1988) Polygenic eruptions on Alba Patera, Mars: Evidence of channel erosion on pyroclastic flows. *Bull.Vol.* **50**, 361 –379.

Mouginis-Mark P.J.,Wilson L.and Zuber M.T. (1992) The Physical Volcanology of Mars. In (eds. Kieffer H. H., Jakosky B. M., Snyder C. W., and Mathews M. S.), *Mars*, Univ.Arizona Press, Tucson, 424 –452.

Mouginis-Mark P. J. and Yoshioka M. T. (1998) The long lava flows of Elysium Planitia, Mars. *J. Geophys. Res.* **103**, No. E8, 19389 – 19400.

Mouginis-Mark P. J. and Rowland S. K. (2001) The geomorphology of planetary calderas. *Geomorphology* **37**, 201 – 223.

Munro D. C. and Mouginis-Mark P. J. (1990) Eruptive patterns and structure of Isla Fernandina, Galapagos Islands, from SPOT – 1 HRN and large format camera images. *Intl. J. Remote Sensing* **8**, 1501 – 1509.

Mutch T. A., Arvidson R. E., Head J. W., III, Jones K. L. and Saunders R. S. (1976) *The geology of Mars*. (ed. Princeton N. J.), Princeton Univ. Press.

Nakamura K. (1977) Volcanoes as possible indicators of tectonic stress orientation – Principle and proposal. *J. Vol. Geotherm. Res.* **2**, 1 – 16.

Neukum G. and Hiller K. (1981) Martian Ages. *J. Geophys. Res.* **86**, No. B4, 3097 – 3121.

Neukum G. and Wise D.U. (1976) Mars: Standard Crater Curve and Possible New Time Scale. *Science* **194**,1381 –1387.

Neumann, G.A., Rowlands D.D., Lemoine F.G., Smith D.E. and Zuber M.T., (2001) Crossover analysis of MOLA altimetric data. *J. Geophys. Res.* **106**, 23753-23768.

Neumann, G.A., Smith D.E. and Zuber M.T. (2003) Two Mars years of clouds observed by the Mars Orbiter Laser Altimeter, *J. Geophys. Res., 108,* no. E4, article 5023.

Nichols R. L. (1936) Flow units in basalt. *J. Geol.* **44**, 617 – 630.

Nichols R. L. (1939) Viscosity of lava. *J. Geol.* **47**, 290 – 302.

Nielson J. and Kocurek G. (1987) Surface processes, deposits and development of star dunes, Dumont dune field, California. *Bull. Geol. Soc. Am.* **99**, 177-186.

Oberbeck V.R., Quaide W.L. and Greeley R. (1969) On the Origin of Lunar Sinuous Rilles. *Mod. Geol., 1*, 75-80.

Orowan E. (1949) Remarks during meeting on the flow of ice and other solids. *J. Glaciol.* **1**, 231 – 240.

Owen, P.R. (1964) Saltation of uniform grains in air. *J. Fluid Mech.* **20**, 225-242.

Park, S. and Iversen, J. (1984) Dynamics of lava flow: thickness growth characteristics of steady two-dimensional flow. *Geophys. Res. Lett.*, **11**, 641–644.

Parker, T. J., Saunders R. S. and Schneeberger D. M. (1989) Transitional Morphology in the West Deuteronilus Mensae Region of Mars: Implications for Modification of the Lowland/Upland Boundary. *Icarus* **82**, 111-145.

Parker T. J., Gorsline D. S., Saunders R. S., Pieri D. C. and Schneeberger D. M. (1993) Coastal geomorphology of the Martian northern plains. *J. Geophys. Res.* **98**, No. E6, 11061 – 11078.

Peterson D. W. and Swanson D. A. (1974) Observed formation of lava tubes during 1970 – 1971 at Kilauea Volcano, Hawaii. *Speleology* **2**, 209- 222.

Pieri D. C. and Baloga S. M. (1986) Eruption rates, areas and length relationships for some Hawaiian lava flows. *J. Volcanol. Geotherm. Res.* **30**, 29 – 45.

Pinkerton H. and Sparks R. S. J. (1976) The 1974 sub-terminal lavas, Mount Etna: A case history of the formation of a compound flow field. *J. Volcanol. Geotherm. Res.* **1**, 167 – 182.

Pinkerton H. and Wilson L. (1988) "The lengths of lava flows" (abstract), *LPSC XIX*, 937 – 938.

Pinkerton H. and Wilson L. (1994) Factors controlling the lengths of channel-fed lava flows. *Bull. Volcanol.* **56**, 108 – 120.

Pissart A. (1965) Les pingos des Hautes Fagnes: le probleme de leur genese. *Annales, Societe Geologique de Belgique*, **88**, 277 – 289.

Plescia J. B. (1981) The Tempe volcanic province of Mars and comparisons with the Snake River plains of Idaho. *Icarus* **45**, 586 – 601.

Plescia J. B. (1990) Recent flood lavas in the Elysium region of Mars. *Icarus* **88**, 465 – 490.

Plescia J. B. (1993) An assessment of volatile release from recent volcanism in Elysium, Mars. *Icarus* **104**, 20– 32.

Plescia J. B. and Saunders R. S. (1979) The chronology of the Martian volcanoes. *Proc. LPSC X,* 2841 – 2859.

Pollack J. B., Haberle R., Greeley R. and Iversen J. (1976) Estimates of the wind speeds required for particle motion on Mars. *Icarus* **29**, 395 – 417.

Porter S. G. (1972) Distribution, morphology, and size frequency of cinder cones on Mauna Kea volcano, Hawaii. *Geol. Soc. Amer. Bull.* **83**, 3607 – 3612.

Pye K. and Tsoar H. (1990), *Aeolian sand and sand deposits*, Unwin Hyman, London.

Reimers C. E. and Komar P. D. (1979) Evidence for explosive volcanic density currents on certain Martian volcanoes. *Icarus* **39**, 88 – 110.

Richey J. E., Thomas H. H., Bailey E. B., Simpson J. B., Eyles V. A., Lee G. W., Radley E. G. and Dixon B. E. (1930) The geology of Ardnamurchan, north-west Mull and Coll. *Mem. Geol. Surv. U.K, H. M. S. O.*.

Richey J. E. and MacGregor A. G. (1961) Scotland: The Tertiary volcanic districts. *Br. Reg. Geol. H. M. S. O.*, 74 – 76.

Robinson M. S., Mouginis-Mark P. J., Zimbelman J. R., Wu S. S. C., Ablin K. K. and Howington-Kraus A. E. (1993) Chronology, eruption duration, and atmospheric contribution of the Martian volcano Apollinaris Patera. *Icarus* **104**, 20 – 32.

Robson G. R. (1967) Thickness of Etnean lavas. *Nature* **216**, 251 – 252.

Rossbacher L. A. and Judson S. (1981) Ground ice on Mars: Inventory, distribution, and resulting landforms, *Icarus*, **45**, 39 – 59.

Rowland S. K. and Walker G. P. L. (1990) Pahoehoe and aa in Hawaii: volumetric flow rate controls the lava structure. *Bull. Volcanol.* **52**, 615 – 628.

Rowlands D. D., Marshall J. A., McCarthy J. J., Rowton S. C., Moore D., Pavlis D. E. and Luthcke S. B. (1993) Geodyn II system description. *Hughes-STX Contractor Report, Greenbelt, MD.*

Rowlands D. D., Pavlis D. E., Lemoine F. G., Neumann G. A. and Luthcke S. B. (1999) The use of cross-over constraint equations derived from laser altimetry in the orbit determination of Mars Global Surveyor. *Geophys. Res. Lett.* **26**, 1191 – 1194.

Russell P.S., and Head J.W., III, (2001), "The Elysium/Utopia flows: Characteristics from topography and a model of emplacement" (abstract), *LPSC XXXII.*

Ryan M. P. (1988) The mechanics and three-dimensional internal structure of active magmatic systems: Kilauea volcano, Hawaii. *J. Geophys. Res.* **93**, 4213 – 4248.

Sagan C. and Pollack J. B. (1969) Windblown dust on Mars. *Nature* **223**, 791-794.

Sagan, C. (1973) Sandstorms and Eolian erosion on Mars. *J. Geophys. Res.*, **78**, No.20, 4155 – 4161.

Sagan, C., Ververka, J., Fox., P., Dubisch, R., Lederberg, J., Levinthal, E., Quam, L., Tucker, R., Eross, B., and Pollack, J.B (1973) Variable features on Mars,2, Mariner 9 global results. *J. Geophys. Res.* **78**, 4163-4196.

Sakimoto S. E. H., Crisp, J. and Baloga S. M. (1997) Eruption constraints on tube-fed planetary lava flows. *J. Geophys. Res.* **102**, 6597 – 6613.

Schenk, P. M. (1993) Central Pit and Dome Craters: Exposing the Interiors of Ganymede and Callisto. *J. Geophys. Res.* **98**, No. E4, 7475 – 7498.

Schneeberger D. and Pieri D. C. (1988) "Morphology of lava flows at Alba Patera" (abstract), *LPSC XIX*, 931 – 932.

Schneeberger D. and Pieri D. C. (1991) Geomorphology and stratigraphy of Alba Patera, Mars. *J. Geophys. Res.* **96**, 1907 – 1930.

Schonfeld E. (1979) "Estimated viscosities of Arsia Mons lava flows" (abstract) LPSC X, 1063.

Schumm, S.A and Kahn H.R (1972) Experimental Study of Channel Patterns. *Bull. Geol. Soc. Am.*, **83**, 1755-1770.

Scott D. H. and Allingham J. W. (1976) Geologic map of the Elysium Quadrangle of Mars. *U.S. Geol. Surv. Misc. Invest. Ser. Map I-935.*

Scott D. H. and Carr M. H. (1978) Geologic map of Mars, scale 1:25, 000, 000. *USGS Misc. Inv. Series Map I-1083.*

Scott D. H. and Tanaka K. L. (1980) Mars Tharsis region: Volcano-tectonic events in the stratigraphic record. *Proc. LPSC XI*, 2403 – 2421.

Scott D. H., Tanaka K. L. and Schaber G. G. (1981a) Map showing lava flows in S.W. Arcadia, scale 1:2, 000, 000. *U.S. Geol. Surv. Misc. Invest. Ser. Map I-1278.*

Scott D. H., Tanaka K. L. and Schaber G. G. (1981b) Map showing lava flows in S. E. Diacria, scale 1:2, 000, 000. *U.S. Geol. Surv. Misc. Invest. Ser. Map I-1276.*

Scott D. H. and Tanaka K. L. (1986) Geologic map of the western equatorial region of Mars, scale 1:15, 000, 000. *U.S. Geol. Surv. Misc. Invest. Ser. Map I-1802-A.*

Scott D. H. and Chapman M. G. (1995) Geologic and topographic maps of the Elysium paleolake basin, Mars. *U.S. Geol. Surv. Misc. Invest. Ser. Map I-2397.*

Scott E. D. and Wilson L. (2000) Cyclical summit collapse events at Ascraeus Mons, Mars. *J. Geol. Soc. Lond.* **157**, 1101 – 1106.

Seidelmann, P. K., Abalakin V. K., Bursa M., Davies M. E., De Bergh C., Lieske J. ., Oberst J., Simon J. L., Standish E. M., Stooke P. and Thomas P. C. (2002) Report of the IAU/IAG working group on cartographic coordinates and rotational elements of the planets and satellites: 2000, *Celest. Mech. Dyn. Astron.* **82**, 83–110.

Self S., Thordarson T. and Keszthelyi L. (1996a) "Inflation features as keys to the emplacement of pahoehoe lava flow fields in the Columbia River Basalt Group" (abstract). In (ed. Whitehead P. W) *Chapman conference on long lava flows: conference abstracts long lava flows, Econ. Geol. Res. Unit Contrib. 56.* Dep. Of Earth Sci. James Cook Univ. of North Queensland., Townsville, Australia.

Self S., Thordarson Th., Keszthelyi L., Walker GPL., Hon K.,Murphy M. T., Long P. and Finnemore S. (1996b) A new model for the emplacement of the Columbia River Basalts as large inflated pahoehoe sheet lava flow fields. *Geophys. Res. Lett.* **23**, 2689–2692.

Self S., Thordarson T. and Keszthelyi L. (1997) "Emplacement of continental flood basalt lava flows", in *Large igneous provinces* (eds. Mahoney J. J. and Coffin M). *Geophys. Monogr. Ser.* **100**, 381 – 410, AGU, Washington D.C.

Self S., Keszthelyi L. and Thordarson Th. (1998) The importance of pahoehoe. *Annu. Rev. Earth Planet. Sci.* **26**, 81 – 110.

Seppala M. and Linde K. (1978) Wind tunnel studies of ripple formation. *Geografiska Annaler* **60A**, 29 – 40.

Sharp R. P. (1973a) Mars: Fretted and chaotic terrain. *J. Geophys. Res.* **78**, 4073-4083.

Sharp R.P. (1973b) Mars: South polar pits and etched terrain. *J. Geophys. Res.* **78**, 4222-4230.

Sharp R. P. and Malin M. C. (1975) Channels on Mars. *Geol. Soc. Amer. Bull.* **86**, 593 – 609.

Shaw H. R., Wright T. L., Peck D. L. and Okamura R. (1968) The viscosity of basaltic magma: an analysis of field measurements in Makaopuhi lava lake, Hawaii. *Am. J. Sci.* **261**, 255 – 264.

Shaw H. and Swanson D. (1970) Eruption and flow rates of flood basalts. *Proc. 2nd Columbia River Basalt Symp.*, 271- 299, Cheney, East Washington State University Press.

Smith,D.E., Lerch F. J., Nerem R. S., Zuber M. T., Patel G. B., Fricke S. K. and F. G. Lemoine (1993) An improved gravity model for Mars: Goddard Mars Model-1 (GMM-1). *J. Geophys. Res.* **98**, 20781-20889.

Smith, D.E., Zuber M.T., Frey H.V., Garvin J.B., Head J.W., Muhleman D.O., Pettengill G.H., Phillips R.J., Solomon S.C., Zwally H.J., Banerdt W.B. and Duxbury T.C. (1998) Topography of the northern hemisphere of Mars from the Mars Orbiter Laser Altimeter. *Science 279,* 1686-1692.

Smith D. E., Sjogren W. L., Tyler G. L., Balmino G., Lemine F. G. and Konopliv A. S. (1999a) The gravity field of Mars: Results from Mars Global Surveyor. *Science* **286**, 94 - 96.

Smith D.E., Zuber M.T., Solomon S.C., Phillips R.J., Head J.W., Garvin J.B., Banerdt W.B., Muhleman D.O., Pettengill G.H., Neumann G.A., Lemoine F.G., Abshire J.B., Aharonson O., Brown C.D., Hauck S.A., Ivanov A.B., McGovern P.J., Zwally H.J. and Duxbury T.C. (1999b) The global topography of Mars and implications for surface evolution. *Science, 284* 1495-1503.

Smith D. E., Zuber M. T., Frey H. V., Garvin J. B., Head J. W., Muhleman D. O., Pettengill G. H., Phillips R. J., Soloman S. C., Zwally H. J., Banerdt, W. B., Duxbury T. C., Golombek M. P., Lemoine F. G., Neumann G. A., Rowlands D. D., Aharonson O., Ford P. G., Ivanov A. B., Johnson C. L., McGovern P. J., Abshire J. B., Afzal R. S. and Sun X. (2001) Mars Orbiter Laser Altimeter (MOLA): Experiment summary after the first year of global mapping of Mars. *J. Geophys. Res.* **106**, 23689 – 23722.

Smith E. I. (1976) Comparison of the crater morphology-size relationship for Mars, Moon and Mercury. *Icarus* **28**, 543-550.

Snyder C. W. (1977) The missions of the Viking Orbiters. *J. Geophys. Res.*, **82**, No. 28, 3971 – 3983.

Snyder C. W. (1979) The planet Mars as seen at the end of the Viking mission. *J. Geophys. Res.*, **84**, 8487 – 8519.

Soderblom L. A. (1977) Historical variations in the density and distribution of impacting debris in the inner solar system: Evidence from planetary imaging. In *Impact and explosion cratering* (eds. Roddy D. J., Pepin R.Oand Merrill R. B.), New York: Pergamon, 629 – 633.

Soderblom L. A. (1992) "The composition and mineralogy of the Martian surface from spectroscopic observations: 0.3 μm to 50 μm". In, (eds. Kieffer H. H., Jakosky B. M., Snyder C. W., and Mathews M. S.) *Mars*, 557 - 593, Univ. of Arizona Press, Tuscon.

Soderblom L. A., Condit C. D., West R. A., Herman B. M. and Kriedler T. J. (1974) Martian planetwide crater distributions: Implications for geologic history and surface processes. *Icarus* **22**, 239 – 263.

Solana M.C., Kilburn C.R.J., Rodriguez Badiola E. and Aparicio A. (2004) Fast emplacement of extensive pahoehoe flow-fields: the case of the 1736 flows from Montaña de las Nueces, Lanzarote. *J. Volcanol. Geotherm. Res.* **132,** 189-207.

Soloman S. C. and Head J. W (1982) Evolution of the Tharsis province of Mars: The importance of heterogeneous lithospheric thickness and volcanic construction. *J. Volcanol. Geotherm. Res.* **87,** 9755 - 9774.

Sparks R. S. J., Pinkerton H. and Hulme G. (1976) Classification and formation of lava levees on Mount Etna, Sicily. *Geology* **4**, 269 – 271.

Spry M. and Stephenson P.J. (1996) "Segregation structures in the Toomba basalt, north Queensland" (abstract). In (ed. Whitehead P. W) *Chapman conference on long lava flows: conference abstracts long lava flows, Econ. Geol. Res. Unit Contrib. 56*, 78 – 79. Dep. Of Earth Sci. James Cook Univ. of North Queensland., Townsville, Australia.

Squyres S. W. (1978) Martian fretted terrain: Flow of erosional debris. *Icarus* **34**, 600 – 613.

Squyres S. W. (1989) Urey Prize lecture: Water on Mars. *Icarus* **79**, 229-288.

Squyres S. W. and Carr M. H. (1986) Geomorphic evidence for the distribution of ground ice on Mars. *Science* **231**, 249 – 252.

Squyres S. W., Wilhelms D. E. and Moosman A. C. (1987) Large-scale volcano-ground ice interactions on Mars. *Icarus* **70**, no. 3, 385 – 408.

Squyres S. W., Arvidson R. E., Bell J. F., Brückner J., Cabrol N. A., Calvin W., Carr M. H., Christensen P. R., Clark B. C., Crumpler L., Des Marais D. J., d'Uston C., Economou T., Farmer J., Farrand W., Folkner W., Golombek M., Gorevan S., Grant J. A., Greeley R., Grotzinger J., Haskin L., Herkenhoff K. E., Hviid S., Johnson J., Klingelhöfer G., Knoll A., Landis G., Lemmon M., Li R., Madsen M. B., Malin M. C.,. McLennan S. M, McSween H. Y., Ming D. W., Moersch J., Morris R. V., Parker T., Rice Jr. J. W., Richter L., Rieder R., Sims M., Smith M., Smith P., Soderblom L. A., Sullivan R., Wänke H., Wdowiak T., Wolff M. and Yen A. (2004) The Spirit Rover's Athena Science Investigation at Gusev Crater, Mars. *Science*, **305**, Issue 5685, 794-799.

Stephenson P. J. and Griffin T. J. (1976) "Some long basaltic lava flows in North Queensland". In, *Volcanism in Australasia* (ed. Johnson R. W.), 41 – 51.

Stephenson P. J. and Whitehead P. W. (1996) *Field Excursion Guide: Long lava flows in North Queensland, Econ. Geol. Res. Unit. Contrib. 57*, 40, Dept. of Earth Sci., James Cook Univ. of North Queensland, Townsville, Australia.

Strom R.G., Croft S.K. and Barlow N.G. (1992) The Martian impact cratering record. In (eds. Kieffer H. H., Jakosky B. M., Snyder C. W., and Mathews M. S.) *Mars*, 383 – 423, Univ.Arizona Press, Tucson.

Swanson D. A. (1973) Pahoehoe flows from the 1969 – 1971 Mauna Ulu eruption, Kilauea Volcano, Hawaii. *Geol. Soc. Am. Bull.* **84**, 615 – 626.

Swanson D. A., Wright T. L. and Helz R. T. (1975) Linear vent systems and estimated rates of magma production and eruption for the Yakima basalt on the Columbia Plateau. *Am. J. Sci.* **275**, 877 – 905.

Tanaka K. L. (1985) Ice-lubricated gravity spreading of the Olympus Mons aureole deposits. *Icarus* **62**, 191 – 206.

Tanaka,K.L. (1986) The Stratigraphy of Mars. *J .Geophys Res* .**91,** Suppl.,139 –158.

Tanaka K.L. and Scott D.H. (1987) Geologic Map of the Polar Regions of Mars, scale 1:15,000,000.*USGS Misc. Inv. Map* I-1802-C.

Tanaka K.L. and Davis P.A. (1988) Tectonic History of the Syria Planum Province of Mars. *J. Geophys. Res.* **93**,14893 –14917.

Tanaka, K.L., Golombek M. P. and Banerdt W. T. (1991) Reconciliation of stress and structural histories of the Tharsis region of Mars. *J. Geophys. Res.* **96**, 15617 – 15633.

Tanaka K. L., Chapman M. G. and Scott D. H. (1992) Geologic map of the Elysium region, Mars. *U.S. Geol. Surv. Misc. Invest. Ser. Map I-2147.*

Theilig E. (1984) "Pressure ridges as indicators of flow emplacement" (abstract). *Geol. Soc. Am. Abstracts with program*, **16**, 674.

Theilig E. and Greeley R. (1986) Lava Flows on Mars: Analysis of Small Surface Features and Comparisons with Terrestrial Analogs. *Proc. Lun. Planet. Sci. Conf. XVII, Part 1, J. Geophys. Res.*, **91**, No. B13, E193 – E206.

Thomas P.C, Ververka, J., Lee., S. and Bloom, A. (1981) Classification of wind streaks on Mars. *Icarus* **45**,124-153.

Thomas P.C., Ververka, J., Gineris, D., and Wong L. (1984) "Dust" Streaks on Mars. *Icarus*, **49**, 398-415.

Thomas P.C, Malin M. C., Carr M. H., Danielson G. E., Davies M. E., Hartmann W. K., Ingersoll A. P., James P. B., McEwen A. S., Soderblom L. A. and Veverka J. (1999) Bright dunes on Mars. *Nature* **397**, 592-594.

Thorarinsson S. (1950) The eruption of Mt. Hekla, 1947 – 48. *Bull. Volcanol.*, Ser. 2, **10**, 157 – 168.

Thorarinsson S. and Sigvaldason G. E. (1962) The eruption of Askja, 1961, a preliminary report. *Am. J. Sci.* **260**, 641 – 651.

Thorarinsson S., Saemundsson K, and Williams R. S., Jr., (1973) ERTS-1 image of Vatnajokull: analysis of glaciological, structural and volcanic features. *Jokull*, **23**, 7 – 17.

Thordarson Th. (1995) *Volatile release and atmospheric effects of basaltic fissure eruptions*. PhD thesis. Univ. Hawaii, Manoa, Honolulu.

Thordarson Th. and Self S. (1996) Sulfur, chlorine and fluorine degassing and atmospheric loading by the Roza eruption, Columbia River Basalt Group, Washington, USA. *J. Volcanol. Geotherm. Res.* **74**, 49–74

Thornhill G. D., Rothery D. A., Murray J. B., Cook A. C., Day T., Muller J. P. and Iliffe J. C. (1993) Topography of Apollinaris Patera and Ma'adim Vallis: Automated extraction of digital elevation models. *J. Geophys. Res.* **98**, 32581 – 32587.

Tolan T. L., Reidel S. P., Beeson M. H., Anderson J. L., Fecht K. R. and Swanson D. A (1989) "Revision to the estimates of the areal extent and volume of the Columbia River Basalt Group". In *Volcanism and tectonism in the Columbia River Flood Basalt province* (eds. Reidel S. P and Hooper P. R), *Geol. Soc. Am. Spec. Pap.* **239**, 1-20.

Turtle E.P, Pathare A. V., Hartmann W. K. and Esquerdo G. (2001) "Investigating Creep of Ground Ice as a Cause of Crater Relaxation in Martian High-Latitude Softened Terrain" (abstract), *LPSC* XXXII, no.2044.

Wadge G. (1978) Effusion rate and the shape of aa lava flow fields on Mount Etna. *Geology* **6**, 503 – 506.

Wadge G. and Lopes R. M. C. (1991) The lobes of lava flows on Earth and Olympus Mons, Mars. *Bull. Volcanol.* **54**, 10 – 24.

Walker G. P. L. (1967) Thickness and viscosity of Etnean lavas. *Nature* **213**, 484 – 485.

Walker G. P. L. (1971) Compound and simple lava flows and flood basalts. *Bull. Volcanol.* **35**, 579 – 590.

Walker G. P. L. (1973) Lengths of lava flows. *Phil. Trans. R. Soc. Lond. A.* **274**, 107 – 118.

Walker G. P. L (1987) The dyke complex of Koolaua volcano, Oahu: Internal structure of a Hawaiian rift zone. *USGS Prof. Paper 1350*, 961 – 993.

Walker G. P. L. (1988) Three Hawaiian calderas: An origin through loading by shallow intrusions? *J. Geophys. Res.* **93**, 14773 - 14784.

Walker G. P. L (1991) Structure and origin by injection under surface crust, of tumuli, "lava rises", "lava rise pits", and "lava inflation clefts" in Hawaii. *Bull. Volcanol.* **53**, 546 – 558.

Walker G. P. L. (1996) "Morphometric study of pahoehoe lava flows" (abstract). In (ed. Whitehead P. W) *Chapman conference on long lava flows: conference abstracts long lava flows, Econ. Geol. Res. Unit Contrib. 56*, 92 – 93. Dep. Of Earth Sci. James Cook Univ. of North Queensland., Townsville, Australia.

Ward, A. W. (1979) Yardangs on Mars: Evidence of recent wind erosion. *J. Geophys. Res.* **84**, 8147-8166.

Ward A. W., Doyle. K. B., Helm P.J., Weisman M. K. and Witback N. E. (1985) Global map of aeolian features on Mars. *J. Geol. Res.*, **90**, 2038-2056.

Warren A. and Knott P. (1983) Desert dunes: A short review of needs in desert dune research and a recent study of micrometeorological dune-initiation mechanisms, in Brookfield and Ahlbrandt (1983), 343 – 352.

Washburn A. L. (1956) Classification of patterned ground and review of suggested origins. *Geol. Soc. Am. Bull.* **67**, 823 – 865.

Washburn A. L. (1979) *Geocryology.* Edward Arnold Ltd.

Weill D.F., Grieve R.A., McCallum I.S. and Bottinga Y. (1971) Mineralogy-petrology of lunar samples: Viscosity of melts. *Proc. LPSC XX*, 413-430.

Wells, E.N, Ververka, J., Thomas, P. (1984) Mars: Experimental study of albedo changes caused by dust fall-out. *Icarus*, **58**, 331-338.

West M. (1974) Martian volcanism: Additonal observations and evidence for pyroclastic activity. *Icarus* **21**, 1 – 11.

Whitehead P. W. and Stephenson P. J. (1998) Lava rise ridges of the Toomba basalt flow, North Queensland, Australia. *J. Geophys. Res.* **103**, No. 11, 27371-27382.

Whitford-Stark J. L. (1982) Tharsis volcanoes: Separation distances, relative ages, sizes, morphologies, and depths of burial. *J. Geophys. Res.* **87**, 9829 – 9838.

Whitney M. I and Dietrich R. V. (1973) Ventifact sculpture by windblown dust. *Bull. Geol. Soc. Am.* **84**, 2561 – 2581.

Wilhelms D. E. (1990) "Geologic Mapping". In, *Planetary mapping* (eds. Greeley R. and Batson R. M.), New York, Cambridge University Press, 208 260.

Wilhelms D. E. and Squyres S. W. (1984) The Martian hemispheric dichotomy may be due to a giant impact. *Nature* **309**, 138 – 140.

Wilson, I. (1971) Desert sandflow basins and a model for the development of ergs, *Geor. J.* **137**, 180-197.

Wilson, L. (1984) The influences of planetary environments on the eruption styles of volcanoes. *Vistas in Astron.* **27**, 333 – 360.

Wilson, L. and Head J. W. (1980) "The formation of eroded depressions around the sources of lunar sinuous rilles: Theory" (abstract) *LPSC XI*, 1260 – 1262.

Wilson, L. and Head J. W. (1983) A comparison of volcanic eruption processes on Earth, Moon, Mars, Io, and Venus. *Nature* **302**, 663-669.

Wilson L. and Head J. W. (1988) "The influence of gravity on planetary volcanic eruption rates" (abstract) LPSC XIX, 1283 – 1284.

Wilson L. and Head J. W. (1994) Mars: Review and analysis of volcanic eruption theory and relationships to observed landforms. *Rev. Geophys.* **32**, 221 – 264.

Wise D.U. (1976) Faulting and stress trajectories near Alba volcano, northern Tharsis Ridge, Mars. *Geol. Romana* **15**, 430 –433.

Wise D. U. (1979) Geologic map of the Arcadia Quadrangle of Mars, scale 1: 5, 000, 000. *US Geol. Surv. Misc. Inv. Ser. Map I-1154.*

Wise D.U., Golombek M.P. and McGill G.E. (1979) Tectonic Evolution of Mars. *J. Geophys. Res.* **84** ,7934 –7939.

Wood C. A., Head J. W. and Cintala M. J. (1978) Interior morphology of fresh Martian craters: The effects of target characteristics. *Proc. Lunar Planet. Sci. Conf.* **9**, 3691-3709.

Wu S. S. C., Garcia P. A., Jordan R., Scahfer F. J. and Skiff B. A. (1984) Topography of the shield volcano Olympus Mons, on Mars. *Nature* **309**, 432 – 435.

Zimbelman J. R. (1985) Estimates of rheologic properties for flows on the Martian volcano Ascraeus Mons. *Proc. Lun. Planet. Sci. Conf. XVI, Part 1, J. Geophys. Res.*, **90**, Supplement, D157 – D162.

Zimbelman J. R. (1998) Emplacement of long lava flows on planetary surfaces. *J. Geophys. Res.* **103**, No. B11, 27503 – 27516.

Zuber M. T., Smith D. E., Soloman S. C., Muhleman D. O., Head J. W., Garvin J. B., Abshire J. B. and Bufton J. L. (1992) The Mars Observer Laser Altimeter Investigation. *J. Geophys. Res.*, **97**, No. E5, 7781 – 7797.

Zuber M.T., Smith D.E., Solomon S.C., Abshire J.B., Afzal R.S., Aharonson O., Fishbaugh K., Ford P.G., Frey H.V., Garvin J.B., Head J.W., Ivanov A.B., Johnson C.L., Muhleman D.O., Neumann G.A., Pettengill G.H., Phillips R.J., Sun X., Zwally H.J., Banerdt W.B. and Duxbury T.C. (1998) Observations of the north polar region of Mars from the Mars Orbiter Laser Altimeter. *Science* **282**, 2053-2060.

Appendix

Data for the Appendix are found on the CD in the pocket adjacent to this page. The user will find several Microsoft Excel files on the CD that contain data for all the lava flows studied in this thesis. This document is intended to explain how to make use of the data on the CD.

Dimensions

The files titled '**Elysium Dimensions**' and '**Alba Dimensions**' contain data regarding the sizes of the flows from the Elysium Mons and Alba Patera volcanic regions respectively. In each file the following data is given for each lava flow: Orbit Number, Distance from start of flow (in metres), Centre thickness (metres) and Flow width (metres). The ways in which the flow dimensions were measured (including the calculation of centre flow thickness from MOLA) are described in Chapter 5. The orbit numbers of MOLA profiles are included to enable the user to access the raw data on the NASA MOLA CDs.

Slopes

The files titled '**Elysium slopes**' and '**Alba slopes**' contain data regarding the underlying slope values for each lava flow for all the Elysium Mons flows and the Alba Patera lava flows respectively. For each lava flow the slope value was obtained at specific points along the flow for where each MOLA profile crossed (column A on the Excel spreadsheet). The elevation value (column C) and distance (column D) along the flow for two points either side of the flow (column B) were collected for each MOLA profile that crossed the flow, and the slope between these points is given (column I). Using the central thickness values measured from MOLA (column H) the values for $h\sin\alpha$ can be calculated (column T).

Calculations

The file titled '**Calculations**' gives the data, calculations and results of calculations for both the Elysium Mons and Alba Patera aa flows using the Flow Growth Model of Kilburn and Lopes (1991). All data and calculations can be found in the bold boxed areas on the spreadsheet. An explanation of any measurements made can be accessed in Chapter 5 of this thesis.